

**SURFACE COMPLEXATION MODELING OF
ARSENIC IN NATURAL WATER AND SEDIMENT SYSTEMS**

by
Gregory P. Miller

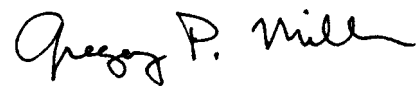
Submitted in Partial Fulfillment
of the Requirements for the

Doctorate of Philosophy in Earth and Environmental Science
with Dissertation in Geochemistry

New Mexico Institute of Mining and Technology
Department of Earth and Environmental Science

Socorro, New Mexico
May, 2001

I have greatly profited from the love, faith, and guidance of two women, my mother, Zena P. Miller, and my wife, Theresa Apodaca. They saved my life. Completion of my Ph.D. truly represents the melding of our collective dreams. I thank you both for being there when I needed you the most.

A handwritten signature in black ink that reads "Gregory P. Miller". The signature is written in a cursive style with a large, stylized 'G' and 'M'.

Gregory P. Miller
December, 2000

Our discussion will be adequate if it has as much clearness as the subject-matter admits of, for precision is not to be sought for alike in all discussions, any more than in all the products of the crafts. Now fine and just actions, which political science investigates, admit of much variety and fluctuation of opinion, so that they may be thought to exist only by convention, and not by nature. And goods also give rise to a similar fluctuation because they bring harm to many people; for before now men have been undone by reason of their wealth and others by reason of their courage. We must be content, then, in speaking of such subjects and with such premises to indicate the truth roughly and in outline, and in speaking about things which are only for the most part true and with premises of the same kind to reach conclusions that are no better. In the same spirit, therefore, should each type of statement be received; for it is the mark of an educated man to look for precision in each class of things just so far as the nature of the subject admits; it is evidently equally foolish to accept probable reasoning from a mathematician and to demand from a rhetorician scientific proofs.

Aristotle, *Nicomachean Ethics*

You can't make the impossible possible by hallucinating new numbers.

Dilbert, in a comic strip by Scott Adams

ABSTRACT

Sorption to solids controls arsenic mobility in most natural waters. Hydrous metal oxides are the dominant sorbing solids in many natural systems. Surface complexation theory will describe water-rock partitioning of arsenic in the laboratory with pure mineral phases; however, published application to arsenic in natural systems is scant. I compare the concentrations of arsenic sorbed to sediments from a geothermally influenced stream in Mexico (100-1200 $\mu\text{g/L}$, 6-20 mg/kg As), and two contaminated sites in Florida (10-450 $\mu\text{g/L}$, 10-44 mg/kg As), to the sediment concentration predicted by a surface complexation model.

Definition of water chemistry and the properties and number of sorption sites is required for surface complexation modeling. General water quality, arsenic speciation, and trace metal chemistry was determined. Arsenic species separation was conducted in the field. The Mexico waters are 90% As^{5+} with the remainder present as organic arsenic compounds and As^{3+} . Small amounts of As^{3+} detected in Mexico allowed determination of an in-stream As^{3+} $t_{1/2}$ of 0.13 h. The water from the Florida sites was approximately an equal mixture of As^{3+} and As^{5+} , with small amounts of organic arsenic present.

Water-sediment ratios were determined from gravimetrically determined porosity and bulk density. The concentration of hydrous metal oxides and sorbed arsenic on the sediments was determined using HNO_3 , H_3PO_4 , citrate-bicarbonate-dithionate, hydroxylamine hydrochloride + HCl, and the Tessier partial extraction techniques. The surface complexation literature provides ion-specific mass-action coefficients (K_{int}) for

the pure mineral phases goethite, ferrihydrite, and gibbsite. Competition simulations used K_{int} for calcium, strontium, barium, zinc, magnesium, manganese, silicic acid, phosphate, carbonate, bicarbonate, sulfate, borate, and fluoride. Coefficients were fitted or substituted if not in the format of the generalized two-layer surface complexation model of Dzombak and Morel. The FITEQL 4.0 code was used for K_{int} fitting. Some coefficients were derived from linear free energy relationships.

The PHREEQC code and the generalized two-layer model were used to model arsenic sorption using a component additivity approach. The component additivity approach is conceptually superior to bulk-characterization of solid-phase sorbing-properties. Partition coefficients (K_d) determined from adsorption isotherms are also inferior to a component additivity approach. Component additivity uses individual surface complexation coefficients measured on pure-mineral phases to represent the sorbing surface. A local equilibrium assumption was made and new solid phases were not allowed to precipitate or dissolve. Water-rock interaction was simulated and the predicted equilibrium concentration of arsenic on sediments is compared to the observed concentration as an indicator of model fit.

The simulations were very sensitive to the extraction method used to define the hydrous metal oxide phases and the iron hydroxide solid phase assumed to be present. The error level in prediction of arsenic concentration can exceed three orders of magnitude if a plausible, but inappropriate, solid sorbing phase is selected. Model fits using iron oxide surfaces defined as ferrihydrite are superior to those using goethite. When metal oxide surfaces are defined using the HNO_3 extraction data the model will closely simulate the observed arsenic concentration. The simulations using HNO_3

extraction data predict approximately 75% of the observed arsenic concentration on the sediments and are superior to simulations using other extraction data.

Sensitivity analysis of the simulations was conducted. The model response to perturbation of silica concentration, pH, or arsenic K_{int} was nonlinear. The competitive effect of silicate, phosphate, carbonate, bicarbonate, sulfate, and boron oxyanions caused large errors in model predictions (20 to 1000 fold) if not treated explicitly. Silica is the most important competing species in the Rio Salado simulations. Phosphate is the most important competing species in the Florida simulations. For Rio Salado, the silica concentration is equal in importance to arsenic sorption as dissolved arsenic concentration, sorbing surface concentration, or pH. Dissolved silica at concentrations as low as 1 mg/kg influenced arsenic surface complexation in the Florida simulations. Phosphate, at half the concentration of silica, out-competes arsenic and silica for sorption sites in the Florida simulations. Estimating porosity resulted in model response differing by a factor of 1.4 to 2.1 from the response to measured porosity. Unfiltered water analysis provided simulations with the greatest internal consistency.

The component additivity approach depends on the transferability of laboratory-derived K_{int} from the literature to field application. Sensitivity analysis of arsenic K_{int} on ferrihydrite indicated that the simulations are 10-fold more sensitive to overestimation of arsenic K_{int} than underestimation. Sensitivity to arsenic K_{int} is greatest at the lowest observed sediment arsenic level. Three published values for silica K_{int} on ferrihydrite were used in the simulations. The various K_{int} for silica caused the simulated sorbed arsenic concentration to vary over four orders of magnitude. The model is sensitive to arsenic and silica K_{int} variability. The variability in K_{int} from the literature should be

evaluated using sensitivity analysis as the simulation error from K_{int} values may equal or exceed that from poor definition of solid phases.

Successful simulation of arsenic component additivity surface complexation in natural systems requires detailed characterization of the aqueous and solid phases. The success of the approach was found to be more dependant the quantification method used for solid phases than quantification of aqueous chemistry. The dependency on definition of iron oxide as amorphous (ferrihydrite) or crystalline (goethite) is equal to the dependency on solid phase quantification method. The breadth of the aqueous analysis used to support the simulation is more important than the accuracy of the individual analyses. Failure to include quantification of competing species in the analysis, and subsequent failure to simulate competition in the model, affects the simulations to a far greater degree than the analytical error inherent to the quantification.

A reasonable simulation of the observed arsenic concentrations was obtained using competitive complexation, sorption constants from the literature, and detailed characterization of the aqueous chemistry and solid phases occurring at field sites. It was apparent that small differences in the conceptual model and data collection techniques have a large effect on the error of the simulation. Without tuning of input parameters, the explicit component additivity approach was able to predict the sediment arsenic concentration to within $\pm 50\%$ of the observed concentrations.

ACKNOWLEDGEMENTS

Without the interest and oversight of Dr. D. I. Norman, Dr. R.M. Prol-Ledesma of Universidad Nacional Autonoma de Mexico, and Dr. I. P. Murarka and Dr. M.E. McLearn of EPRI (formerly the Electric Power Research Institute), this effort would never have been started. It requires scientists of a breed apart to guide graduate students; for their dedication, I thank my advisors Drs. D.I. Norman, C. J. Popp, R. S. Bowman, and G. W. Gross. I am greatly indebted to David Welch of the New Mexico Institute of Mining and Technology for his help in the field and laboratory. Similarly, Lynn A. Brandvold provided laboratory resources at the New Mexico Bureau of Mines and Mineral Resources that would have been unavailable otherwise. David Parkhurst of the US Geological Survey provided assistance with the PHREEQC model as did Sabine Goldberg and Bruce Manning with an early review of the modeling. John Vitti made for plant identifications, Joseph Kelliher provided field assistance, and Shannon Krause performed Tc/Tkl coding. Dr. Dante J. Moran Zenteno of Universidad Nacional Autónoma de Mexico, Alfredo Ramirez Orozco of Comisión Federal de Electricidad, and Oscar A. Escolaro Fuentes, both of Comisión Nacional del Agua were of great aid in providing logistics support in Mexico, and obtaining historical data.

The field investigation and modeling were funded by EPRI under Agreement No. 4CH6890. The refinement of arsenic species field-separation was funded by the New Mexico Waste-Management Environmental Research Consortium (WERC).

TABLE OF CONTENTS

	Page
TABLE OF CONTENTS	iii
LIST OF TABLES	vi
LIST OF FIGURES	ix
LIST OF SYMBOLS AND ABBREVIATIONS	xi
CHAPTER 1 INTRODUCTION	1
1.1 Arsenic Health Effects	3
1.2 Arsenic Geochemistry	4
1.3 Geochemical Models and Modeling	6
1.4 Surface Complexation Theory	8
1.5 Related Research on Surface Complexation Modeling	13
CHAPTER 2 FIELD SITES	18
2.1 Methods	18
2.2 Rio Salado, Mexico	18
2.2.1 Filtered and Unfiltered Analysis	22
2.2.2 Sediment Geochemistry	30
2.2.3 Rio Salado Flow and Chemical Flux	31
2.2.4 Arsenic Speciation and Transformation Kinetics	33
2.3 Florida Sites	36
2.3.1 Tyndall Air Force Base	39
2.3.2 Fort Walton	40
2.3.3 Water Sample Chemistry	40
2.3.4 Sediments	41
CHAPTER 3 METHODS	42
3.1 Modeling Approach	42
3.2 Selection of Computational Model	49
3.3 Input Data Sets	50
3.3.1 Rio Salado Surface Chemistry	51
3.3.2 Florida Surface Chemistry	52
3.3.3 Water-Mineral Ratio	53
3.4 Sensitivity Analysis	54
3.5 Computational and Data-Processing Environment	55
3.6 Model Output and Post-Processing	56
CHAPTER 4 RESULTS	58
4.1 Rio Salado	58
4.1.1 Median R-values	58
4.1.2 Trends in R as Compared to Select Input Data	61
4.2 The Effect of Ion Competition	64

4.3 Florida Sites.....	76
4.4 Sensitivity Analysis	79
4.4.1 Variation in Conceptual Model.....	79
4.4.2 Perturbation of Select Input Parameters	80
4.4.3 Perturbation of Arsenic K_{int}	83
CHAPTER 5 DISCUSSION.....	86
5.1 Known Limitations to Approach	86
5.1.1 Surface Phase Limitations	86
5.1.2 Operationally Defined Extractions	86
5.1.3 Equilibrium Assumption.....	90
5.1.4 Organic Substrates.....	92
5.1.5 Organic Arsenic.....	93
5.2 Extraction Method for Geochemical Modeling.....	93
5.2.1 Rio Salado	93
5.2.2 Florida Sites	94
5.3 Findings Regarding the Sorbing Mineral Phase	95
5.3.1 Iron Oxides.....	95
5.3.2 Gibbsite.....	96
5.4 Arsenic Speciation to Support Surface Complexation Modeling.....	96
5.5 Competition for Sorption Sites by Common Anions	98
5.6 Trends in R: The Ratio of Modeled to Observed Arsenic	100
5.7 General Observations	102
5.8 Suggested Approach	105
CHAPTER 6 RECOMMENDATIONS FOR FUTURE WORK	107
CHAPTER 7 CONCLUSIONS	109
REFERENCES CITED	111
APPENDIX A RIO SALADO FIELD INVESTIGATIONS	119
A.1. Site Selection	119
A.2. Stream Flow.....	126
A.2.1. Tracer Tests.....	126
A.2.1.1 Dye Tests.....	127
A.2.1.2 Sodium Chloride Test	127
A.2.2. Velocity-Area Method	127
A.3. Surface Water Sampling.....	130
A.3.1. Field Parameters	130
A.3.2. Arsenic Source Variability.....	133
A.3.3. Arsenic Diurnal Variation – Replicate Sampling.....	133
A.4. Stream Sediment Sampling	136
A.5. Plant and Algae Sampling	137
A.6. Analytical Methods	137
A.6.1. Analytical Techniques and Detection Limits.....	137
A.6.2. Sediment Extractions	139
A.6.2.1 Selective Extraction	139
A.6.2.2 HNO ₃ Digestions	140
A.6.2.3 Speciation of Arsenic in Sediments	140
A.7. Sediment Mineralogy	142

A.7.1. Carbonate Analysis.....	142
A.7.2. Electron Microprobe Analysis	144
A.7.3. Reflectance Spectrophotometry	144
A.7.4. Surface Area Measurements	144
A.7.5. Determination of Total Organic Carbon (TOC).....	145
A.7.6. X-Ray Diffraction.....	145
A.7.7. X-Ray Fluorescence	146
A.7.8. Barium Arsenate.....	146
A.7.9. Algae Digestions and Arsenic Speciation.....	146
A.7.10. Plant Digestions.....	147
A.7.11. Rio Salado Plants.....	147
A.7.11.1 Arsenic Speciation of Algae	147
A.7.11.2 Arsenic in Plants	148
A.7.11.3 Plant Descriptions and Taxonomy	149
A.8. Rio Salado Tabular Data	151
A.9. Data Quality.....	168
A.9.1. Reagents and Standards	168
A.9.2. Quality Assurance	168
A.9.3. Quality Control.....	171
A.9.4. Rio Salado Data Quality Assessment	172
A.9.4.1 Speciation Method Modification	172
A.9.4.2 Speciation Method Performance.....	173
APPENDIX B FLORIDA INVESTIGATION.....	179
B.1. Sampling and Analysis.....	179
B.1.1. Tyndall AFB.....	181
B.1.2. Fort Walton Beach.....	182
B.1.3. Field Parameters	183
B.2. Speciation of Arsenic in Water	184
B.3. Sediment Extractions.....	184
B.3.1. Selective Extraction	184
B.3.2. HNO ₃ Digestions	185
B.3.3. Citrate-Bicarbonate-Dithionate Extractions	185
B.3.4. Speciation of Arsenic in Sediments.....	186
B.4. Sediment Petrology and Mineralogy.....	186
B.4.1. Determination of Total Organic Carbon (TOC).....	186
B.4.2. X-Ray Fluorescence.....	186
B.5. Florida Tabular Data	187
B.6. Data Quality.....	193
B.6.1. Reagents and Standards	193
B.6.2. Quality Assurance.....	193
B.6.3. Quality Control.....	195
B.6.4. Florida Data Quality Assessment	195
APPENDIX C CD-ROM OF DATA AND MODEL OUTPUT	197

LIST OF TABLES

Table	Page
Table 1. In-stream arsenic species concentration, unfiltered samples ($\mu\text{g/L}$).	24
Table 2. In-stream arsenic species concentration, filtered samples ($\mu\text{g/L}$).	25
Table 3. Rio Salado unfiltered water samples, major elements.	26
Table 4. Rio Salado filtered water samples (0.45 μm), major elements.	27
Table 5. Rio Salado anions and alkalinity.	28
Table 6. Rio Salado sediment arsenic concentrations.	28
Table 7. Rio Salado field parameters.	29
Table 8. Florida field parameters and alkalinity.	36
Table 9. Florida anions in water.....	36
Table 10. Florida arsenic concentration in water (ppb).....	37
Table 11. Florida arsenic species as percentage of total filtered arsenic concentration in water and method recovery as compared to the total (ppb).	37
Table 12. Florida unfiltered water samples, major elements.	37
Table 13. Florida filtered water samples (0.45 μm), major elements.	38
Table 14. Surface complexation mass-action coefficients for ferrihydrite surfaces and the generalized two-layer model.	45
Table 15. Surface complexation mass-action coefficients used for goethite surfaces and the generalized two-layer model.	45
Table 16. Surface complexation mass-action coefficients used for gibbsite surfaces and the generalized two-layer model.	46
Table 17. Results of Rio Salado simulations: Summary statistics of the ratio of modeled to observed arsenic concentration, R, on sediment.	59
Table 18. Results of Rio Salado simulations, trends in R-value as compared to selected input parameters for Rio Salado.....	61
Table 19. Relative site occupation by silica and arsenic under varied K_{int} for silica.	72
Table 20. Results of Florida simulations: Summary statistics of the ratio of modeled to observed arsenic concentration, R, on sediment.	78
Table 21. Results of Florida simulations: summary statistics of the ratio of modeled to observed arsenic concentration, R, on sediment, with outliers censored.	78
Table 22. Slopes from linear regression analysis of changes in model output by perturbing input parameters plotting the response as a percent change in sorbed arsenic concentration.	81
Table A-1. Rio Salado sampling and measurement station locations.	124
Table A-2. Point velocity and discharge values.....	128
Table A-3. Tracer test flow velocities, Rio Salado, January 1998.....	129
Table A-4. Field parameters for Rio Salado.	132

Table A-5 Rio Salado arsenic concentration (ppb) source variation summary statistics.	133
Table A-6. Arsenic analytical values for diurnal sampling (ppb).	134
Table A-7. Metals and anion analytical values for diurnal sampling (ppm).	134
Table A-8. Diurnal field measurements.	134
Table A-9. Reconnaissance sampling data collection.	138
Table A-10. In-stream arsenic species concentration: Unfiltered samples ($\mu\text{g/L}$).	151
Table A-11. In-stream arsenic species concentration: Filtered samples ($\mu\text{g/L}$).	152
Table A-12. Unfiltered water samples, major elements.	153
Table A-13. Filtered water samples (0.45 μm), major elements.	154
Table A-14. Anions and uncorrected alkalinity.	155
Table A-15. Arsenic concentrations of time series samples.	155
Table A-16. Sediment Eh, organic carbon (TOC), and grain size distribution (Welch, 1999).	156
Table A-17. Arsenic bound in each size fraction as % of total arsenic and BET surface area (Welch, 1999).	157
Table A-18. Counts of arsenic measured for iron oxide and glasses by electron microprobe (Welch, 1999).	157
Table A-19. Description of sediment >2 mm (Welch, 1999).	158
Table A-20. Fe, Mn, and As extracted by HNO_3 from whole sediment (Welch, 1999).	159
Table A-21. Fe, Mn, Al, Si, and As extracted by HNO_3 from -80 mesh sediment (Welch, 1999).	159
Table A-22. Fe, Mn, Al, Si, and As extracted by Chao reagent with ground -80 mesh sediment (Welch, 1999).	160
Table A-23. As species, Fe, and Mn extracted by 0.1M H_3PO_4 with ground -80 mesh sediment (Welch, 1999).	161
Table A-24. Results of Tessier partial extractions (Welch, 1999).	162
Table A-25. XRF determinations of elemental concentrations in whole sediment, mg/kg unless noted (Welch, 1999).	163
Table A-26. Mineral surface sorbing sites determined by HNO_3 digestion on -80 mesh sediment.	164
Table A-27. Mineral surface sorbing sites determined by HNO_3 digestion on whole sediment.	165
Table A-28. Mineral surface sorbing sites determined by H_3PO_4 digestion on -80 mesh sediment.	166
Table A-29. Mineral surface sorbing sites determined by Chao reagent digestion on -80 mesh sediment.	167
Table A-30. Ion exchange chromatography - GFAA recovery rates.	174
Table A-31. Acid disassociation constants for arsenic compounds.	174
Table B-1. Florida sampling station locations.	180
Table B-2. Florida data collection.	180
Table B-3. Florida field parameters.	183
Table B-4. Concentration of As, Fe, Al, Si by sediment extraction method.	187
Table B-5. Florida anions in water.	188
Table B-6. Arsenic concentration in water (ppb).	189

Table B-7. Arsenic species as percentage of total filtered arsenic concentration in water and method recovery as compared to the total (ppb).....	189
Table B-8. Unfiltered water sample analytical results.	189
Table B-9. Filtered water sample analytical results.	190
Table B-10. Arsenic by partial extraction methods as compared to arsenic by total digestion.	190
Table B-11. Mineral surface sorbing sites determined by HNO ₃ digestion.	190
Table B-12. Mineral surface sorbing sites determined by citrate-bicarbonate-dithionate (CBD) digestion.....	191
Table B-13. Mineral surface sorbing sites determined as the sum of all Tessier sequential extraction steps.....	191
Table B-14. Mineral surface sorbing sites determined by the Chao reagent step of the Tessier sequential extraction.	191
Table B-15. Porosity, density, and organic carbon content (TOC).....	192

LIST OF FIGURES

Figure	Page
Figure 1. Location of the La Primavera watershed and Rio Salado, Mexico.....	19
Figure 2. Location of the Rio Salado sampling stations, springs, and weirs.	20
Figure 3. Results of PHREEQC modeling of carbonate alkalinity and calcite saturation index for the main channel of Rio Salado.....	23
Figure 4. Rio Salado discharge and chemical flux for chloride and filtered (F) and unfiltered (UF) total arsenic.	34
Figure 5. As ³⁺ disappearance in Rio Salado downstream of the Powerline spring.....	35
Figure 6. Eh-pH plot for the As-H ₂ O-S system from Sadiq (1997), with observations from the Florida (T and FW) and Rio Salado (RS) field sites.	51
Figure 7. Data analysis and modeling process schematic.	56
Figure 8. Relationships between BET surface area and the number of model sites available to fit factor R.	62
Figure 9. Trends in R as compared to arsenic extraction method and surface composition.	63
Figure 10. Trends in R as compared to iron extraction method and surface composition.	65
Figure 11. Trends in R as compared to total organic carbon and surface composition. ..	66
Figure 12. Trends in R as compared to water temperature and surface composition.	67
Figure 13. Trends in R as compared to pH and surface composition.	68
Figure 14. Trends in R as compared to conductivity and surface composition.	69
Figure 15. Trends in R as compared to porosity and surface composition.	70
Figure 16. Ranked occupied site population for Rio Salado simulations using silica K _{int} refit from Meng and Letterman [102] data by percentage (a) and concentration (b).	73
Figure 17. Ranked occupied site population for Rio Salado simulations using published silica K _{int} from Dzomback and Morel [20] by percentage (a) and concentration (b).	74
Figure 18. Ranked occupied site population for Rio Salado simulations using published silica K _{int} from Swedlund and Webster [50] by percentage (a) and concentration (b).	75
Figure 19. Ranked occupied site population for Florida simulations using K _{int} refit from Meng and Letterman [102] data for Tyndall (a) and Fort Walton (b) samples.....	77
Figure 20. Variation in R by sample station, extraction method, and surface assemblage for the Florida sediments and unfiltered (UF) water samples.....	82
Figure 21. Sensitivity of sorbed arsenic concentration to perturbation in input pH value for Rio Salado Station 12 and Florida Sample T-1.	84
Figure 22. Sensitivity of Rio Salado simulations to perturbation of arsenic K _{int}	85

Figure 23. Sensitivity of Florida simulations to perturbation of arsenic K_{int} .	85
Figure 24. Flowchart for initial application of a surface complexation component additivity modeling approach to a field site.	106
Figure A-1. Location of the La Primavera watershed and Rio Salado, Mexico	120
Figure A-2. Rio Salado sampling stations, January 1998.	123
Figure A-3. Replicate arsenic sampling at spring sources to determine variability.	134
Figure A-4. Diurnal variation in arsenic speciation and Redox parameters for Station 3.	135
Figure A-5. Extraction of arsenic from plants, sediments, and water.	148
Figure A-6. Arsenic in plants by field name.	148
Figure A-7. Examples of early validation runs for ion exchange separation of arsenic species.	176
Figure A-8. Comparison of the late mass peaks produced by As^{5+} and the mass of 'DMAA' detected at Rio Salado.	177

LIST OF SYMBOLS AND ABBREVIATIONS

As ³⁺	arsenous acid, H ₃ AsO ₃ , arsenite
As ⁵⁺	arsenic acid, H ₃ AsO ₄ , arsenate
ACS	American Chemical Society
BET	Brunauer-Emmett-Teller surface area
CA	Component Additivity SC method
CBD	citrate-bicarbonate-dithionate
CC	Constant Capacitance
CD-MUSIC	Charge Distribution - Multi Site Complexation
CFE	Comisión Federal de Electricidad, Mexico
DLM	Double-Layer Model
DMAA	dimethylarsinic acid
DO	dissolved oxygen
EDL	Electrical Double Layer
Eh	Redox potential
EPRI	Electric Power Research Institute
<i>F</i>	Faraday constant
F	filtered
g/cm ³	grams per cubic centimeter (density)
GC	generalized composite SC method
h	hour
K _{int}	constant for chemical-specific complexation with an oxide surface
K _{S-}	SC constant for de-protonation of an oxide surface
K _{S+}	SC constant for protonation of an oxide surface
kg	kilogram
L	liter
LFER	linear free-energy relationships
m	meter
M	mole
MDL	method detection limit
mg/kg	milligrams per kilogram
mg/L	milligrams per liter
mV	millivolts
min	minute
MMAA	monomethylarsonic acid
NCCP	no competition, constant porosity
NMBMMR	New Mexico Bureau of Mines and Mineral Resources
NMIMT	New Mexico Institute of Mining and Technology
ORP	oxidation-reduction potential (Redox potential)
PARCC	precision, accuracy, representativeness, completeness, comparability

pH	negative logarithm of the hydrogen ion concentration
pKa	log acid disassociation constant
ppb	part per billion
ppm	part per million
PQL	practical quantification limit
S	Siemens
s	second
SC	Surface Complexation
R	ratio of modeled to observed arsenic concentration
T	temperature, Kelvin
TLM	Triple-Layer Model
TOC	Total Organic Carbon
UF	unfiltered
USEPA	United States Environmental Protection Agency
μg/L	micrograms per liter
μS/cm	conductivity in microSiemens per centimeter
XRD	X-ray diffraction
XRF	X-ray fluorescence
ψ_0	surface potential (volts)

This dissertation is accepted on behalf of the
Faculty of the Institute by the following committee:

David L. Norman
Advisor

Robert A. Bowman

Carl J. Papp

Ulrich Wolfgang Gross

Feb. 1, 2001
Date

I release this document to the New Mexico Institute of Mining and Technology.

Greg P. Miller 02/01/01
Student's Signature Date

CHAPTER 1 INTRODUCTION

Arsenic is a common element, generally present at low concentration in water, soil, and rock. When present in drinking water it can cause debilitating and fatal disease, including cancer [1,2,3]. Ingestion of water containing physiologically significant levels of arsenic has affected the health of millions worldwide and caused thousands of premature deaths. High-arsenic drinking water generally comes from a groundwater source [4,5,6]. With the exception of man-made contamination, there is a link between arsenic present in groundwater and geology. Increased groundwater use in areas of naturally-occurring arsenic is the basis for the current worldwide arsenic health crisis. Better understanding of arsenic geochemistry is essential to alleviating the suffering of millions of human beings. A critical area of arsenic geochemistry to investigate is the environmental partitioning of arsenic between water and aquifer solids.

Chemical interaction with solids controls the mobility of arsenic in aquifers, streams, lakes, and estuaries [6, 7, 8, 9, 10, 11, 12, 13]. The most common and dominant arsenic attenuation reaction is surface complexation (SC) with hydrous metal oxides [14, 15, 16, 17]. Surface complexation is a physical and chemical process [18, 19, 20]. Electrostatic forces draw ions to a solid where they may chemically bond to the solid surface [21, 22, 23].

Surface complexation theory will predict the interaction of arsenic and hydrous metal oxides in the laboratory [18, 19, 24, 25, 26, 27], however, there is little reported on

the predictive ability of the theory as applied to natural systems [8, 28, 29, 30, 31]. Estimates of error in SC laboratory experiments are published [20], however, error sources and magnitude in field application of the theory to arsenic are unknown. This dissertation examines the sources and levels of error that arise when predicting the sediment-water field distribution of arsenic using SC theory.

The research evaluates error levels in modeling arsenic SC using a component additivity (CA) approach. Samples collected as sediment-water pairs from three different hydrogeologic systems, a geothermally influenced stream in Mexico, and two contaminated sites in Florida, are used. Laboratory-developed, pure-mineral, SC coefficients from the literature constrained the model. Wet-chemical partial extractions of the sorbing solid phase from the sediments were used to reconstruct the hydrous metal oxide surface components.

The application of a CA approach to the distribution of arsenic in natural water-rock systems is not well understood. I propose that a CA approach will have error levels comparable to those currently possible with less mechanistic methodologies, such as a partition coefficient approach. The hypothesis is tested by comparison of the CA SC model against observations of arsenic in three natural systems. The model includes competition for sorption sites by both cations and anions. Competitive effects of the common carbon and silica aqueous species are explored explicitly. Error analysis is conducted in a detailed and rigorous manner. By evaluating the error in application of a CA SC approach areas for improvement are identified and ranked.

1.1 ARSENIC HEALTH EFFECTS

Arsenic is a known Class A human carcinogen [1, 2] that is toxic when ingested or inhaled. Over the past decade, there has been accumulating evidence that arsenic at low levels in drinking water can seriously affect health [3]. Cancerous lesions are associated with waters containing 100's of ppb arsenic. Increased rates of skin cancer, heart disease, infant mortality, and birth defects are related to arsenic levels less than 100 ppb. This has prompted the United States Environmental Protection Agency (USEPA) to reexamine health-based limits of arsenic in drinking water supplies, which is currently set at 50 ppb. A new USEPA limit is proposed at 5 ppb; the World Health Organization recommends arsenic concentrations <10 ppb. The American Water Works Association estimates that the US cost of compliance to a 10 ppb arsenic limit will be \$6.3 billion (1999) dollars for the first year of implementation.

The United States has a problem with arsenic in surface water and groundwater. It affects most major cities in New Mexico, including Albuquerque, Los Alamos, and Socorro that have arsenic in some water sources just lower than the USEPA limit of 50 µg/L. It is a problem common in the western US [4, 5, 6, 7], where volcanic rocks are common.

Arsenic exposure can affect human health. In Bangladesh, there is an environmental catastrophe with an estimated 500,000 dying of arsenic-related cancer, and about 1,200,000 persons with some level of arsenic poisoning from ingestion of arsenic contaminated groundwater [19, 20]. It has been noted that the number of people worldwide that are suffering from arsenic-related disease is greater than previously estimated [32, 33, 34]. There are latent effects from long-term low-level exposures,

raising concerns about the protective ability of our current drinking water standard. The National Academy of Science has recently reported that the 50 ppb drinking water level for arsenic can cause bladder cancer with lifetime exposure at the rate of 1 in 1000 individuals exposed [3]. These factors are increasing the general level of public concern regarding the presence of arsenic, in any form, in all media.

1.2 ARSENIC GEOCHEMISTRY

Arsenic occurrence in water is controlled by geochemical constraints. Several wells in Albuquerque have been closed because of poorly understood increases in arsenic concentration. An unspecified geochemical mechanism is postulated [35, 36]. The City of Los Angeles is using the results of arsenic geochemistry studies to evaluate its options regarding the siting of water treatment plants, required capacity, and capital cost [14, 37, 38]. Improved understanding of arsenic geochemistry is critical to the efforts to supply millions of people in Bangladesh with water that is safe to drink [18]. Radically different geochemical mechanisms for the Bangladesh arsenic exposure have been published [18, 19, 20], but have not been tested or a quantitative model proposed. The areas of the world most impacted by arsenic in drinking water have, at best, qualitative understanding of the geochemical processes that are governing arsenic occurrence and distribution.

Arsenic is found in all geological environments with normal concentrations ranging from 1 to 9 ppm in rocks and soils [39, 40]. In the western United States the concentration of arsenic in water, soils, and rocks can be much higher [7, 41]. For example, large areas of Nevada have been found to contain rocks that have total arsenic concentrations > 200 ppm [15]. Arsenic is generally present in water and sediments as the inorganic species As^{3+} , As^{5+} , and the organic compounds monomethylarsonic acid

(MMAA) and dimethylarsinic acid (DMAA) [36, 42, 43, 44]. These different forms of arsenic each have individual toxicities and environmental pathways. Each of these arsenic compounds has several pH-dependant ionic forms.

Arsenic is a minor element. Its aqueous geochemistry is poorly understood. Arsenic environmental pathways are complex. The complexity is caused by the large number of possible interactions and transformations of arsenic [6, 24, 36, 45]. There are problems with quantifying arsenic species during analysis. This confounds the interpretation of the toxicity of arsenic-containing waters [5, 17, 32, 46, 47]. There are kinetic limitations to the inorganic reactions that are not well quantified [8, 45, 48]. Diurnal variation of total arsenic concentrations is reported in contaminated streams [8]. The presence of aqueous species such as silica, sulfate, or organic ligands changes the mobility of arsenic [49, 50]. Clearly, there are a large number of controls on the environmental behavior of arsenic compounds.

The inorganic species As^{3+} and As^{5+} form a Redox (oxidation-reduction) couple. The inorganic arsenic compounds are often in Redox disequilibrium with the environment [5, 6], resulting in thermodynamic disequilibrium [5, 17, 22, 24, 36, 51, 52, 53, 54]. For many inorganic compounds in natural waters, speciation, sorption, and supersaturation (precipitation) conditions can be successfully predicted using a thermodynamic equilibrium approach. However, arsenic disequilibrium investigation requires knowledge of the general equilibrium state and chemical dynamics of the system, because evaluation of disequilibrium requires reference to an equilibrium relationship. In general, reactions between Redox couples are rapid as compared to other dynamics, such as groundwater flow rates and lacustrine sedimentation [16]. However,

the arsenic Redox couple may transform slowly, with half-lives of days to weeks [54, 55]. Current understanding of arsenic geochemistry is not able to accurately predict inorganic or organic arsenic Redox conditions [24, 52, 53, 54, 56, 57].

The bulk of current research on arsenic chemistry is focused on the occurrence and treatment of inorganic arsenic, particularly As^{5+} . This is appropriate since inorganic arsenic is the dominant fraction found in drinking water. However, there is increasing evidence indicating the ubiquitous presence of organic arsenic compounds in the environment, most often as the methyl arsenic compounds MMAA and DMAA [9, 10, 11, 12, 13, 22, 36, 42, 46, 53, 59, 60, 62, 63]. These compounds are produced by biologic transformations.

Predictions of total arsenic behavior can be made in simple systems [8, 11] but there have been few attempts to quantitatively predict arsenic speciation or behavior when there are a large number of geochemical variables. The behavior of arsenic in natural waters is not easily predictable [24, 54, 64]. Evaluation of arsenic environmental behavior requires better understanding of arsenic geochemistry.

1.3 GEOCHEMICAL MODELS AND MODELING

The mobility of metals in the environment is very complex and controlled by a large number of competitive biogeochemical processes. In the last 20 years, there has been remarkable progress in our understanding of controlling mechanisms for metal transport [16, 23, 38, 63, 65, 66]. Werner Stumm initiated this progress in great measure. He started work in 1958 that established the basic mechanisms by which ions react with metal oxides in aqueous systems. This was the beginning of the surface complexation approach [67].

There are relatively large numbers of computer codes designed to simulate aqueous geochemistry and water-rock interaction using thermodynamics. In most cases, the codes have been shown to be capable of providing a realistic representation of equilibrium solution chemistry processes [8, 18, 19, 38, 63, 68, 69], including the SC of trace elements. In order to evaluate complex natural chemistry it is essential to use numerical models. The models must be applicable under a broad range of chemical and physical conditions and have tested and well supported criteria for input data quality. The application of competitive, mechanistic, multi-component modeling shows great promise to allow general predictions of metal behavior in the environment [25, 70]. Mechanistic approaches rely on descriptions of metal behavior at the molecular level [21, 22]. The processes include but are not limited to ion complexation (pairing), precipitation, sorption or SC, oxidation-reduction reactions, gas exchange, ionic strength effects on molecular activity, temperature corrections to thermodynamic parameters, and chemical buffering [69, 70], requiring solution of hundreds of equations for an optimized solution. This is only possible using computerized numerical methods. In theory, it is possible to combine and scale many individual processes, allowing their competitive interaction to fully describe the behavior of complex geochemical systems in a mathematical framework [22, 29, 71]. In reality, there has been little field-scale testing of the theory, approach, or practice of mechanistic modeling [30, 72, 73, 74].

Ideally, mechanistic approaches are descriptive of all observed behaviors; SC modeling is ideally a mechanistic approach. Mechanistic modeling of contaminant interactions with the environment has long been preferable to fully empirical methods, but the necessary data have generally been unavailable [18, 19, 20, 21, 22, 23]. The

unique environmental properties of arsenic have generally prevented reliable prediction of its behavior [9, 17, 23, 24, 25, 26, 28, 29, 30, 36, 39, 43, 45, 52, 55, 58, 63, 64, 65, 71, 74, 76, 77, 78, 79, 80, 81, 82, 83, 84, 85, 86, 87, 88, 89, 90]. The dominant factor affecting the mobility of arsenic species in natural systems is speciation-controlled complexation on the surface of hydrous metal oxides [9, 24, 49], closely followed by interaction with organic matter [16, 20]. The mechanistic approach has successfully described oxyanion interactions with hydrous metal oxides in simple, tightly constrained, laboratory experiments [16, 20, 21, 22, 23].

The modeling approach assumes that the abundance of hydrous metal oxide sorbing surfaces can be determined by chemical extractions. In general, these extractions use acids, bases, and/or reducing agents to dissolve the surface oxides in a manner that is aggressive enough to remove the surface coating, but not so aggressive that the substrate is attacked. Since these extractions cannot be purely specific for hydrous metal oxides, they are empirical or operationally defined rather than mechanistic. However, these operationally defined extractions are practical, have a long history, and have been validated in a variety of media types.

1.4 SURFACE COMPLEXATION THEORY

A broad spectrum of chemical reactions controls the composition of water in contact with soils, sediments, and rocks. Elements and compounds are leached from the rocks while changing conditions can cause the precipitation of new solids. Included in these reactions are ion exchange processes. A process similar to ion exchange is surface complexation. In natural systems, hydrous metal oxides are the most common minerals participating in SC reactions. In SC, ions are drawn near and held at the mineral surface

by electrostatic forces. The ions can be held electrostatically, surrounded by water molecules in a diffuse layer near the oxide surface (outer-sphere complex), or lose the water molecules and covalently bond with the oxide directly, or through a ligand exchange process (inner-sphere complex) [23]. The As^{3+} and As^{5+} ions form inner sphere complexes [26, 27, 91].

Scientists have advanced a number of mathematical descriptions of sorption equilibrium behavior [16, 18, 19, 20, 21, 23, 38]. Use of adsorption isotherms to calculate metal water-solid partitioning distribution coefficients is common. However, field studies revealed problems in the application of adsorption isotherms to calculate partition coefficients (the K_d approach) [92]. The SC approach is thought superior to the K_d approach for modeling oxyanion sorption [8, 20, 21, 22, 23, 92].

In groundwater systems the aquifer material controls water composition. Hydrous metal oxides that form grain coatings dominate aquifer geochemistry but are a very small portion of the total aquifer solids [93]. Sorption reactions that take place at metal oxide surfaces are fully describable using surface complexation theory [16, 20, 23, 38, 72, 94]. Hence, quantification of aquifer geochemistry depends on quantification of SC reactions.

The SC properties of hydrous metal oxides have been studied for over 100 years, mainly by soil scientists [20]. Various theories for the sorption process have been constructed to try to get around the empirical and poorly transferable description of water-mineral interaction of ions using adsorption isotherms [21, 28, 95]. The Gouy-Chapman and Stern electric double layer (EDL) theory was proposed in the 1940's. Electrostatic effects dominate EDL sorption. A turning point was made in theory development by Schindler and Stumm in the late 1960's with their proposal of a SC

approach where the sorbing ions specifically interact with definable, functional, surface molecular groups, yet the electrostatic effects in EDL theory are retained. This differs from the approach of EDL theory in that a specific chemical bond is made with the surface at defined sites that are finite in size and number. Since that time, there have been various modifications of the SC theory. Although the number of fitting parameters, required data, and mathematical construct of the models are significantly different they all have certain commonality. Dzomback and Morel [20] expressed the focus of SC models in the following four statements:

“Sorption on oxides takes place at specific coordination sites. Sorption reactions on oxides can be described quantitatively via mass law equations. Surface charge results from the sorption reactions themselves. The effect of surface charge on sorption can be taken into account by applying a correction factor derived from the EDL theory to mass law constants for surface reactions.”

It should be noted that the fundamental bonding reactions that take place on hydrous metal oxide surfaces are the subject of ongoing research, as are the number and type of functional surface groups available for bonding, the location of the sorbed ions, and the mechanistic theory used for quantification. This results in first-principle differences in how calculations are made in the different SC models. The concepts behind several models and an excellent review of the current state of SC modeling theory were presented by Goldberg in 1998 [38].

Several mathematical formulations of SC models are currently available. The four most commonly cited [38] are the:

1. Schindler and Stumm Constant Capacitance model (CC) [23];
2. Dzomback and Morel Generalized Two-Layer or Diffuse Layer Model (DLM) [20];
3. Triple Layer Model (TLM) of Davis and Leckie [18, 19]; and,

4. Hiemstra and vanRiemsdijk Charge Distribution-Multi-Site Complexation model (CD-MUSIC) [86, 96].

These models have all been used to fit laboratory-derived pure mineral SC data with equal success [38, 71]. In application, each has limitations. The chemical significance of model approach to the problem under consideration must be evaluated. The DLM formulation was tested for arsenic SC in laboratory systems [20]. Hiemstra and vanRiemsdijk's CD-MUSIC model [97, 98] is a newer approach to SC modeling. It is not included in a multicomponent geochemical code, hence was not used in this study.

Surface complexation models use the law of mass-action, expressed as an equilibrium constant, to define protonation (K_{S+}), deprotonation (K_{S-}), and ion-specific sorption to a surface (K_{int}). To implement SC in PHREEQC these K's must be known for each mineral phase and ion modeled. Central to the SC model approach is that protonation and disassociation reactions and ion-specific complexation constants are reversible and apply over a range of pH and ionic strength conditions. The equilibrium constants K_{S-} and K_{S+} are determined for protonation-deprotonation reactions at the oxide surface. The protonation reaction with the surface, S, in the CC, DLM and TLM models are described by the two step reversible process below,

$$\begin{array}{cc}
 SOH + H^+ \rightleftharpoons SOH_2^+ & SOH \rightleftharpoons SO^- + H^+ \\
 K_{s+} = \frac{[SOH_2^+]}{[SOH][H^+]} \exp \frac{(F\psi_0)}{(RT)} & K_{s-} = \frac{[SO^-][H^+]}{[SOH]} \exp \frac{(-F\psi_0)}{(RT)}
 \end{array}$$

where F is the Faraday constant (9.65×10^4 coulomb/mole), ψ_0 is the surface potential in volts, R is the universal gas constant, and T is the absolute temperature. This exponential

electrostatic term appended to the standard form of the equilibrium mass-action equation is used to account for the change in surface potential because of the adsorption of the modeled ion.

The K_S and K_{S+} constants allow the surface-sorbing properties to change with changing pH. Constants for specific sorbing ions that meet these constraints are referred to as “intrinsic constants” or K_{int} . In order to apply these models to SC, K_{int} for surface reactions must be known for each surface to be used, each sorbing ion, and each site defined on the surface. To some degree K_S , K_{S+} , and K_{int} values determined for a single mineral may be used interchangeably among the CC, DLM and TLM (single site, 2-pK) models. This requires refitting and corrections for model geometry. Refitting of experimental data to different SC models can be accomplished using the FITEQL 4.0 model [99].

The Dzombak and Morel [20] DLM model requires two populations of sites to fit the sorption data for cations. They used a small number of high-affinity sites and a large number of low-affinity sites. Dzombak and Morel used a single site for anions. PHREEQC database modifications are needed to account for the total number of sites available to anions. The modified database is contained in Appendix C. Modifications were made after consultation with the author of the PHREEQC code, David Parkhurst of the USGS. To account for the total number of sites available to anions a dummy K_{int} (analogous to the cation $K_{int\ weak}$) was used to make the small number of strong sites available to anions.

The electric layer geometries of the models differ, but they all reduce to mass-action equations that are solved numerically. With respect to broad multicomponent

modeling as proposed here, the most important part of the commonality and formulation among the SC models is the universal application of the mass law constraint. The mass law formulation allows the sorption reactions to be used in the existing theoretical and mathematical framework of thermodynamic equilibrium models. Surface complexation reactions become a part of the general mathematical solution of an equilibrium state between an aqueous solution and a solid sorbing phase. As demonstrated here, this allows use of a single, broadly defined geochemical model to test several SC approaches.

Each protonation state of an oxyanion has a unique K_{int} . For example, K_{int} for DLM SC have the following forms for arsenate sorbing to a single site:

$$K_{As_{\text{int}}}^1 = \frac{[SH_2AsO_4]}{[SOH][H_3AsO_4]}$$

$$K_{As_{\text{int}}}^2 = \frac{[SHAso_4^-][H^+]}{[SOH][H_3AsO_4]} \exp \frac{(-F\psi_0)}{(RT)}$$

$$K_{As_{\text{int}}}^3 = \frac{[SAsO_4^{2-}][H^+]^2}{[SOH][H_3AsO_4]} \exp \frac{(-2F\psi_0)}{(RT)}$$

1.5 RELATED RESEARCH ON SURFACE COMPLEXATION MODELING

The current knowledge of metal environmental behavior suggests that it is possible to predict metal mobility and partitioning over a wide range of environmental conditions using SC [20, 21, 22, 24, 30, 38, 69]. SC theory is used successfully to predict metal distribution in natural waters and sediments [25, 28, 58, 70, 72, 73, 74, 100]. The

SC mechanism is cited as responsible for observed arsenic distributions [17, 20, 24, 25, 49, 58, 63, 72, 73, 74, 76, 101].

Much of the SC research investigates chemically simple systems in the laboratory. There are hundreds of publications describing bench-top surface complexation experiments, see [16, 20, 21, 26, 38, 72, 71, 80, 102] and references therein. The experimental procedure commonly involves conducting titrations of hydrous metal oxide suspensions to determine mineral surface electrostatic potential and adsorption experiments over a range of pH and ionic strength [16, 20, 23]. The intent of the experiments is to obtain K_{S-} , K_{S+} , and K_{int} values for specific hydrous metal oxides. Pure-mineral K's are obtained by fitting the observations using inverse SC models [99]. These K's are the heart of the approach to using SC modeling to fit or predict the mobility of metals.

Experimentally determined K's should be useable in more complex geochemical systems than those tested. There are published pure-mineral K_{S-} , K_{S+} , and K_{int} values (K's) for arsenate and arsenite SC on naturally occurring or synthesized amorphous hydrous ferric oxide (ferrihydrite or HFO), alumina, activated alumina, goethite, gibbsite, kaolinite, montmorillonite, illite, sulfides, soils, and sediments [27, 50, 87, 96]. A few researchers have investigated competition for sorption sites by binary mixtures of arsenic and another oxyanion [26, 50, 76, 79, 87, 103, 105]. The study of surface complexation has not advanced to the point where a ranking of anion and cation competition for hydrous metal oxide surfaces is available.

Bench-top studies on geomeia have used laboratory-derived K's to support SC in natural systems [28, 30, 31]. Apparent K_{int} values are estimated from the field distribution

of aqueous metal concentrations and iron oxyhydroxides and compared to laboratory K_{int} data [25, 30]. The results have been favorable, as indicated by author's subjective indications that a 'good fit' to observation was obtained. However, it is difficult to use either of these methods to make predictions without parameter fitting. Once parameter fitting has taken place error evaluation is meaningless, since the error of fit is reduced by tweaking of input data.

The type and amount of each sorbing surface on a natural material must be known in order to use pure-mineral K 's to predict metal partitioning. Determining the surface composition and summing the parts, or measuring the bulk properties of the whole, are termed respectively the "component additivity" (CA) and the "generalized composite" (GC) methods [100, 104]. There is little published on testing of either principle in natural systems or in a predictive capacity. Davis et al. and Coston et al. describe zinc and lead sorption on quartz sand from Cape Cod by the CA and GC methods [100, 104]. In order to determine the composition of sediment surfaces for their CA approach, Davis et al. used a partial extraction procedure that requires a large number of sediment preparation steps [100]. Their GC method required independent determination of K 's for all geomeedia to be modeled, including adsorption isotherm experiments for all species of interest including competitive ions [100]. Davis et al. concludes that the GC approach is better because it is more practical and accurate.

Several studies suggest that SC models incorporating surface mineralogy and laboratory-derived pure mineral phase K 's, are not currently as effective or accurate as models using other methods [21, 100]. The proposed alternate methods move in the direction of greater simplicity at the cost of generality [100], and are less mechanistic

than CA [16, 20, 21, 22, 38]. The sensitivity of CA or GC methods to input parameter perturbation is not reported. Without a sensitivity analysis, a judgment of fit quality is subjective at best [88].

Davis et al. suggest that the GC method is more accurate. However, they do not present a numerical evaluation of the quality of fit of predicted vs. observed metal sorption [100]. Davis et al. show model fits of about $\pm 25\%$ the observed values for both the GC and CA method [100]. They note that the CA method does not require any data fitting and has predictive capability. Davis et al. make a case for not needing to use the electrostatic terms for correction of K_{int} in surface complexation. The composite method, as advanced by Davis et al., does not determine surface electrical properties of the media. Their method cannot account for change in the surface charge resulting directly from complexation of ions, which is one of the four tenets of Dzomback and Morel's SC theory [20]. Regarding the EDL modifications made to fit the Cape Cod data Davis et al. state:

“The mass-action equations that describe ion adsorption in a nonelectrostatic model are not expected to provide accurate representation of the stoichiometry at the molecular scale.”

This is contrary to another tenet of SC theory; SC reactions are stoichiometric with specific sites on the molecular scale [20, 21, 38].

The nonelectrostatic method employed by Davis et al. is reasonable for the specific application, but is inappropriate for oxyanions. As stated by Dzomback and Morel [20];

“Only a few anions, such as phosphate or arsenate, sorb sufficiently strongly to hydrous ferric oxide to promote substantial PZC and PZNPC shifts.”

Dzomback and Morel's finding that arsenate sorption can affect the point of zero charge (PZC) and the point of zero net proton charge (PZNPC) of a mineral means that the effect on surface charge should not be neglected. The Davis et al. GC approach does not account for details intrinsic to the definition of SC and necessary for arsenic.

CHAPTER 2 FIELD SITES

2.1 METHODS

Details of sample collection and analysis are presented in Appendices A and B. Water analysis includes common field parameters, all major anions and cations, and a suite of common trace elements. Sediment analysis included chemical, mineralogical, and physical determinations. Arsenic speciation was determined in water samples and sediment extracts. The objective was to collect a broad base of data of known accuracy. Tables A-9 and B-2 list analytes, analytical methods, and detection limits.

Chemical analysis of the Rio Salado sediments was conducted by David M. Welch as part of his thesis [106]. His effort includes petrology, petrography, grain size analysis, and chemical extractions. The author conducted all water analysis, and the Florida sediment extractions and petrology. Sediment porosity, density, and organic carbon content was determined at all three sites. Rio Salado discharge was measured by the velocity-area method, and travel times determined by tracer tests.

2.2 RIO SALADO, MEXICO

The upper Rio Salado, Guadalajara, Mexico (Figure 1) was selected for study after a site visit in June 1997 revealed a suitable chemical and physical setting [107, 108, 109, 110]. Rio Salado sampling was conducted in January of 1998. The details of the Rio Salado field investigation are contained in Appendix A. Major components of

Appendix A were previously published [89, 106]. Some analytical results contained in Appendix A are reproduced here as Tables 1-7 for the convenience of the reader. The Rio Salado is a small stream fed by sodium bicarbonate thermal springs; it has approximately 1 ppm aqueous arsenic (Table 1 and 2). Baseflow discharge during the study was constant at $\sim 0.5 \text{ m}^3/\text{s}$. The Rio Salado was sampled over 10 km of the stream reach (Figure 2).

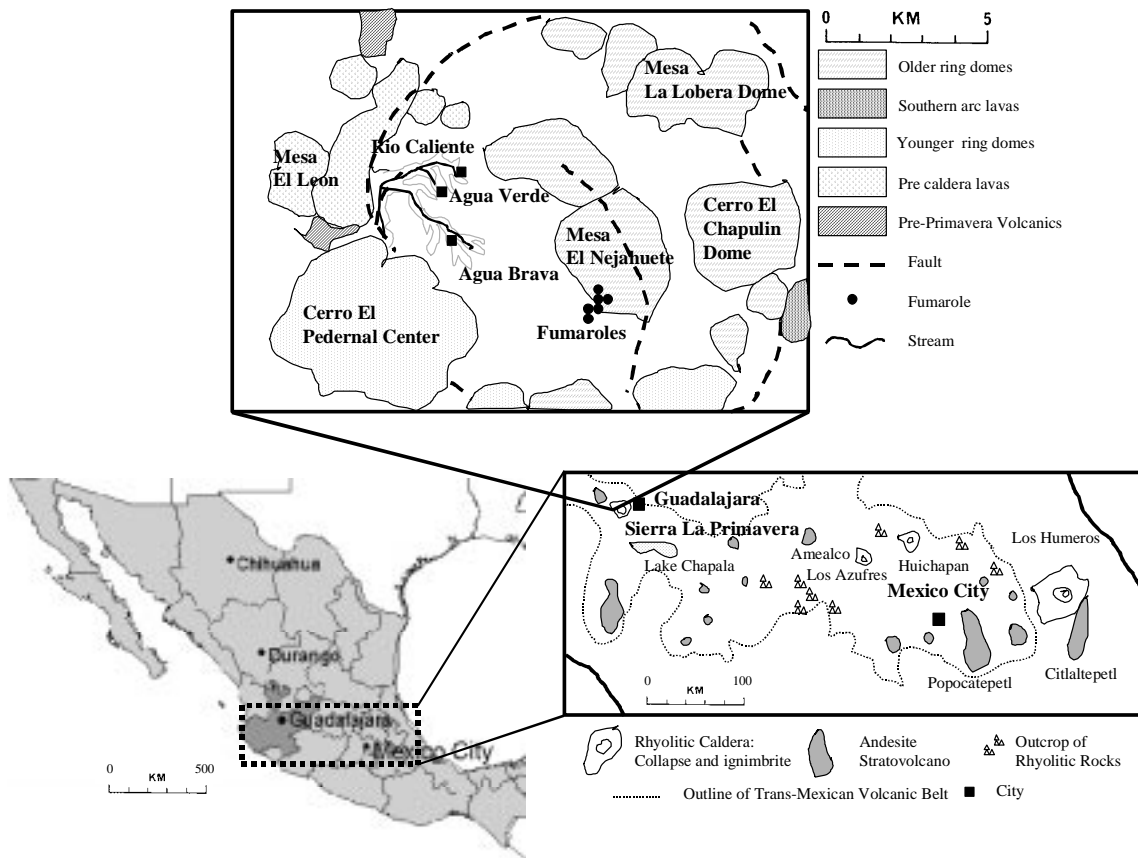


Figure 1. Location of the La Primavera watershed and Rio Salado, Mexico.

A geothermal chemical signature is seen in Rio Salado's higher than usual temperatures and concentrations of silica, fluorine, and boron (Tables 3-6). Stream sediment is dominantly coarse-grained volcanic glass (>95%). This means that the sediments are conceptually similar to hydrous metal oxide-coated glass beads used in

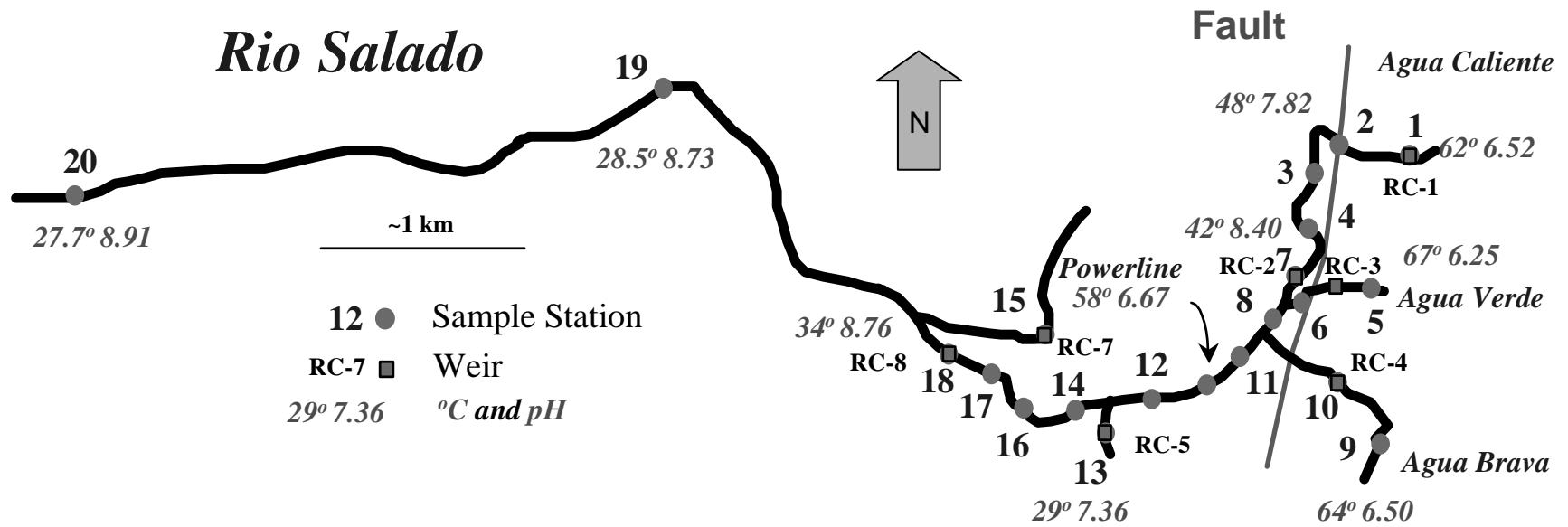


Figure 2. Location of the Rio Salado sampling stations, springs, and weirs. Temperature and pH corrected to 25°C for selected sample locations and all major springs are given.

laboratory bench-scale experiments. The water and sediments are oxidized. The spring discharges provided a reasonably constant arsenic flux during sampling. The principal arsenic species is As^{5+} . Most of the stream channel is free of algae mats, thus allowing sediment-water interaction.

Field parameters (Table 7) show a positive relationship between temperature, Cl^- , H^+ , and conductivity. All the thermal springs are supplied by the same fault system [109, 110, 111, 112], but they vary in the degree of mixing between geothermal and shallow groundwater. There is a change of almost two pH units as the water cools in the stream channels from about 65 to 45 °C. This occurs in short distances from the springs with less change at lower temperatures as the water moves downstream.

Analysis of Rio Salado data in Appendix A and Welch's thesis [106] indicate:

1. Rio Salado is at steady state with respect to discharge, chemical flux, and chemical equilibria after extended baseflow conditions.
2. The sediment-water system is well mixed due to the coarse nature of the sediments and relatively rapid flow.
3. The source of arsenic in the system is constant on the time scale of the sampling event in both flux and concentration, as are other compounds.
4. Hydrous metal oxide phases are present as goethite or ferrihydrite (Fe phase), diaspore, gibbsite, amorphous aluminum hydroxide and/or kaolinite (Al phase), chalcedony or cristobalite (Si phase), and manganese oxide. There are few clay-sized particles or clay minerals. Of the inorganic sorbants, iron oxides dominate SC.

The field parameters indicate that Agua Brava and Powerline springs differ from Agua Caliente and Agua Verde. All springs are pH buffered by carbonate and silica

equilibria. In general, the springs at the north end of the fault system (Agua Caliente and Agua Verde) are hotter, more oxidized, and more acidic than the springs at the southern end of the fault (Agua Brava and Powerline). The waters of Agua Dulce and RC-5 (Station 13) represent local groundwater with little influence from geothermal activity.

Deep thermal waters at La Primavera are charged with CO₂ [107] and effervescence occurs at spring mouths. The stream pH increases in proportion to travel time and distance from a thermal spring. Field alkalinity cannot be used directly to evaluate changes in carbonate equilibrium because of the high silica content. With pH and total alkalinity fixed at the observed values PHREEQC was used to correct the field alkalinity for the effect of acid-consuming species and calculate a carbon species distribution (Figure 3). The downstream variation in pH is explained by CO₂ degassing and changes in pCO₂ from mixing of waters from high CO₂ first order streams. Welch's [106] carbonate measurements and sediment field checks of carbonate reaction with dilute acid (Appendix A) compare well with the modeled calcite saturation index (SI) in Figure 3.

2.2.1 Filtered and Unfiltered Analysis

Aluminum, silica, and iron concentrations in filtered and unfiltered water samples (Tables 3 and 4) indicate that these elements may be precipitating out of the water at some sample stations. Between Kilometer Two and Ten, the unfiltered aluminum concentration rises to five times that of the filtered. It is probable that colloidal aluminum compounds are forming in the water as it cools and the pH rises. A similar, but smaller, trend is noted for iron downstream of Kilometer Four. At Stations 14-18 the filtered silica values deviate from the unfiltered. Given that a similar small trend in lower

concentrations of arsenic in filtered samples is observed, it is likely that some of the arsenic in the lower stream reaches is adsorbing on to Fe and Al colloids. The effect is small with respect to arsenic concentrations. In general, the unfiltered samples provide the most consistent data with the most reasonable trends. I used unfiltered analyses for modeling.

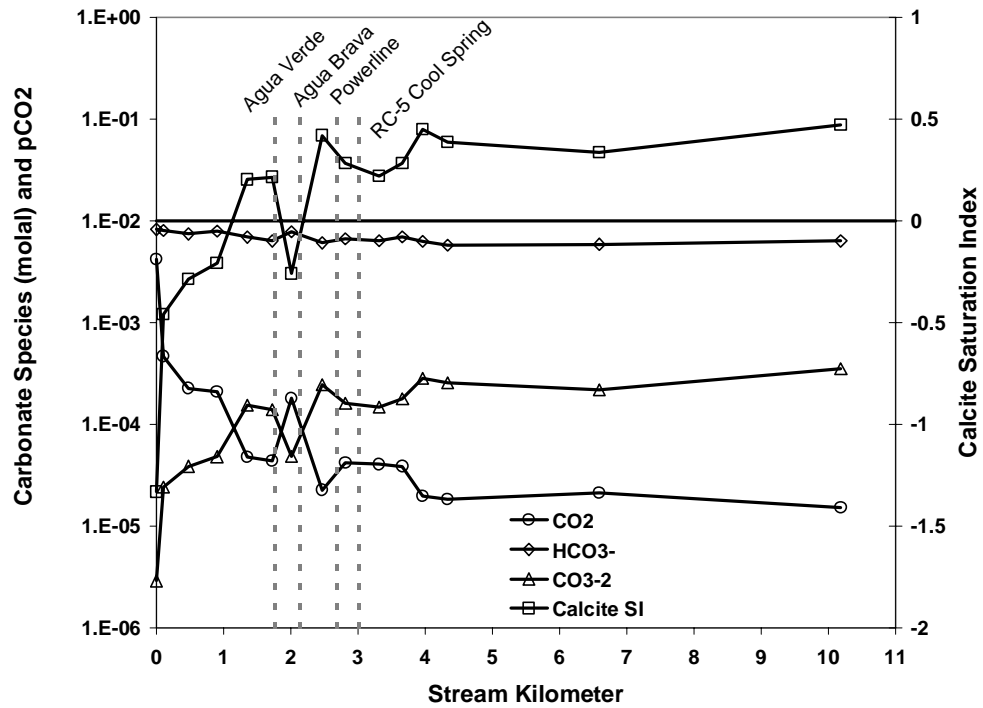


Figure 3. Results of PHREEQC modeling of carbonate alkalinity and calcite saturation index for the main channel of Rio Salado.

Table 1. In-stream arsenic species concentration, unfiltered samples ($\mu\text{g/L}$).

Station	As ³⁺	MMAA	As ⁵⁺	DMAA	Sum of Species	Total As	MMAA (%)	DMAA (%)	MMAA+DMAA (%)
1	0	0	1095	182	1290	1109	0%	14%	14%
2	64	0	1088	102	1267	1189	0%	8%	8%
3.3 (PM)	0	0	1171	113	1296	1042	0%	9%	9%
3.6 (AM)	0	41	973	228	1248	1073	3%	18%	22%
4	0	13	1178	91	1287	1142	1%	7%	8%
5	0	0	1076	62	1146	937	0%	5%	5%
6	0	0	1014	32	1052	985	0%	3%	3%
7	0	25	1048	171	1246	1119	2%	14%	16%
8	11	18	986	127	1141	1065	2%	11%	13%
9	0	24	827	28	883	909	3%	3%	6%
10	0	16	889	101	1005	897	2%	10%	12%
11	0	16	1038	107	1162	1002	1%	9%	11%
12	145	27	888	96	1156	983	2%	8%	11%
13	0	0	235	28	274	242	0%	10%	10%
14	26	16	968	96	1106	949	1%	9%	10%
16	13	13	1055	63	1144	909	1%	6%	7%
17	0	13	911	52	981	935	1%	5%	7%
18	0	20	956	36	1011	903	2%	4%	6%
19	0	0	867	16	892	848	0%	2%	2%
20	0	11	878	22	911	804	1%	2%	4%

Table 2. In-stream arsenic species concentration, filtered samples ($\mu\text{g/L}$).

Station	As ³⁺	MMAA	As ⁵⁺	DMAA	Sum of Species	Total As	MMAA (%)	DMAA (%)	MMAA+DMAA (%)
1	0	18	1130	146	1293	1065	1%	11%	13%
2	69	23	1085	94	1269	1121	2%	7%	9%
3.3 (PM)	0	11	1178	91	1284	1126	1%	7%	8%
3.6 (AM)	0	34	998	154	1193	1088	3%	13%	16%
4	0	18	1188	72	1281	1109	1%	6%	7%
5	0	0	1044	24	1077	970	0%	2%	2%
6	0	148	962	18	1130	964	13%	2%	15%
7	0	20	918	121	1060	1119	2%	11%	13%
8	16	50	896	94	1055	1046	5%	9%	14%
9	0	23	827	83	932	893	2%	9%	11%
10	0	16	750	74	840	888	2%	9%	11%
11	0	23	951	80	1058	722	2%	8%	10%
12	133	27	815	70	1044	983	3%	7%	9%
13	0	0	218	22	254	227	0%	9%	9%
14	28	23	756	66	872	911	3%	8%	10%
16	15	45	1006	36	1102	918	4%	3%	7%
17	0	0	957	51	1023	918	0%	5%	5%
18	0	18	956	33	1006	890	2%	3%	5%
19	0	0	1083	9	1098	821	0%	1%	1%
20	0	11	981	25	1017	756	1%	2%	4%

Table 3. Rio Salado unfiltered water samples, major elements.

Station	Ca ppm	Na ppm	Mg ppm	K ppm	SiO ₂ ppm	Ba ppb	Al ppb	Mn ppb	Fe ppb	Li ppm	Sr ppb	Mo ppb	Cu ppb	As ppb
1	3.2	296	0.19	13.6	531	ND	7	56.83	88.2	1.02	10.0	40.7	1.30	1109
2	3.8	312	0.20	13.7	533	ND	7	79.2	14.0	1.04	10.1	37.4	1.28	1189
3.3 (PM)	3.4	280	0.27	13.5	504	ND	9	77.6	28.2	1.02	9.1	39.8	1.38	1042
3.6 (AM)	3.6	280	0.28	13.3	518	ND	10	117.2	26.7	1.01	9.7	40.5	1.65	1073
4	3.4	306	0.26	13.5	522	ND	9	28.9	50.1	1.04	10.4	41.7	1.34	1142
5	3.7	276	0.28	13.6	496	ND	10	148.9	2.0	0.95	10.2	35.6	1.47	937
6	2.7	270	0.20	14	514	ND	7	10.4	0.6	0.97	6.9	42.9	0.12	985
7	3.8	300	0.30	13.6	513	ND	11	28.7	42.0	1.04	9.5	35.2	2.11	1119
8	3.7	298	0.29	14.1	505	ND	10	40.0	23.2	1.02	9.0	38.6	1.68	1065
9	4.2	275	0.33	13.7	452	ND	12	90.4	5.2	0.94	8.1	31.8	2.18	909
10	4.1	275	0.32	13.7	454	ND	9	43.2	4.0	0.91	8.4	37.2	2.53	897
11	3.7	287	0.32	13.9	482	ND	17	32.5	14.0	0.94	9.9	36.3	1.12	1002
12	3.8	280	0.60	13.8	488	6.4	24	63.5	32.0	0.91	9.9	37.2	1.29	983
13	2.5	64	1.38	3.7	254	ND	9	1.3	4.4	0.23	5.6	24.0	1.23	242
14	3.7	270	0.63	13.4	478	5.6	19	39.6	30.3	0.91	9.7	35.9	1.34	949
16	3.7	266	0.63	13.7	488	5.1	17	29.3	23.5	0.9	9.05	38.5	2.63	909
17	3.7	265	0.63	13.6	469	5.4	19	35.3	20.3	0.9	9.4	37.9	1.45	935
18	3.5	266	0.65	12.9	459	5.0	17	20.4	18.3	0.9	8.6	37.9	1.42	903
19	3.7	255	0.94	12.6	442	4.9	42	12.7	26.7	0.83	10.5	36.1	1.31	848
20	3.4	244	0.93	12.2	421	3.9	56	10.9	52.5	0.77	9.9	35.4	1.43	804
Powerline		280		22.6			103	74.9	0.8					
Agua Dulce		68		4.5			8	273.4	0.2					

Table 4. Rio Salado filtered water samples (0.45 μm), major elements.

Station	Ca ppm	Na ppm	Mg ppm	K ppm	SiO ₂ ppm	Ba ppb	Al ppb	Mn ppb	Fe ppb	Li ppm	Sr ppb	Mo ppb	Cu ppb	As ppb
1	3.8	292	0.19	12.7	486	ND	12	64.0	10.9	1.01	10.5	36.4	1.40	1065
2	3.8	306	0.19	13.2	511	ND	8	66.5	14.2	1.02	10.9	34.0	1.26	1121
3.3 (PM)	3.1	307	0.25	13	504	ND	11	90.2	26.4	1	9.2	35.5	1.36	1126
3.6 (AM)	3.5	297	0.28	13	494	ND	22	104.9	41.5	0.98	11.0	35.9	2.19	1088
4	3	295	0.25	13.3	513	ND	7	26.3	21.8	0.98	8.7	36.3	1.15	1109
5	3.7	290	0.3	13.5	476	ND	55	165.1	5.9	0.98	11.5	29.0	1.27	970
6	2.8	267	0.21	13.5	519	ND	7	61.1	3.9	0.93	9.7	39.8	0.55	964
7	3.8	294	0.3	13.5	507	ND	9	18.5	36.8	0.99	10.4	29.7	1.00	1119
8	3.8	285	0.32	13.6	500	ND	5	37.5	19.2	0.95	9.0	31.9	1.00	1046
9	4.2	268	0.34	13.6	446	ND	9	53.2	7.6	0.87	8.1	25.9	1.14	893
10	4.2	269	0.34	13.6	465	ND	13	38.2	2.1	0.86	8.5	24.9	1.12	888
11	3.8	289	0.32	14.2	488	ND	10	26.6	10.8	1	9.6	29.4	1.10	722
12	3.8	271	0.62	13.8	477	6.2	12	50.0	20.6	0.96	9.4	20.1	3.24	983
13	2.6	68	1.41	ND	251	ND	8	1.8	1.0	0.22	5.4	31.1	1.16	227
14	3.7	254	0.65	13.4	462	4.5	5	30.8	28.7	0.92	9.4	31.1	1.36	911
16	3.8	265	0.64	13.4	458	5.9	11	23.9	178.3	0.93	10.6	28.7	1.29	918
17	3.7	260	0.61	13.4	471	5.4	8	21.9	148.3	0.91	9.5	28.9	1.32	918
18	3.6	262	0.63	12.9	476	4.6	7	22.1	25.7	0.92	9.7	28.2	1.11	890
19	3.7	242	0.91	12.7	440	3.7	5	7.2	16.4	0.84	11.7	27.9	1.88	821
20	3.5	226	0.91	12.4	412	3.5	6	7.1	31.6	0.75	10.2	23.5	2.74	756

Table 5. Rio Salado anions and alkalinity.

Station	Cl ppm	F ppm	Br ppm	B ppm	SO ₄ ppm	CO ₃ ppm	HCO ₃ ppm	NO ₃ ppm
1	93.1	14.8	0.81	7.3	26.8	ND	416	0.3
2	92.6	14.9	0.46	8.7	27.8	ND	392	ND
3.3 (PM)	92.6	15.7	0.37	7.1	28.5	ND	424	ND
3.6 (AM)	91.7	15.5	0.37	4.3	27.8	ND	408	ND
4	89.9	15.9	0.39	7.3	28.8	80	328	0.1
5	73.6	13.7	0.06	6.8	20.1	ND	328	0.1
6	79.2	15.0	0.50	9.4	20.3	88	300	0.1
7	92.0	16.0	0.42	8.9	28.5	56	320	ND
8	86.5	15.5	0.36	7.8	25.8	76	334	0.1
9	73.8	13.3	0.42	8.8	18.6	ND	368	0.2
10	75.4	14.0	0.25	9.3	19.1	104	270	0.1
11	82.5	15.1	0.33	5.7	22.9	160	236	ND
12	77.1	14.6	0.27	6.6	21.8	88	308	ND
13	16.9	6.1	ND	4.1	6.5	ND	88	ND
14	74.2	15.1	0.29	6.5	22.1	40	336	ND
16	75.9	14.7	ND	5.2	21.7	152	252	0.3
17	76.1	14.5	0.23	5.1	21.8	152	256	0.1
18	74.5	14.6	0.32	5.0	21.3	96	280	ND
19	70.9	13.8	0.27	4.7	20.3	144	220	ND
20	63.9	12.5	0.05	4.3	18.2	140	284	ND

Table 6. Rio Salado sediment arsenic concentrations.

Location	As by XRF (mg/kg)	As by HNO ₃ (mg/kg)	Eh (mV)	TOC wt.%	
1		6	3.7	280	1.5
2		6	4.4	200	1.8
3 a.m.		9	4.1	80	2.0
3 p.m.		10	5.9	325	1.9
4		7	5.1	310	1.7
5		13	12.8	200	2.5
6		20	15.3	267	3.0
7		10	6.3	220	2.6
8		8	5.3	230	1.6
9		9	7.1	212	1.9
10		8	5.2	250	1.8
11		13	10.4	210	3.0
12		10	5.0	225	1.8
13		9	2.9	200	3.1
14		10	6.8	70	2.3
16		13	11.1	280	3.1
17		16	7.3	290	3.7
18		9	6.6	280	1.3
19		9	7.0	350	1.3
20		7	3.0	340	1.2

Table 7. Rio Salado field parameters.

Station	Date	Time (MST)	Temp (° C)	Conductivity (µS/cm)	pH	ORP (mV)	CO ₃ ²⁻ (ppm)	HCO ₃ ⁻ (ppm)	
RC-1 North	1/10/98	830			6.52	273			
RC-1 South	1/10/98	830			6.53	280			
RC-1 West	6/26/97	1300	62.1	1674	7.01				
RC-3	1/6/98	1145	53	1289	7.64	224			
RC-3	1/7/98	919	49	1359	7.87	251			
RC-3	1/12/98	1601	60.5	1412	7.67	240			
AV Source 1	1/5/98	1032	31	1500	7.42	226			
AV Source 2	1/5/98	1035	25	1340	7.85	310			
AV Source 3	1/5/98	1036	61	1475	6.83	275			
AV Source 4	1/5/98	1040	63	1385	6.56	330			
AV Source 5	1/5/98	1045	64	1360	6.49	300	0	328	
AV Source 5	1/12/98	1045	67.5						
AV Source 5	6/26/97	1500	67	1566	6.25				
AB Source 1	1/6/98	1320	57	1335	7.7	231			
AB Source 2	1/6/98	1321	64	1329	6.5	219			
AB Source 2	1/12/98	1355	67.5						
AB Source 3	1/6/98	1322	46	1049	7.67	217			
Powerline	1/7/98	1017	51	1182	6.8	187			
Powerline	1/12/98	1242	58.5	1242	6.67	174			
RC Down AV	1/5/98	1457	36	1312	8.46	285			
RC Down	1/12/98	1140	42.8						
RC Up AV	1/5/98	1457	35	1287	8.45	282			
RC Up	1/7/98	1039	27	1241	8.3	196			
RC Up	1/12/98	1330	41.5	1241	8.3	196			
1	1/6/98	756	58	1415	7.16	240	0	416	
1	1/7/98	724	57	1333	7.29	284			
1	1/10/98	800	61	1406	7.47	290			
2	1/5/98	1703	46	1395	7.75	58	0	392	
3	1/8/98	815		1220	7.81	327	0	408	
3	1/10/98	1614	48	1291	7.82	280	0	424	
4	1/10/98	1210	42.5	1277	8.4	287	80	328	
6	1/5/98	1332	48	1310	8.48	280	88	300	
7	1/6/98	1002	42	1287	8.4	218	56	320	
8	1/9/98	1040		1269	7.89	308	76	334	
9	1/6/98	1416		1289	7.64	226	0	368	
9	1/12/98	1345	61.5						
10	1/6/98	1601		1188	8.45	226	104	270	
10	1/7/98	942	42	1250	8.45	248			
10	1/12/98	1328	51.5	1310	8.53	206			
11	1/7/98	1642		1232	8.67	240	160	236	
12	1/7/98	1459		1207	8.44	222	88	308	
14	1/7/98	1303		1130	8.45	264	40	336	
16	1/8/98	1505		1130	8.51	269	152	252	
17	1/8/98	1310		1233	8.76	257	152	256	
18	1/8/98	1130		<u>DO (mg/L)</u> 936	8.76	66	96	280	
18	1/12/98	1200	34	5.2					
19	1/11/98	1110	28.5	5.3	1245	8.73	75	144	220
20	1/11/98	1451	27.7	6.3	1005	8.91	95	140	284
AD	1/11/98	1238	29	443	7.96	67			
13	1/7/98	1116		5.2	316	7.36	8	0	88
13	1/12/98	1334	29						

AV - Agua Verde. AB - Agua Brava. RC - Rio Caliente. AD - Agua Dulce. DO - Dissolved Oxygen.

2.2.2 Sediment Geochemistry

Rio Salado sediment geochemistry was quantified by Welch [106]. Welch's partial extractions of sediment were used to define hydrous metal oxide surfaces for modeling. I quote Welch's findings directly from his thesis [106]. Welch's findings are used to support a conceptual model for the sediments. Additional details are contained in Appendix A. Welch makes the following points:

“Very little variation was seen in local geology and sediment mineralogy over the 10 km of stream reach. Study of the >2 mm fraction showed sediments to be composed of varying proportions of pumice, welded rhyolite tuff fragments and obsidian with Fe-oxides coating some grains... XRD analyses revealed the predominance of amorphous phases representing glasses and could only positively identify quartz.”

“Sediment size fraction analysis conducted for each sample station showed the sediments to be dominated by coarse-grained material with over 50% coarser than 0.5 mm. On average less than 2% of the sediments fell into the <63 μm size fraction (silt-clay).”

“Iron oxides, present as mineral coatings, discrete grains, and as partially oxidized mafic minerals were identified as hematite and goethite by reflectance spectrophotometry.”

“Total As in sediments is not much higher than normal crustal abundance averaging about 8 ppm...”

“Results of the sequential extraction show As to be dominantly associated with organic matter and Fe/Mn-oxides with smaller amounts associated with the carbonate and exchangeable fractions.”

“Point-counts using the electron microprobe showed Fe-oxide grains to contain As at levels 2-3 times above [those in] background glasses and minerals.”

“Results of speciation of sediments for As^{3+} , As^{5+} , MMAA and DMAA show As^{5+} to be the dominant species present in La Primavera sediments. As^{3+} is also present in all samples and is proportional to As^{5+} ...”

The saturation indices of common minerals were calculated using PHREEQC. This was done in order to evaluate anion and cation sources and sinks. Calculations show that the system is strongly oversaturated for the iron oxides goethite, magnetite, and hematite, and often amorphous FeOOH [89, 106] (Appendixes A and C). The Rio Salado system is also oversaturated with respect to amorphous silica phases, slightly undersaturated with respect to amorphous hydrous aluminum oxides, saturated for diaspore, and oversaturated for closely related kaolinite. PHREEQC predicts that aluminum and iron hydrous metal oxides are thermodynamically stable over all modeled sample stations. Ferrihydrite is below but near saturation in the upper stream reaches and above saturation in the lower reaches.

2.2.3 Rio Salado Flow and Chemical Flux

The velocity-area method measurements were used to construct the base flow (steady state) profile for Rio Salado depicted in Figure 4(a). There were instrument difficulties at Stations 1 and 3, hence, flows at those stations were estimated from CFE values. The known first-order springs and streams can account for almost all of the observed flow. Most of the Rio Salado discharge at stream Kilometer Ten was contributed before stream Kilometer Four.

Flux is the product of a concentration and a rate. In the case of Rio Salado, it is the product of the dissolved constituents and the streamflow discharge. Other than a few perturbations by input from first-order streams and groundwater contributions, the dissolved phase concentration of compounds decreases rather uneventfully downstream (Appendix A). Figures 4(a) and (b) depict the total arsenic concentration and arsenic flux

profiles for the main channel of Rio Salado. Figure 4(a) uses measured discharges and 4(b) uses corrected discharge values for stations 18, 19 and 20 that are explained below.

There is a relatively minor groundwater component to the flow (gaining stream) past stream Kilometer Four (RC-8 and Station 18). Changes in Rio Salado water chemistry can be explained by dilution with groundwater similar in composition to that discharging from non-thermal spring RC-5 (Station 13). RC-5 water has approximately $\frac{1}{4}$ of the potassium, sodium, lithium, chloride, sulfate and fluoride found in Rio Salado. Even though RC-5 enters the main channel above Kilometer Four, its cool water discharge is not readily discernible except for an increase in manganese concentration. This being the case the chemistry of Rio Salado is dominated by thermal waters above Kilometer Four and is influenced by shallow, cooler, groundwater downstream.

Assuming that RC-5 is mostly shallow groundwater, chemical concentrations should indicate significant cool groundwater infiltration to Rio Salado. The stream discharge curve in Figure 4(a) shows gaining discharge while the arsenic flux decreases. The total arsenic curve mimics that for chloride. Calculated mass flux of lithium, sodium, sulfate, chloride, boron, bromine, and fluoride indicates that the flux of these elements all decrease as the discharge of Rio Salado increases in the stream reach below Kilometer Four (see chloride flux in Figure 4(a) for example). Conservative tracer flux cannot decrease unless there is a sink, and a sink that uniformly effects arsenic, lithium, sodium, sulfate, chloride, boron, bromine, and fluoride is improbable. Hence, a systematic error in the flow measurements below Kilometer Four (Station 18) is indicated.

The Rio Salado above Station 18 is a high gradient stream with rapids and riffles contained in a bedrock channel. Below Station 18 the gradient decreases and the stream meanders through alluvial valley fill. It is reasonable that a major component of stream flow is moving through the alluvium. Under-measurement of flow can account for the flux reductions seen below Station 18. Figure 4(b) depicts the flux profiles obtained after correction of systematic underestimation of flow.

The curves in Figure 4(b) are obtained by increasing the measured discharge by 4% for each kilometer of stream reach below Station 18. The flux curves produced are more reasonable; this correction produces an increasing flux profile for chloride. The 4% value was determined by trial and error attempts to smooth the chloride flux curve. Fitting was discontinued when the chloride curve assumed a pseudo-asymptotic appearance. As such, the 4% discharge increase per kilometer determined is a minimum value. The chloride-arsenic conservative relationship, and filtered and unfiltered sample trends pointing towards colloid formation with arsenic removal, remain supported by the corrected flux presented in Figure 4(b).

The divergence of filtered arsenic from the unfiltered results may indicate some colloidal sorption of dissolved arsenic. However, total arsenic concentration decreases in Rio Salado can be attributed to dilution. Other than dilution, the flux of total arsenic in Rio Salado at baseflow is conservative, as are most other compounds.

2.2.4 Arsenic Speciation and Transformation Kinetics

The arsenic speciation in Rio Salado is dominantly inorganic as As^{5+} , with minor As^{3+} present at Stations 2, 3 and downstream of the Powerline spring. The As^{3+} point discharge into Rio Salado at Powerline spring allowed determination of As^{3+}

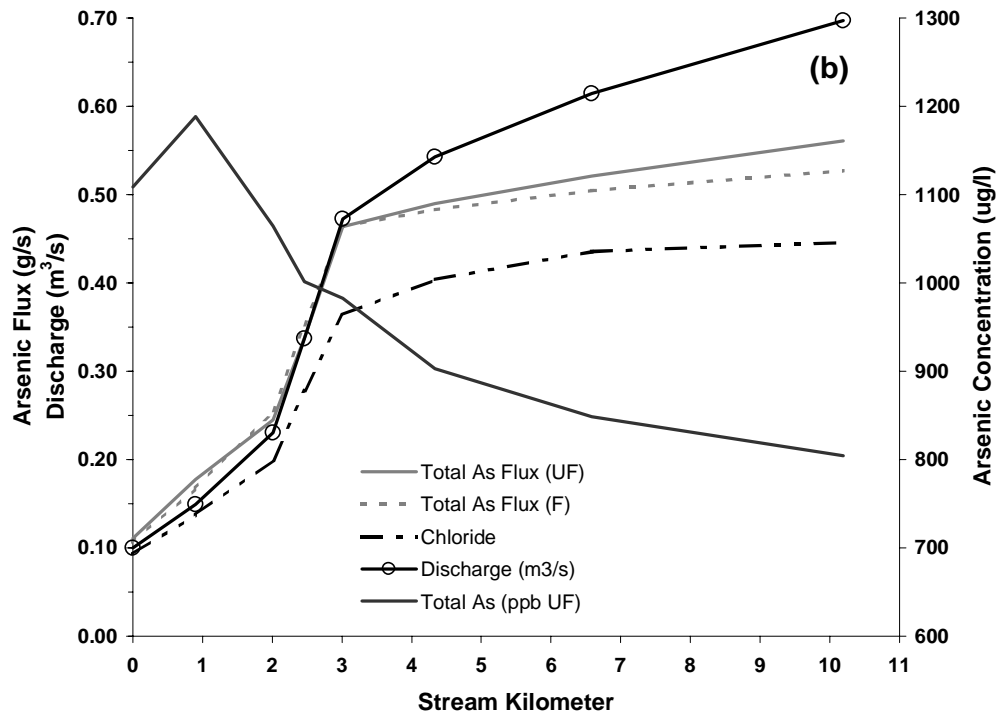
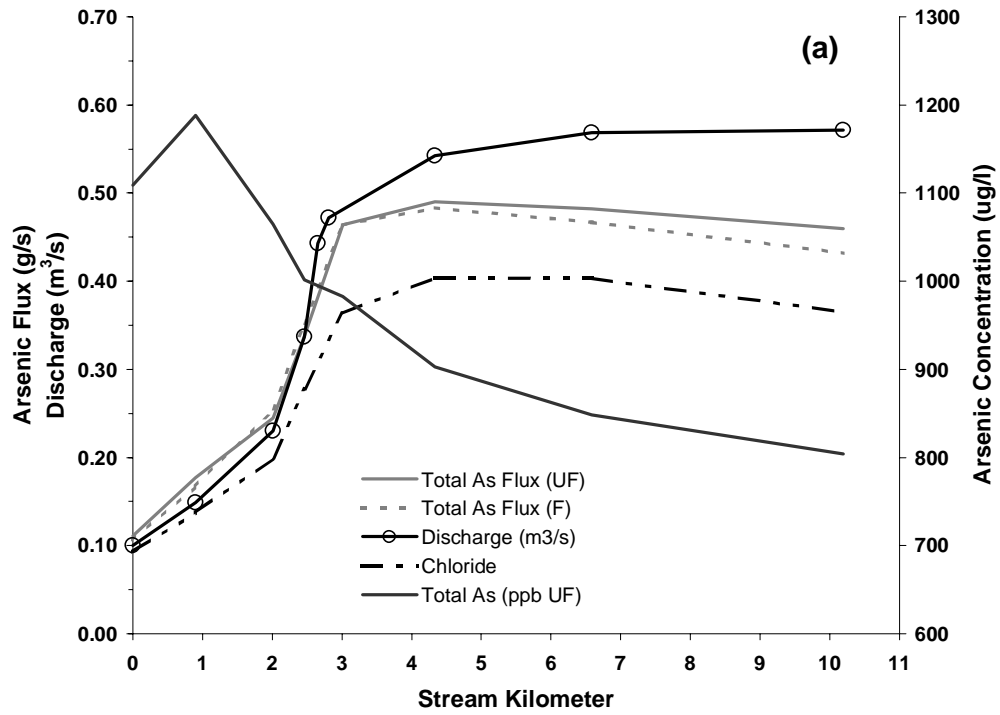


Figure 4. Rio Salado discharge and chemical flux for chloride and filtered (F) and unfiltered (UF) total arsenic. Figure 4(a) uses measured discharge values. Figure 4(b) increments measured flows downstream of Kilometer Four by +4% per kilometer.

transformation rates (Figure 5). Critical for the calculation is knowledge of stream velocities.

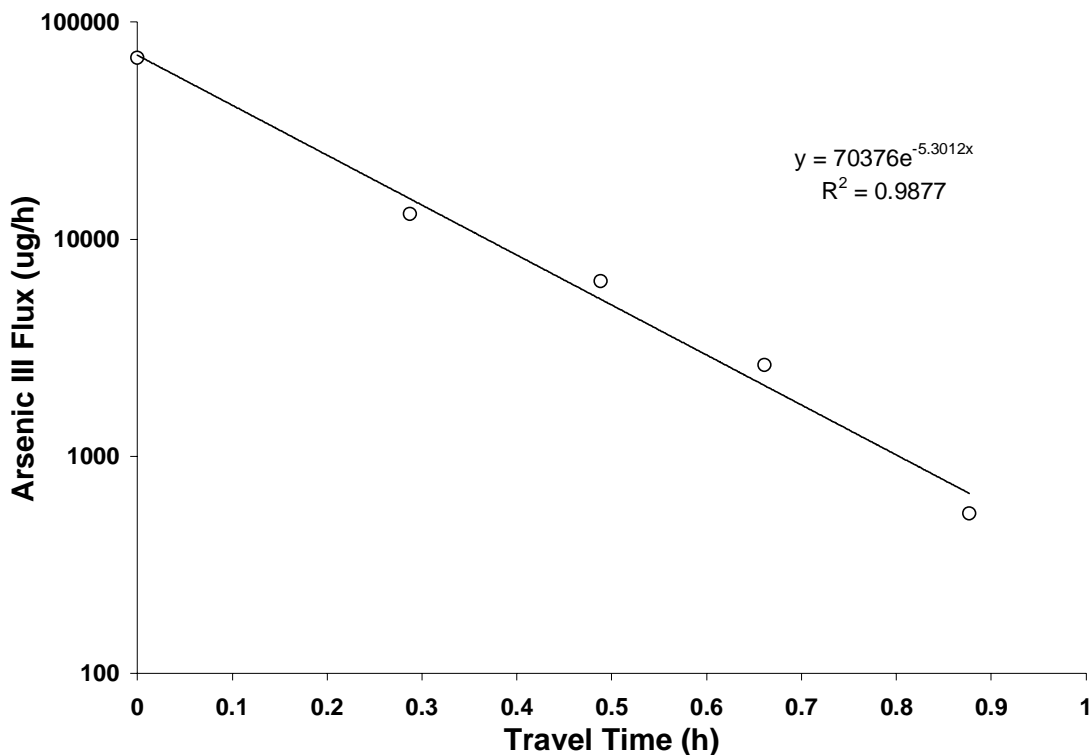


Figure 5. As^{3+} disappearance in Rio Salado downstream of the Powerline spring.

There is good agreement between dye average peak velocity and salt average peak velocity with the dye faster by 1.8%, indicating that the dye tended to behave in an ideal manner (Appendix A). Statistics indicate a modal stream velocity for locations downstream of the Powerline spring of 0.55 km/h and standard deviation of 0.092 km/h. This value is quite close to the velocity of the dye peak, hence used for the kinetics calculations. Figure 5 data indicate a pseudo-first order reaction. The straight line fit allows calculation of an As^{3+} $t_{1/2}$ of 0.13 hours. Wilkie and Hering found a $t_{1/2}$ of 0.3 hours for As^{3+} in Hot Creek, California that was attributed to biologic reductive pathways [48].

2.3 FLORIDA SITES

Arsenic-contaminated sites at Fort Walton and Tyndall Air Force Base (AFB), Florida, have arsenic-contaminated groundwater plumes discharging to open drainage ditches. The plumes result from application of arsenic trioxide (As_2O_3) as a herbicide. Fort Walton provides a sampling opportunity similar to that exploited at Rio Salado, whereby, sediment-water pairs could be collected synoptically by hand with little disturbance. Unlike the purely surface water Rio Salado or Fort Walton investigations, Tyndall samples allowed testing the model on a shallow groundwater system. Aqueous arsenic is dominantly in the As^{3+} and As^{5+} forms in roughly equal proportions. Approximately 10% of the total arsenic present occurs as organic arsenic species MMAA and DMAA at the Tyndall site. The details of the Florida field investigation are contained in Appendix B, of which portions were previously published [89]. Water and sediment analytical data are in Tables 8-13.

Table 8. Florida field parameters and alkalinity.

Station	Date	Time (CST)	Temp ($^{\circ}\text{C}$)	Conductivity ($\mu\text{S}/\text{cm}$)	pH	ORP (mV)	CO_3^{2-} (ppm)	HCO_3^- (ppm)
T-1	1/8/00	1401	15.6	97	5.07	103	0	10.1
T-2	1/8/00	1050	15.5	111	4.85	128	0	13.0
T-3	1/8/00	1613	15.6	60	5.00	105	0	19.1
FW-1	1/9/00	938	17.3	284	6.95	354	0	118.3
FW-2	1/9/00	1224	20.5	264	6.74	327	0	127.2

Table 9. Florida anions in water.

Station	Cl ppm	SO_4 ppm	F ppm	NO_3 ppm	PO_4 ppm
T-1	19.9	43.8	0.28	0.95	100
T-2	16.9	13.5	0.26	0.81	50
T-3	8.6	13.4	0	0.44	100
FW-1	14.8	5.1	0	0.92	225
FW-2	12.4	4.5	0	1.39	350

Table 10. Florida arsenic concentration in water (ppb).

Station	Total Unfiltered	Total Filtered	As III by Two Species Method	As V by Two Species Method	As III by Four Species Method	As V by Four Species Method	MMAA by Four Species Method	DMAA by Four Species Method
FW-1	10.7	9.5	4.6	5.2	6.3	7.5	0.0	0.0
FW-2	10.2	9.7	4.0	4.6	5.0	7.5	0.0	0.0
T-1	210.7	189.9	123.2	19.4	137.5	24.4	4.5	8.1
T-2	524.2	474.7	214.0	160.0	207.5	150.0	43.5	33.0
T-3	107.2	71.1	42.0	6.2	34.4	15.0	4.5	8.7

Table 11. Florida arsenic species as percentage of total filtered arsenic concentration in water and method recovery as compared to the total (ppb).

Station	As III by Two Species Method	As V by Two Species Method	Two Species Method % Recovery	As III by Four Species Method	As V by Four Species Method	MMAA by Four Species Method	DMAA by Four Species Method	Four Species Method % Recovery
FW-1	48%	55%	103%	66%	66%	0%	0%	131%
FW-2	41%	47%	89%	52%	52%	0%	0%	103%
T-1	65%	10%	75%	72%	72%	2%	4%	151%
T-2	45%	34%	79%	44%	44%	9%	7%	104%
T-3	59%	9%	68%	48%	48%	6%	12%	115%
Average FW	45%	51%	96%	59%	59%	0%	0%	117%
Average Tyndall	50%	31%	81%	50%	50%	5%	6%	112%

37

Table 12. Florida unfiltered water samples, major elements.

Station	Ag (ppb)	Al	Ba (ppb)	Ca	Cd (ppb)	Co (ppb)	Cr (ppb)	Cu (ppb)	Fe (ppb)	K	Mg	Mn (ppb)	Mo (ppb)	Na	Ni (ppb)	Pb (ppb)	Sb (ppb)	Si (ppb)	Sr (ppb)	V (ppb)	Zn (ppb)
FW-1	0.06	1.27	82	34.6	0.02	0.6	0.8	11.5	68.0	9.3	1.98	6.7	3.9	21	2	ND	7.9	799	311	2.8	39
FW-2	0.04	1.43	125	34	0.04	0.1	0.7	6.6	27.0	10	1.50	5.2	2.6	18	1.9	ND	3.6	2272	420	ND	30
T-1	0.13	3.66	ND	7.5	0.23	0.4	0.5	8.9	11.1	1.8	3.03	2.1	ND	6	1.5	1.1	0.9	1605	11	5.7	13
T-2	0.22	1.98	ND	8.5	0.19	0.8	1.2	12.6	26.0	1	1.74	2.0	ND	10	3	3.7	2.2	3299	20	ND	26
T-3	0.24	2.32	ND	7.8	0.03	0.2	1	5.3	36.0	2.1	1.26	3.4	ND	4	4	2.5	2.7	2197	72	ND	20

Table 13. Florida filtered water samples (0.45 µm), major elements.

Station	Ag (ppb)	Al	Ba (ppb)	Ca	Cd (ppb)	Co (ppb)	Cr (ppb)	Cu (ppb)	Fe (ppb)	K	Mg	Mn (ppb)	Mo (ppb)	Na	Ni (ppb)	Pb (ppb)	Sb (ppb)	Si (ppb)	Sr (ppb)	V (ppb)	Zn (ppb)
FW-1	ND	1.95	68	34	0.02	0	0.7	1.9	23.0	8	1.99	12.0	2.7	21	0.7	ND	6.9	801	304	ND	124
FW-2	ND	1.98	110	34	0.02	0	0.9	3.3	23.0	8.1	1.52	9.6	1.6	18	1.2	ND	6.8	1849	372	2.5	93
T-1	ND	2.44	ND	7.3	0.04	0.2	0.5	3.7	2.1	0.5	2.40	2.3	ND	6	0.5	0.7	3	646	17	ND	12
T-2	ND	2.55	ND	7.9	ND	0.2	0.9	7.4	21.0	1.2	1.71	15.7	ND	13	0.4	2.7	ND	1542	17	ND	30
T-3	ND	2.57	ND	4.1	ND	0.3	ND	4.5	1.0	2.1	0.81	2.0	ND	6	0	1.1	ND	1001	44	ND	20

2.3.1 Tyndall Air Force Base

Studies of arsenic in groundwater and soil related to herbicide treatment of a site on Tyndall AFB were conducted by the Air Force. It was determined by previous workers that a portion of the arsenic-contaminated groundwater discharged to a drainage swale located ~450 ft from the site. Sediment-water pairs were collected ~1 m below the ditch bottom, in the shallow groundwater system up-flow zone. The groundwater discharge was pronounced and estimated at 1-2 L/min-m² of ditch surface area. The sediments present in the Tyndall ditch are typical of the regional shallow aquifer materials. They consist of fine-grained quartz sand with a small percentage of heavy minerals, clays, and organic debris. The following assumptions form the conceptual model.

1. The sediment-water system in the ditch was at steady state with respect to discharge, chemical flux, and chemical equilibria.
2. Arsenic Redox disequilibrium effects on total sorbed arsenic are small.
3. The sediment-water system is well mixed in the groundwater discharge zone.
4. The source of arsenic in the system is constant on the time scale of the sampling event in both flux and concentration, as are other compounds.
5. Although there is ~10% organic arsenic, and organic solid phases that sorb arsenic, arsenic attenuation in the Tyndall ditch is dominantly an inorganic process and can be modeled as such.
6. Sediments are quartz sand with hydrous metal-oxide grain coatings.
7. Arsenic sorption on the Tyndall ditch sediments can be modeled in a representative manner using the same methodology as was employed for Rio Salado.

2.3.2 Fort Walton

The Fort Walton samples were taken from an urban drainage ditch that receives inflow from arsenic-contaminated groundwater. The sediments are fine to medium quartz sand with a small percentage of heavy minerals, clays, and organic debris. Oxidized iron staining was noticed on the sediments. The sediments at Fort Walton differ from Tyndall AFB mainly by coarser grain size. Fort Walton samples were taken as stream water and sediment pairs, in the same manner as Rio Salado. Flow at the sample locations was approximately 0.010 m³/s. The site has greater similarity to Rio Salado than Tyndall AFB. The assumptions list for Fort Walton is the same as for Tyndall AFB with the exception that organic arsenic is assumed not to be present.

2.3.3 Water Sample Chemistry

Florida data are contained in Appendix B. There are a number of contrasts between Rio Salado and Florida that are worthy of emphasis. The Florida waters are at ambient temperatures of ~15-20 °C. The total dissolved solids are lower; the conductivity values are 100-350 μS/cm vs. >1000 μS/cm at Rio Salado. Water at the Florida sites tends to be more acidic; Tyndall AFB samples exhibit pH of 4.85 to 5.07 and Fort Walton samples 6.74 to 6.95. Total arsenic concentration is approximately 10 ppb at Fort Walton and ranged from 71 to 475 ppb at Tyndall AFB, which is substantially lower than the Rio Salado concentrations. Rio Salado waters have proportionately little As³⁺ or organic arsenic. Arsenic speciation was near an equal mix of As³⁺ and As⁵⁺ at Fort Walton and Tyndall AFB. Fort Walton had no detection for MMAA or DMAA while Tyndall AFB organic arsenic varied from 6-18% of the total.

2.3.4 Sediments

Florida sediments are different from those at Rio Salado. Florida sediments are composed almost entirely of sub-angular, fine sand-sized, quartz grains. There is some dark organic matter associated with the Tyndall sediments, and minor urban debris with the Fort Walton samples.

CHAPTER 3 METHODS

3.1 MODELING APPROACH

I simulated equilibrium inorganic arsenic SC reactions with hydrous metal oxides and competition for oxide sorption sites on those oxides by ions other than arsenic. The SC simulations use a multi-component thermodynamic geochemical modeling code, PHREEQC. This work is confined to the use of the DLM mathematical formulation as contained in PHREEQC. The approach assumes that the dominant anions competing for sorption sites with arsenic are silicic acid, phosphate, carbonate, bicarbonate, sulfate, borate, and fluoride. The sorption of the common cations calcium, strontium, barium, zinc, magnesium, and manganese is included in the simulations. Complementary to the equilibrium assumptions used, new solid phases are not allowed to precipitate or dissolve. I assume that the abundance of hydrous metal-oxide sorbing surfaces can be determined by operationally defined chemical extractions of sediments. Published data are used for SC input parameters [20, 26, 102, 103, 135].

The major simplifying assumption for the modeling is that the system is at a steady state and equilibrium condition. The primary factors controlling arsenic partitioning via SC under these assumptions are the surface available for sorption, pH, and competing ions. The organic arsenic speciation distribution, kinetically limited reactions, sorption by organic matter, and biotransformation are assumed to be secondary

effects. Model Redox conditions were not used to simulate or fix observed $\text{As}^{3+}/\text{As}^{5+}$ ratios. Arsenic kinetic constraints are not used because they are not well known and have poorly defined mechanisms and reactions [52, 77, 78, 134].

The above assumptions are not valid for all systems, but may apply to many. The test of transferability of laboratory surface complexation approaches to the field is assumed to be limited to the primary factors. There are some known problems with this approach (i.e. known presence of organic arsenic and organic carbon solid-phase sorption phenomena) but it is too difficult and impractical to attempt the simulation of all facets of the system, all at once, for all variables. The Florida sites were sampled to evaluate arsenic partitioning using SC in a geochemical setting different from Rio Salado, using the approach developed with the Rio Salado samples.

Published physical and chemical SC parameters are available. These include arsenate and arsenite on hydrous metal oxides. Analytical determinations of metal concentration on the sediment grain surfaces are used to define the distribution of hydrous metal oxide surfaces. PHREEQC is used to bring the observed water chemistry to thermodynamic equilibrium with the sediments. In the manner described above, the ability to mechanistically model arsenic sorption is tested. Additional details of model construction are contained in following sections.

The general two-layer model (DLM) was selected for use over the TLM model because of the large number of publications that cite the approach of Dzombak and Morel, the relatively low number of fitting parameters, and the use of the Dzombak and Morel generalized two-layer model [20] in the PHREEQC code.

Mass-action relationships are quantified by several equilibrium constants, or ‘K’. Constants for specific sorbing ions on specific minerals are referred to as “intrinsic constants” or K_{int} . Lewis acids and bases will have more than one K_{int} . The K_{S^-} and K_{S^+} constants allow the surface-sorbing properties to change with changing pH. This change in charge occurs because of the protonation and deprotonation of the oxide surface. They are determined by titration of pure mineral phases in solution. K_{int}^1 , K_{int}^2 and K_{int}^3 provide sorption of ions at different levels of protonation associated with the ion’s pK_a for strong and weak sites. K_{a1} , K_{a2} , and K_{a3} are K_{int} that are associated with the single-site goethite and gibbsite models. The K values used in the simulations are presented in Tables 14-16.

Dzomback and Morel’s DLM uses a mix of a small number of strong high affinity sites with a large number of weaker sites with different K_{int} to fit divalent cation data. K_{strong} and K_{weak} are K_{int} that are associated with only strong or weak sites. The different sorbing properties of cation hydroxide complexes are accounted for by additional K_{weak} mass-action relationships. The DLM strong site density for ferrihydrite is set at 0.005 mol/mol Fe, the weak site density at 0.2 mol/mol Fe, and the surface area as 600 m^2/g [20]. The use of two sites is not required to fit anion data, such as arsenate and arsenite, but model bookkeeping requires that the strong and weak site definition be carried through all ferrihydrite sorption.

For goethite and gibbsite, only one sorbing site is specified in the model. This is consistent with the K_{int} for arsenic found in Manning and Goldberg [26]. Surface complexation models have been found to be insensitive to site density when the ratio of

Table 14. Surface complexation mass-action coefficients for ferrihydrite surfaces and the generalized two-layer model.

Complex	log K _{strong}	log K _{weak}	log K _{weak}	Source
K _{S+}	7.29	7.29		Dzomback and Morel, 1990
K _{S-}	-8.93	-8.93		Dzomback and Morel, 1990
Ca	4.97	-5.85		Dzomback and Morel, 1990
Sr	5.01	-6.58	-17.6	Dzomback and Morel, 1990
Ba	5.46	^a		Dzomback and Morel, 1990
Mg	^a	-4.6		Dzomback and Morel, 1990
Mn	-0.4	-3.5		Dzomback and Morel, 1990
	log K _{int} ¹	log K _{int} ²	log K _{int} ³	
AsO ₄ ³⁻ strong & weak	29.31	23.51	10.58	Dzomback and Morel, 1990
H ₃ AsO ₃ strong& weak	5.41			Dzomback and Morel, 1990
H ₃ BO ₃ strong & weak	0.62			Dzomback and Morel, 1990
SO ₄ ⁻ strong & weak	7.78	0.79		Dzomback and Morel, 1990
F ⁻ strong & weak	8.7	1.6		Dzomback and Morel, 1990
H ₄ SiO ₄ strong & weak		4.4	-4.5	Meng and Letterman, 1996, Refit of TLM
SiO ₃ ²⁻ strong & weak	28.4	15.9	8.3	Dzomback and Morel, 1990 ^c
H ₄ SiO ₄ strong & weak	4.28	-3.22	-11.69	Swedlund and Webster, 1999 ^c
CO ₃ ²⁻ strong & weak	13.5	6.25		LFER ^b

^a LFER were not derived in Dzomback and Morel (1990).

^b LFER estimates of K_{int} made using graphics from Dzomback and Morel (1990) and pKa's from Van Geen et al. (1994).

^c Used for sensitivity analysis

Table 15. Surface complexation mass-action coefficients used for goethite surfaces and the generalized two-layer model.

Complex	log Ka ₁	log Ka ₂	log Ka ₃	Source
K _{S+}	7.52			Manning and Goldberg, 1996
K _{S-}	-10.6			Manning and Goldberg, 1996
Ca	-5.85			Dzomback and Morel, 1990
Sr	-6.58			Dzomback and Morel, 1990
Ba	-7.2			Dzomback and Morel, 1990
Mg	-4.6			Dzomback and Morel, 1990
Mn	-3.5			Dzomback and Morel, 1990
	log Ka ₁	log Ka ₂	log Ka ₃	
AsO ₄ ³⁻	9.1	0.0 ^c	10.58	Manning and Goldberg, 1996, Refit from CC ^a
H ₃ AsO ₃	5.41			Dzomback and Morel, 1990
H ₃ BO ₃	0.62			Dzomback and Morel, 1990
SO ₄ ⁻	7.78	0.79		Dzomback and Morel, 1990
F ⁻	8.7	1.6		Dzomback and Morel, 1990
H ₄ SiO ₄	4.48	-3.43		Goldberg, 1985 ^d
CO ₃ ²⁻	20.78	12.71		Van Geen et al., 1994

^a Manning and Goldberg data refitted to DLM using FITEQL.

^b LFER estimates of K_{int} made using graphics from Dzomback and Morel (1990) and pKa's from Van Geen et al. (1994).

^c Fitting insensitive to the value of this parameter and FITEQL fails to converge if not fixed, set to 0.0.

^d Constant capacitance parameters for goethite, refitting not possible due to lack of ionic strength data.

Table 16. Surface complexation mass-action coefficients used for gibbsite surfaces and the generalized two-layer model.

Complex	log K_{a1}	log K_{a2}	log K_{a3}	Source
K_{S+}	9.1			Manning and Goldberg, 1996
K_{S-}	-10.5			Manning and Goldberg, 1996
Ca	-5.85			Dzomback and Morel, 1990 ^a
Sr	-6.58			Dzomback and Morel, 1990 ^a
Ba	-7.2			Dzomback and Morel, 1990 ^a
Mg	-4.6			Dzomback and Morel, 1990 ^a
Mn	-3.5			Dzomback and Morel, 1990 ^a
	log K_{a1}	log K_{a2}	log K_{a3}	
AsO_4^{3-}	8.7	1.1	-5.2	Manning and Goldberg, 1996 Refit from CC
H_3AsO_3	5.41			Dzomback and Morel, 1990 ^a
H_3BO_3	0.62			Dzomback and Morel, 1990 ^a
SO_4^-	7.78	0.79		Dzomback and Morel, 1990 ^a
F ⁻	8.7	1.6		Dzomback and Morel, 1990 ^a
H_4SiO_4	4.48	-3.43		Goldberg, 1985 ^a
CO_3^{2-}	20.78	12.71		Van Geen et al., 1994 ^a

^a Direct substitution of ferrihydrite or goethite data from original source for gibbsite.

^b Manning and Goldberg data refitted to DLM using FITEQL.

sites to ions is high [6, 21, 38, 50,]. For consistency, Manning and Goldberg's site density of 3.84×10^{-6} mol/m² is used. Using a surface area value of 45 m²/g, a goethite site density of 0.01 mol/mol Fe is calculated for goethite. Using a gibbsite surface area of 43.7 m²/g, I calculated a site density of 0.009 mol/mol Al.

The two-layer model was selected over the constant capacitance formulation because of the explicit charge balance option available in PHREEQC. This option uses the 1983 method of Borkovec and Westall [133] to account for the composition of the double layer. This method requires artificial charge balancing for convergence of the numerical solution. By accounting for the composition of the double layer, it is possible to model the advection of pore fluid away from the system without numerical instability in charge balancing. This is accomplished by insignificant changes in the value of chloride ion, a species enabled in PHREEQC for this purpose as a variable concentration. This is the most realistic way to handle charge balance and enhanced model convergence in the model runs. For sorption of arsenate, the sorption process is generally agreed to be

covalent bonding as inner-sphere complexes [26, 95], and the dominant bonding mechanism is bidentate-binuclear, [27, 91]. Arsenite also forms an inner sphere complex with the probable bonding being monodentate mononuclear [91].

Whenever possible, published diffuse double layer or general two layer constants (DLM) were used directly as published in the literature. The PHREEQC database contained the DLM surface complexation constants published in Dzombak and Morel [20] for hydrous ferrous oxide and a number of heavy metal ions. It was necessary to modify the supplied database for this study to be able to model the influence of common anions and cations on arsenic complexation (Appendix C). There are many more published coefficients for trace metals than there are for the common anions and cations known to compete for sorbent sites. When necessary, published data was refitted to the DLM using the FITEQL 4.0 code [99], or determined using linear free energy relationships (LFER) between the pKa and K_{int} of an oxyanion [20, 28].

In order to extend the simulation to comparison of goethite, ferrihydrite, and gibbsite conceptual models some compromises were made. Surface areas of the hydrous metal oxides and the number of sites per unit area were obtained from the source that supplied the relevant $K_{\text{S-}}$, $K_{\text{S+}}$, and K_{int} data. Where complexation data for specific ions of interest could be located only for goethite, or ferrihydrite, direct substitution of K_{int} values between these two iron phases was used.

The Dzombak and Morel (1990) general two-layer model for ferrihydrite uses two types of sorbing sites, a small number of strong sites and a much larger number of weak sites. The PHREEQC database required modification to use both these strong and weak sites. Other than the SC modifications to the WATEQ4F database supplied with

PHREEQC, no other alterations were made. Goldberg [38] correctly indicates that generalized two-layer model ligand exchange reactions do not require use of strong and weak sites, however, in order to model competition for sorbing sites accurately in the ferrihydrite system these sites were both represented consistently in the database for both anions and cations.

The silica sorption data of Meng and Letterman [102] were refitted from the triple-layer model to the two-layer model using FITEQL 4.0 [99]. These data were used in preference to the LFER derived relationships for silica of Dzomback and Morel [20] because the Meng and Letterman [102] results are experimental and were conducted in a CO₂ free atmosphere. Published data for carbonate and bicarbonate on ferrihydrite were not located. These coefficients were derived for this study using LFER's and published data.

Tables 15 and 16 present the mass-action coefficients used in simulation of goethite and gibbsite surfaces. K_{S+} , K_{S-} , and arsenic K_{int} for goethite were from Manning and Goldberg [26]. They suggest a single sorbing site for arsenic that has two states of protonation for goethite. Accordingly, the PHREEQC database was modified so that goethite simulations use a single sorbing site consistently, rather than the two sites used for ferrihydrite [20]. To test competition for sorption sites by divalent cations, and phosphate, sulfate, fluoride, and borate anions, in the goethite and gibbsite simulations, I applied Dzomback and Morel [20] ferrihydrite K_{int} values for these ions to the goethite and gibbsite mineral surfaces. Silica coefficients were applied directly from a constant capacitance model derived from experiments on goethite [103]. The carbonate-bicarbonate K's are from Van Geen et al. [135]. Other than the Manning and Goldberg

[26] coefficients for arsenate complexation with gibbsite, all gibbsite coefficients are directly substituted from goethite and/or ferrihydrite.

3.2 SELECTION OF COMPUTATIONAL MODEL

Thermodynamic models for aqueous solutions are of three main types. MINTEQA2 [115] is an example of the first type that uses Gibbs free energies and sorption parameters to calculate aqueous speciation and solid phase equilibrium. The second type, represented by PHREEQC [68], adds the capability of reaction path simulation, mixing of two waters, addition and removal of reactants, and changing temperature to the capabilities of the first type. A third type of model will handle non-equilibrium conditions, such as kinetic limitations or variable reactant flux in addition to equilibrium conditions. A public domain version of the third type of model was not located.

PHREEQC [68] is the equilibrium thermodynamic model supported by the United States Geological Survey (USGS). Details on the construction and operation of the model are found in the user's manual [68]. According to the author of the manual and code,

“PHREEQC is based on an ion-association aqueous model and has capabilities for (1) speciation and saturation-index calculations, (2) reaction-path and advective-transport calculations involving specified irreversible reactions, mixing of solutions, mineral and gas equilibria, surface-complexation reactions, and ion-exchange reactions, and (3) inverse modeling, which finds sets of mineral and gas mole transfers that account for composition differences between waters, within specified compositional uncertainties.”

The WATEQ4F database supplied with PHREEQC was modified to support the SC approach (Appendix C).

3.3 INPUT DATA SETS

The PHREEQC input data sets contain solution chemistry, a hydrous metal oxide surface representation, and instructions on how to make the two interact. Portions of the SC data are contained in the input data sets and the remainder in the thermodynamic database used by PHREEQC. The water analyses presented in Appendixes A and B were used for the simulations. Input data sets and raw data are contained in Appendix C.

The Florida simulations required a modification of input data to promote numerical stability. PHREEQC cannot hold pH or Eh fixed during transport simulations involving SC. This is because these variables are not explicitly accounted for in the iterative numerical solution of the SC equations. From the Eh-pH overlay depicted in Figure 6 (modified from Sadiq, [24]) it can be seen that the Tyndall (T) samples lie in the As^{3+} stability field while the Fort Walton (FW) and Rio Salado (RS) samples lie predominantly in the oxidized As^{5+} field. In the case of the Florida simulations, the concentration of nitrate (NO_3^-) is high enough (~1 ppm) to numerically ‘oxidize’ all of the As^{3+} at simulated equilibrium and cause Eh numerical runaway. This is because the As^{3+} , As^{5+} , or NO_3^- was not in Redox equilibrium. I omitted nitrate from the Florida simulations to gain numerical stability. I did not use the alternative of balancing unknown, but plausible, Redox reactions by adding species that were not quantified.

Dzomback and Morel ferrihydrite K_{int} values for phosphate, sulfate, fluoride, and borate were used as substitutes with the goethite and gibbsite mineral surfaces in order to allow and test competition in the goethite and gibbsite simulations. This was done because DLM K_{int} are not available for all combinations of ions and minerals modeled.

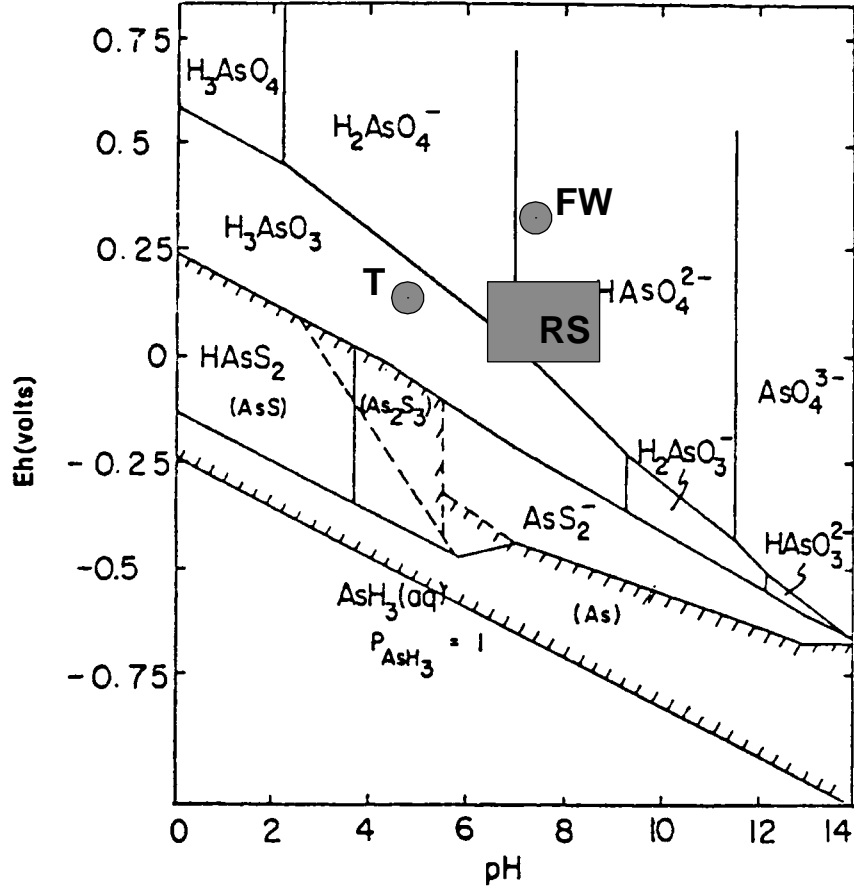


Figure 6. Eh-pH plot for the As-H₂O-S system from Sadiq (1997), with observations from the Florida (T and FW) and Rio Salado (RS) field sites.

3.3.1 Rio Salado Surface Chemistry

The molar mass of hydrous metal oxide phase per kilogram of sediments was calculated from sediment iron and aluminum extract values. Rather than *a priori* selection of a single extraction method as representative, Welch [106] evaluated several extraction methods by correlations between iron, manganese, TOC, and operationally defined arsenic extraction and quantification schemes. I compare the ability of those different extraction methods to support the simulation of arsenic partitioning in Rio Salado. The sediment extract data used for iron and aluminum surface concentrations

was derived from whole sediment extracts using hot nitric acid (HNO_3 'Whole'); -80 mesh homogenized sediment extracts using hot nitric acid (HNO_3 'Fine'); -80 mesh homogenized sediment extracts using hydroxylamine hydrochloride (Chao Reagent); and, -80 mesh homogenized sediment extracts using phosphoric acid (H_3PO_4) [106]. The HNO_3 'Whole' and H_3PO_4 extractions did not have aluminum determined, therefore aluminum extract values from respective HNO_3 'Fine' and Chao Reagent extractions were substituted. This provided four input data sets for each sample station, with surface combinations of iron and aluminum as ferrihydrite, ferrihydrite + gibbsite, goethite, and goethite + gibbsite. This resulted in 16 combinations of different extraction methods and SC assemblages for each sample station water chemistry determination, or 320 sorbing surface - water chemistry input data sets for modeling. Calculated surface concentrations of hydrous metal oxides are contained in Appendix A (Tables A-26 through A-29).

3.3.2 Florida Surface Chemistry

The molar mass of hydrous metal oxide phase per kilogram of sediments was calculated from sediment iron and aluminum extract values. The sediment extract data were derived from whole sediment extracts with hot nitric acid (HNO_3) [136]; with citrate-bicarbonate-dithionate (CBD) [85]; with hydroxylamine hydrochloride (Chao Reagent) [123]; and with the Tessier method of partial extractions [122]. Whole sediment extractions using phosphoric acid (H_3PO_4) were unsuccessful on the Florida samples, probably due to readsorption of arsenic on other phases during the extraction process.

This provided four input data sets for each sample station, with surface combinations of iron and aluminum as ferrihydrite, ferrihydrite + gibbsite, goethite, and

goethite + gibbsite. This resulted in 16 combinations of different extraction methods and SC assemblages for 5 sample stations or 90 input data sets for modeling.

3.3.3 Water-Mineral Ratio

PHREEQC uses a kilogram of water as its reaction volume. This requires that a ratio between the water and sediment surface be set. A sediment porosity of 30% (close-packed sand) and a grain density of 2.5g/cm³ (volcanic glass) were assumed for Rio Salado input data. The assumed porosity and density model (30% and 2.5 g/cm³) results in 1 kg water contacting 2.33 liters of sediments (5.825 kg). The water-mineral ratio is 1 kg of water to the mass of hydrous metal oxide that is found on 5.825 kg of sediments. Gravimetric determinations of porosity and bulk density were also made on both the Florida and Rio Salado samples. Gravimetric porosity was determined by weighing 50 ml of hand-packed sediments in a graduated cylinder. Water was added to the 50 ml mark and the sample shaken to remove air bubbles and the sample reweighed. Bulk density and porosity were calculated using the equations below.

$$\text{Mean Particle Density} = \frac{\text{Mass of Solids}}{\text{Volume of Solids}} = \rho_s$$

$$\text{Dry Bulk Density} = \frac{\text{Mass of Solids}}{\text{Total Volume}} = \rho_b$$

$$\text{Porosity} = 1 - \frac{\rho_b}{\rho_s}$$

The gravimetric porosity data are used for water-rock ratio determinations in the same manner as the assumed porosity and density. Molar surface areas of the hydrous metal oxides and the number of sites per unit area were obtained from the source that

supplied the relevant K_{S-} , K_{S+} , and K_{int} data. Calculated surface concentrations of hydrous metal oxides are contained in Appendixes A and B.

The model was constrained to simulate the advection of water of the sampled composition through the sediments, a pore volume at a time, until the modeled water chemistry matched the observed water chemistry. This simulates the field condition of steady-state flow and chemical equilibrium. After several iterations of model testing four to ten pore volumes were generally found to be sufficient for model convergence for most input data sets.

3.4 SENSITIVITY ANALYSIS

There is an unknown level of error in constants obtained from the literature, and the numerical and conceptual models. It is difficult to assess the true source of error present in this analysis. It is less difficult to determine the effect of a predetermined range of error on the simulation by conducting a sensitivity analysis. Sensitivity analysis was executed by systematically changing the value of select input variables (perturbation) to determine the effect on model output. Eight parameters were varied in eight steps resulting in 128 simulations for the sensitivity analysis. Sensitivity examination of K_{int} for silica and site populations required 65 model runs.

Sensitivity analysis was done in order to answer the questions:

1. What is the quantitative variation in the model output obtained by systematic variation of the input parameters?
2. How much error in data collection is acceptable before the error propagation is noted in the model predictions?

3. What input parameters are the most sensitive, that is, when do small changes in input values cause large changes in model output?

I used the Tyndall T-1 and Rio Salado Station 12 data sets for whole-sediment nitric acid extractions represented as ferrihydrite and gibbsite. The varied parameters were pH, alkalinity, total arsenic, total silica, ferrihydrite surface, gibbsite surface, two K_{int} for arsenic, and K_{int} for silica.

3.5 COMPUTATIONAL AND DATA-PROCESSING ENVIRONMENT

All simulations were conducted on IBM clone personal computers using the Microsoft Windows 98 Second Edition™ operating system. Computational power was enhanced by over-clocking of the bus and processor and use of a minimum of 512 megabytes of error checking and correcting memory. Over-clocking requires enhanced thermal management to prevent equipment failure but can halve PHREEQC run-times as compared to factory motherboard settings. Over-clocking results in lower cost for increased computational ability as compared to conventional upgrade solutions. Intel Pentium III® 450 MHz Coppermine processors, Alpha heat sinks, and ASUS P3B-F and P3V4X motherboards were used for over-clocking.

Input and output files were formatted and manipulated using Greenleaf Software's V-Edit™ program. Pre- and post-processing mathematical and statistical operations were accomplished using Microsoft Excel™ spreadsheets. PHREEQC version 1.6 was run in batch mode using the public domain Tcl/Tk scripting language. All raw and processed data, scripts, databases, public domain software, models, and spreadsheets are contained in Appendix C.

3.6 MODEL OUTPUT AND POST-PROCESSING

The PHREEQC output is in the form of the molal surface concentration of arsenic complexed with hydrous metal oxides. The output data sets were grouped in major categories of location, surface assemblage, and extraction method, then statistically evaluated for the combination of categories that provide the best fit. A perfect simulation of the partitioning of arsenic would reveal all samples having a ratio of unity for modeled to observed arsenic found on the sediments. I refer to this ratio of modeled to observed sediment arsenic concentration as 'R' (equation below). Figure 7 depicts a simplified modeling process flowchart.

$$R = \frac{\textit{Modeled As Concentration}}{\textit{Observed As Concentration}}$$

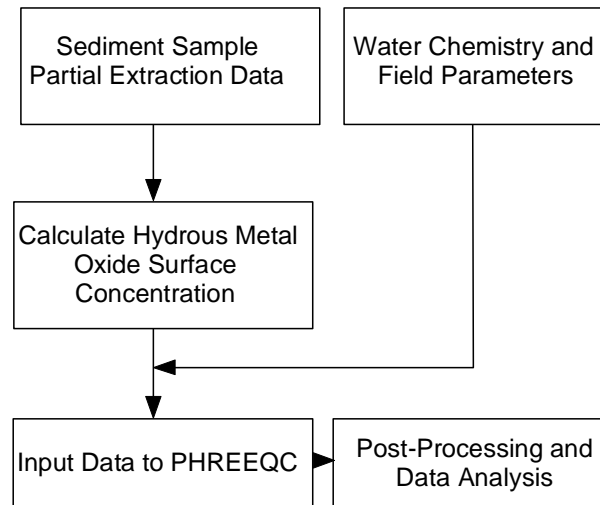


Figure 7. Data analysis and modeling process schematic.

Arsenic surface concentrations determined by extraction vary for each method used. For any given extraction, an R of unity indicates that simulation and extraction concentration are the same. Simulations with R less than unity under-predict the

observed arsenic and those with R greater than unity over-predict. It is assumed that the extraction method removes only the modeled arsenic and sorbing phases.

In order to conduct a statistical evaluation of the modeling, the median and standard deviation of R was calculated for all samples; sorted first according to location, second according to the extraction method, and third by the mineral phase(s) used to create the input data set. The median is used for comparison, rather than the mean. This was done because the median is more representative of the central tendency in skewed data and is resistant to tails and outliers. Only Gaussian distributions of R have the mean equal to the median. cursory examination of general statistics (Appendix C) revealed that most distributions of R are skewed and/or log-normally distributed.

Model output is contained in Appendix C. A 'readme.txt' file is included in the root directory of the CD that describes the file and directory nomenclature. The CD is readable using a DOS, Linux, or Windows[®] operating system.

CHAPTER 4 RESULTS

4.1 RIO SALADO

4.1.1 Median R-values

The R statistics for Rio Salado are presented in Table 17. The standard deviation divided by the median was also calculated as a measure of scatter in results. The standard deviation is used only as a rough estimator of the scatter about the median since it is truly a measure of the spread about the mean and not resistant to outliers. In cases like the HNO₃ extractions on whole sediments as ferrihydrite and ferrihydrite + gibbsite where the mean is very near the median, the data is close to normally distributed. The median is used to rank the results. The mean and standard error of R are listed for comparison purposes. Surface assemblages of ferrihydrite or ferrihydrite + gibbsite provide the best match of the amount of sorbed arsenic for Rio Salado. Goethite or goethite + gibbsite Rio Salado surface assemblages under-predict the extracted arsenic. Gibbsite complexation of arsenic was not significant as compared to the iron oxide simulations for Rio Salado. Nitric acid (HNO₃) extractions provided the best results.

Rio Salado models (Table 17) using goethite as the hydrous iron oxide phase grossly under-predict the observed arsenic concentration (R of 0.001 to 0.003) and suffer from the greatest proportional scatter in the data between sample stations (SD/Median of 811 to 1301%). Models using ferrihydrite as the hydrous iron phase, excluding the

Table 17. Results of Rio Salado simulations: Summary statistics of the ratio of modeled to observed arsenic concentration, R, on sediment.

Extraction ^a	Mineral Phase	Median ^b	SD	SD/ Median	Mean	Standard Error
H ₃ PO ₄	Goethite	0.001	0.009	900%	0.005	0.002
H ₃ PO ₄	Goethite and Gibbsite	0.001	0.011	1100%	0.006	0.002
HNO ₃ 'Whole'	Goethite	0.003	0.022	733%	0.014	0.005
HNO ₃ 'Fine'	Goethite and Gibbsite	0.003	0.031	1033%	0.016	0.007
HNO ₃ 'Whole'	Goethite and Gibbsite	0.003	0.029	997%	0.018	0.006
Chao	Goethite	0.003	0.037	1233%	0.021	0.008
HNO ₃ 'Fine'	Goethite	0.003	0.028	933%	0.018	0.006
Chao	Goethite and Gibbsite	0.003	0.042	1400%	0.023	0.009
H ₃ PO ₄	Ferrihydrite	0.245	0.222	90%	0.275	0.050
H ₃ PO ₄	Ferrihydrite and Gibbsite	0.245	0.222	91%	0.275	0.050
HNO ₃ 'Whole'	Ferrihydrite	0.737	0.366	50%	0.734	0.082
HNO ₃ 'Whole'	Ferrihydrite and Gibbsite	0.744	0.369	50%	0.743	0.082
HNO ₃ 'Fine'	Ferrihydrite and Gibbsite	0.762	0.407	53%	0.825	0.091
HNO ₃ 'Fine'	Ferrihydrite	0.779	0.402	52%	0.818	0.090
Chao	Ferrihydrite	0.881	0.615	70%	0.963	0.137
Chao	Ferrihydrite and Gibbsite	0.882	0.612	69%	0.963	0.137
Chao NoComp	Goethite	2.413	1.504	62%	2.526	0.336
Chao NoComp	Goethite and Gibbsite	3.746	2.483	66%	4.284	0.555
Chao NCCP	Goethite	4.691	2.662	57%	4.997	0.595
Chao NCCP	Goethite and Gibbsite	7.679	4.976	65%	8.682	1.113
Chao NoComp	Ferrihydrite	19.680	13.734	70%	22.122	3.071
Chao NoComp	Ferrihydrite and Gibbsite	21.546	14.880	69%	24.378	3.327
Chao NCCP	Ferrihydrite	26.720	16.943	63%	29.636	3.789
Chao NCCP	Ferrihydrite and Gibbsite	29.320	18.954	65%	33.307	4.238

^aAll extractions performed on -80 mesh ground and homogenized sediments other than HNO₃ 'Whole' conducted on homogenized <2mm sediments.

^bSample size is 20 for all statistics.

H₃PO₄ extractions, offer the best predictions with R ranging from 0.737 to 0.882. Of the operational extractions, Chao reagent yields the highest R-values, HNO₃ next, and H₃PO₄ the lowest R-values.

The HNO₃ extractions yield arsenic levels close to the maximum possible concentration as determined by XRF [106]. The best fit for HNO₃ extractions to the observations is for -80 mesh (HNO₃ 'Fine') surfaces as ferrihydrite and gibbsite with an R of 0.779. HNO₃ extractions represent arsenic complexed with amorphous and

crystalline metal oxides and organic material and offer a good fit to the total arsenic available.

Phosphoric acid extracts arsenic by phosphate ions displacing the sorbed arsenic. Phosphoric acid extractions yield best match R-values of 0.254 for ferrihydrite and gibbsite. A poor SC recombination is exhibited by this method.

The best fit to the measured extractable arsenic data is for Chao reagent with ferrihydrite and gibbsite surfaces at an R of 0.882. Chao extractions should be specific for amorphous iron and manganese phases. This indicates that the Chao extractions and simulations are internally consistent in that 88% of the amount of arsenic extracted can be simulated in a SC framework. The material operationally defined by the Chao extraction as ferrihydrite and gibbsite will accurately recombine with the extracted arsenic, but at levels lower than available arsenic as defined by the HNO_3 or H_3PO_4 extractions. The concentration of arsenic on the modeled surfaces is less than half of that extracted by H_3PO_4 or HNO_3 . The Chao extractions are thus only successful for modeling a portion of the surface available arsenic.

The absence of simulated competition results in gross over-prediction of the amount of adsorbed arsenic (Table 17). In all Rio Salado simulations, silica is preferentially sorbed over arsenic on goethite, ferrihydrite, and gibbsite and occupied more sites than arsenic. Carbonate and bicarbonate are preferentially sorbed over arsenic on gibbsite and compete with, but do not exceed, arsenic on iron oxide minerals. The role of common oxyanions in arsenic sorption is significant, as presented in detail in Section 4.1.3 and 4.3.

Table 18 shows relationships between R and other variables. Ideally, R should be independent of all variables in Table 18.

Table 18. Results of Rio Salado simulations, trends in R-value as compared to selected input parameters for Rio Salado.

Component	Trend in R	Nature of Trend^a	Figure
Distance downstream (sample station)	Yes	Inverse	
BET N ₂ surface area	Yes	Inverse	8
Total arsenic extracted from sediments	Yes	Inverse	9
TOC	Yes	Inverse	11
pH	Yes	Inverse	13
Porosity	Yes	Inverse	15
Temperature	Yes	Proportional	12
Conductivity	Yes	Proportional	14
The number of sites in the simulation	No		8
Total iron extracted from sediments	No		10
Total arsenic in water	No		
Alkalinity	No		
Bulk density	No		
Particle density	No		
Redox potential	No		

^a Inverse trends are where R-value decreases as the component value increases.

4.1.2 Trends in R as Compared to Select Input Data

Figure 8 depicts the relationship of R to the number of sorbing sites contained in the model and the Brunauer-Emmett-Teller (BET) surface area. R is not proportional to the number of sorbing sites assigned to the simulation, but there is a trend towards lower R at higher BET surface area.

Figure 9 shows R compared to the amount of sediment arsenic extracted using four methods, and for four definitions of the sorbing surface. Goethite simulations do not provide a good match with respect to R. However, the trend in R for goethite simulations is similar to ferrihydrite. The data indicate a tendency for R to decrease with extracted arsenic for samples that are -80 mesh. The HNO₃ extracts of whole sediments do not clearly show a trend. There is no relationship between R and iron extracted from the sediments, for three methods, but there is a relationship between Chao Fe and R (Figure

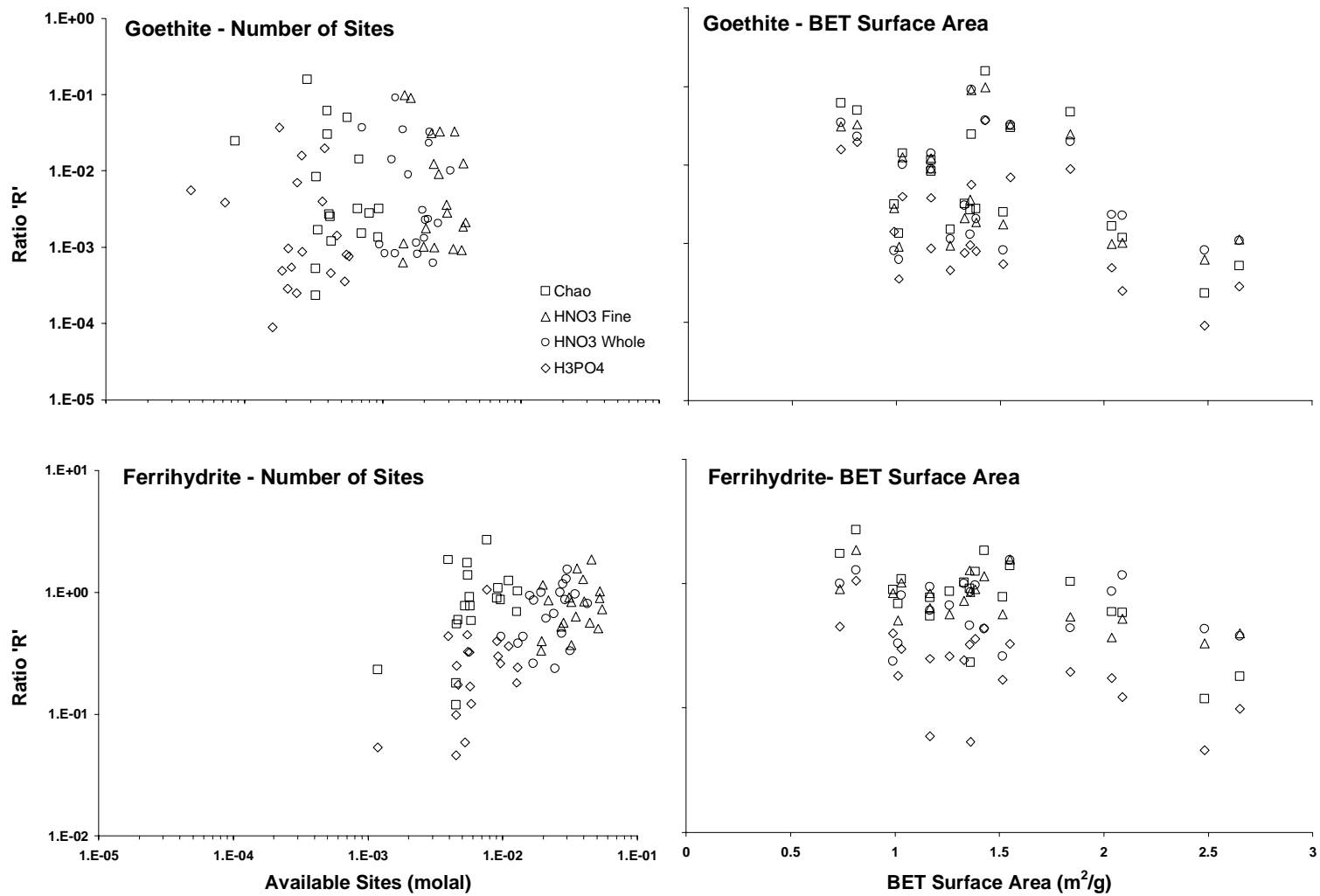


Figure 8. Relationships between BET surface area and the number of model sites available to fit factor R.

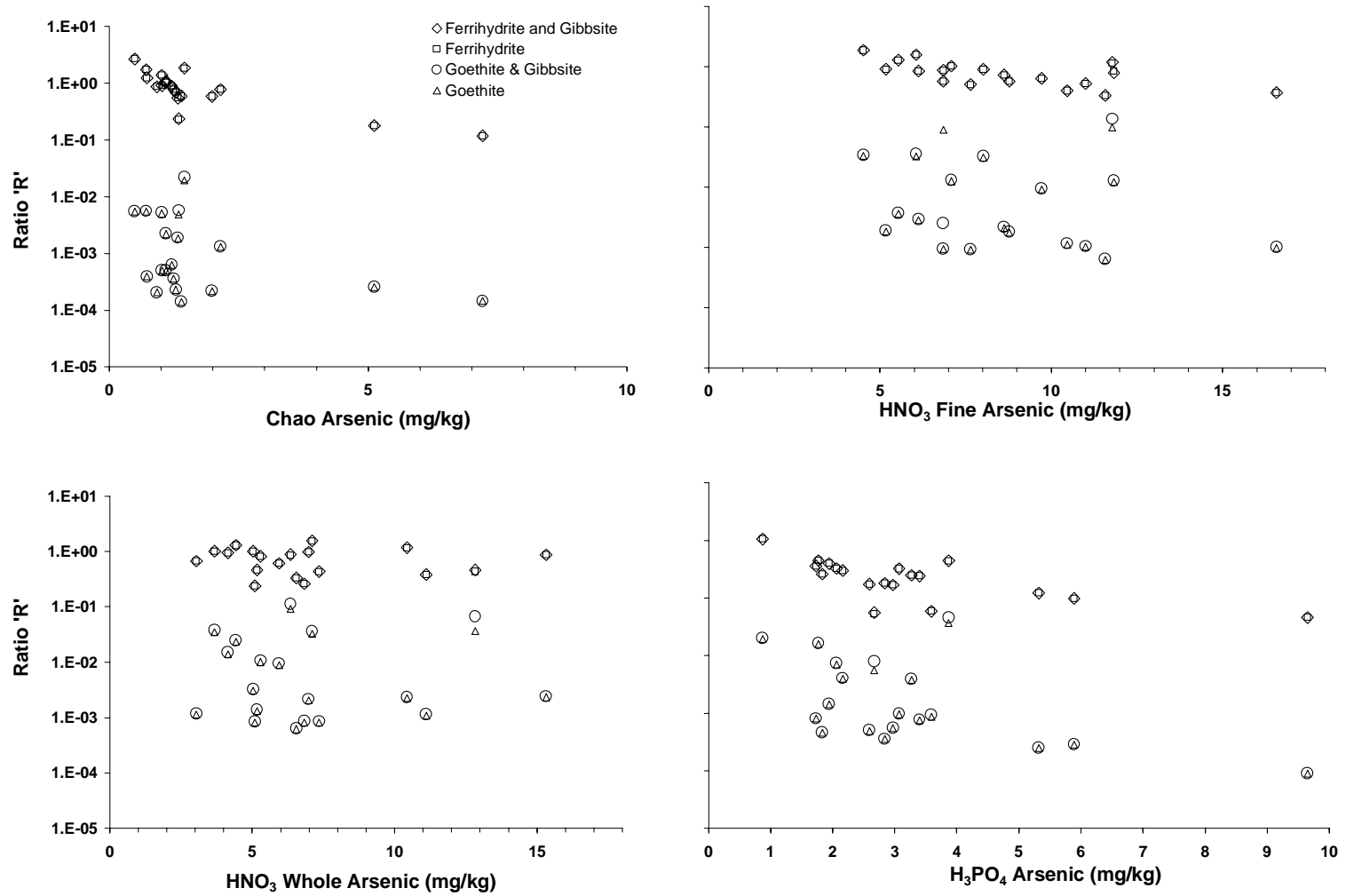


Figure 9. Trends in R as compared to arsenic extraction method and surface composition.

10). Overall, correlation of HNO₃ 'Whole' models to observed arsenic is better than that exhibited by the other three extraction methods. Figure 11 shows R compared to TOC (total organic carbon). There is a negative relationship between R and TOC content that is least evident in the HNO₃ 'Whole' simulations. The relationships between R and temperature, pH, and conductivity are presented in Figures 12, 13, and 14. There are weak correlations between these parameters and R. Temperature shows the least correlation with R. Temperature, pH, total arsenic, and conductivity relationships with R may not be attributable to a particular parameter because they together vary in a systematic and related manner. Generally, HNO₃ 'Whole' R-values show the lowest level of relationship with the variables.

In Table 17, 'NCCP' refers to simulations using constant rather than measured porosity. Using a fixed porosity resulted in over-prediction because the measured porosity was generally larger than the assumed porosity of 30%. This results in a greater amount of hydrous metal oxide present in the PHREEQC unit volume of water thus raising the modeled molal concentration of arsenic. The relationship of R to porosity (Figure 15) is for the sediments that were processed by grinding. The HNO₃ 'Whole' samples show no relationship whereas for the other extraction methods there is a weak inverse relationship of R to porosity.

4.2 THE EFFECT OF ION COMPETITION

As shown in Table 17, the effect on R-value of disallowing competition for sorption sites can be large. 'NoComp' refers to simulations where there were no ions competing for sorption sites other than arsenic, OH⁻ and H⁺. Allowing competition in the Chao extracted goethite simulations results in an R of 0.001 to 0.003. For the same input

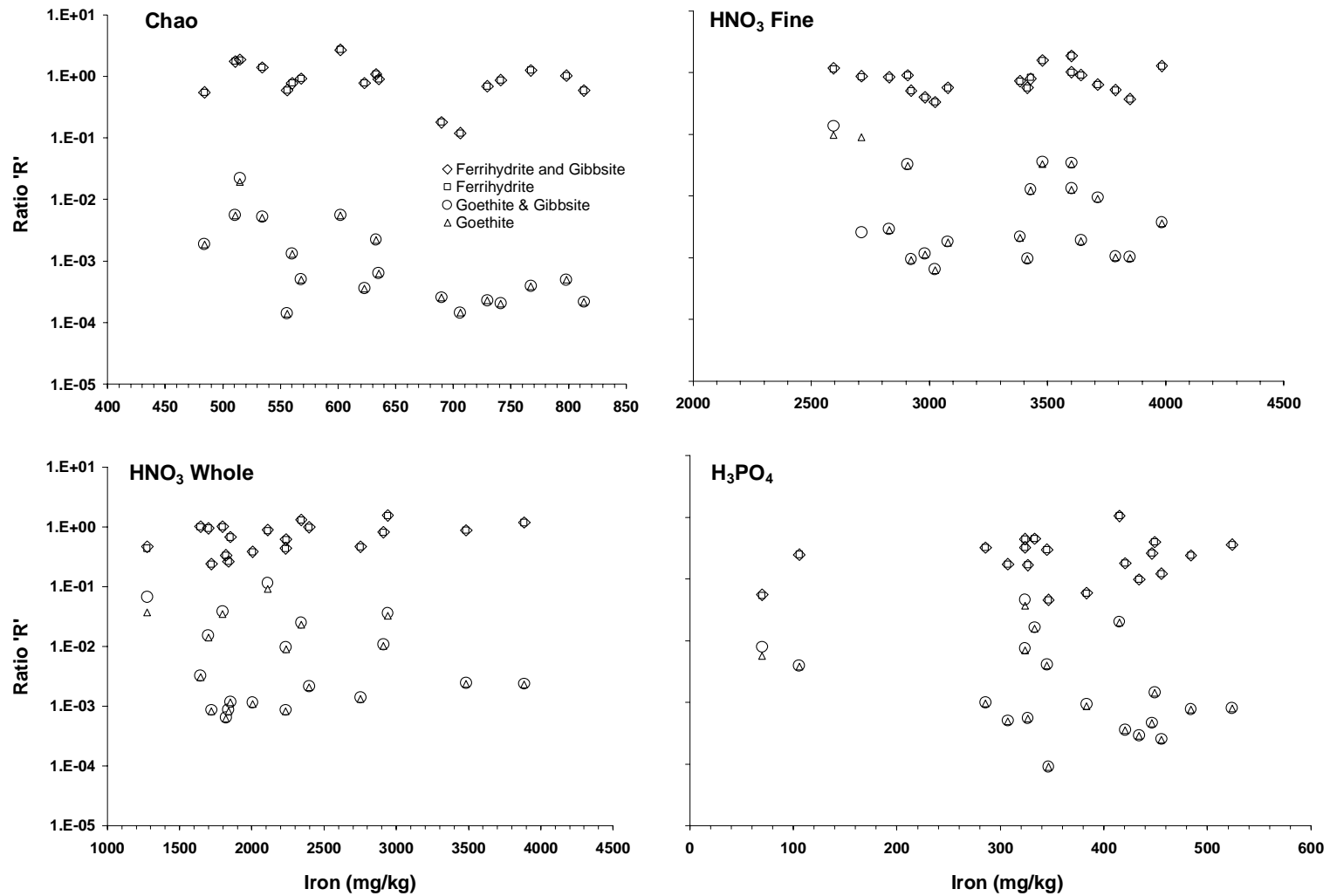


Figure 10. Trends in R as compared to iron extraction method and surface composition.

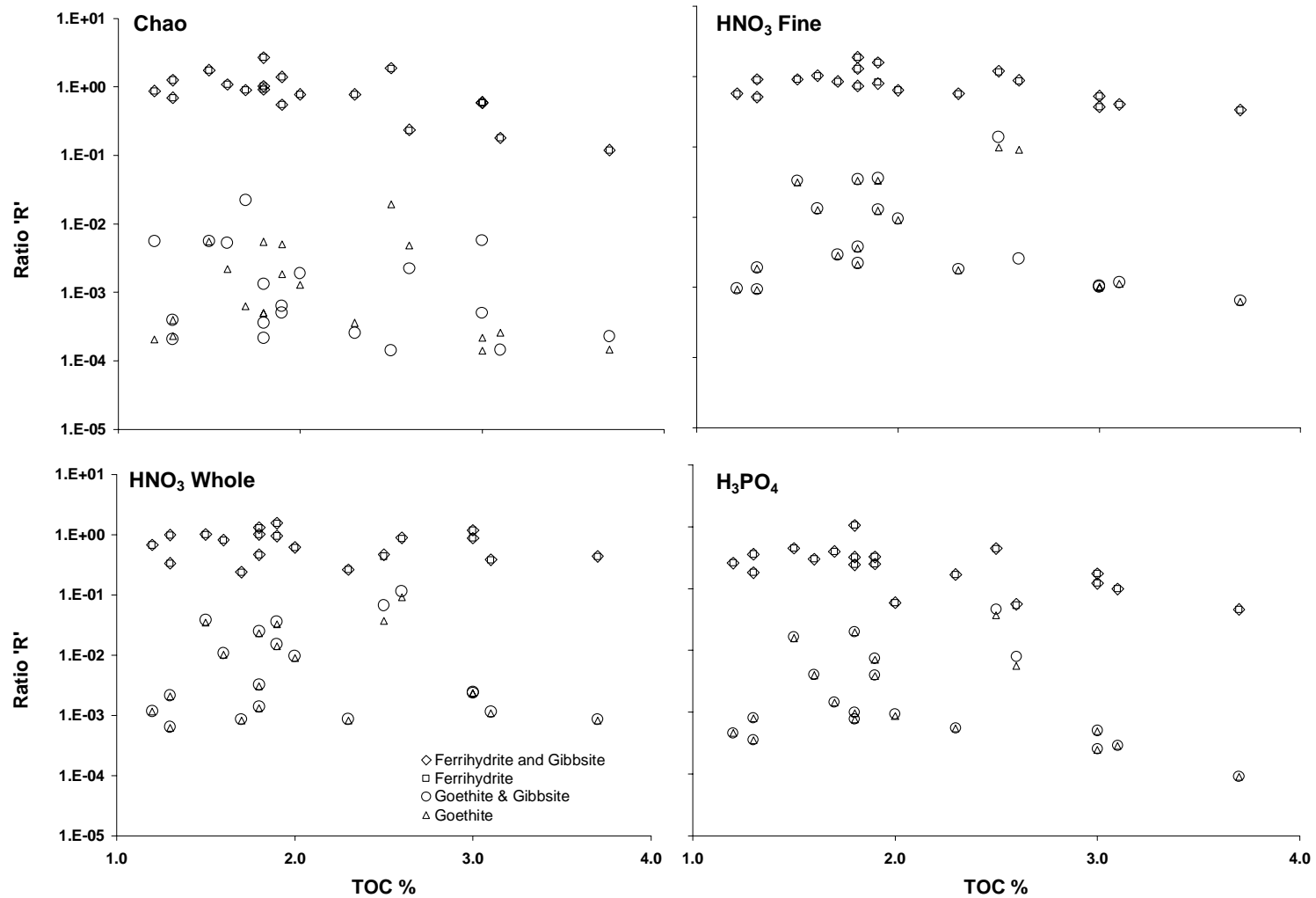


Figure 11. Trends in R as compared to total organic carbon and surface composition.

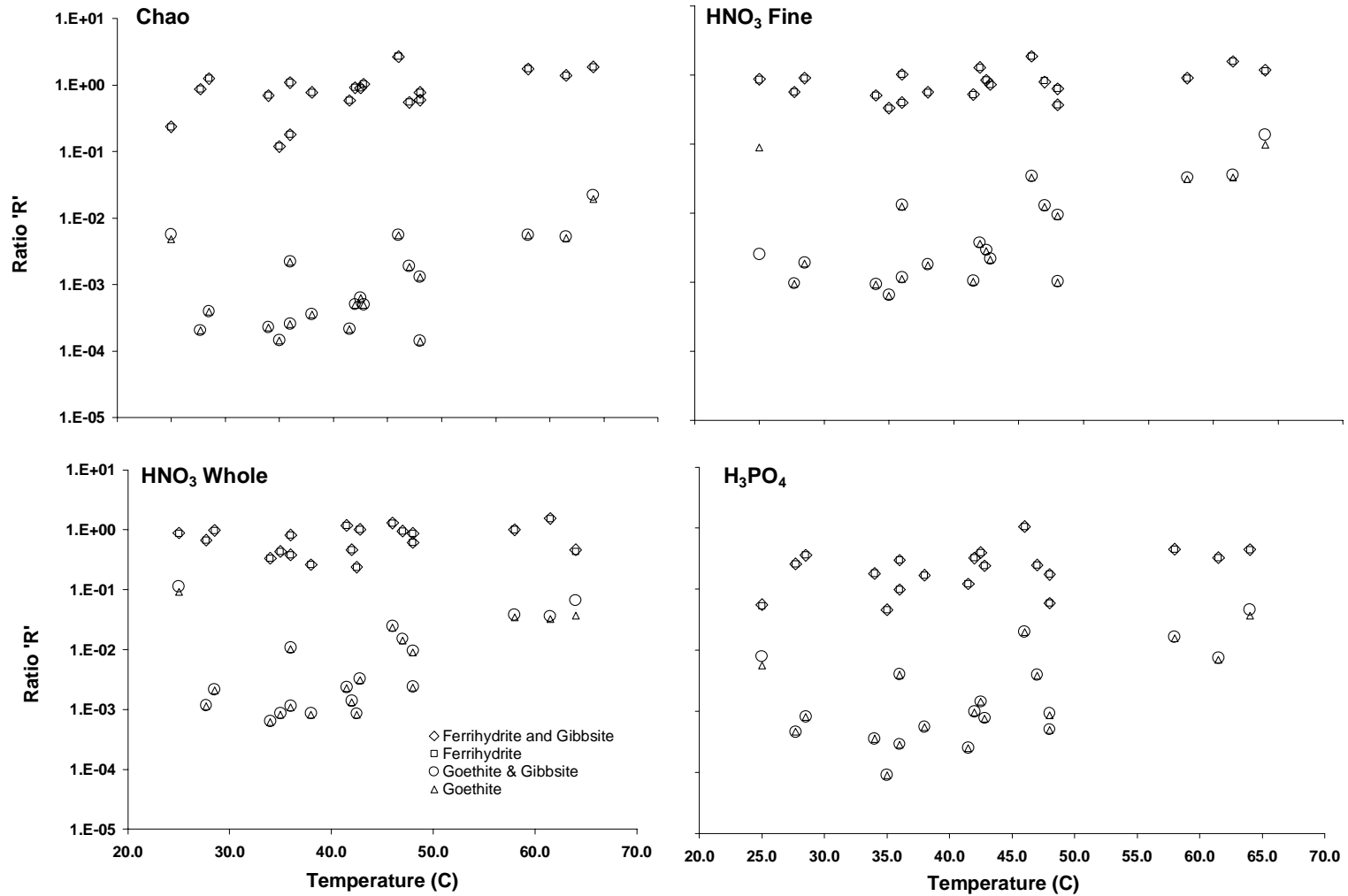


Figure 12. Trends in R as compared to water temperature and surface composition.

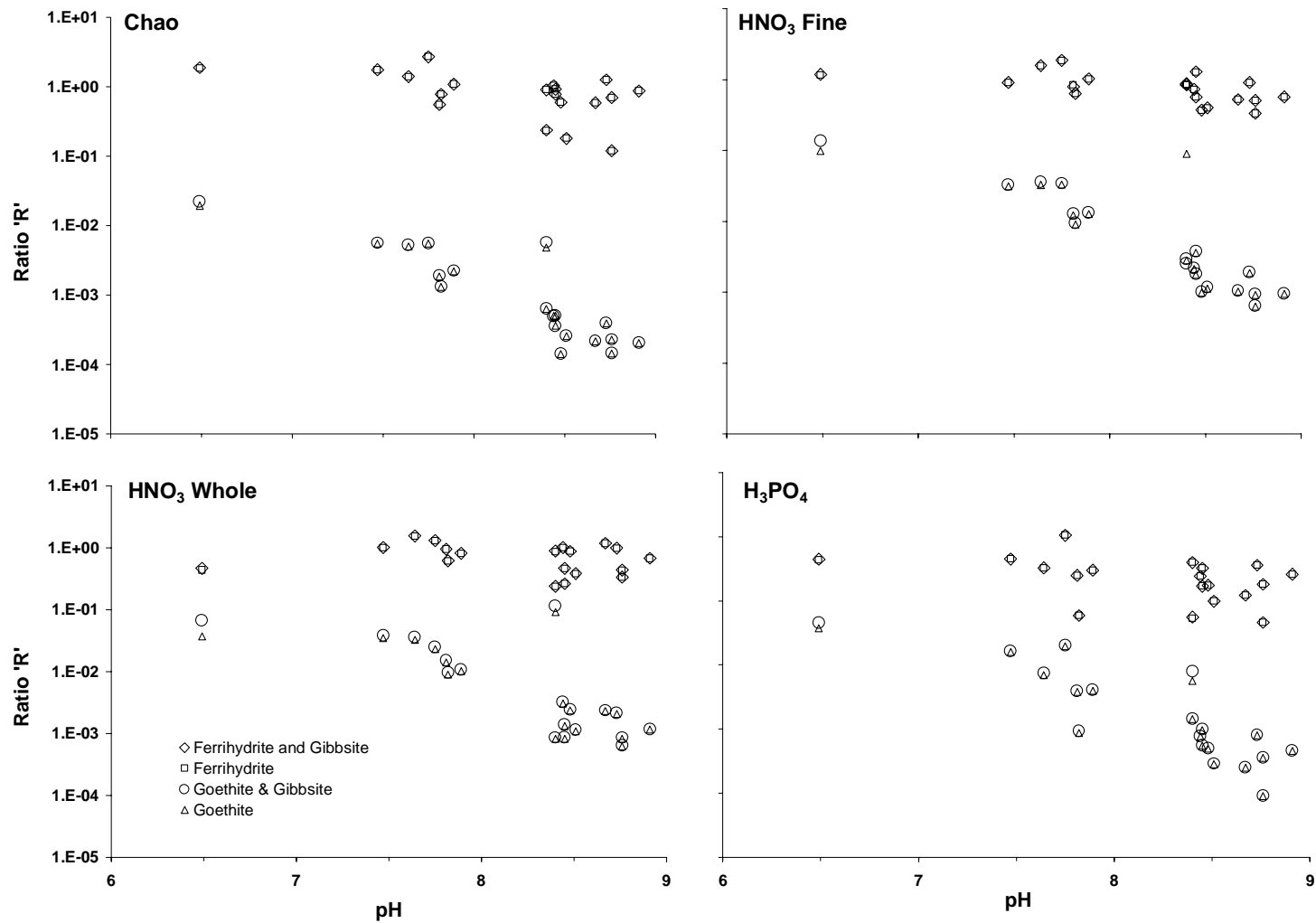


Figure 13. Trends in R as compared to pH and surface composition.

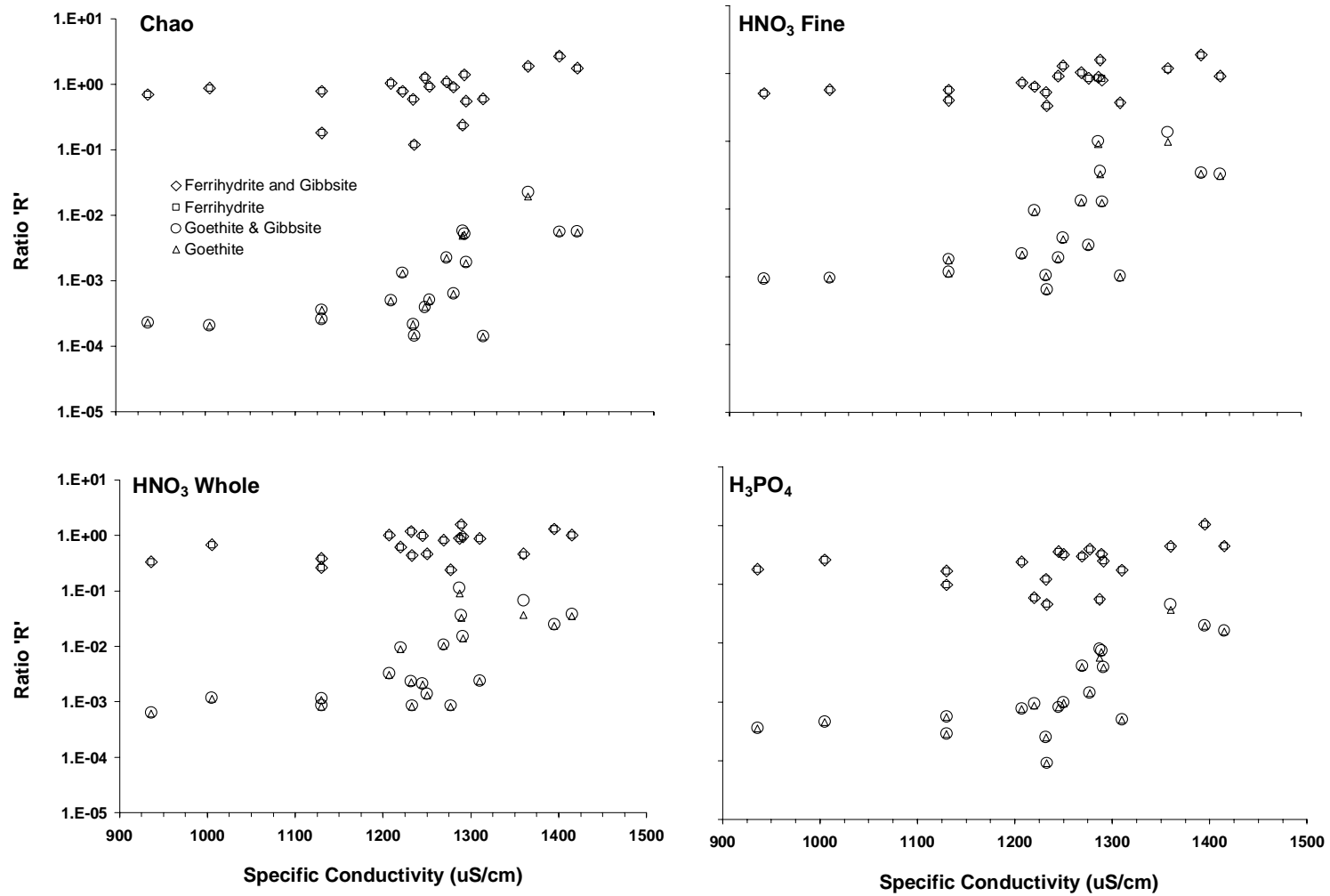


Figure 14. Trends in R as compared to conductivity and surface composition.

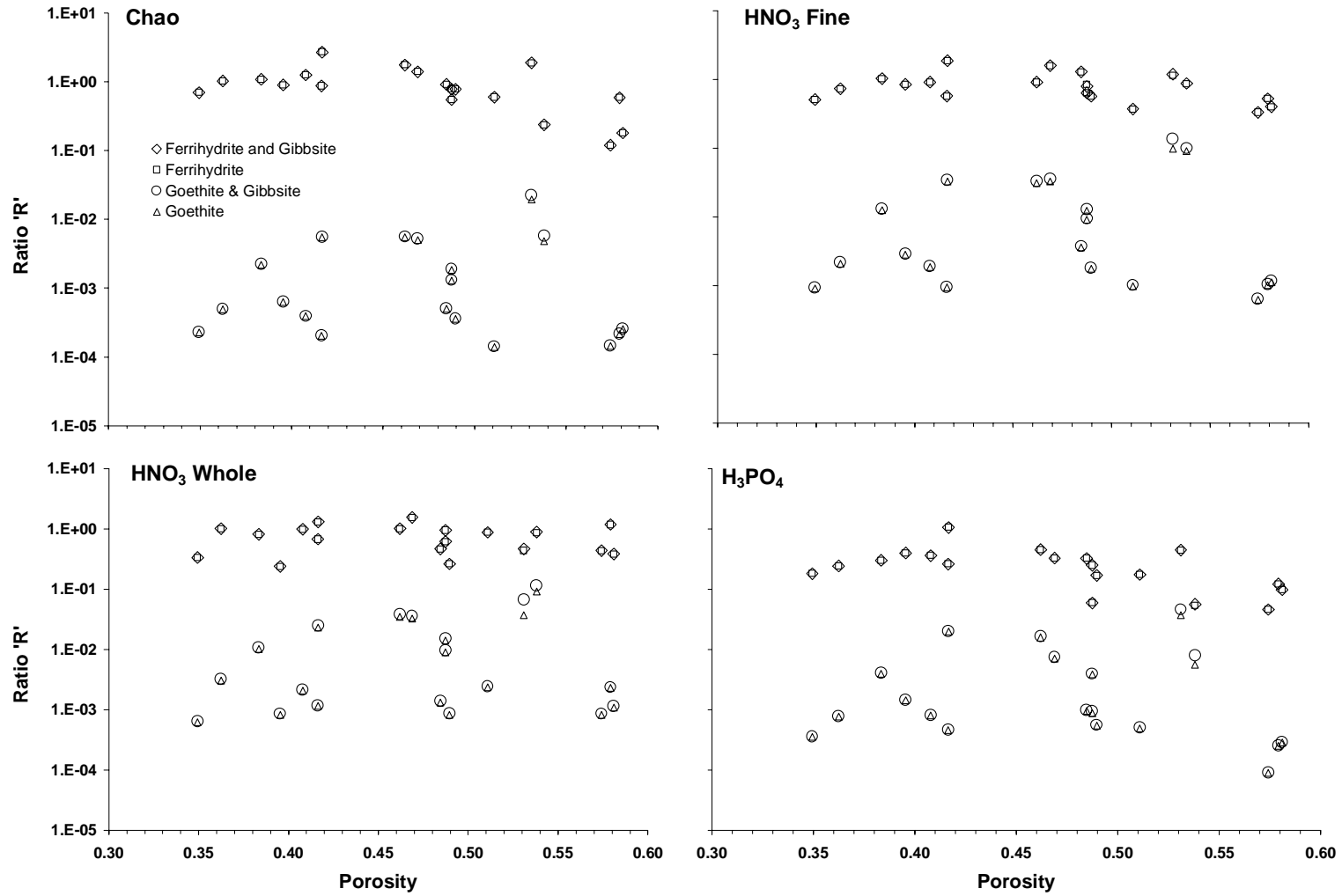


Figure 15. Trends in R as compared to porosity and surface composition.

data with competition not allowed R-values range from 2 to 4, which is change on the order of three orders of magnitude. The effect is lesser in scale but significant in magnitude for the Chao extracted simulations using ferrihydrite as the iron phase. Here, R from non-competitive models reaches 22 to 24 times the R-values obtained using SC competition. The ‘NoComp’ sensitivity analysis indicates that the competition effect on arsenic sorption in Rio Salado was significant for silica and carbonate-bicarbonate (Table 17). I used competition in all subsequent simulations, save those in Table 17, for determining R-value best-fit.

The number of sites occupied by sorbing compounds on HNO₃ ‘Whole’ extracted sediments with surfaces simulated as ferrihydrite and gibbsite are calculated (Figures 16-20). The average of surface populations for all Rio Salado stations (Figure 16-19) or Florida simulations (Figure 20) are depicted as plots of the percentage of occupied sites (bar graphs labeled ‘a’). The range of surface populations of each surface complex are presented as box-and-whisker plots. The sites without a surface complexed species are designated as OH₂⁺, OH⁻, and O⁻. The ‘Alk’ complex is the sum of sorbed carbonate and bicarbonate. Elements with multiple sorbing species are represented by a single sum. These calculations reveal that silica SC dominates the sorbing sites on Rio Salado sediments using K_{int} data from three sources [20, 50, 102]. Phosphate dominates the Florida samples (Figure 20).

The effect of predicted silica competition is related to the K_{int} value selected from the literature. The database modifications for the three sets of silica K_{int} data are included in Appendix C. The numerical values for the critical K_{int} are in Table 16. The Meng and Letterman [102] value of K_{int} for silica on ferrihydrite was derived by refitting their

titration data to the DLM using FITEQL 4.0 (Appendix C). Dzomback and Morel [20] estimated their silica K_{int} through LFER and pKa relations. Swedlund and Webster [50] determined their K_{int} from titrations in competitive sorption experiments with arsenate, arsenite, and silica. Use of the Meng and Letterman data results in simulations that reflect observed arsenic concentrations; the Dzomback and Morel silica K_{int} simulations indicate that complexed arsenic on Rio Salado sediments should be almost undetectable (Table 19). One simulation, Rio Salado Station 6, failed to converge using the Swedlund and Webster K_{int} values. Removing Station 6 from consideration yields results similar to that of the Meng and Letterman simulations, albeit with significantly reduced modeled arsenic concentrations.

Table 19. Relative site occupation by silica and arsenic under varied K_{int} for silica.

	Si Sites (molal)	As Sites (molal)	As Ratio to Meng	Si Ratio to Meng
Silica K_{int} Meng Model	0.0283	1.70E-04	1	1
Silica K_{int} S&W Model	0.0256	1.18E-05	0.0694	0.9048
Silica K_{int} D&M Model	0.0276	8.19E-07	0.0048	0.9755

Box-and-whisker plots (labeled ‘b’) in Figures 16-19 allow qualitative observations regarding silica K_{int} effects on model predictions. The Dzomback and Morel K_{int} display the largest inter-quartile spread for the greatest number of sorbing species of the three K_{int} employed, and the largest number of outliers. The Swedlund and Webster K_{int} simulations display tighter statistical distributions for sorbed species, however the inter-quartile spread for arsenic is equally as inaccurate as the Dzomback and Morel results. Meng and Letterman simulations have the smallest inter-quartile spread for the greatest number of sorbing species of the three K_{int} employed. The inter-quartile spread for arsenic is smallest for the Meng and Letterman silica K_{int} , which indicates the lowest sensitivity to other variables (e.g. pH, T, [As]). The arsenic

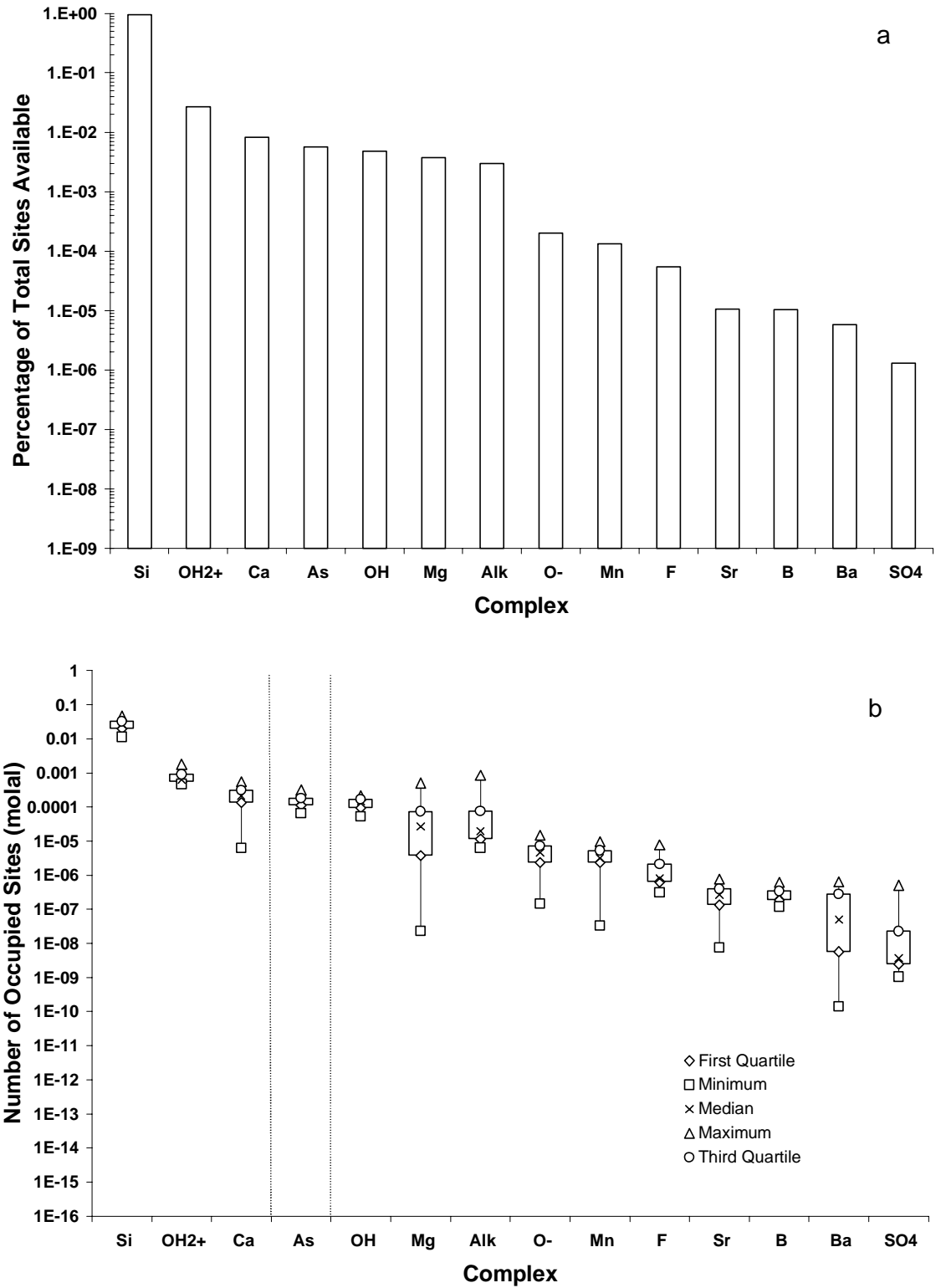


Figure 16. Ranked occupied site population for Rio Salado simulations using silica K_{int} refit from Meng and Letterman [102] data by percentage (a) and concentration (b).

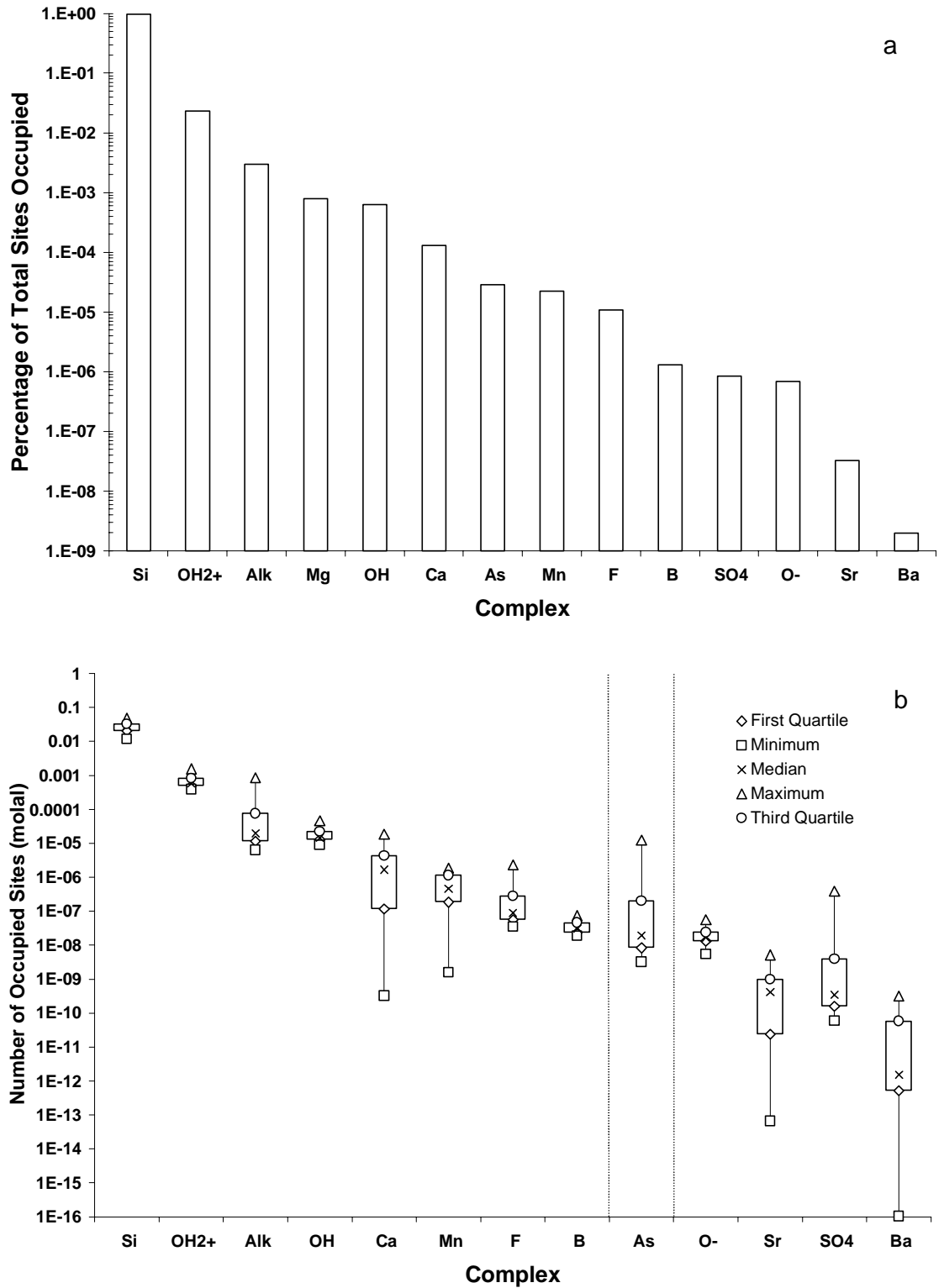


Figure 17. Ranked occupied site population for Rio Salado simulations using published silica K_{int} from Dzomback and Morel [20] by percentage (a) and concentration (b).

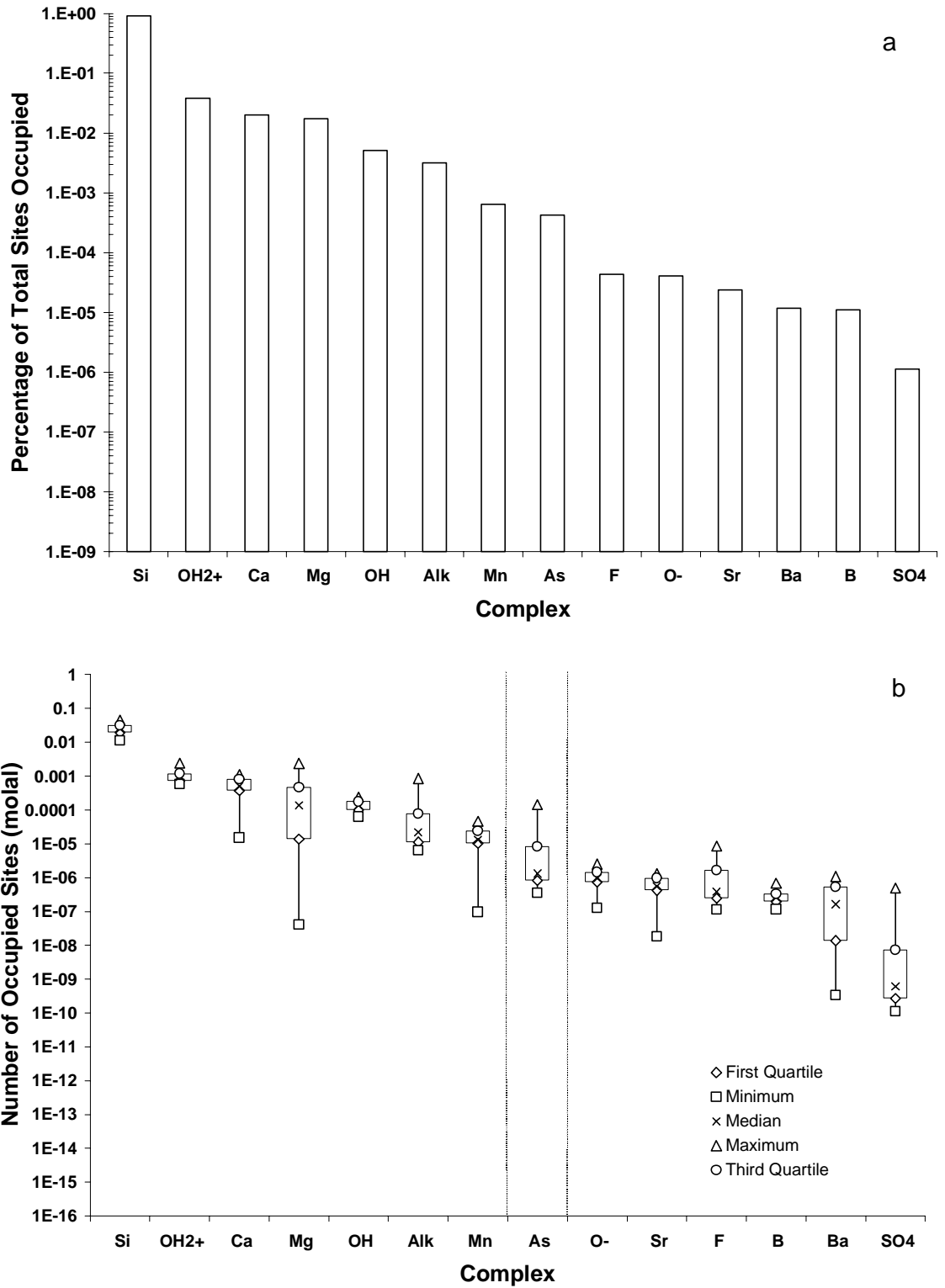


Figure 18. Ranked occupied site population for Rio Salado simulations using published silica K_{int} from Swedlund and Webster [50] by percentage (a) and concentration (b).

concentration simulation using Meng and Letterman silica K_{int} is the most precise and accurate of the three silica K_{int} employed.

Figure 19 depicts the average site population for the Florida simulations using Meng and Letterman silica K_{int} . Phosphate dominates the site population for the Florida simulations. This suggests that phosphate affects arsenic sorption at the Florida sites. Phosphate competes with arsenic on metal oxides in laboratory systems [68, 79, 90].

There has been a fair amount of research on the role of sulfate in surface complexation [69, 70, 79, 90, 102, 101]. The efforts have included laboratory determination of K 's on various solid phases, competitive complexation investigations, and some attempts at simulation of natural systems. In all of the Rio Salado simulations conducted here the role of sulfate was insignificant in either competition or surface site occupation. In the Florida simulations sulfate maintained site occupation at levels near that of arsenic (Figure 19). The sulfate concentration in the three simulated systems are somewhat different. Rio Salado concentrations are from 22-32 ppm, Tyndall at 4.5-13.5, and Fort Walton 13.5 and 43.8 ppm. Tyndall shows the highest degree of sulfate competition for sites while having lowest sulfate concentrations.

4.3 FLORIDA SITES

Table 20 presents the Florida sample R-value determinations. Statistical calculations were performed prior to table composition causing the seemingly incorrect SD/Median values. Values prior to rounding are contained in Appendix C. The results are ranked by median value in the same manner as the Rio Salado data. Evaluation of the Florida R-values (Table 20) is less straightforward than for Rio Salado R-values (Table 18). Determination of the best fit by inspection is difficult. There is not an extraction

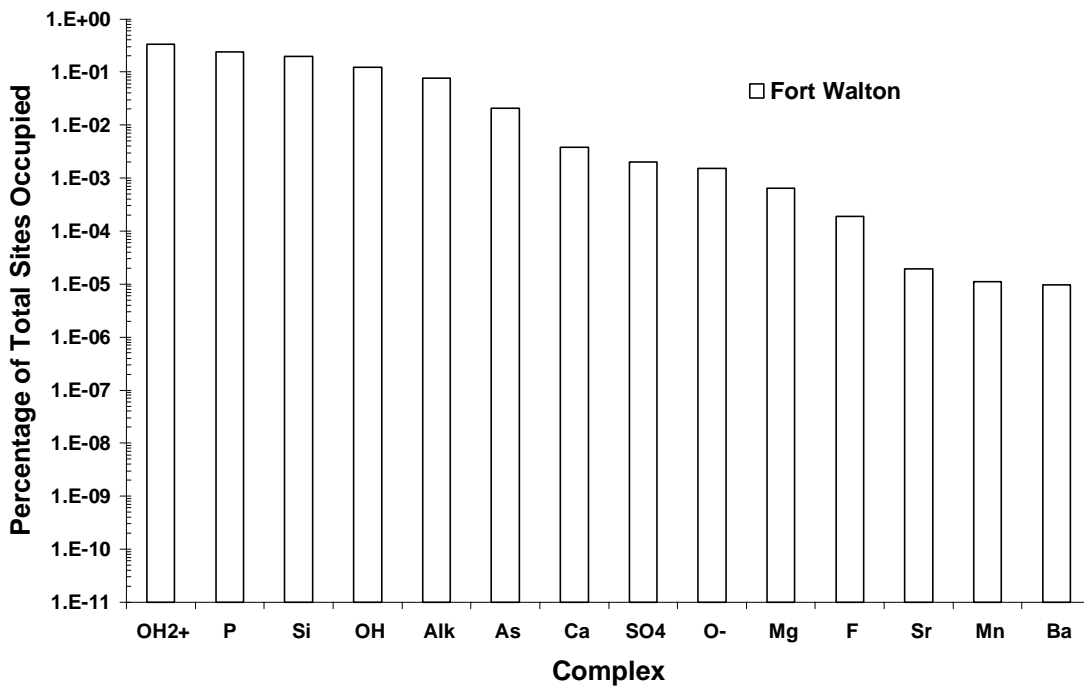
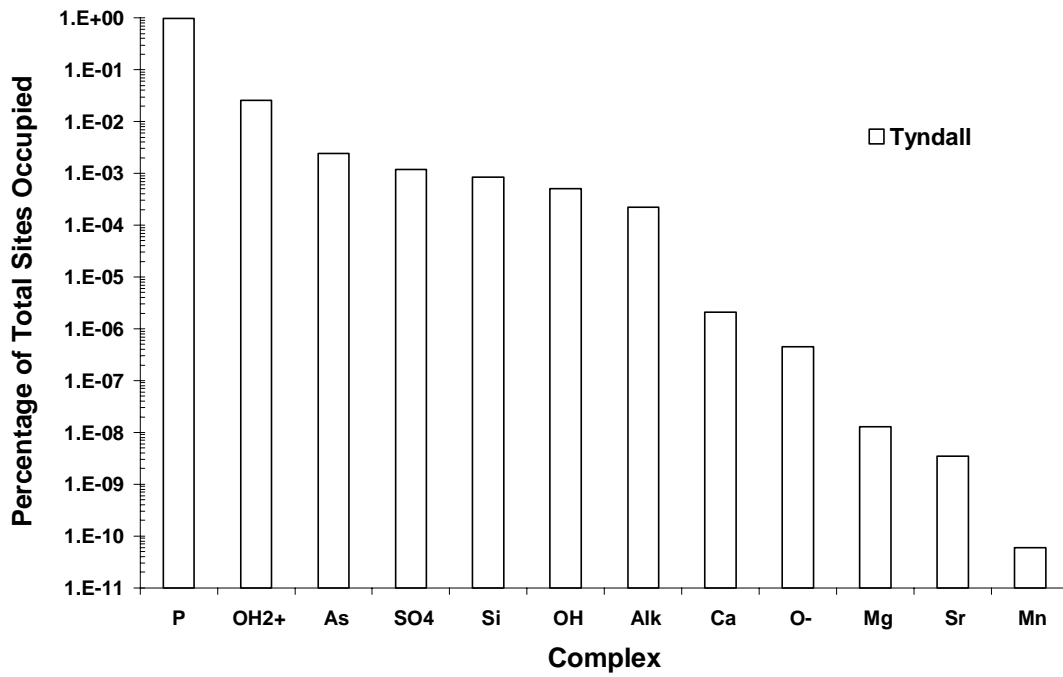


Figure 19. Ranked occupied site population for Florida simulations using K_{int} refit from Meng and Letterman [102] data for Tyndall (a) and Fort Walton (b) samples.

Table 20. Results of Florida simulations: Summary statistics of the ratio of modeled to observed arsenic concentration, R, on sediment.

Extraction	Mineral Phase	Median	SD	SD/Median	Mean	Standard Error
CBD	Goethite	0.01	0.0	195%	0.02	0.01
Total Tessier	Goethite	0.02	0.0	135%	0.03	0.01
Chao	Goethite	0.07	6.8	10394%	3.68	1.97
Total Tessier	Goethite and Gibbsite	0.08	0.2	297%	0.20	0.07
CBD	Ferrihydrite	0.15	0.1	84%	0.17	0.04
HNO ₃	Goethite	0.18	0.3	163%	0.28	0.09
Total Tessier	Ferrihydrite	0.24	0.6	233%	0.48	0.17
CBD	Goethite and Gibbsite	0.34	0.7	216%	0.62	0.21
Total Tessier	Ferrihydrite and Gibbsite	0.47	0.6	127%	0.63	0.17
HNO ₃	Goethite and Gibbsite	0.49	0.6	129%	0.68	0.18
CBD	Ferrihydrite and Gibbsite	0.63	0.8	119%	0.77	0.22
Chao	Ferrihydrite	0.96	37.5	3905%	19.65	10.83
Chao	Goethite and Gibbsite	1.12	19.0	1700%	10.03	5.49
HNO ₃	Ferrihydrite	1.16	13.2	1144%	8.10	3.82
Chao	Ferrihydrite and Gibbsite	1.49	49.7	3341%	26.00	14.35
HNO ₃	Ferrihydrite and Gibbsite	1.55	13.5	872%	8.49	3.90

Table 21. Results of Florida simulations: summary statistics of the ratio of modeled to observed arsenic concentration, R, on sediment, with outliers censored.

Extraction	Mineral Phase	Median	SD	SD/Median	Mean	Standard Error
CBD	Goethite	0.02	0.02	110%	0.03	0.01
Total Tessier	Goethite	0.03	0.03	100%	0.04	0.01
Total Tessier	Goethite and Gibbsite	0.10	0.23	247%	0.23	0.07
CBD	Ferrihydrite	0.19	0.11	59%	0.20	0.04
HNO ₃	Goethite	0.21	0.31	150%	0.32	0.10
Total Tessier	Ferrihydrite	0.31	0.59	190%	0.57	0.19
HNO ₃	Goethite and Gibbsite	0.58	0.63	109%	0.79	0.20
Total Tessier	Ferrihydrite and Gibbsite	0.61	0.58	96%	0.75	0.18
CBD	Goethite and Gibbsite	0.69	0.76	110%	0.74	0.24
CBD	Ferrihydrite and Gibbsite	0.97	0.74	76%	0.92	0.23
HNO ₃	Ferrihydrite	1.24	14.04	1131%	9.69	4.44
HNO ₃	Ferrihydrite and Gibbsite	1.65	14.32	866%	10.14	4.53

method or mineral surface composition that is universally superior to the others, as was the case for HNO₃ extractions on Rio Salado sediments. The Chao extractions have a poor fit as evidenced by the very high values for standard deviation, the ratio of standard deviation to median, and the standard error. Because of the broad scatter in the Chao data indicated by the SD/median, the extraction is not considered further. The scatter in the HNO₃ is of only slightly less magnitude than the Chao fit. The citrate-dithionate-

bicarbonate (CBD) extraction as ferrihydrite and gibbsite has the superior fit. All of the Florida R-values indicate that gibbsite has a significant role in sorption of arsenic and in some cases dominates the sorption process.

Three extraction methods are represented in Figure 20, HNO₃, CBD, and a summation of the Tessier extractions (TT). T-1D is a replicate extraction of the T-1 sediments. Examination of Figure 20 indicates that the behavior of sample T-3 is atypical. Station T-3 extracted arsenic values are 2-50 times higher than other Tyndall samples for extraction methods other than Chao and CBD (Appendix B, Table B-4). The T-3 R-values for the three extraction methods in Figure 20 tend to cluster together, other Florida sample R values show more sensitivity to extraction method than T-3. Omitting T-3, the match between the HNO₃ and CBD extractions improves, as does the model fit. Table 21 presents the calculated R-values omitting all Chao extraction and T-3 data. CBD extraction as ferrihydrite and gibbsite is superior, with a median R almost identical to the mean and very near 1.0.

4.4 SENSITIVITY ANALYSIS

4.4.1 Variation in Conceptual Model

Several conceptual models that vary the type and quantity of the sorbing oxide surfaces were tested. I conducted that phase of sensitivity analysis by varying the extraction methods used to define the sorbing mineral surfaces, by varying the type of iron oxide defined from the extraction data, and by inclusion or omission of gibbsite. The ability of the model to fit arsenic sorption observations over a range of conditions was tested by using samples from different locations. The sensitivity of these models

was presented previously in the R-value analysis. It is very difficult to determine from those simulations how the predictive capability would change if input values were perturbed. These simulations do quantify information on the sensitivity of the approach to the operationally defined extraction method and surface assemblage of minerals.

4.4.2 Perturbation of Select Input Parameters

I varied the values for pH, alkalinity, total arsenic, and silica in the input data sets for Rio Salado Station 12 and Florida sample T-1. These samples were selected because the calculated R-values for surfaces as ferrihydrite + gibbsite were near unity. The water-sediment pairs also did not have any extreme values as compared to other samples taken from that field site. The output from perturbed simulations was used to calculate molal concentrations of total sorbed arsenic and the percent change from the unperturbed simulations determined. The input parameters of pH, total arsenic, silica, alkalinity, number of ferrihydrite sites, and number of gibbsite sites were varied over a range of values. The pH perturbations were ± 0.05 , 0.1, 0.5, and 1.0 pH units. All other input value perturbations were made at ± 1 , 5, 10, and 25% of the original value. Results from linear regression of the perturbation and model response are presented in Table 22. The absolute values (magnitudes) of the slopes are used for ranking, A slope of 1.1 indicates that a +1% change in the input parameter results in a +1.1% change in the sorbed arsenic concentration. Negative slopes for alkalinity and silica indicate that a positive perturbation in input parameters causes a decrease in sorbed arsenic concentration. The regression of response to perturbation in silica concentration or pH was non-linear for the Rio Salado analysis. The linear slope approximation of the Rio Salado silica regression is included in Table 22.

Table 22. Slopes from linear regression analysis of changes in model output by perturbing input parameters plotting the response as a percent change in sorbed arsenic concentration.

Florida Sample T-1		Rio Salado Station 12	
Parameter	Slope	Parameter	Slope
Arsenic	0.87	Silica ^a	-1.06
Ferrihydrite	0.68	Ferrihydrite	1.0
Gibbsite	0.28	Arsenic	0.7
Silica	-0.02	Alkalinity	-0.07
Alkalinity	-0.0025	Gibbsite	0.0001

^a The best fit to the Rio Salado silica sensitivity analysis data is in the form: percent change in sorbed arsenic = $1.1655x^2 - 1.0602x + 0.0509$ where x is the percent change in silica concentration.

Some of the input parameters cannot be perturbed without causing the PHREEQC code to adjust other parameters in response. This is due to the equilibrium relationships between pH, alkalinity, and the activity of polyprotic acids (e.g. arsenic and silica) that are treated explicitly in the PHREEQC code. Perturbation of the concentration of a polyprotic acid such as silica also changes the equilibrium pH. Since polyprotic acids contribute to alkalinity this parameter (and thereby the PHREEQC calculated carbonate equilibria) is also perturbed at convergence. Although these effects make the interpretation of the sensitivity analysis more difficult, useful information is obtained. The result is that although the change in modeled arsenic concentration may vary linearly with the percent change in the input parameter, a best-fit line through the perturbed simulation output will not pass through the graph origin in the pH, alkalinity, silica, and arsenic sensitivity relationships. The graph origin represents the unperturbed case, therefore, failure to pass through the origin indicates non-linear sensitivity.

As evidenced in the slopes of the regressions, the Rio Salado Station 12 and Florida T-1 sample models have different sensitivities to parameter perturbation. T-1 simulations are most sensitive to aqueous arsenic concentration, less so than to the

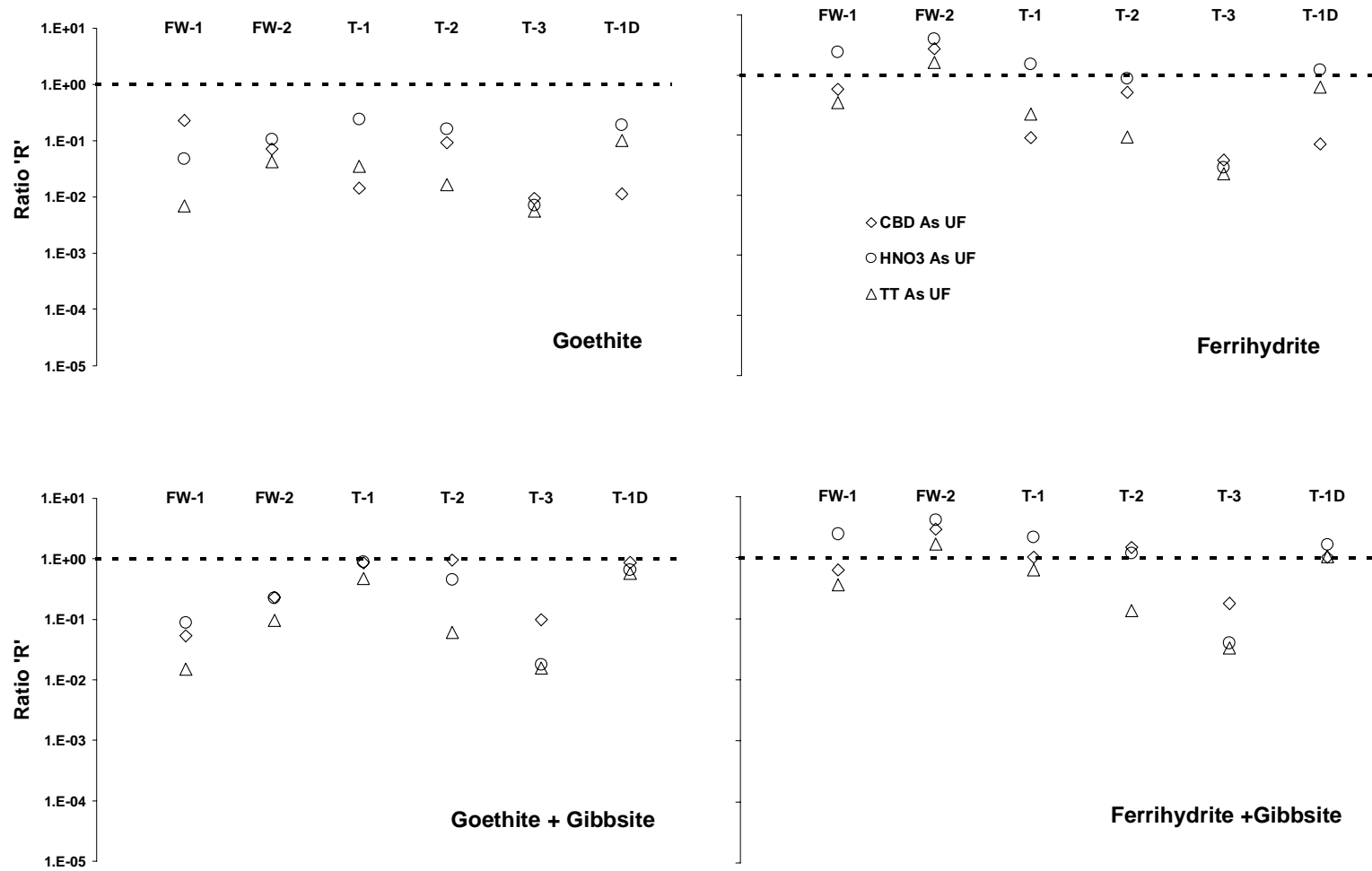


Figure 20. Variation in R by sample station, extraction method, and surface assemblage for the Florida sediments and unfiltered (UF) water samples.

amount of the sorbing phase. Rio Salado is sensitive to silica concentration, the amount of ferrihydrite, and aqueous arsenic concentration.

Sensitivity to change in pH is depicted in Figure 21. Perturbation of pH produced a non-linear response for both samples. When the pH of Rio Salado Station 12 was perturbed by plus one pH unit the response was far from the trend shown by lesser positive levels of perturbation. This point is plotted individually. It is probable that this is due to the interdependence of pH and other variables in PHREEQC causing an abrupt and large shift in some equilibrium relationship. The Florida and Rio Salado samples display a different magnitude and direction of sensitivity to changes in input pH.

4.4.3 Perturbation of Arsenic K_{int}

Dzombak and Morel cite a standard deviation of ± 0.07 to ± 1.50 of the log value of ion-specific K_{int} for ferrihydrite [20]. Arsenic K_{int} were adjusted ± 1.0 to explore the effect of perturbing K_{int} on the predicted arsenic surface concentration. The perturbations were conducted on all Rio Salado and Florida sample stations using the HNO_3 extraction as ferrihydrite + gibbsite. The observations indicate some complex relationships.

For the Rio Salado samples (Figure 22), lowering K_{int} (K_{int} Down) resulted in a relatively uniform lowering of the modeled arsenic concentration by ~85%. This is independent of observed arsenic concentration. Raising K_{int} (K_{int} Up) was sensitive to the observed amount of arsenic on the surfaces. Raising the K_{int} for Rio Salado caused the greatest changes in surfaces with the lowest observed arsenic levels. The magnitude of change in modeled arsenic concentration for perturbation of K_{int} is greater with decreasing temperature and increasing pH. There is bifurcation of the K_{int} Up trend for Rio Salado at higher observed arsenic levels. The Florida sample data are similar (Figure

23). For both Florida and Rio Salado the model is more sensitive to raising the arsenic K_{int} than lowering it, and most sensitive to K_{int} at the low range of observed arsenic concentration.

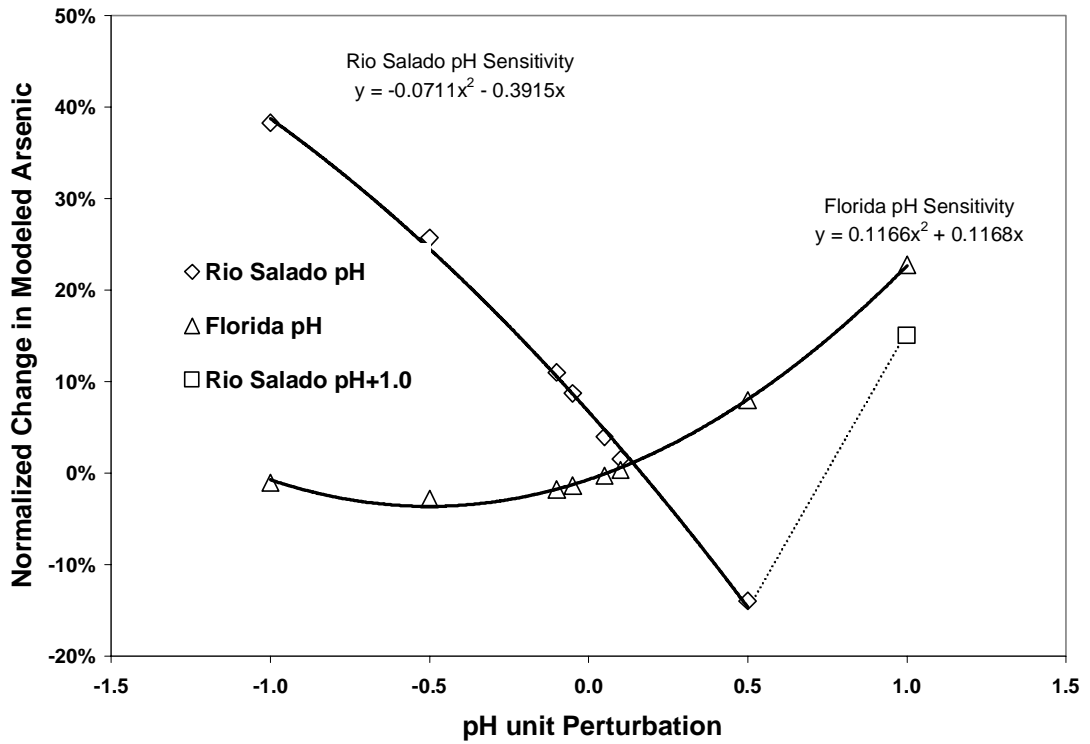


Figure 21. Sensitivity of sorbed arsenic concentration to perturbation in input pH value for Rio Salado Station 12 and Florida Sample T-1.

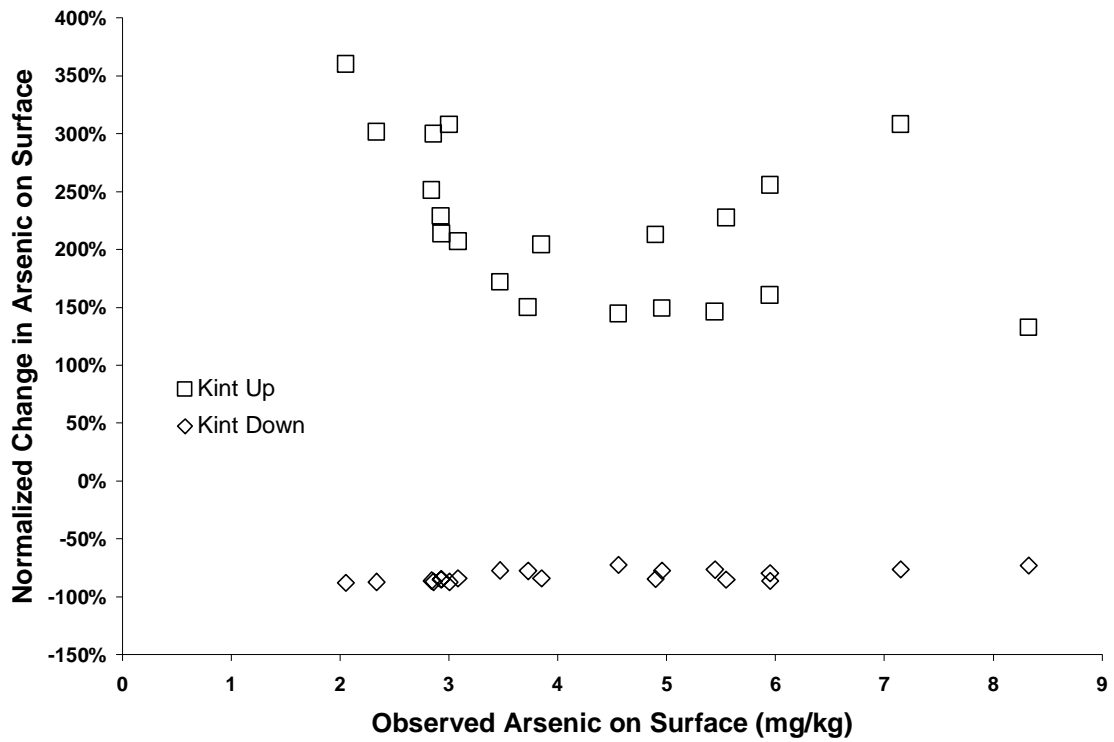


Figure 22. Sensitivity of Rio Salado simulations to perturbation of arsenic K_{int} .

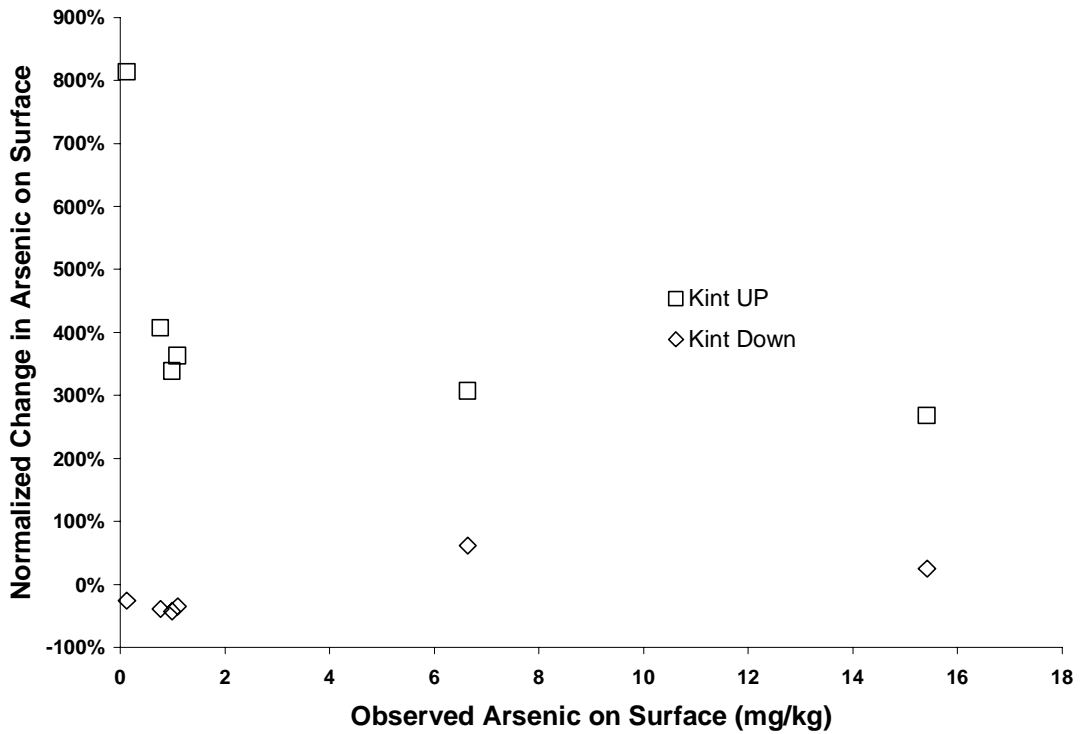


Figure 23. Sensitivity of Florida simulations to perturbation of arsenic K_{int} .

CHAPTER 5 DISCUSSION

5.1 KNOWN LIMITATIONS TO APPROACH

5.1.1 Surface Phase Limitations

Only hydrous metal oxide surfaces for aluminum and iron are used here. No other sorbing phases are simulated or considered directly. Although it is known that carbonates sorb [24], they were omitted due to low abundance. Manganese was observed to be correlated with arsenic in Rio Salado [106] but little data exists to apply these oxides to arsenic attenuation without invoking kinetics [72]. Silica was found in operationally defined extractions, and silica surfaces are probable in the Rio Salado system. The choice of gibbsite as the aluminum oxide phase was based on the availability of arsenic K_{int} ; another aluminum phase may be more appropriate. Clay minerals are assumed to be present but not abundant. In order to limit the system simulated to probable first-order sorbing phases only ferrihydrite, goethite and gibbsite phases were used.

5.1.2 Operationally Defined Extractions

Choices are made regarding how the solid phases will be quantified. Here, I quantify the mineral phases using operationally defined wet-chemical extractions. The extractions are ‘operationally defined’ because past use has indicated that the methods

will generally dissolve the mineral of interest. I can not be certain that the extraction dissolved only the minerals of interest. This requires that I make choices regarding the best operationally defined extraction for the intended use, it is inevitable that some compromises from the ideal will be made.

Extractions used for determining the hydrous metal oxide surface population on sediment are known and accepted in the scientific community. The hydrous metal oxide surfaces are defined as individual components of a multicomponent site distribution using elemental values determined from the operationally defined extractions. Specifically, iron and aluminum concentrations in sediment extracts are used to back-calculate the amount of hydrous metal oxide that was present on the surface of the sediment grains. The amount of modeled arsenic should only be compared to observed arsenic values from the same extraction. There are problems with this procedure in that:

1. The amount of arsenic leached may not correspond with the amount of hydrous metal oxide ions that are used to create mineral surfaces for the model, due to preferential leaching of one component over the other [60, 122];
2. The selection of solid phases to represent the extraction data may not be correct;
3. The selection of solid phases to simulate and their relative importance is dependent on the specific geochemical reactions controlling the environmental process of interest. This is often poorly understood.
4. Explicitly supporting selection of solid phases to simulate is very difficult. This is most often due to the extreme complexity of direct detection and quantification of low concentrations of minerals and amorphous phases in sediment [93].

5. There are questions regarding the theoretical vs. empirical treatment of multiple competing sorbing species and surfaces [21, 22]; and,
6. There is debate as to if mixed-mineral-phase complexation behavior is additive as compared to the pure-mineral-phase behavior [50, 102].

What is at issue is defining the appropriate extraction method to define mineral phases that result in accurate simulation of environmental processes. Due to the difficulty of defining and quantifying mineral phases directly, I have defined them empirically using operationally defined extractions. Discussion of the validity of this approach was not found in the literature, but there appear to be few alternatives in implementing a mechanistic approach [93]. Rather than truly defining the surface area of available minerals, the extraction and subsequent calculations estimate the potential number of sorption-site-forming metal atoms. The result is that the best-fitting models are those that provide results that are internally consistent with the ratios of arsenic and hydrous metal oxide forming elements found in the extractions. At best, this is semi-empirical, and is certainly not purely mechanistic.

The issues with operationally defined extractions are reflected in comparison of extract to x-ray fluorescence (XRF), or total digestion elemental concentrations. Welch [106] indicates that the Rio Salado Chao extractions removed 15% of the arsenic detectable using XRF where the HNO_3 extraction removed 85%, and the H_3PO_4 extraction 25%, on average. All extracted iron values were well below (4-21%) the total iron value determined by XRF. XRF provides a measure of the total concentration of an element in the sediments. Similar results were found with the extractions on the Florida samples.

Before the Rio Salado effort it was not known whether the arsenic extractions would provide meaningful results for use in a SC model. It is possible the extractions would remove the 'correct' surface-active phases responsible for sorbing the arsenic, and the arsenic complexed with those phases, but not support stoichiometric recombination in a SC scheme. This could be due to the extraction removing portions of the sediment grain coatings that were not surface-active. I tested the extractions here, found them successful, and hope for broader validation of the approach in the future.

Major questions remain regarding the use of sequential extractions in study of the bioavailability of metals. Are the extracted phases and elements physically meaningful for estimates of metal toxicity from the geomeedia? Can the technique used here provide consistent results in modeling retardation and attenuation? These questions remain to be investigated, but the underlying mechanistic approach appears to be supported by the extractions.

The Chao extraction is designed to remove amorphous phases by reductive dissolution. HNO_3 extractions should remove amorphous iron oxides, and crystalline iron oxides, manganese and aluminum hydrous oxides, and organic material by oxidation and acid attack. The H_3PO_4 extractions work by acid attack and displacement of complexed arsenic by phosphate. The citrate-bicarbonate-dithionate (CBD) extractions [85] remove amorphous and crystalline secondary iron, manganese and aluminum minerals by reductive dissolution and complexation in a buffered system. These same extractions also provide data on surface silica but with exception of the CBD method, the effectiveness for silica and its complexes is not well described in the literature. The extractions are operationally defined in that they are not as specific for dissolution of

mineral types as may be desirable. This effort provides information on the suitability of the methods to match observation when used for modeling. It does not validate any selective dissolution analysis method as mechanistically correct.

5.1.3 Equilibrium Assumption

The modeling approach assumes that in all cases the system is in chemical equilibrium and is describable without using kinetic constraints. This is probably not completely valid, because arsenite is often present in disequilibrium with the oxidation state of the environment [39, 48, 52, 54] and has sorption properties significantly different from arsenate. Arsenic Redox disequilibrium has been observed in the Rio Salado and Florida sampling locations. The presence of As^{3+} in Rio Salado downstream of the Powerline spring, and subsequent oxidative transport, indicates that the system will move towards equilibrium in travel times of tens of minutes over hundreds of meters. Little is known regarding the natural transformation rates of the As^{3+} - As^{5+} Redox couple [48]. Redox disequilibria, as noted in Welch's [106] sediment extracts and at other sites, complicate any interpretation of arsenic mobility based on oxidation state because the assumption of As^{3+} - As^{5+} Redox equilibria is generally not valid [53].

Redox disequilibria of many metal pairs are due to biogeochemical reactions and the controls imposed by biological terminal electron acceptors; they can be modeled using fitted kinetic corrections [72]. The PHREEQC modeling here does not attempt to calibrate the model to observed As^{3+} concentrations. However, I use As^{3+} concentrations predicted to be complexed with sediments as part of the total arsenic used in model comparisons to field data. The total arsenic mass input as determined from analytical values is accounted for.

In the case of the Florida samples, significant As^{3+} (~50% of the total) was determined to be present at both Fort Walton and Tyndall AFB. Simulations were conducted for relative Redox endpoints of the system to evaluate the sensitivity of the modeled sorption to the oxidation state of the arsenic. There were no attempts made to adjust the Redox chemistry to simulate the observed arsenic speciation. Based on the discussion above, regarding the prevalence of non-equilibrium conditions for the arsenic Redox couple, such simulations are probably meaningless.

For Rio Salado, it was possible to simplify the conceptual model because of ample evidence that the system was near equilibrium. Over 90% of the arsenic is present as a single specie, As^{5+} . Most of Rio Salado simulations converged with only limited change in Redox condition from the input Eh. Redox simulation and measurement can be difficult and error prone. However, the Rio Salado modeling did not require manipulation of measured Eh or “fixing” or “hard wiring” of Redox couples to obtain numerical convergence or meaningful results.

These Redox and equilibrium simplifications are not as reasonable for the Florida simulations given the presence of several species of arsenic at significant concentrations. In simulations using raw input, and simulations where Redox equilibria were manipulated, charge balance requirements of the diffuse layer simulation caused oxidation of As^{3+} and subsequent sorption of the resultant As^{5+} . Redox condition became strongly oxidizing due to the reduction of nitrate and other species. Redox manipulations were limited to zeroing input concentrations of Redox-sensitive NO_3 from the observed level of up to 1.4 mg/L. This did not prevent the simulation from oxidizing most of the As^{3+} in solution to As^{5+} , or altering the resultant R-value at convergence, but resulted in

less As^{3+} oxidation and Eh closer to the input value than simulations where NO_3 was not zeroed. It is probable that an As^{3+} to As^{5+} ratio at convergence can be obtained that matches input values by manipulation of input parameters. The geochemical meaning of such simulations would be questionable for all but the As^{3+} - As^{5+} Redox couple.

The general applicability of an equilibrium assumption can be difficult to prove. Even when good evidence exists for equilibrium there can be problems with the thermodynamic constants used by the model. Problems arise from inconsistent reference points for calculated values, experimental error, and activity corrections.

5.1.4 Organic Substrates

Arsenic chemisorption is not limited to hydrous metal oxides. Organic substrates such as living and dead plant material, bacteria, and other surface coatings or colloidal organic forms are known to sorb anions and cations. It is recognized that there is an organic substrate effect on arsenic sorption and SC. This has not been factored into the conceptual model or simulations for Florida or Rio Salado. There is also adsorption of dissolved organic compounds such as fulvic and humic acids on hydrous metal oxides that would act in a competitive manner with arsenic. There is some bearing on the findings herein. Given Welch's [106] observed correlation between total organic carbon (TOC) and arsenic in Rio Salado, and the observations for the Florida samples, it is quite probable that some of the observed chemisorption is on organic or biologic material rather than on mineral surfaces. TOC to arsenic correlations were weak for the Florida samples but this fact alone cannot discount probable organic substrate sorption of arsenic.

5.1.5 Organic Arsenic

The organic arsenic concentrations detected at Rio Salado and Tyndall AFB are not fully represented in the simulations. Organic arsenic is treated as As^{5+} . The evaluation of Rio Salado organic arsenic data was hampered by false positives for DMAA. This is attributable to the specific ion exchange separation elution sequence used at that time. MMAA detection was unaffected. Although Rio Salado organic arsenic content is probably less than 10% in water, it is considerably greater in sediments. Florida analysis reveals no organic arsenic at Fort Walton and approximately 10% organic arsenic at Tyndall AFB. Since the K_{int} for MMAA and DMAA are reasonably close to that of As^{5+} [81, 82], the effect of substitution is small for the current simulations. To ensure generality of future efforts, organic arsenic should be rigorously incorporated into SC modeling.

5.2 EXTRACTION METHOD FOR GEOCHEMICAL MODELING

5.2.1 Rio Salado

Care must be used in selection of ‘the best’ operationally defined extractions. Considering the best-fit as a combination of prediction of total available arsenic and internal consistency in a SC framework, the Rio Salado HNO_3 ‘Whole’ extractions offer the best match overall. The HNO_3 ‘Whole’ extract does not represent the best model based on R approaching unity; that distinction belongs to the Chao extractions. The median values for model fit (Table 18) also favor the HNO_3 ‘Fine’ extractions on ground sediments as good simulations. However, it is the case that the HNO_3 ‘Whole’ extract provides the best model, based on the tendency for HNO_3 ‘Whole’ R-values to be more

resistant to non-ideal behavior. The HNO₃ extractions provide the best match (85% average for Rio Salado) to total arsenic as defined by XRF. The HNO₃ 'Whole' median R of 0.74 under-predicts the observed arsenic by about 26%. The relationships between BET, total sites in the model, and R indicates that the under-prediction is not due to a problem with the numerical simulation. It is probably the result of an underrepresented sorbing phase, or a deficiency in the conceptual model. I believe that under-prediction is due to complexation by a combination of organic, manganese, silica, and carbonate surfaces that are not represented in the model.

The HNO₃ extractions have been operationally defined as removing surface-active organic, amorphous and crystalline phases. The HNO₃ extractions solubilize organically-bound arsenic. It is known that there is an organic carbon component in the sediments, and that the organic carbon (TOC) is associated with arsenic. The 26% under-prediction of the inorganic HNO₃ model is close to the 36% average amount of arsenic associated with organic material as determined by Tessier partial extraction [106]. Based on the magnitude of arsenic in the organic partial extractions, it is possible that the organic fraction of the Rio Salado sediments may account for most of the arsenic 'missing' from the HNO₃ 'Whole' simulations.

5.2.2 Florida Sites

Complexation simulation of arsenic sorption for the Florida sites using surfaces defined by extraction was generally successful. Sample T-3 R values were lower than other Tyndall samples for all extractions and surface combinations. T-3 has anomalously high sediment arsenic levels as compared to other Tyndall samples. Arsenic contamination in the T-3 sample that is not associated with aluminum or iron hydrous

metal oxides could account for this inability to predict arsenic sediment concentrations in the T-3 sample. As revealed in the tabular data and graphical analysis, inclusion of aluminum hydrous metal oxide phases resulted in better representations of the observed arsenic distributions than iron oxides alone. The simulations using the HNO₃ extractions tended to over-predict. Absence of an aluminum phase caused gross under-prediction. The importance of the aluminum phase in the Florida samples as compared to Rio Salado probably stems from the higher Al/Fe ratio in the Florida sediment extracts (Table A-21 and B-4). The testing of CBD extractions on the Florida sediments indicates promise for this operationally defined method. Development of a standard protocol among practitioners for sample collection and extraction will enhance comparability of modeling efforts.

5.3 FINDINGS REGARDING THE SORBING MINERAL PHASE

5.3.1 Iron Oxides

Examination of Table 18 clearly indicates that the choice of sorbing iron oxide phase, goethite vs. ferrihydrite, is one of the most significant factors affecting model fit. The dominant difference between these two phases with respect to application of SC modeling is the specific surface area of the mineral. Definition of the appropriate mineral phase for use, via separate lines of evidence, has not unambiguously indicated the correct mineral assemblage to use in modeling the Rio Salado arsenic distribution. Evidence for both phases exists. Defining the appropriate mineral assemblage as the one that best fits the modeling is circular with respect to defense of a mechanistic modeling approach, but is used here given the lack of alternatives. The contribution of goethite to arsenic

sorption is insignificant as physically defined in the Rio Salado simulation. Based on the modeling, ferrihydrite is the appropriate iron phase to use for Rio Salado.

Based on observation and modeling, the Rio Salado system appears to have mixed iron oxide sorbing surfaces, goethite and ferrihydrite. The ferrihydrite used in the simulations has a surface area over 13 times greater than the goethite. Field evidence for the presence of ferrihydrite, such as iron staining or coating observable with a hand lens, was absent in Rio Salado. Saturation index calculations show goethite to be thermodynamically stable over the entire stream reach and ferrihydrite only partially so. Spectrophotometric detection of goethite was accomplished and goethite was observed petrographically. Partial and operationally defined extractions show the presence of both phases.

5.3.2 Gibbsite

The Rio Salado modeling results were not greatly affected by the presence or absence of gibbsite; yet its inclusion is justified by slightly improved fits. Including an aluminum-oxide-based sorption site as gibbsite increased the transferability of the model from Rio Salado to the Florida data. Florida simulations are sensitive to the inclusion of gibbsite. Given the success in using two minerals in a CA approach, the incorporation of additional inorganic phase(s) may improve the model fit.

5.4 ARSENIC SPECIATION TO SUPPORT SURFACE COMPLEXATION

MODELING

Speciation has a direct influence on the environmental availability of chemicals, their behavior over time, and attenuation under transport conditions. Speciation provides

a better quantification of toxicity than use of total arsenic determinations. The literature on the occurrence of arsenic species shows that organic arsenic is a common component in natural systems. The presence of organic arsenic as a small (<10%), but measurable component of high-arsenic natural waters was confirmed. From the literature, organic arsenic is present in low arsenic (<100 ppb) systems at 5-60% of the total arsenic available. From this work, it appears that the presence of organic arsenic cannot be ruled out in high-arsenic geothermal watersheds or inorganically contaminated sites.

Field speciation of arsenic is readily accomplished and inexpensive. When speciation techniques are employed, the error in toxicity calculation attributable to the difficulty in preserving arsenic species is eliminated. The speciation and modeling of inorganic arsenic indicated that when As^{3+} was detected it was generally not in equilibrium with the Redox potential of the water. The simulations were not constrained to force Redox conditions so that the model would predict the observed As^{3+} concentration. Because As^{3+} is more toxic and more mobile than As^{5+} , it is important to be able to predict As^{3+} concentrations separately from As^{5+} . Forcing Redox conditions in the model is not appropriate because of the unrealistic constraints imposed on the entire simulation. Based on my observations of in-stream As^{3+} oxidation rate ($t_{1/2}$ of 0.13 hours), and the similar rates in the literature, I believe that As^{3+} modeling will need to be kinetically constrained. Although the approach is more complex than the effort reported here, the most recent versions of PHREEQC support kinetics, and there is a large body of literature on reactive transport simulations. Kinetically-limited modeling of As^{3+} water-mineral partitioning can be accomplished within the framework presented here, although at an unknown error level.

5.5 COMPETITION FOR SORPTION SITES BY COMMON ANIONS

Appropriate application of ion competition for sorbing sites is essential to SC modeling. The results indicate that the error due to neglecting competition can be very high. This is shown by the orders of magnitude in the variation of R. The error can equal or exceed that due to inappropriate choice of mineral phases. Examination of the model output indicates that silica occupies more sorption sites than any other sorbing compound or ligand does. The degree of competition cannot be predicted without modeling due to the interplay between surface charge, complexation constants, pKa's of polyprotic species, and pH. The values of K_{int} used for competing species will have a significant effect on the success of the effort. Silica was found to be an important species in ferrihydrite and gibbsite SC. Use of K_{int} derived from LFER [23] was inaccurate.

Silica concentration in water, and the K_{int} for silica sorption play an important role in regulating the surface complexation of arsenic. Swedlund and Webster's laboratory investigation into the competition between silica and arsenic for sorbing sites is in qualitative agreement with my result [50]. Some inconsistencies in the arsenic K_{int} derived from other published values [20] were noted by the authors. They showed that adsorption of arsenate and arsenite could be inhibited 20-80% at a fixed pH with ratios of dissolved silica to sorbing sites as low as 0.026. Silica complexation is a primary control on arsenic surface complexation. The sensitivity analysis indicates that the competitive effects of silica cannot be predicted a priori, and must be quantified using numerical modeling methods.

Alternate K_{int} for silica have a large effect on the sorbed arsenic concentrations. Table 19 shows that the reduction in modeled arsenic concentration is not accompanied

by increased occupation of sites by silica (Table 19). This is an example of the interplay between pKa's of polyprotic acids, pH dependant K_{int} , and the interrelationship of parameters in PHREEQC. A similar effect is seen in arsenite sorption in laboratory experiments, and has been attributed to these same types of feedback, albeit without quantification [50, 90]. Arsenite, although an anion, increases its complexation with ferrihydrite as pH decreases, the inverse of expectation, and inverse of the behavior of related arsenate [27, 90, 91]. This is attributable to the pH-controlled speciation of arsenite and the relative affinity of the species for ferrihydrite [90]. It is probable that a similar feedback process causes the simulations to behave as observed.

It is notable that with exception of phosphate, the Rio Salado and Florida simulations have the same rank and same percentage of site population for the majority of the modeled surface populations. The level of correlation between the simulations is remarkable given the very different water composition between Florida and Rio Salado. Silica and arsenic concentrations alone vary two orders of magnitude between the locales (2-200 mg/L). This again confirms that the K_{int} of silica on hydrous metal oxides is a critical parameter to SC modeling of field relationships.

The published information on carbonate sorption is limited, presumably due to experimental difficulty [135]. I found that model error levels depend on the inclusion of common anion competition with arsenic for sorption sites. This includes the carbonate and bicarbonate ions. The competitive interaction of the carbon species is not as great as that of silica, but is still significant. Carbonate and bicarbonate species occupy approximately the same number of sites as arsenic in the simulations.

Based on this work, field application of SC modeling will rarely be successful if competition is neglected. This simplification should be avoided in model conceptualization. Increasing numbers of laboratory determinations of single-species single-mineral SC parameters, particularly major anions and cations in natural waters or surrogate solutions, are needed for testing of the CA approach. The generality of the approach could be tested more rigorously if there were more complexation parameters available for mineral surfaces and common ions, particularly silica.

5.6 TRENDS IN R: THE RATIO OF MODELED TO OBSERVED ARSENIC

Several major changes in water chemistry take place as Rio Salado water flows downstream. The water cools, the pH rises, and the conductivity of the water decreases downstream. Correlation of these variables with R allows some assessment of model fit. Arsenate and arsenite form inner sphere complexes with hydrous metal oxides. Inner sphere complexes in the DLM are not affected by small changes in ionic strength (conductivity). It is possible that temperature effects on the K's are responsible for the slight downstream trend towards lower R-values; PHREEQC does not calculate SC temperature dependencies. The observed trend in R with pH may be from in-situ K_{int} , K_{S+} , and K_{S-} differing from the values used in the model. The trends indicate that the model does not fully account for changes in SC as a function of pH, conductivity, or temperature.

Some sediment samples were homogenized to enhance reproducibility between replicates [106]. This should probably be avoided. The total arsenic extracted from sediment is inversely proportional to R (Figure 9) in samples that were homogenized using grinding, sieving, and quartering. This trend is not as apparent in the whole

sediment samples (HNO₃ 'Whole'). The trend towards lower R with higher arsenic is due to liberation of arsenic during grinding that is not normally surface-available. The model would then be predicting lower than observed arsenic concentrations because the observed concentrations are biased by sample preparation. At first glance, the explanation above requires that the amount of iron extracted be less enhanced by grinding than the arsenic, otherwise the model would have sufficient sites to use for the increased level of arsenic and there would not be a trend in R. However, surface complexation models are generally insensitive to the number of available sites [21, 38, 100], as is apparent in Figure 13. Support is also found in the poor correlation between extracted iron and arsenic for Rio Salado sediments [106], in the lack of a relationship between R and iron (Figure 15), and in that hydrous metal oxides are dominantly found as grain coatings.

A lower R is associated with the larger BET surface area. The general relationship for increasing chemical reactivity with increasing solid phase surface area applies here. The sediments with the highest BET surface areas should have the greatest number of potential reaction sites. However, these sediments exhibit the lowest R-values; the inverse of expected. This could be explained by the presence of a constant-proportion sorbing phase not included in the model.

The R-values for the HNO₃ 'Whole' extractions are not dependent on the amount of extracted arsenic or measured porosity. This indicates that the extraction process removes surface material and sorbed arsenic proportionally. Rio Salado samples have a natural variation in porosity and extractable arsenic that was addressed by the methods used here. Common sediment preparation techniques should be evaluated before use to

avoid bias in R. Whole grain, air-dried sediment samples are preferred. Use of larger than normal sample aliquots to avoid nugget effects and other bias resulting from inhomogeneity may be appropriate. Evaluation of sample inhomogeneity should be conducted before modeling.

It is important to acknowledge that all of the R-value trends are relatively weak. It appears that input parameters, singly or in groups, do not provide good empirical predictors for the quality of model fit. Some inferences can be made from this observation. First, the model is able to make predictions of arsenic sorption that are of equal quality over the moderately high variability in chemistry and sediment characteristics at Rio Salado. Second, since some of the parameters that R is insensitive to are critical to the mechanistic conceptual and numerical model (e.g. extracted arsenic and iron, pH, alkalinity), the observation helps validate the mechanistic approach. Lastly, the trends observed may indicate areas where the model and data should be queried. This includes determining if the thermodynamic database or conceptual model can be tuned for greater accuracy, and data review for analytical bias that may have propagated in the modeling. Analytical bias is seen in decreasing R-values at higher sediment arsenic concentrations for -80 mesh samples; whereas the phenomenon is absent from whole sediment extractions. This type of review is valuable because any trend in R indicates a systematic deviation from the ideal.

5.7 GENERAL OBSERVATIONS

Surface complexation modeling can be used to predict the distribution of trace elements, including arsenic. Additional testing of SC modeling in complex but well understood geochemical systems is needed. Modeling SC by biological and mixed

organic-mineral substrates may be critical to the mechanistic approach. This should be advanced in parallel with the development of a field data collection protocol for use in support of geochemical modeling.

In order to expand the use of laboratory-determined sorption parameters to environmental studies, the practice of defining solid phases and sorbed ions on natural materials needs additional development and agreement among practitioners. It would be useful to assess the ability of other extraction schemes to support the application of complexation modeling. It is necessary to build consensus on the appropriate extraction methods for natural sediments to emulate the laboratory results if there is to be general transference of laboratory parameters to field use. Without this consensus the method for proper application of laboratory results to the field remains ambiguous.

Simulations using filtered sample water data under-predict arsenic sorption as compared to unfiltered samples (Appendix C). The effect is variable in magnitude depending on the individual differences between samples. There is some evidence, in the form of Rio Salado saturation index and mass flux calculations (Appendix A), that unfiltered samples are better for use in geochemical modeling. The use of measured vs. assumed porosity significantly decreases the error level. Sampling and analysis protocol is a factor in successful mechanistic modeling.

The potential error in SC modeling arsenic water-mineral partitioning in natural systems is first presented here. Because the modeling effort was conducted without fitting by artificial parameter variation, this study shows that the Rio Salado approach is transferable to other systems. Modeling of the Florida sediments indicates suitability for

contaminated sites. However, the general question of how to implement the results of this study to meet arsenic management goals remains unresolved.

Knowledge of contaminant water-mineral partitioning is essential to contaminant transport evaluation. Accurate contaminant transport determination forms the underpinnings of risk assessment, remedial design and feasibility studies, and of natural attenuation quantification. The more accurate the assessment, the lower the uncertainty in cost or in probability of success. Numerical modeling is used to make these determinations. There are mechanistic and empirical strategies to determine a contaminant's transport parameters. The mechanistic strategies would generally employ geochemical modeling and flow-field determination using sequential iteration of the geochemical and the flow code. Although computationally intensive, and requiring expert implementation, mechanistic strategies are intrinsically better than empirical ones.

The modeling approach can be used in a semi-empirical manner. In contaminant transport models, some sort of a retardation or decay factor is used to numerically account for contaminant chemical and physical interaction. These interactions cause changes in the aqueous and solid phase distribution of the contaminant over the flow-field. Each of the Rio Salado sampling stations is a point in the surface water flow-field of Rio Salado. The modeled water-mineral partitioning for each station is converted into a partition coefficient or retardation factor (K_d). These numbers can be used in existing contaminant transport models. This approach has been used for estimation of radionuclide transport [29]. Whether the mechanistic sequential iteration strategy is used, or the semi-empirical approach employed, the data collection and geochemical modeling approach presented here provide guidance on implementation of arsenic SC modeling.

The fundamental principles of arsenic chemisorption by SC will continue to be investigated and debated in the years to come. This should not inhibit testing the current state of the theory against field data. This effort uses the results of decades of laboratory work by others to support testing of SC theory on arsenic partitioning in a natural setting. As the theory is revised, some of the constants employed here will certainly change, as will the mathematical approach. However, given the commonalities in the details of describing surface chemistry, the conceptual approach used here will remain the same for some time to come.

5.8 SUGGESTED APPROACH

I explored a large number of variables in the use of a component additivity approach to SC modeling of the field distribution of arsenic. The success of the effort suggests that the method is transferable. However, a large number of uncertainties remain in application to other arsenic field problems. If the CA SC method can be validated on a few samples at a field site use of a CA SC approach is supported. I suggest a pathway for validation of CA SC in Figure 24. In the flowchart, the items to the left are generally indicative of actions or data sources. Items to right are more representative of decision points or findings.

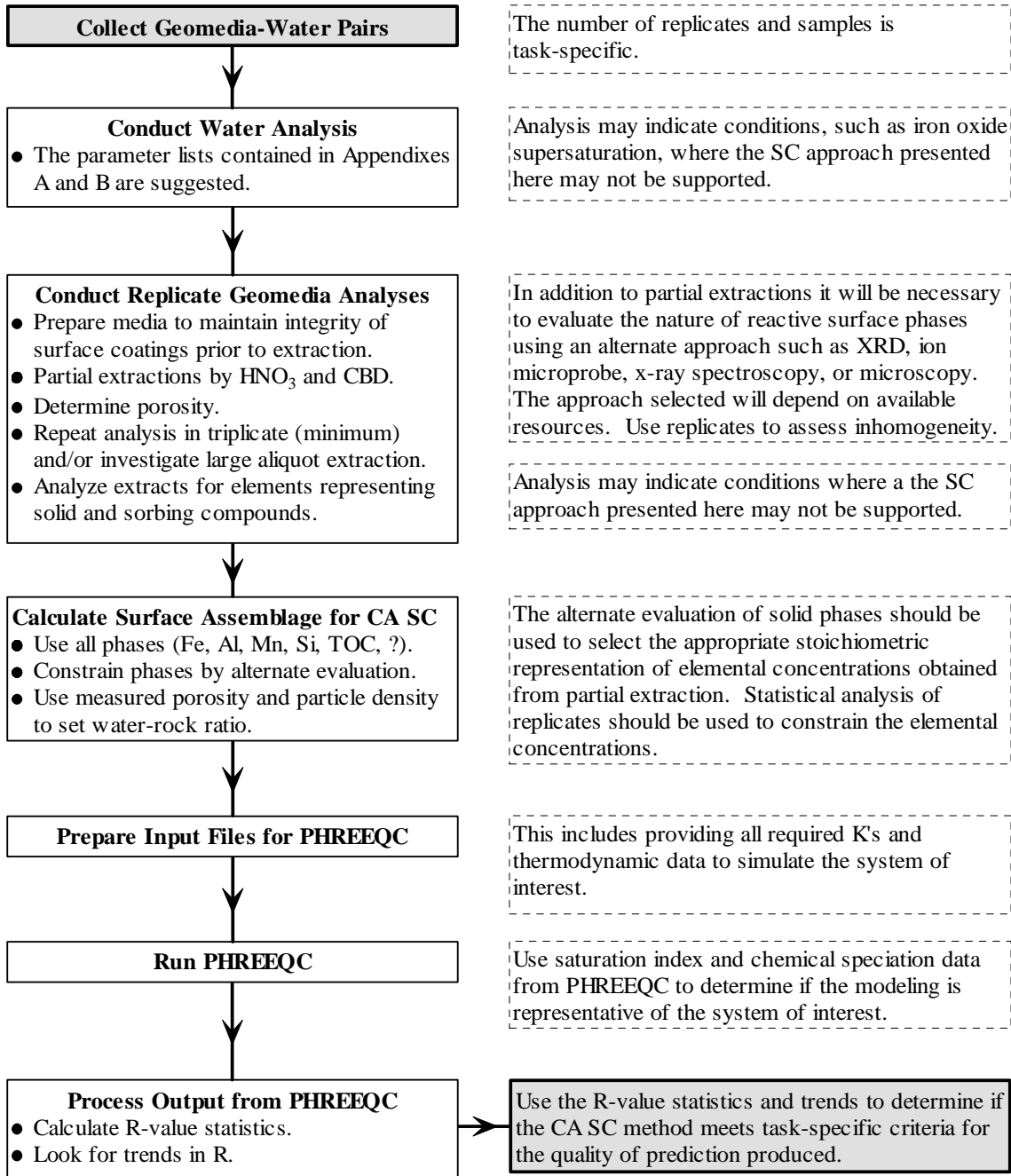


Figure 24. Flowchart for initial application of a surface complexation component additivity modeling approach to a field site.

CHAPTER 6

RECOMMENDATIONS FOR FUTURE WORK

Specific recommendations for future efforts are:

1. A higher level of validation of partial extractions to support surface complexation models in the field is needed. Combination of partial extractions with observations at the atomic scale would explore what is really removed from the surface by the extraction. The Rio Salado is an unusually simple system for testing of mechanistic approaches to the modeling of arsenic attenuation. It would be worthwhile to continue examination of Rio Salado sediments at the atomic scale.
2. Additional testing of CA SC modeling in natural systems would be useful. This should be advanced in parallel with the development of protocol for field data collection used in support of geochemical modeling, specifically sediment characterization in support of surface complexation modeling.
3. Evaluation of surface complexation of individual arsenic species was not explored explicitly here. Arsenic species competition with each other has been explored empirically, but not computationally. It would be useful to compare observation to modeling for arsenic species competitive complexation as influenced by Redox and pH.
4. Given the demonstrated importance of silicate and carbonate species in competitive complexation, and the very few studies to develop K_{int} for these species, additional

studies are warranted. This also applies to many other common anions and cations that are not well represented in the literature.

5. Rather than the difficult quantification of specific mineral species it may be fruitful to use a chemical site approach to determining surface properties from partial extraction data. Because the extract data supplies elemental values, the concept of representing the surface as a combination of aluminol-, silinol-, or ferrinol-like sites may be a more realistic approach.
6. Intermediate to laboratory batch reaction studies that provide mineral specific K's and the application of the CA SC approach to the field are flow-through reactors. Column studies of natural and synthetic materials are suited to surface complexation modeling approaches. Column studies of Rio Salado and synthetic materials would provide a wealth of information on the surface complexation of arsenic.

CHAPTER 7 CONCLUSIONS

The conclusions I reached are:

1. The surface complexation approach used here was able to model the actual concentrations of arsenic present on Rio Salado and Florida sediments to about \pm 50%. Considering that surface complexation modeling is a developing science, this is a success.
2. A component-additivity surface complexation model can predict arsenic environmental distribution using relatively simple field and laboratory techniques, public domain models, and surface complexation modeling parameters obtained from the literature.
3. Common compounds such as silica and bicarbonate will strongly affect surface complexation of arsenic by competition for sorption sites. The conceptual model for field application should consider competitive complexation of carbonate and silica.
4. Incorrect definition of the solid phase provides the greatest level of error in the modeling process (orders of magnitude). The solid phase used in the model should be selected using multiple methods of identification or inference.
5. It is difficult to select an appropriate extraction method prior to modeling the data. The extraction method must be selected based on the intended use of the model. I found that the HNO_3 extraction gave the best overall performance.

6. The K_{int} values chosen have a strong effect on simulation results. Care must be used in selection of K_{int} from the literature.
7. The component additivity model approach was transferable. Modeling arsenic surface complexation using the component additivity approach was successful at Rio Salado. With exception of one sample, the Rio Salado component additivity method predicted the arsenic concentration on sediments at two contaminated sites in Florida.

REFERENCES CITED

1. Journal of AWWA. 1994. In Search of an Arsenic MCL. Journal AWWA. September 1994. p.43.
2. U.S. Environmental Protection Agency. 1998. IRIS Substance File: Arsenic, Inorganic. Integrated Risk Information System.
<http://www.epa.gov/ngispgm3/iris/subst/0278.htm>
3. National Academy of Sciences. March 1999. Arsenic in Drinking Water. Subcommittee on Arsenic in Drinking Water, Committee on Toxicology, Board on Environmental Studies and Toxicology, Commission on Life Sciences, National Research Council. National Academy Press, Washington, D.C.
4. Reid, J. 1994. Arsenic Occurrence: USEPA Seeks A Clearer Picture. Journal AWWA. September 1994. pp. 44-51.
5. Korte, N.E., 1991. Naturally Occurring Arsenic in the Groundwaters of the Midwestern United States. Environ. Geol. Water Sci. 18:137-141.
6. Welch, A. H., M.S. Lico, J.L. Hughs. 1988. Arsenic in the Groundwater of the Western United States. Ground Water 26(3):333-347.
7. Welch, A. H., and Lico, M. S, 1998, Factors Controlling As and U in Shallow Ground Water, Southern Carson Desert, Nevada: Applied Geochemistry, 13:521-539.
8. U.S. Geological Survey. 1994. Arsenic Contamination in the Whitewood Creek-Belle Fourche River-Cheyenne River System, Western South Dakota, Bibliography of Publications From the Toxic Substances Hydrology Program. U.S. Geological Survey Open-File Report 94-91.
9. Aurillo, A.C., R.P. Mason and H.F. Hemond. 1994. Speciation and Fate of Arsenic in Three Lakes of the Aberjona Watershed. Environ. Sci. Technol. 28:577-585.
10. Azcue, J.M. and J.O. Nriagu. 1993. Arsenic Forms in Mine Polluted Sediments of Moira Lake, Ontario. Environ Int. 19(4):405-416.
11. Baker, L.A., T.M. Qureshi, and M.M. Wyman. 1998. Sources and Mobility of Arsenic in the Salt River Watershed, Arizona. Water Resources Research 34(6):1543-1552.
12. Howard, A.G., M.H. Arbab-Zavar, and S. Apte. 1982. Seasonal Variability of Biological Arsenic Methylation in the Estuary of the River Beaulieu. Marine Chemistry. 11:493-498.
13. Maher, W.A. 1984. Mode of Occurrence and Speciation of Arsenic in Some Pelagic and Estuarine Sediments. Chemical Geology, 47:333-345.
14. Hering, J.G., and J. Wilkie. 1996. Arsenic Geochemistry in Source Waters of the Los Angeles Aqueduct. Preliminary Report to the Water Resources Center, University of California, Davis.
15. Shevenell, L., K.A. Conoors, and C.D. Henry. 1999. Controls on Pit Lake Water Quality At Sixteen Open-Pit Mines in Nevada. Applied Geochemistry, 14(5): 669-687.

16. Langmuir, D. 1997. *Aqueous Environmental Geochemistry*. Prentice Hall, New Jersey.
17. Korte, N.E. and Q. Fernando. 1991. A Review of As(III) in Groundwater. *Critical Reviews in Environmental Control*. 21:1-39.
18. Bhattacharya, P., A. Sracek, and G. Jacks. 1998. Groundwater Arsenic in Bengal Delta Plains: Testing of Hypotheses. *Dhaka Conference on Arsenic*. February, 1998.
18. Davis, J.A., R.O. James and J.O. Leckie. 1978. Surface Ionization and Complexation at the Oxide/Water Interface: I. Computation of Electrical Double Layer Properties in Simple Electrolytes. *J. Coll. Inter. Sci.* 63:480-499.
19. Davis, J.A and J.O. Leckie. 1978. Surface Ionization and Complexation at the Oxide/Water Interface: II. Surface Properties of Amorphous Iron Oxyhydroxide and Adsorption of Metal Ions. *J. Coll. Inter. Sci.* 67:90-107.
20. Dzombak, D.A. and F.M.M. Morel. 1990. *Surface Complexation Modeling: Hydrous Ferric Oxide*. John Wiley and Sons, New York.
21. Davis, J.A., Kent, D.B., 1990. Surface Complexation Modeling in Aqueous Geochemistry. in: Hochella, M. F., Jr., White, A. F., Ribbe, P. H. (Eds). *Reviews in Mineralogy: Mineral-Water Interface Geochemistry*, Vol. 23. Mineralogical Society of America, Washington D.C., pp. 177-248 (Chapter 5).
22. Hochella, M.F., Jr., White, A.F, 1990. Mineral-Water Interface Geochemistry: An Overview. in: Hochella, M. F., Jr., White, A. F., Ribbe, P. H. (Eds). *Reviews in Mineralogy: Mineral-Water Interface Geochemistry*, Vol. 23. Mineralogical Society of America, Washington D.C., pp. 1-15 (Chapter 1)
23. Hemond, H.F., 1995. Movement and Distribution of Arsenic in the Aberjona Watershed. *Environmental Health Perspectives*. Vol 103, Supp. 1, February.
23. Stumm, W. 1992. *Chemistry of the Solid-Water Interface*. John Wiley and Sons, Inc. Wiley-Interscience Publication. New York. 428 Pages.
24. Sadiq, M. 1997. Arsenic Chemistry in Soils: An Overview of Thermodynamic Predictions and Field Observations. *Water, Air, and Soil Pollution* 93:117-136.
25. Belzile, N. and A. Tessier. 1990. Interactions Between Arsenic and Iron Oxyhydroxides in Lacustrine Sediments. *Geochimica et Cosmochimica Acta* 54:103-109.
26. Manning, B.A., Goldberg, S., 1996. Modeling Competitive Adsorption of Arsenate with Phosphate and Molybdate on Oxide Minerals. *Soil Soc. Am. J.* (60):121-131.
27. Manning, B.A., Goldberg, S., 1997. Arsenic(III) and Arsenic(V) Adsorption on Three California Soils. *Soil Science*, V. 162(12) p.886-895.
28. Wang, F. Chen, J., Forsling, W., 1997. Modeling Sorption of Trace Metals on Natural Sediments by Surface Complexation Model. *Environ. Sci. Technol.* 31:448-453.
29. Turner, D.R. and R. T. Pabalan. 1999. Abstraction of Mechanistic Sorption Model Results for Performance Assessment Calculations At Yucca Mountain, Nevada. *Waste Management*. 19:375-388.
30. Tessier, A., D. Fortin, N. Belzile, R. R. Devitre, and G. G. Leppard, 1996. Metal Sorption To Diagenetic Iron and Manganese Oxyhydroxides and Associated Organic Matter: Narrowing the Gap Between Field and Laboratory Measurements. *Geochimica et Cosmochimica Acta*, 60(3):387-404.

31. Mok, W. M., and Wai, C. M., 1990, Distribution and Mobilization of Arsenic and Antimony Species in the Cour D'Alene River, Idaho: *Environ. Sci. Technol.*, 24:102-108
32. Chappell, W. R., C. O. Abernathy, C. R. Cothorn. 1994. Arsenic Exposure and Health. *Science and Technology Letters*. Northwood. 318 p.
33. Chen, S. L., S. R Dzung, M. H. Yang, K. H. Chiu, G. M. Shieh, and C. M. Wal. 1994. Arsenic Species in Groundwaters of the Blackfoot Disease Area, Taiwan. *Environ. Sci. Technol.* 28(5):877-881.
34. Mushak, P. 1994. Arsenic and Human Health: Some Persisting Scientific Issues. *Arsenic Exposure and Health. Science and Technology Letters*. Northwood, pp. 305-318
35. Soussan, T. 1997a. Arsenic Study Nearly Finished. *Albuquerque Journal*, January 21, 1997, Sec. C, p.1.
36. Cullen, W.R., and K.J. Reimer. 1989. Arsenic Speciation in the Environment. *Chem. Rev.* 89:713-764.
36. Soussan, T. 1997b. Arsenic Levels in River Over Isleta Standard. *Albuquerque Journal*, December 13, 1997, Sec. C, p.1.
37. Los Angeles Department of Water and Power . 1997. Arsenic Removal Strategies. <http://www.ladwp.com/bizserv/water/quality/topics/arsenic/arsenic.htm>
38. Goldberg, S. 1998 Ion Adsorbtion At the Soil Particle-Solution Interface: Modeling and Mechanisms. in *Structure and Surface Reactions of Soil Particles*, P.M. Huang Ed. pp 378-408. Wiley and Sons, New York.
39. Onishi, H., and Sandell, E. B., 1955, *Geochemistry of Arsenic: Geochimica et Cosmochimica Acta*, 7:1-33.
40. Rice, K.C. 1999. Trace-Element Concentrations in Streambed Sediment Across the Conterminous United States. *Environ. Sci. Technol.* 33:2499-2504.
41. Focazio, M.J., A.H. Welch, S.A Watkins, D.R. Helsel, and M.A. Horn. 2000. A Retrospective Analysis on the Occurrence of Arsenic in Ground-Water Resources of the United States and Limitations in Drinking-Water-Supply Characterizations. *Water Resources Investigations Report 99-4279*. U.S.G.S. and U.S. Dept. of the Interior. 27 p.
42. Gailer, J. and K.J. Irgolic. 1994. The Ion-Chromatographic Behavior of Arsenite, Arsenate, Methylarsonic Acid and Dimethylarsinic Acid on the Hamilton PRP-X100 Anion-Exchange Column. *Applied Organometallic Chemistry*. 8:129-140.
43. Hasegawa, H., M. Masakazu, S. Okamura, M. Hojo, N. Iwasaki, and Y. Sohrin. 1999. Arsenic Speciation Including 'Hidden' Arsenic. *Applied Organometallic Chemistry*. 13:113-119
44. Hasegawa, H., Y.S. Sohrin, M. Matsui, M. Hojo, and M. Kawashima. 1994. Speciation of Arsenic in Natural Waters by Solvent Extraction and Hydride Generation Atomic Absorption Spectrometry. *Analytical Chemistry*, Vol. 66, No. 19, pp. 3247-3252.
45. Nimick, D.A. 1998. Arsenic Hydrogeochemistry in An Irrigated River Valley: A Reevaluation. *Ground Water*, 36(5):743-753.
46. Eaton, A., H.C. Wang, and J. Northington. 1998. *Analytical Chemistry of Arsenic in Drinking Water*. AWWA Research Foundation and American Water Works Association, Denver.

47. Hydrogeologic, Inc., Allison Geoscience Consultants, Inc., 1998. MINTEQA2/PRODEFA2, A Geochemical Assessment Model for Environmental Systems: User Manual Supplement for Version 4.0. Herndon, VA and Flowery Branch, GA.
48. Wilkie, J.A. and J.G. Hering. 1998. Rapid Oxidation of Geothermal Arsenic(III) in Streamwaters of the Eastern Sierra Nevada. *Environ. Sci. Technol.* 32:657-66.
49. Bowell, R.J. 1994. Sorption of Arsenic By Iron Oxides and Oxyhydroxides in Soils. *Applied Geochemistry* 9:279-286.
50. Swedlund, P.J. and J.G. Webster. 1999. Adsorption and Polymerisation of Silicic Acid on Ferrihydrite, and Its Effect on Arsenic Adsorption. *Wat. Res.* 33(16):3413-3422.
51. Stauffer, R.E. and J.M. Thompson. 1984. Arsenic and Antimony in Geothermal Waters of Yellowstone National Park, Wyoming, U.S.A. *Geochimica et Cosmochimica Acta.* 48:2547-2561.
52. Cherry, J.A., A.U. Shaikh, D.E. Tallman, and R.V. Nicholson. 1979. Arsenic Species As An Indicator of Redox Conditions in Groundwater. *J. Hydrol.* 45:373-392
53. Lindberg, R.D. Runnels, D.D., 1984. Ground Water Redox Reactions: An Analysis of Equilibrium State Applied to Eh Measurements and Geochemical Modeling. *Science*, 225(31):925-927.
54. Holm, T.R., Curtiss, C.D., 1989. A Comparison of Oxidation-Reduction Potentials Calculated From the As(V)/As(III) and Fe(III)/Fe(II) Couples With Measured Platinum-Electrode Potentials in Groundwater. *J. Contaminant Hydro.* 5:67-81.
55. Holm, T.R., M.A. Anderson, R.R. Stanforth, and D.G. Iverson. 1980. the Influence of Adsorption on the Rates of Microbial Degradation of Arsenic Species in Sediments. *Limnol. Oceanogr.* 25(1):23-30.
56. Deuel, L.E., and A.R. Swoboda. 1972. Arsenic Solubility in a Reduced Environment. *Soil Sci. Soc. Amer. Proc.* 36:276-278.
57. Elkhatib, E.A., O.L. Bennett, and R.J. Wright. 1984. Kinetics of Arsenite Sorption in Soils. *Soil Sci. Soc. Am. J.* 48:758-762.
58. Ford, C.J., J.T. Byrd, J.M. Grebmeier, R.A. Harris, R.C. Moore, S.E. Madix, K.A. Newman, and C.D. Rash. 1996. Final Project Report on Arsenic Biogeochemistry in the Clinch River and Watts Bar Reservoir, Volume 1 ORNL/ER-206/V1/H3.
59. Bowell, R J. 1992. Supergene Gold Mineralogy At Ashanti, Ghana: Implications for the Supergene Behavior of Gold. *Mineralogical Magazine* 56:545-560.
60. Braman, R.S. and C.C. Foreback. 1973. Methylated Forms of Arsenic in the Environment. *Science* 182:1247-1249.
62. Nriagu, J.O. and J. M. Azcue. 1989. Food Contamination with Arsenic in the Environment. National Water Research Institute. Burlington, Ontario, Canada. February, 1989.
63. Welch, A.H. and M.S. Lico. 1998. Factors Controlling As and U in Shallow Ground Water Southern Carson Desert, Nevada. *Applied Geochemistry* 13:521-539.
64. Kuwabara, J.S. 1992. Associations Between Benthic Flora and Diel Changes in Dissolved Arsenic, Phosphorus, and Related Physico-Chemical Parameters. *Journal of North American Benthological Society* 11(2):218-228.
65. Hess, R.E. and R.W. Blanchar. 1976. Arsenic Stability in Contaminated Soils. *Soil Sci. Soc. Am. J.* 40:847-852.

66. Hem, J. D. 1970. Study and Interpretation of the Chemical Characteristics of Natural Waters. U. S. Geological Survey. Water-Supply Pap. 1473. 363 p.
67. Morgan, J.J. 1999. Introduction of Werner Stumm. Geochemistry in Aqueous Systems. *Geochimica et Cosmochimica Acta*. 63(19/20):Viii-X.
68. Parkhurst, D.L. 1995. Users Guide to PHREEQC - A Computer Program for Speciation, Reaction-Path, Advective-Transport, and Inverse Geochemical Calculations. US Geological Survey Water-Resources Investigations Report 95-4227, 143 p.
69. Parkhurst, D.L., Thorstenson, D. C., and L.N. Plummer. 1980. PHREEQE -A Computer Program for Geochemical Calculations. US Geological Survey Water-Resources Investigations 80-96, 210 p.
70. Kimball, A.K., Broshears, R.E., Bencala, K.E., Mcknight, D.M., 1994. Coupling of Hydrologic Transport and Chemical Reactions in Stream Affected By Acid Mine Drainage. *Environ. Sci. Technol.*, 28(12):2065-2073.
71. Westall, J. and H. Hohl. 1980. A Comparison of Electrostatic Models for the Oxide/Solution Interface. *Advances in Colloid and Interface Science*. 12:265-294.
72. Smith, S.L., Jaffe, P.R., 1998. Modeling the Transport and Reactions of Trace Metal in Water Saturated Soils and Sediments. *Water Res. Research*, 34(11):3135-3147.
73. Eary, L.E., 1999. Geochemical and Equilibrium Trends in Mine Pit Lakes. *Applied Geochemistry* 14(8): 963-987.
74. Brown, J.G., Bassett, R.L., Glynn, P.D., 2000. Reactive Transport of Metal Contaminants in Alluvium-Model Comparison and Column Simulation. *Applied Geochemistry* 15(1):35-49.
76. Livesey, N.T. and P.M. Huang. 1981. Adsorption of Arsenate by Soils and Its Relation to Selected Chemical Properties and Anions. *Soil Sci.* 131:88-94.
77. Brockbank, C.I., G.E. Batley, and G. K-C Low. 1988. Photochemical Decomposition of Arsenic Species in Natural Water. *Environmental Technology Letters*. 9:1361-1366.
78. Garland, T.R., R.E. Wildung, and H.P. Harbert. 1983. Influence of Irrigation and Weathering Reactions on the Composition of Percolates from Retorted Oil Shale in Field Lysimeters. Pacific Northwest Laboratories. Richland, Washington. Oct. 1983.
79. Qafoku, N.P., U.Kukier, M.E. Sumner, W.P. Miller, and D.E. Radcliffe. 1997. Sulfate and Phosphate Displacement of Arsenic from Fly Ash Amended Soil. *Proceedings of the 1997 Georgia Water Resources Conference*. pp 516-517.
80. Goldberg, S. 1991. Sensitivity of Surface Complexation Modeling To the Surface Site Density Parameter. *Journal of Colloid and Interface Science*. 145(1):1-9.
81. Ghosh, M.M., Yuan J.R., 1987. Adsorption of Inorganic Arsenic and Organoarsenicals on Hydrous Oxides. *Environmental Progress* 6(3):150-157.
82. Cox, C.D., Ghosh, M.M., 1994. Surface Complexation of Methylated Arsenates by Hydrous Oxides. *Water Resources* 28(5):1181-1188.
83. Aggett, J. and G.A. O'Brien. 1985. Detailed Model for the Mobility of Arsenic in Lacustrine Sediments Based on Measurements in Lake Ohakuri. *Environ. Sci. Technol.* 19:231-238.
84. Kheboian, C. and F. Bauer. 1987. Accuracy of Selective Extraction Procedures for Metal Speciation in Model Aquatic Sediments. *Anal. Chem.* 59:1417-1423.

85. Jackson, M.L., and L.W. Zelazny. 1986. Oxides, Hydroxides, and Aluminosilicates. in *Methods of Soil Analysis, Part 1. Physical and Mineralogical Methods*. Second Edition, Agronomy Monograph No. 9. Arnold Klute, Ed. pp. 101-148.
86. Waychunas, G.A., B.A. Rea, C.C. Fuller, and J.A. Davis. 1992. Surface Chemistry of Ferrihydrite: Part 1. EXAFS Studies of the Geometry of Coprecipitated and Adsorbed Arsenate. *Geochimica et Cosmochimica Acta*. 57:2251-2269.
87. Manning, B.A., Goldberg, S., 1996. Modeling Arsenate Competitive Adsorption on Kaolinite, Montmorillonite and Illite. *Clays and Clay Minerals*. 44(5):609-623.
88. Kempton, J.H., W. Locke, D. Atkins, and A. Nicholson. 2000. Probabilistic Quantification of Uncertainty in Predicting Mine Pit-Lake Water Quality. *Mining Engineering*. 10:59-64.
89. Miller, G. P., 2000. Prediction of the Environmental Mobility of Arsenic: Evaluation of a Mechanistic Approach to Modeling Water-Rock Partitioning. EPRI, Palo Alto, CA 2000. Doc. No. 1000547.
90. Jain, A. and R. H. Loeppert. 2000. Effect of Competing Anions on the Adsorption of Arsenate and Arsenite by Ferrihydrite. *Journal of Environmental Quality* 29(5):1422-1430.
91. Manning, B.A., Fendorf, S.E., Goldberg, S., 1998. Surface Structures and Stability of Arsenic(III) on Goethite: Spectroscopic Evidence for Inner-Sphere Complexes. *Environ. Sci. Technol.* 32:2383-2388.
92. Bethke, C.M., and P.V. Brady. 2000. How the Kd Approach Undermines Groundwater Cleanup. *Ground Water*, 38(3):435-443.
93. Rakovan, J., Becker, U., Hochella, M.F., Jr., 1999. Aspects of Goethite Microtopography, Structure, Chemistry, and Reactivity. *American Mineralogist*. 84:884-894.
94. Felmy, A.R. and J.R. Rustad. 1998. Molecular Statics Calculations of Proton Binding To Goethite Surfaces: Thermodynamic Modeling of the Surface Charging and Protonation of Goethite in Aqueous Solution. *Geochimica et Cosmochimica Acta* 62(1):25-31.
95. Ficklin, W. H. 1983. Separation of Arsenic(III) and Arsenic(V) in Ground Waters By Ion Exchange. *Talanta*. 30(5):371-373.
96. Meng, X. and R.D. Letterman. 1993. Modeling Ion Adsorption on Aluminum Hydroxide Modified Silica. *Environ. Sci. Technol.* 27(9):1924-1929.
97. Hiemstra, T. and W.H. Van Riemsdijk. 1995. A Surface Structural Approach To Ion Adsorption: the Charge Distribution (CD) Model. Dept. of Soil Science and Plant Nutrition, Wageningen Agricultural University, the Netherlands. pp. 488-143.
98. Hiemstra, T. and W.H. Van Riemsdijk. 1998. Surface Structural Ion Adsorption Modeling of Competitive Binding of Oxyanions By Metal (Hydr)Oxides. Dept. of Environmental Sciences, Wageningen Agricultural University, the Netherlands. pp. 182-193.
99. Herbelin, A.L., Westall, J.C., 1999 FITEQL 4.0 - A Computer Program for Determination of Chemical Equilibrium Constants From Experimental Data. Report 99-01, Department of Chemistry, Oregon State University, Corvallis.
100. Davis, J.A., J.A. Coston, D.B. Kent, and C.C. Fuller. 1998. Application of the Surface Complexation Concept to Complex Mineral Assemblages. *Environ. Sci. Technol.* 32(19):2820-2828.

101. Cherry, J.A., Morel, F.M.M., Rouse, J.V., Schnoor, J.L., Wolman, M.G., 1986. Hydrogeochemistry of Sulfide and Arsenic-Rich Tailings and Alluvium Along Whitewood Creek, South Dakota, (Parts 1,2,3), in: Mineral and Energy Resources: A Review of Developments, Colorado School of Mines. 29(4), July 1986.
102. Meng, X., Letterman, R.D., 1996. Modeling Cadmium and Sulfate Adsorption By Fe(OH)₃/SiO₂ Mixed Oxides Water Research, V.30(9) p.2148-2154.
103. Goldberg, S., 1985. Chemical Modeling of Anion Competition on Goethite Using the Constant Capacitance Model. Soil Sci. Soc. Am. J 49:851-856.
104. Coston, J.A., C.C. Fuller, and J.A. Davis. 1995. Pb²⁺ and Zn²⁺ Adsorption by a Natural Aluminum- and Iron-Bearing Surface Coating on an Aquifer Sand. Geochimica et Cosmochimica Acta. 59(17):3535-3547.
105. Meng, X. and R.D. Letterman. 1993. Effect of Component Oxide Interaction on the Adsorption Properties of Mixed Oxides. Environ. Sci. Technol. 27(5):970-975.
106. Welch, D.M., 1999. Arsenic Geochemistry of Stream Sediments Associated With Geothermal Waters At the La Primavera Geothermal Field, Mexico. Master of Science Thesis, New Mexico Institute of Mining and Technology, Socorro, New Mexico.
107. Prol-Ledesma, R.M., S.I. Hernandez-Lombardini and R. Lozano-Santa Cruz, 1996. Chemical Variations in the Rocks of the La Primavera Geothermal Field Related With Hydrothermal Alteration. in Press, University of Mexico, Mexico City.
108. Ramirez-Silva, G.R. 1981. Informe Climatologico De La Zona Geotermica La Primavera-San Marcos-Heveres De La Vega, Jalisco. Informe 16-81. Comisión Federal De Electricidad, Mexico, Subgerencia De Estudios Geotérmicos, Departamento De Exploración, May, 1981.
109. Ramirez-Silva, G.R. 1982. Hidrología Superficial Y Subterránea En Las Zonas Geotermicas La Primavera-San Marcos Heveres De La Vega, Jalisco. Informe 19-82. Comisión Federal De Electricidad, Mexico, Subgerencia De Estudios Geotérmicos, Departamento De Exploración, April, 1982.
110. Mahood, G.A., A.H. Truesdell, and L.A. Templos M. 1983. A Reconnaissance Geochemical Study of La Primavera Geothermal Area, Jalisco, Mexico. Journal of Volcanology and Geothermal Research. 16:247-261.
111. Alatorre-Zamora, M.A. and J.O. Campos-Enriquez. 1992. La Primavera Caldera (Mexico): Structure Inferred From Gravity and Hydrogeological Considerations. Geofisica Internacional 31(4):371-382.
112. Santoyo-Gutierrez, S.,A. Garcia, M. Morales, J. Perezvera and A. Rosas. 1991. Applied Technology in the Solution of Geothermal Drilling Problems of Deep Wells in La Primavera Caldera (Mexico). Journal of Volcanology and Geothermal Research. 47:195-208.
113. U.S. Geological Survey. 1977. National Handbook of Recommended Methods for Water Quality Data Acquisition. Office of Water Data Coordination, United States Geological Survey, Reston Virginia.
114. Maiorino, R.M. and H.V. Aposhian. 1985. Dimercaptan Metal-Binding Agents Influence the Biotransformation of Arsenite in the Rabbit. Toxicology and Applied Pharmacology. 77:240-250.

115. Onysko, S.J. and R.L. McNearny. 1997. GIBBTEQ: A MINTEQA2 Thermodynamic Error Detection Program. *Ground Water, Computer Notes* 35(5): 912-914.
116. Chen, S.L., S.R Dzen, M.H. Yang, K.H. Chiu, G.M. Shieh, and C.M. Wal. 1994. Arsenic Species in Groundwaters of the Blackfoot Disease Area, Taiwan. *Environ. Sci. Technol.* 28(5):877-88
118. Takamatsu, T., H. Aoki, and T. Yoshida. 1982. Determination of Arsenate, Arsenite, Monomethylarsonate, and Dimethylarsinate in Soil Polluted With Arsenic. *Soil Science* 133(4):239-246.
122. Tessier, A., P.G.C. Campbell, and M. Bisson. 1979. Sequential Extraction Procedure for the Speciation of Particulate Trace Metals. *Analytical Chemistry*. 51(7):844-851.
123. Chao, T.T. and L. Zhou. 1983. Extraction Techniques for Selective Dissolution of Amorphous Iron Oxides from Soils and Sediments. *Soil Sci. Soc. Am. J.* 47:225-232.
124. Grabinski, A.A. 1981. Determination of Arsenic(III), Arsenic(V), Monomethylarsonate, and Dimethylarsinate by Ion-Exchange Chromatography with Flameless Atomic Absorption Spectrometric Detection. *Analytical Chemistry*. 53:966-968.
125. Barranco, F.T., Jr., W.L. Balsam, and B.C. Deaton. 1989. Quantitative Reassessment of Brick Red Lutites: Evidence From Reflectance Spectrophotometry. *Marine Geology* 89:299-314.
126. Davies, B.E. 1974. Loss-on-Ignition as an Estimate of Soil Organic Matter. *Soil Sci. Soc. Amer. Proc.* 38:150-151.
128. Xiao-Quan, S., and C. Bin. 1993. Evaluation of Sequential Extraction for Speciation of Trace Metals in Model Soil Containing Natural Minerals and Humic Acid. *Anal. Chem.* 65:802-807.
129. Lawrence, G.H.M. 1951. *Taxonomy of Vascular Plants*. Macmillan Publ. Co., New York.
130. Mcvaugh, R. 1983. *Flora Novo-Galiciana: A Descriptive Account of the Vascular Plants of Western Mexico*. Univ. Mich. Press, Ann Arbor.
131. Pesman, M.W. 1962. *Meet Flora Mexicana*. Northland Press, Flagstaff.
132. Miller, G.P., D.I. Norman, and P.L. Frisch, 2000. A Comment on Arsenic Species Separation Using Ion Exchange. *Wat. Res.* 34(4):1397-1400.
133. Borkovec, M., Westall, J., 1983. Solution of the Poisson-Boltzman Equation for Surface Excesses of Ions in the Diffuse Layer At the Oxide-Electrode Interface. *Journal of Electroanalytical Chemistry* 150:325-337.
134. Grossl, P.R., M. Eick, D.L. Sparks, S. Goldberg, and C.C. Ainsworth, 1997, Arsenate and Chromate Retention Mechanisms on Goethite. 2. Kinetic Evaluation Using A Pressure-Jump Relaxation Technique. *Environ. Sci. Technol.* 31:321-326.
135. Van Geen, A., Robinson, A.P., Leckie, J.O., 1994. Complexation of Carbonate Species At the Goethite Surface: Implications for Adsorption of Metal Ions in Natural Waters. *Geochimica et Cosmochimica Acta*, 58(9):2073-2086.
136. U.S. Environmental Protection Agency. 1992a. Test Methods for Evaluating Solid Waste, Physical/Chemical Methods, EPA/SW-846/92.

APPENDIX A

RIO SALADO FIELD INVESTIGATIONS

A.1. SITE SELECTION

Rio Salado (Salty River), in the Bosque La Primavera (Spring Forest) conservation area 25 km west of Guadalajara, Mexico, was selected for evaluation of some of the processes controlling arsenic occurrence and transport (Figure A-1). The closest community to the field site is the village of La Primavera with less than 500 inhabitants. Rio Salado lies within a national conservation area consisting of bathing, hiking, and camping areas, a private spa, an elder hostel, hot springs, and the headwaters of the Rio Caliente-Rio Salado drainage. La Primavera was selected for study due to a number of favorable factors, including that:

1. It is a relatively undisturbed watershed with national conservation area protection, eliminating anthropogenic influences to the highest degree possible;
2. The total arsenic concentration exceeds 1 ppm, allowing reactions to be studied in detail that could be below quantification limits for other sites; and,
3. General water chemistry and geology data was available.

The site allows access to arsenic waters at the ground surface. Groundwater is shallow in the region, so groundwater investigations can be conducted less expensively. Biota can be examined for arsenic uptake and effect outside of a laboratory. Access to the site is relatively easy. Universidad Nacional Autonoma de Mexico (UNAM), Comision Federal de Electricidad (CFE) and the Comision Nacional del Agua (CNA) support and welcome investigative efforts at Rio Salado. UNAM has a program to investigate in detail the geology and hydrology in the area providing regional and site-specific supporting data and research to the project. UNAM, CFE and CNA also provide logistical support when possible. The climate is conducive to year-round research and provides for experimental stability. Having arsenic waters at the surface allows easy testing of passive, innovative, or low-cost treatment alternatives. Establishment of the Bosque La Primavera conservation area has allowed unique, multidisciplinary, research and technology development to be conducted without fear of the effects of major human encroachment on the site.

There has been little or no residential, commercial, or industrial activity within the boundaries of the watershed other than the previously mentioned recreational facilities. The Rio Salado system provides a temperature and Redox gradient along the length of its primary and secondary streams, forcing changes in surface water and sediment chemistry. Distinct changes in biotic zonation have been observed. Alluvium along and under the streams allows for shallow groundwater investigation. The physical and biologic setting is conducive to the examination of the rate of change between arsenic species.

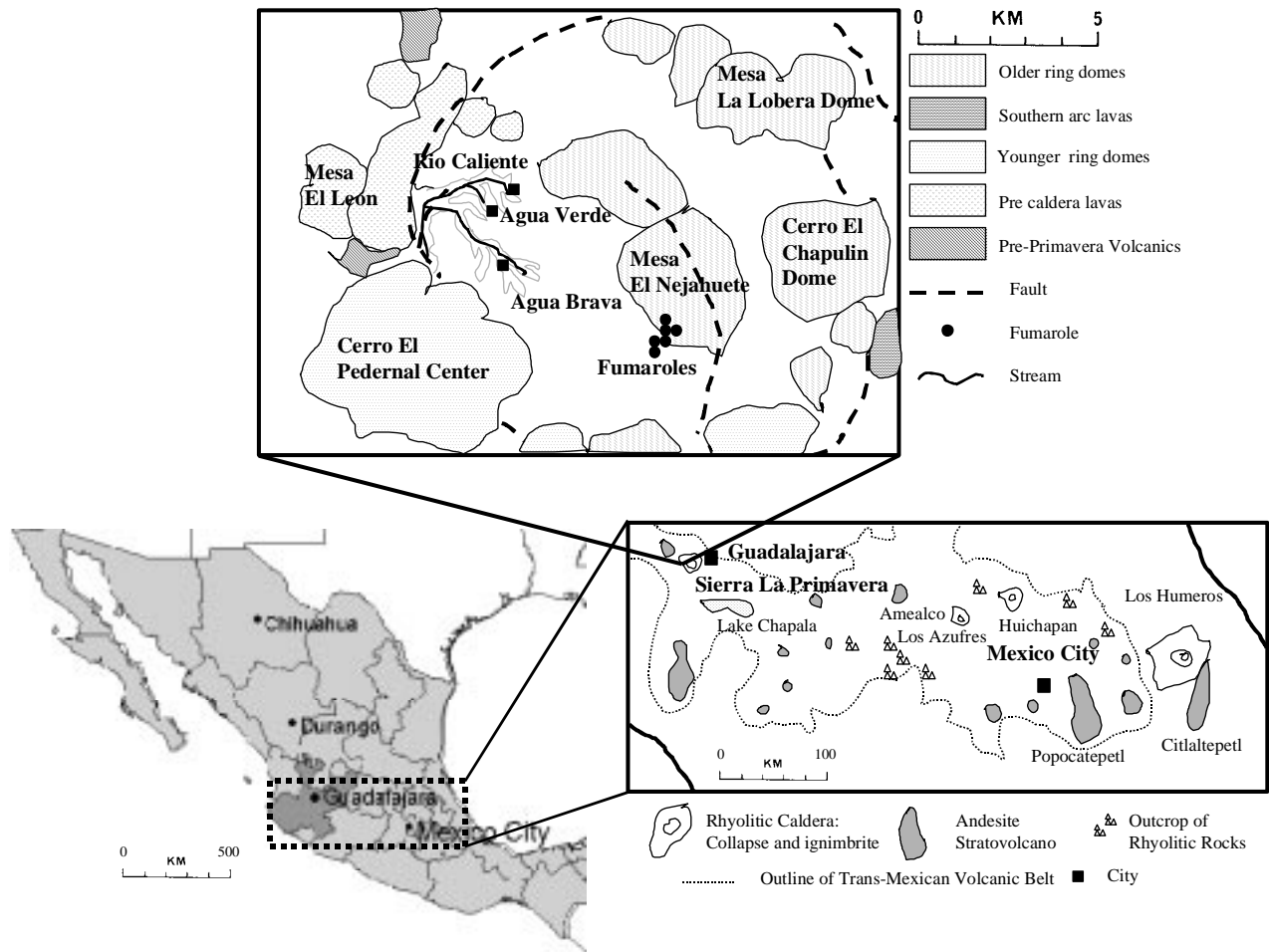


Figure A-1. Location of the La Primavera watershed and Rio Salado, Mexico

The primary source of arsenic in Rio Salado streams is geothermally impacted groundwater discharging from springs. Other sources of arsenic can include groundwater infiltrating stream channels or releases from sediments or rocks brought about by changing environmental conditions. Although there are probably some minor man-made sources of arsenic in the Rio Salado system, these sources must be quite small when compared to average concentrations in volcanic rocks and geothermal water, and the total flux of arsenic from the Rio Salado site. The waters of Rio Salado can exceed 1200 ppb total arsenic, a level well above established health thresholds. I have determined that methyl arsenic compounds are present in the Rio Caliente-Rio Salado watershed. The naturally high arsenic concentrations at Rio Salado reduce the analytical error that occurs when investigating arsenic transformation and attenuation near the limit of quantification. The high concentrations at Rio Salado may result in arsenic availability and detectability over a much greater stream reach than at many other sites, allowing the arsenic transformations to be observed in greater detail. The site naturally releases about 11,000 kg/year of arsenic to the environment.

La Primavera is composed of acidic volcanic rocks (dominantly rhyolitic) and is quite young. Caldera formation started about 150,000 years ago, with the last eruptions occurring 30,000 years ago. It is part of the Trans-Mexican Volcanic Belt, a structure that spans Mexico east to west (Figure A-1). The Trans-Mexican Volcanic Belt is a target for CFE's geothermal power development efforts. The volcanic rocks provide the heat source for geothermal activity and are responsible for the high levels of arsenic present in La Primavera groundwater. The springs of La Primavera surface at the western caldera rim and form Rio Caliente that drains to the Rio Salado. In this report, "Rio Salado" is used to refer to the study area. The site geomorphology is typical of faulted volcanic terrain. Topographic relief is rolling to steeply sloping in the watershed, with the watershed boundaries formed by mesas and escarpments. Elevations range from 1500 to 1600+ meters above sea level. In the areas with a sediment bottom, vegetation has stabilized sand and gravel bars. Base flow through the alluvium may represent a substantial portion of the total flow in these areas. Generally, the portion occupied by stream flow varies from <1 m to 5 m wide. Small rapids and braided stream sections are common. Air temperatures are moderate (average 20.8 °C) with little variation. The area is subject to a dry season and a wet season, with the dry season occurring in late fall through mid winter. The area receives an average of 945 mm of precipitation with evapotranspiration of 658 mm resulting in recharge to shallow groundwater.

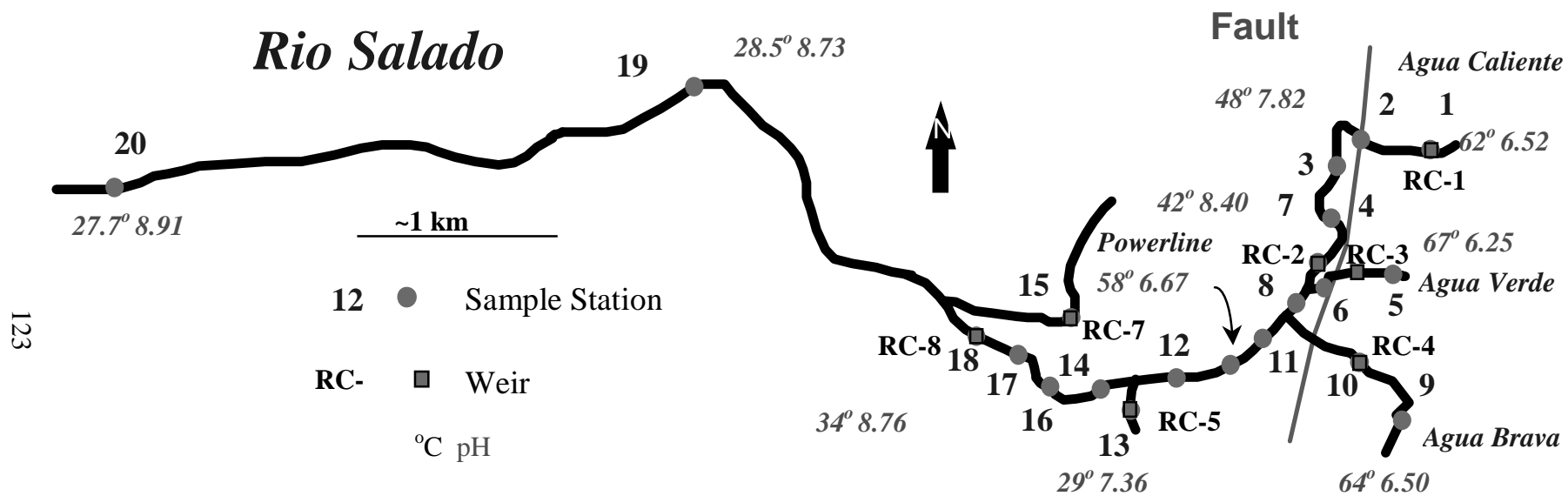
The sodium bicarbonate waters of Rio Salado are discharged from a network of thermal springs associated with a fault at approximate rates of 1-200L/s. There are four dominant point thermal discharges and numerous smaller seeps and springs. The fault is a 5 km north-south trending structure that forms the escarpment to the east of Rio Salado and is collocated with three of the four main springs. The springs discharge mixed geothermal waters that contain about 1 ppm arsenic and 100 ppm chloride versus the 14 ppm arsenic and 900 ppm chloride found in the deeper geothermal reservoir fluids. Silica content is high but precipitates found at spring mouths are carbonate (travertine). Mixing with cool, meteorically derived groundwater has taken place prior to spring discharge. Spring temperatures are variable with some approaching 70 °C, and flow from the major springs is fairly constant throughout the year. Flow and chemistry appear to be stable, over time based on review of historical data [107, 108, 109, 110, 111, 112].

Rio Caliente is the local name for the stream that forms the headwaters of Rio Salado. The four primary thermal springs of the headwater area have consistent high-arsenic, and high-temperature discharge. In the early 1980's, CFE began investigating the La Primavera geothermal field for power production. As part of the development, eight surface water flow measurement structures (sharp crested weirs) were constructed on the streams of interest to this study. These stations are numbered RC-1 through RC-8 in Figure A-2 (RC for Rio Caliente). These structures were evaluated for use as part of this project in June and July of 1997, and again in January 1998.

Currently, there are seven known flow measurement stations spread over four kilometers of stream reach. RC-6 was not found and is presumed to have been destroyed. Five of the stations are on first order streams, three of which originate from large thermal springs (RC-1, RC-3, and RC-4), two from non-thermal waters (RC-5 and RC-7). Two of the structures are on the main channel of Rio Salado (RC-2 and RC-8), a second order stream. Flow measurements were conducted by CFE during part of 1981 and 1982. The CFE data has been used for this effort when appropriate. The stations have not been maintained since that time. Although these structures require upgrades and rehabilitation, they can be restored to function, if the data would be useful. This would consist primarily of cleaning of upstream pools and fitting of new weir plates and data logging equipment.

The primary location control used for this effort is the 1:50,000 scale Cetenal Carta Geologica, Guadalajara Oeste F-13-D-65, 19 topographic and geologic map produced by Geología de México, the Mexican equivalent of the US Geological Survey. The scale limited the accuracy of position determinations. Global Positioning System (GPS) equipment was used to resolve these problems with some success. However, steep walled canyons and heavy vegetative cover limited the accuracy of GPS readings. Compass and pace methods were used to locate sample stations when difficulties arose. The subjectively best determinations were used with the base map to estimate the distance between sampling stations. It is estimated that the maximum error in any sample station's location is ± 30 m. Stream kilometer was set to zero at the northern most sample location, Station 1, the headwaters of Rio Salado.

Sampling points used for the reconnaissance sampling (Stations 1-20 and Agua Dulce) are described in Table A-1 and depicted in Figure A-2. Some explanation of the nomenclature used here might be useful. The headwaters and upper watershed of Rio Salado lie in the Bosque de La Primavera, a national conservation area. Locally, the headwaters of Rio Salado are known as Rio Caliente and the northernmost spring as Agua Caliente. Three major thermal springs enter Rio Caliente from the east. CFE does not name the northern most spring, and uses Arroyo Agua Brava for the middle spring and Agua Verde for the southern spring. Mahood [110] refers to the northern spring as Rio Caliente, the middle as Agua Brava, and Arroyo Verde to the south. The nomenclature used here is that used locally and by UNAM staff and students. Agua Caliente is used for the headwaters spring, moving south from the headwaters the names used in order are Agua Verde then Agua Brava. Powerline is used for a major thermal spring that is not mentioned in the literature. La Primavera, Rio Salado, and Rio Caliente can be used interchangeably in the current study area.



123

Figure A-2. Rio Salado sampling stations, January 1998.

Table A-1. Rio Salado sampling and measurement station locations.

Station	Description	Use
1	Rio Salado-Rio Caliente headwaters sampling station. Stream kilometer 0.0. Samples taken just below weir. Sand and gravel bottom. Little or no algae or in-stream vegetation. Rio Caliente of Mahood [110].	Water samples. Tracer test injection point.
2	On Rio Salado. Broad sand and gravel bottom. Abundant brown and green algae.	Water samples. Tracer test monitoring.
3	On Rio Salado just upstream of concrete bridge into Rio Caliente Spa. Gravel and cobble bottom. Abundant brown and green algae. Sampled twice, once early morning once in the afternoon.	Water samples. Tracer test monitoring. Flow measurement.
4	On Rio Salado downstream of spa. Broad sand and gravel bottom. Sparse brown and green algae. Stream braided with plants established on sandbars	Water samples. Tracer test monitoring.
5	Headwaters of Agua Verde. Rock and gravel bottom. Under trees. Sprigs issue from network of rock openings. Sample taken from largest and hottest thermal source. Agua Brava of Mahood, 1983. No algae at sample location.	Water samples. Tracer test injection point.
6	15 meters upstream Agua Verde from confluence with Rio Salado. Rock and gravel bottom. Under trees. Abundant algae at sample location. Downstream of RC-3. Two meter waterfall 35 meters upstream.	Water samples. Tracer test monitoring.
7	On Rio Salado in upstream pool of flow structure RC-2. Rock and boulder bottom with braids, riffles, eddies and rapids upstream. No algae at sample location.	Water samples. Tracer test monitoring.
8	On Rio Salado between Agua Verde and Agua Brava confluence. Gravel bottom. Gentle steady flow. Braided stream upstream of location. Sparse algae at sample location.	Water samples. Tracer test monitoring. Flow measurement.
9	Headwaters of Agua Brava. Rock and gravel bottom. Under trees. Sample taken from well mixed location 20 meters downstream of a cluster of large thermal springs. Arroyo Verde of Mahood, 1983. Thick algae mat on bottom through entire length of stream.	Water samples. Tracer test injection point.
10	In upstream pool of flow structure RC-4 on Agua Brava. Sand, gravel and boulder bottom with braids, riffles, eddies and rapids upstream. No algae at sample location.	Water samples. Tracer test monitoring. Flow measurement.
11	On Rio Salado below Agua Brava confluence. Gravel bottom. Gentle steady flow. Algae at sample location.	Water samples. Tracer test monitoring. Flow measurement.
12	On Rio Salado below Powerline confluence, above RC-5 confluence. Gravel and bolder bottom. Rapid steady flow, riffles, eddies. Algae at sample location.	Water samples. Tracer test monitoring. Flow measurement.
13	First order stream with seep and spring source that enters Rio Salado ~100 m upstream of Station 14. 240 ppb total arsenic. May be representative of less thermal groundwater.	Water samples.
14	On Rio Salado below RC-5 confluence. Gravel bottom. Gentle steady flow, braided upstream with vegetation in sand bars. Under trees. Sparse algae at sample location.	Water samples. Tracer test monitoring.

Station	Description	Use
15	Name for total metals water sample taken at RC-7. Not used otherwise.	Water samples
16	On Rio Salado. Gravel bottom. Gentle steady flow. Sparse algae at sample location.	Water samples. Tracer test monitoring.
17	On Rio Salado. Gravel bottom. Gentle steady flow. Moderate algae at sample location.	Water samples. Tracer test monitoring.
18	On Rio Salado in pool below RC-8. Sand and gravel bottom. Gentle steady flow. Under trees. Thick black algae on stream edge. Last location for monitoring of tracer tests.	Water samples. Tracer test monitoring. Flow measurement.
19	On Rio Salado. Gravel bottom. Gentle steady flow. Sparse algae at sample location. Near small cattle operation and downstream of a public bathing area. Stream kilometer 6.6.	Water samples. Flow measurement.
20	On Rio Salado below RC-5 confluence. Sand bottom. Gentle steady flow. Near corn and sugar cane fields. Sparse algae at sample location. Stream kilometer 10.2, farthest downstream station.	Water samples. Flow measurement.
RC-1 Weir	One meter concrete sharp crested weir at the most upstream point of Rio Salado. Triangular cross section. Collocated with Station 1, monitors all Agua Caliente flow. Weir and pool are in need of rehabilitation.	Sampled for total metals several times.
RC-2 Weir	Three meter wide concrete sharp crested rectangular weir in Rio Salado rock channel. No low flow provisions. Weir and pool are in need of rehabilitation.	
RC-3 Weir	One meter rectangular weir with steel edge. Can be fitted with weir plate. Monitors all flow from Agua Verde. Pool needs cleaning.	Sampled for total metals several times.
RC-4 Weir	One meter rectangular weir with steel edge. Can be fitted with weir plate. Monitors all flow from Agua Brava. Pool needs cleaning.	Sampled for total metals several times.
RC-5 Weir	One meter rectangular weir with steel edge. Can be fitted with weir plate. Monitors all flow from cool low arsenic spring between Stations 12 and 14. Pool needs cleaning and vegetation removal. Collocated with Station 13.	Water samples.
RC-6 Weir	Never located. Probably located at Station 14.	
RC-7 Weir	Located in drainage that enters downstream of RC-8 and Station 18. One meter triangular concrete weir. May not be repairable. Located too far upstream to capture full flow contribution to Rio Salado. Stagnant ponded condition. Station 15.	Sampled for total metals once.
RC-8 Weir	Three meter wide concrete sharp crested rectangular weir with wing walls in Rio Salado. No low flow provisions. Weir and pool are in need of serious rehabilitation. Weir undercut by stream channel across entire width. Collocated with Station 18.	
Powerline Spring	Spring that enters main channel of Rio Salado from stream bank. May be submerged in high flow conditions. Lies between Stations 11 and 12.	Sampled for total metals several times.
Agua Dulce	First order stream with seep and spring source that enters Rio Salado ~100 m upstream of Station 19. 115 ppb total arsenic. May be representative of non-thermal groundwater.	Sampled for total metals once.

A.2. STREAM FLOW

The principles of streamflow measurement are well established. Two streamflow measurement techniques were used: tracer tests, to determine average time of travel between sampling points, and a direct measurement velocity-area method that provides point-velocity measurements and calculated discharges.

A.2.1. Tracer Tests

Tracer tests track the movement and concentration of a foreign substance in a fluid to determine chemical and physical properties of the flow system. One use of tracer tests is to determine surface water travel time between two points. This is accomplished by the detection at known time and location of a tracer substance that was introduced upstream. Ideally, a tracer is not chemically reactive with the water or sediments and is easy and inexpensive to detect. Solids, liquids, and gasses have all been successfully employed as tracers. The known ideal behavior of a tracer allows the interpretation of tracer test data.

The tracer is usually dumped into the stream as rapidly as possible to provide a “slug” initial condition (instantaneous introduction of tracer). Tracer tests are subject to the influence of in-stream mixing (dispersion and diffusion components), and physical or chemical reactions (predominantly sorption). Because of these influences, the tracer spreads out from its initial highly concentrated slug into an elongated parcel of water, where tracer concentrations diminish to zero at the upstream and downstream edges, with size constantly increasing as it moves downstream. The concentration tail later can be quite long. Tracer determinations of velocity provide the range of possible stream velocities during the test. The velocity determined from first detection of the tracer approximates the behavior of a small parcel of water that has always taken the fastest route downstream. The velocity associated with the concentration peak approximates the velocity of the average parcel of water in the stream. Velocities determined from the late-time tail represent parcels of water that were trapped or retarded in their movement downstream. A precise and accurate tracer test can be used to determine a probability distribution of travel times, or quantify diffusion, dispersion, and sorption parameters. These parameters may be necessary for detailed evaluation of in-stream chemical evolution.

Tracer tests were conducted on January 12 and 13, 1998 after all sampling had been completed. The tracer tests were intended to support investigation of arsenic speciation kinetics and provide data for the design of future experiments at Rio Salado. Some questions cannot be answered by velocity-area discharge determination investigations as easily and/or as well as by tracer tests. Specifically:

1. What is the general range of streamflow velocities at the site?
2. What are the fast, average, and slow travel times between sampling stations?
3. Qualitatively, what is the mixing length, time, area, and volume of a slug injection as it moves downstream?

Time and budget constraints would not allow use of sophisticated tracer detection methods, such as quantitative fluorescence, nor were they necessary for the given purposes. Tracer tests were limited to the upper 4 km of the watershed, e.g. upstream of

Station 18. Two types of tracers were used, fluorescent dyes and sodium chloride. The detection methods used were qualitative visual detection of fluorescent dyes and detection of changes in conductivity caused by introduction of the salt.

A.2.1.1 Dye Tests

Three individual dye tests were conducted. Agua Brava and Agua Verde were traced from their respective sources to the junctions with Rio Salado on January 12. The main channel test, from Station 1, Agua Caliente, to Station 18, was completed on January 13. The dyes used were 51 wt. % Rhodamine WT and 78 wt. % fluorescein supplied by the Ben Meadows company. Fluorescein was used for Agua Brava and Agua Verde, and Rhodamine WT was used for the main channel test. Permission to conduct the tests was provided verbally by Oscar A. Escolero Fuentes of CNA, Mexico City. The use of two dyes was planned to compare visual effectiveness, and guard against possible interference or misinterpretation. Sufficient dye was used to ensure visual detection for the entire duration of the test, two liters of Rhodamine WT for the main channel and 0.5 liter Fluorescein for each Agua Verde and Agua Brava. Fluorescein was by far the superior dye for visual detection in Rio Salado at base flow. Subjective visual estimation of dye concentration and wristwatches were used to determine travel times between stations for the first dye arrival, approximate dye centroid, and length of the tail. Not all stations had all measurements. The travel times and calculated velocities determined from the dye tracer tests are given in Table A-2.

A.2.1.2 Sodium Chloride Test

The sodium chloride (salt) tracer test was conducted at the same time as the main channel Rhodamine WT tracer test. The test was conducted by introducing 40 liters of saturated salt solution (~350g/L at 20°C) that was prepared from common processed water softener rock salt and Type II water. The need for this amount of salt solution was based on desiring a 30% increase over background conductivity at Station 18, assuming that a dilution of 1:2000 would occur over the stream reach. The salt solution was introduced at the same time as the two liters of Rhodamine WT for the dye tracer test. The travel times and calculated velocities determined from the salt tracer test are given in Table A-2.

A.2.2. Velocity-Area Method

The velocity-area method is a direct measurement of stream velocity taken with a paddle-wheel current meter, and a stopwatch. In combination with cross-sectional area measurements this method can be used to calculate discharge. Velocities determined in this manner are generally not representative of travel times. The ideal stream section in which to use the velocity-area method is a straight stream channel section much longer than wide, with little variation in depth, and no in-stream obstructions. Most Rio Salado locations for measurement required some accommodation from the ideal.

The current meter used was a Model F583 Price-Pygmy vertical-axis rotating element meter, SN# 4887, maintained by the New Mexico Bureau of Mines and Mineral Resources. The meter is factory calibrated with no adjustment necessary unless the meter

is damaged or extremely worn. All calibrations and repairs are made by the factory. The meter is rated to a maximum velocity of 0.76 m/s. The discharge equation used is: $V = 0.665 N + 0.04$, where V is velocity in m/s and N is the paddle-wheel revolutions per second. The discharge equation was supplied by the manufacturer and is unique to the meter. Maximum suggested stream depth for this model meter is less than 0.46 m. The stream channel is divided into equal width segments (generally 10-12) using a fiberglass tape measure. Depth measurements are taken at the midpoint of each segment using the current meter wading rod and/or a plastic ruler. Areas used are the product of the segment width and corresponding segment midpoint depth. The most accurate and recommended method for discharge determination under these conditions is to make the measurement at 0.6 of the stream total depth below the stream surface [113]. This method was used exclusively.

With the following exception, all point discharge measurements were made within the operational range of the equipment. The discharge measurements made at Station 3 are suspect. These measurements exceeded the maximum rated velocity of the meter by over 40%. Discharge and velocity measurements made on June 27-28, 1997 and January 11-13, 1998 are tabulated below (Table A-2) with flows determined in 1981-82 by CFE.

Table A-2. Point velocity and discharge values.

Station	Date	Velocity (km/h)	Discharge (m ³ /s)	Comments
RC-4	6/27/97	1.461	0.195	Upstream of weir
RC-4	6/27/97	1.367	0.195	Duplicate test
8	6/27/98	1.741	0.214	~100 m upstream of confluence of Agua Brava and Rio Caliente
6	6/28/98	0.794	0.059	Downstream RC-3
RC-8	1/12/98	1.285	0.543	Below RC-8 weir 50 m, weir washed out
19	1/11/98	1.411	0.569	At intersection of Granjas Road and Rio Salado
20	1/11/98	1.230	0.571	At intersection of El Mirador Road and Rio Salado
12 +	1/12/98	1.356	0.472	40 m downstream of Powerline Spring
11 +	1/12/98	0.959	0.443	30 m upstream of Powerline Spring
11	1/12/98	1.338	0.337	~100 m upstream of sample point 11
8	1/12/98			~100 m upstream of confluence of Agua Brava and Rio Caliente
RC-1	1/2/82	No Value	0.060	CFE
RC-2	1/2/82	No Value	0.133	CFE
RC-3	1/2/82	No Value	0.043	CFE
RC-4	1/2/82	No Value	0.156	CFE
RC-5	1/2/82	No Value	0.010	CFE
RC-6	1/2/82	No Value	0.379	CFE
RC-7	1/2/82	No Value	0.102	CFE
RC-8	1/2/82	No Value	No Value	CFE

Powerline Discharge = 0.029 m³/s

Table A-3. Tracer test flow velocities, Rio Salado, January 1998.

Station	Stream Kilometer	Observation	Velocity (km/hr)	First arrival (km/h)	Peak Dye (km/h)	Dye Tail (km/h)	Salt Peak (km/h)	Salt Tail (km/h)
1	0.00	Dropped Dye and Salt						
2	0.48	First Arrival	0.864	0.864				
2	0.48	Peak Dye	0.375		0.375			
3	0.90	First Arrival	0.614	0.614				
3	0.90	Peak Dye	0.587		0.587			
3	0.90	Salt Peak	0.574				0.574	
3	0.90	Salt Tail	0.524					0.524
3	0.90	Dye Tail	0.514			0.514		
4	1.35	First Arrival	0.704	0.704				
4	1.35	Peak Dye	0.669		0.669			
4	1.35	Dye Tail	0.453			0.453		
7	1.73	First Arrival	0.525	0.525				
7	1.73	Salt Peak	0.518				0.518	
7	1.73	Peak Dye	0.512		0.512			
7	1.73	Dye Tail	0.458			0.458		
8	2.01	First Arrival	0.532	0.532				
Agua Brava	2.14	First Arrival	0.553	0.553				
Powerline	2.69	First Arrival	0.527	0.527				
14	3.31	First Arrival	0.595	0.595				
16	3.66	First Arrival	0.561	0.561				
17	3.96	First Arrival	0.587	0.587				
18	4.34	First Arrival	0.618	0.618				
18	4.34	Salt Peak	0.547				0.547	
18	4.34	Peak Dye	0.537		0.537			
18	4.34	Dye Tail	0.510			0.510		
18	4.34	Salt Tail	0.505					0.505
18	4.34	Background	0.499					
Agua Verde				1.421	1.080			
Agua Brava				0.428	0.422	0.363		
Rio Salado Averages				First arrival	Peak Dye	Dye Tail	Salt Peak	Salt Tail
				0.607	0.536	0.484	0.546	0.515

A.3. SURFACE WATER SAMPLING

The Rio Salado was sampled along ~10 km of stream reach. At most sampling locations, sediments, rocks, soils, and plants were sampled in addition to surface water. There were three water sampling programs during the reconnaissance sampling: 1) Broad sampling, conducted for all parameters at most all sites; 2) Repeated opportunistic total arsenic source sampling, conducted at the RC-1, RC-3, and RC-4 weirs, and the Powerline Spring, to examine the variability of total arsenic over time; and, 3) Diurnal sampling, conducted at Station 3 to examine arsenic speciation in light and dark conditions and check for variability over time of the broad parameter list.

All water samples were grab samples collected before any sediment, rock, or plant sampling. Every reasonable effort was made not to perturb the stream bottom before and during water sampling. Field parameters (with exception of alkalinity) were measured in-stream following water sample collection. At all sample stations the water sample was collected from the stream position that appeared to be best mixed and most representative of the main flow (thalweg), or directly from a spring source. A pre-washed high-density polyethylene (HDPE) pail was rinsed several times in this flow and used to dipper out a sample. This sample was split with 0.5L being immediately filtered through a 0.45 μm cellulose acetate membrane (Millipore) under hand-pump vacuum, and 0.5 L being retained as an unfiltered aliquot. A 1.0 L Nalgene HDPE graduated cylinder was used to measure water aliquots for filtration. The unpreserved filtered and unfiltered aliquots were subsampled for arsenic speciation, then one aliquot was preserved to $\text{pH} \leq 2$ with concentrated nitric acid that had been double distilled at the New Mexico Bureau of Mines and Mineral Resources (NMBMMR). Another 1 L aliquot was obtained for an unpreserved sample for anion and alkalinity determination. Speciated arsenic samples did not receive additional acid preservation. For time series sampling a 125 ml container was pre-rinsed with sample a few times, filled, and preserved with nitric acid. At the end of each field day the samples were checked for plastic bag, label, and container integrity and iced. All samples were kept on ice in the custody of the sampling team until return to the laboratory in New Mexico where they were refrigerated at $4 \pm 2^\circ\text{C}$ until analysis.

A.3.1. Field Parameters

Field parameters of pH, conductivity, temperature, and oxidation reduction potential (ORP) were measured using calibrated probes. The field parameters data collected in this effort are presented in Table A-4. Measurements were conducted at the time of sampling and during tracer tests. Field measurements were made as close as practical to the stream channel location that was sampled, within several minutes of sample collection. All meters were calibrated and stored according to the manufacture's instructions and cleaned between uses with a Type I water rinse. Occasional physical cleaning of probe sensors was accomplished with Kim-wipes tissue or cotton swabs. All calibrations, equipment malfunctions, or failures to spot check were recorded in the project logbooks. Over the course of two weeks one pH meter-thermometer and one conductivity sensor failed and backups had to be brought into use.

A Cole-Parmer TDSTestr 40 with a temperature compensated range of 0-1999 and 0-199 $\mu\text{S}/\text{cm}$ and accuracy of $\pm 2\%$ of full scale was used to monitor conductivity. A conductivity calibration standard of 1333 and 133 $\mu\text{S}/\text{cm}$ was used to check instrument response several times a day. The instrument was calibrated to the same standards daily before use.

An OMEGA model PHH-82 meter was used to measure pH and ORP. The glass-bulb gel-filled combination electrode pH meter has a range of 0-14 pH units, resolution of 0.01 pH units, and accuracy of ± 0.02 pH units over an automatically temperature compensated range of 0-70°C to 25°C. Fresh National Institute of Testing and Standards (NITS) traceable pre-mixed buffer solutions of 4.01, 7.00, and 10.01 pH units at 25°C, accurate to ± 0.02 pH units (OMEGA), were used for daily calibrations. The true buffer values were calculated using the manufacturer supplied temperature dependent pH corrections appropriate for each buffer. Since Rio Salado waters were found to have a pH range of 6.25 to 8.91, calibration was checked frequently. Very little drift in calibration was noted during these checks. The ORP meter is a platinum electrode type with range of ± 1000 mV, resolution of 1 mV, and accuracy of ± 15 mV. The ORP meter is factory calibrated at time of manufacture and is not intended for user adjustment. The meter is referenced to the Ag/AgCl electrode in the pH sensor with the meter reading the differential voltage between the Pt and Ag/AgCl electrodes. This reading is corrected to Eh by addition of the standard potential for the Ag/AgCl electrode (200 mV) to the meter reading. The meter was new at project initiation.

Temperature was initially measured using an OMEGA model PHH-3X combination thermometer and pH meter with a range of 0-70°C. This unit has a resolution of 1°C and accuracy of ± 1 °C. The PHH-3X failed on January 6, 1998. The meter was replaced with a mercury thermometer with resolution of 0.1°C and accuracy of ± 0.2 °C on January 9, 1998. This resulted in some loss of planned data. Temperature dependent pH meter calibrations were made on the morning of January 7 and 8 using morning temperature values from January 6. No temperature reading was made at Station 14.

Dissolved oxygen was measured only at three cool sample locations (<40 °C) using a Yellow Springs Instruments model 53 DO meter. Streamflow was rapid enough that a stirrer was not necessary. The DO probe sensor would be damaged at temperatures above 40°C. The meter was calibrated according to the manufacturer's instructions using water-saturated air as a standard. It was originally intended that other gas measurements would be provided by quadrupole mass spectrometry (QMS). Equipment difficulties were not resolved quickly enough to have confidence in the QMS gas analysis for the majority of samples obtained in January. It was several weeks after return from the field before the samples could have been run. One gas analysis of a spring was completed.

Alkalinity was determined by titrating a 50 ml sample with standardized 0.020 N H_2SO_4 to phenolphthalein (colorless, pH~8.3) and bromcresol green-methyl red (light pink, pH~4.5) endpoints. Titrations were conducted at the end of each field day. Carbonate (CO_3^{2-}) concentrations can be estimated as two times the phenolphthalein alkalinity. The bicarbonate (HCO_3^-) concentration estimate is the bromcresol green-methyl red alkalinity, minus two times the phenolphthalein alkalinity. Due to the high silica content, and some lesser ions, there is a non-carbonate contribution to the total alkalinity. The alkalinity values and other field data are presented in Table A-4.

Table A-4. Field parameters for Rio Salado.

Station	Date	Time (MST)	Temp (° C)	Conductivity (uS/cm)	pH	ORP (mV)	CO ₃ ²⁻ (ppm)	HCO ₃ ⁻ (ppm)	
RC-1 North	1/10/98	830			6.52	273			
RC-1 South	1/10/98	830			6.53	280			
RC-1 West	6/26/97	1300	62.1	1674	7.01				
RC-3	1/6/98	1145	53	1289	7.64	224			
RC-3	1/7/98	919	49	1359	7.87	251			
RC-3	1/12/98	1601	60.5	1412	7.67	240			
AV Source 1	1/5/98	1032	31	1500	7.42	226			
AV Source 2	1/5/98	1035	25	1340	7.85	310			
AV Source 3	1/5/98	1036	61	1475	6.83	275			
AV Source 4	1/5/98	1040	63	1385	6.56	330			
AV Source 5	1/5/98	1045	64	1360	6.49	300	0	328	
AV Source 5	1/12/98	1045	67.5						
AV Source 5	6/26/97	1500	67	1566	6.25				
AB Source 1	1/6/98	1320	57	1335	7.7	231			
AB Source 2	1/6/98	1321	64	1329	6.5	219			
AB Source 2	1/12/98	1355	67.5						
AB Source 3	1/6/98	1322	46	1049	7.67	217			
Powerline	1/7/98	1017	51	1182	6.8	187			
Powerline	1/12/98	1242	58.5	1242	6.67	174			
RC Down AV	1/5/98	1457	36	1312	8.46	285			
RC Down	1/12/98	1140	42.8						
RC Up AV	1/5/98	1457	35	1287	8.45	282			
RC Up	1/7/98	1039	27	1241	8.3	196			
RC Up	1/12/98	1330	41.5	1241	8.3	196			
1	1/6/98	756	58	1415	7.16	240	0	416	
1	1/7/98	724	57	1333	7.29	284			
1	1/10/98	800	61	1406	7.47	290			
2	1/5/98	1703	46	1395	7.75	58	0	392	
3	1/8/98	815		1220	7.81	327	0	408	
3	1/10/98	1614	48	1291	7.82	280	0	424	
4	1/10/98	1210	42.5	1277	8.4	287	80	328	
6	1/5/98	1332	48	1310	8.48	280	88	300	
7	1/6/98	1002	42	1287	8.4	218	56	320	
8	1/9/98	1040		1269	7.89	308	76	334	
9	1/6/98	1416		1289	7.64	226	0	368	
9	1/12/98	1345	61.5						
10	1/6/98	1601		1188	8.45	226	104	270	
10	1/7/98	942	42	1250	8.45	248			
10	1/12/98	1328	51.5	1310	8.53	206			
11	1/7/98	1642		1232	8.67	240	160	236	
12	1/7/98	1459		1207	8.44	222	88	308	
14	1/7/98	1303		1130	8.45	264	40	336	
16	1/8/98	1505		1130	8.51	269	152	252	
17	1/8/98	1310		1233	8.76	257	152	256	
18	1/8/98	1130		DO(mg/L) 936	8.76	66	96	280	
18	1/12/98	1200	34	5.2					
19	1/11/98	1110	28.5	5.3	124	8.73	75	144	220
20	1/11/98	1451	27.7	6.3	100	8.91	95	140	284
AD	1/11/98	1238	29	443	7.96	67			
13	1/7/98	1116		5.2	316	7.36	8	0	88
13	1/12/98	1334	29						

AV - Agua Verde. AB - Agua Brava. RC Rio Caliente. AD - Agua Dulce

A.3.2. Arsenic Source Variability

It was unknown if the spring discharge chemistry was highly variable prior to the reconnaissance sampling. There are north-south trends in water chemistry revealed by the field parameters. There are also trends in total arsenic concentration. The highest arsenic concentrations were found at Agua Caliente and the lowest at Powerline. Figure A-3 and the summary statistics in Table A-5 display these trends clearly. The arsenic mean concentration decreases by 24% from the north to the south. The arsenic concentrations also varied in time, with RC-1 varying by 184 µg/L (about 16%) over seven days time. This is not to suggest evaluating temporal trends with such a small data set is appropriate. The variation presented here is felt to be real.

Table A-5 Rio Salado arsenic concentration (ppb) source variation summary statistics.

	RC-1	RC-3	RC-4	Powerline
Mean	1182	1023	959	894
95% Confidence Interval About the Mean	84	23	39	60
Median	1188	1034	951	919
Range	214	90	95	137
Standard Deviation	80	30	37	57

A.3.3. Arsenic Diurnal Variation – Replicate Sampling

Station 3 was sampled on January 8 and 10 with the intent of determining if there is change in arsenic speciation between light and dark conditions. The sampling effort also served as replicate to evaluate other metal and anion day-to-day variability. To maximize the possibility of detecting a difference in arsenic speciation, a sample should be taken in a full sun location as possible late in the day, and again at or before the dawn twilight. This provides the maximum sun without shadows and as long a dark period as possible. Station 3 was selected because of its proximity to the camp, full sun location, and single spring and channel source without tributaries. The location is proximal to the spa, but is probably not impacted by runoff or groundwater flow from the spa facilities (septic system and laundry). The data for this station contained elsewhere is repeated here for ease of reference.

All data from the replicate sampling is in very close agreement with exception of conductivity, Eh, manganese, and arsenic speciation. Higher levels of manganese are found in the morning, under more oxidizing conditions, in the absence of As^{3+} . There is an increase in As^{5+} and As^{3+} in the afternoon that is approximately equal to the increase in MMAA and DMAA overnight. Total arsenic at Station 3 varied less than 15 ppb between January 8 and 10. This indicates that the source concentration was consistent at these two times. Since the sampling was separated by another full day it is not possible to estimate the kinetics of the diurnal variation in arsenic speciation for these data. The diurnal variation in chemistry for filtered and unfiltered samples is depicted in Figure A-4. A separate scale is not provided for Eh.

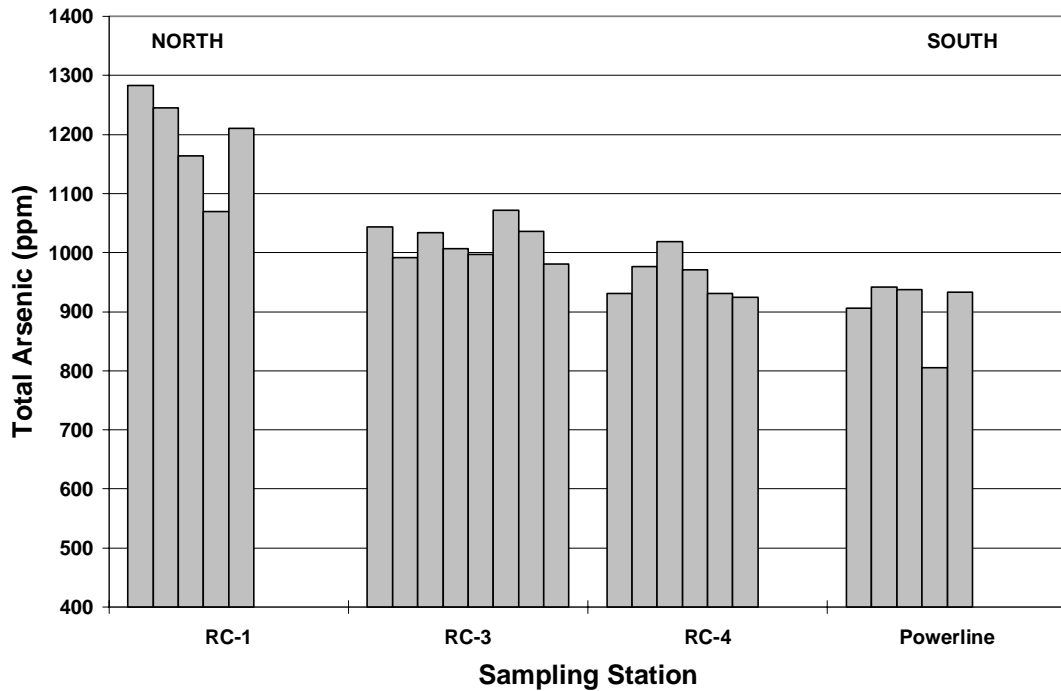


Figure A-3. Replicate arsenic sampling at spring sources to determine variability.

Table A-6. Arsenic analytical values for diurnal sampling (ppb).

Unfiltered	Date	Time	As ³⁺	MMAA	As ⁵⁺	DMAA	Species Total	Total As
3-Afternoon (3.3)	1/10/98	1621	0	0	1171	113	1296	1042
3-Morning (3.6)	1/8/98	0815	0	41	973	228	1248	1073
Filtered								
3-Afternoon (3.3)	1/10/98	1621	0	11	1178	91	1284	1126
3-Morning (3.6)	1/8/98	0815	0	34	998	154	1193	1088

Table A-7. Metals and anion analytical values for diurnal sampling (ppm).

Unfiltered	Ca	K	Na	Li	Mg	Si	Fe	Mn	Cl	SO ₄	F
							(ppb)	(ppb)			
3-Afternoon (3.3)	3.4	13.5	280	1.02	0.27	236	28	78	93	28	16
3-Morning (3.6)	3.6	13.3	280	1.01	0.28	242	27	117	92	28	16
Filtered											
3-Afternoon (3.3)	3.1	13	307	1.00	0.25	236	26	90			
3-Morning (3.6)	3.5	13	297	0.98	0.28	231	41	105			

Table A-8. Diurnal field measurements.

Station	Date	Time	°C	Conductivity (µS/cm)	pH	Eh (mV)	CO ₃ ²⁻ (ppm)	HCO ₃ ⁻ (ppm)
3-Afternoon (3.3)	1/10/98	1614	48	1291	7.82	80	0	424
3-Morning (3.6)	1/8/98	0815	48	1220	7.81	127	0	408

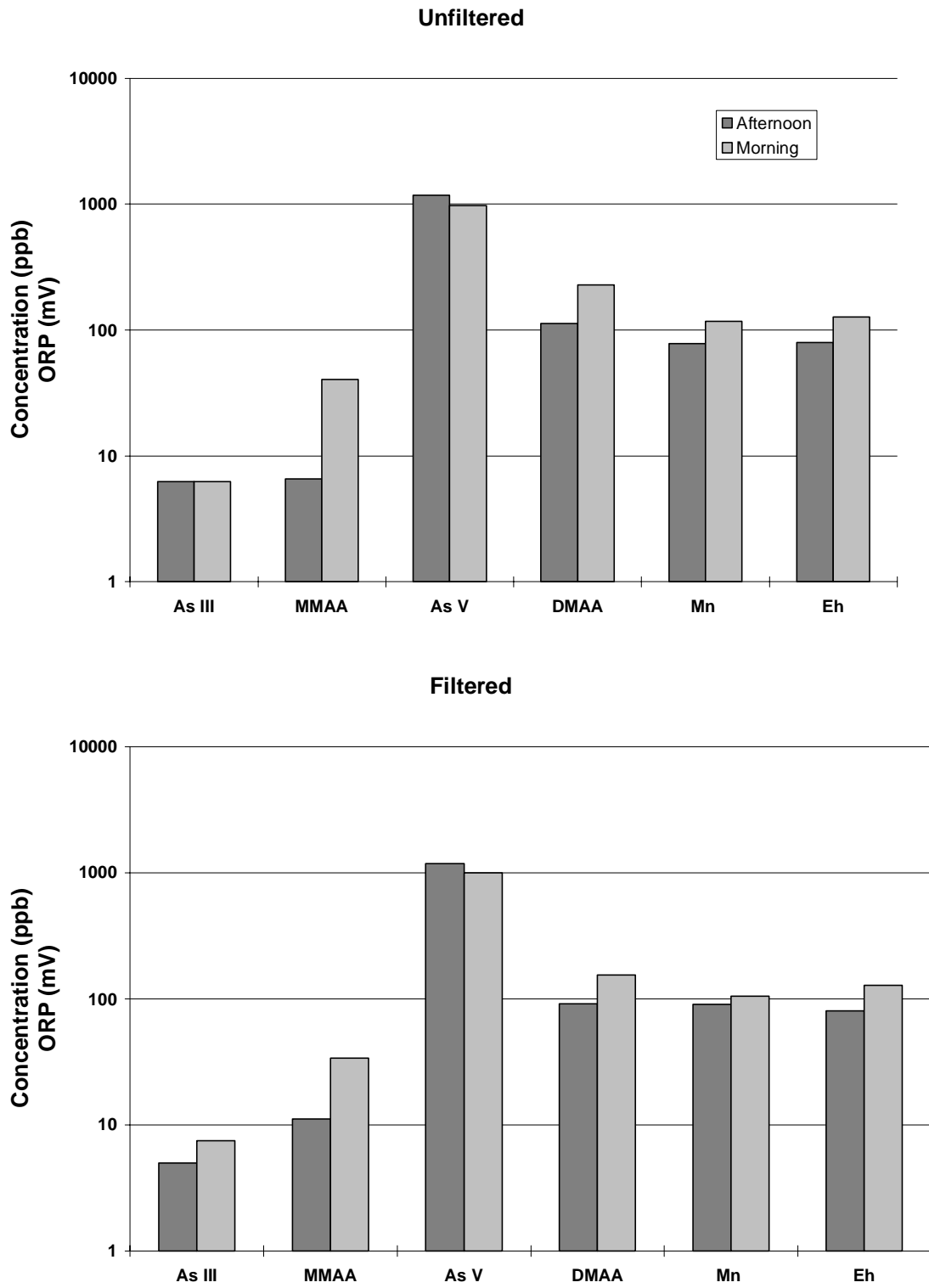


Figure A-4. Diurnal variation in arsenic speciation and Redox parameters for Station 3.

The Rio Salado was sampled along ~10 km of stream reach. At most sampling locations, sediments, rocks, soils, and plants were sampled in addition to surface water. There were three water sampling programs during the reconnaissance sampling: 1) Broad sampling, conducted for all parameters at most all sites; 2) Repeated opportunistic total arsenic source sampling, conducted at the RC-1, RC-3, and RC-4 weirs, and the Powerline Spring, to examine the variability of total arsenic over time; and, 3) Diurnal sampling, conducted at Station 3 to examine arsenic speciation in light and dark conditions and check for variability over time of the broad parameter list.

All water samples were grab samples collected before any sediment, rock, or plant sampling. Every reasonable effort was made not to perturb the stream bottom before and during water sampling. Field parameters (with exception of alkalinity) were measured in-stream following water sample collection. At all sample stations the water sample was collected from the stream position that appeared to be best mixed and most representative of the main flow (thalweg), or directly from a spring source. A pre-washed high-density polyethylene (HDPE) pail was rinsed several times in this flow and used to dipper out a sample. This sample was split with 0.5L being immediately filtered through a 0.45 μm cellulose acetate membrane (Millipore) under hand-pump vacuum, and 0.5 L being retained as an unfiltered aliquot. A 1.0 L Nalgene HDPE graduated cylinder was used to measure water aliquots for filtration. The unpreserved filtered and unfiltered aliquots were subsampled for arsenic speciation, then one aliquot was preserved to $\text{pH} \leq 2$ with concentrated nitric acid that had been double distilled at the New Mexico Bureau of Mines and Mineral Resources (NMBMMR). Another 1 L aliquot was obtained for an unpreserved sample for anion and alkalinity determination. Speciated arsenic samples did not receive additional acid preservation. For time series sampling a 125 ml container was pre-rinsed with sample a few times, filled, and preserved with nitric acid. At the end of each field day the samples were checked for plastic bag, label, and container integrity and iced. All samples were kept on ice in the custody of the sampling team until return to the laboratory in New Mexico where they were refrigerated at $4 \pm 2^\circ\text{C}$ until analysis.

A.4. STREAM SEDIMENT SAMPLING

Stream sediment collection was accomplished by David Welch of the New Mexico Institute of Mining and Technology (NMIMT). Welch conducted the sampling and analysis in support of this effort and his evaluation was used as partial completion of his master's degree in Geochemistry at NMIMT [106]. Welch's sampling and analysis procedures and evaluations of the Rio Salado sediments are presented as edited excerpts from his thesis. Due to the complexity of his methodology and the importance of his findings to the modeling effort, they are included in this report generally as excerpts from the thesis rather than by paraphrasing the text. Accurate sediment analytical work is essential to testing of the modeling approach presented later. Welch's effort provided the raw data necessary to define mineral surfaces for the Rio Salado modeling approach.

Samples were collected at 20 sample stations separated by approximately 500 meters along Rio Caliente and its tributaries. Sediments were collected within 20 meters of locations where stream waters were sampled so that direct comparisons could be made between water and sediment chemistry. Where possible, sediments were collected midstream by plastic scoop and contained in one-half gallon plastic buckets and one-liter

plastic bottles that were refrigerated to 4 ± 2 °C until time of sample preparation. In some locations larger cobbles and algae mats were removed before scooping.

Before sample collection, Redox conditions at the sediment-water interface and several inches within the sediments were tested using an OMEGA model PHH-82 meter. Though measured Eh conditions within sediments ranged from +70 to +350 mV, only samples with Eh values greater than +200 mV (corrected for 200 mV difference between standard platinum electrode and Ag/AgCl reference electrode) were used for direct comparison between sample stations. This was done to reduce heterogeneity of samples resulting from different mineral assemblages stable under differing Redox conditions. Also, the procedures involved in preservation of reduced sediments are elaborate and were beyond the scope of what could be accomplished on this sampling trip.

Sediments were air-dried and split into manageable portions using the cone and quartering method. With this method, a cone was initially made by pouring the sediments through a plastic funnel. The sediment cone was then quartered on a sheet of plastic. Two of the opposite quarters were then mixed and quartered again. This procedure was repeated several times until a manageable sample size was obtained. Air-drying of the samples was done because it is believed to have a lower possibility of affecting secondary mineral phases and organic matter than heat-drying or freeze-drying.

A.5. PLANT AND ALGAE SAMPLING

Algae and plant specimens were also collected at each of the La Primavera sample locations. An attempt was made to collect each type of plant and algae present at sample sites. Algae and plants were stored in separate ziplock bags and refrigerated at 4 ± 2 °C until time of sample preparation. Algae samples were first patted dry with a paper towel to remove excess moisture and weighed to obtain a “wet weight” then dried overnight at 105 °C. The dried algae was re-weighed to obtain a dry weight and ground to a powder in a ceramic mortar for analysis.

A.6. ANALYTICAL METHODS

A.6.1. Analytical Techniques and Detection Limits

Other than field measurements and separations, all analytical procedures were conducted at New Mexico Institute of Mining and Technology (NMIMT) and New Mexico Bureau of Mines and Mineral Resources (NMBMMR) facilities. Water analysis was conducted by Gregory P. Miller and sediment analysis by David Welch of NMIMT. The principal instruments used for water and sediment extract analyses are an IL Video Model 12 flame atomic absorption spectrophotometer (FAA), Varian 600 Zeeman, graphite furnace atomic absorption spectrophotometer (GFAA), and Dionex 4000 ion chromatograph (IC). The determinations and analyses that were performed for this effort are listed in Table A-9. Tabular analytical data for all analyses described here is presented later.

Table A-9. Reconnaissance sampling data collection.

Parameter	PQL ¹	Method	Comments
Field Measurements			
pH	± 0.02 units	Field Probes	Calibrated daily and checked frequently through the day. Calibrated daily against temperature corrected KCl standard. Measured with calibrated probes and mercury thermometer. Platinum electrode values corrected for Ag/AgCl reference electrode (add 200 mV to meter reading). Field titrated alkalinity at pH 8.3 and 4.5 endpoints. Performed in field daily.
Conductivity	±10 µS/cm	Field Probes	
Temperature	± 1 °C	Field Probes	
Eh	± 10 mV	Field Probes	
Alkalinity	5 mg/L as CaCO ₃	Titration	
Metals			
Aluminum	0.005 mg/L	GFAA	
Arsenic	0.002 mg/L	GFAA	
Barium	0.003 mg/L	GFAA	
Boron	1 mg/L	GFAA	
Cadmium	0.001 mg/L	GFAA	Cadmium not detected.
Calcium	0.2 mg/L	FAA	
Chromium	0.001 mg/L	GFAA	Chromium not detected.
Copper	0.0005 mg/L	GFAA	
Iron	0.003 mg/L	GFAA	
Lithium	0.05 mg/L	GFAA	
Magnesium	0.05 mg/L	FAA	
Manganese	0.005 mg/L	GFAA	
Molybdenum	0.005 mg/L	GFAA	
Potassium	0.1 mg/L	FAA	
Selenium	0.005 mg/L	GFAA	Selenium not detected.
Silica	20 mg/L	FAA	
Sodium	0.2 mg/L	FAA	
Strontium	0.004 mg/L	GFAA	
Vanadium	0.005 mg/L	GFAA	Vanadium not detected.
Zinc	0.03 mg/L	FAA	Zinc not detected.
Anions			
Bromine	1 mg/L	IC	Samples field-filtered, 0.45 micron, lab filtered-using 0.22 micron cellulose acetate filter (Millipore) and direct injected to the Dionex 4000 IC. Phosphate not detected.
Chloride	1 mg/L	IC	
Fluoride	0.2 mg/L	IC	
Nitrate	0.1 mg/L	IC	
Phosphate	0.1 mg/L	IC	
Sulfate	0.1 mg/L	IC	
Sediments		Comments	
Sediment preparation was highly variable and dependent on the analytical method used.	Specific surface area. Trace elements by XRF. Grain size distribution. Trace level carbonate solid phases. Amorphous digestion for Fe, Mn, and Al concentrations. Strong acid digestion for Fe, Mn, and Al concentrations. Hydroxylamine hydrochloride extraction for Fe, Mn, and Al concentrations (Chao reagent). Arsenic speciation by phosphate ion –exchange displacement followed by ion chromatography. Electron microprobe and reflectance spectrophotometry of polished sections. Total organic carbon by loss on ignition.		

¹ Practical Quantification Limit Note: mg/L = parts per million (ppm) and µg/L = parts per billion (ppb)

A.6.2. Sediment Extractions

The sediment extraction text presented below has been excerpted from Welch [106]. Welch's text has been annotated, modified, or reorganized as necessary to ensure nomenclature and organizational compatibility with this report. All excerpts, graphics, and text modifications have been used or made with permission of the author. Data is presented in the tabular data section of this appendix.

“Sediments were air-dried and split into manageable portions using the cone and quartering method. With this method, a cone was initially made by pouring the sediments through a plastic funnel. The sediment cone was then quartered on a sheet of plastic. Two of the opposite quarters were then mixed and quartered again. This procedure was repeated several times until a manageable sample size was obtained. Air-drying of the samples was done because it is believed to have a lower possibility of affecting secondary mineral phases and organic matter than heat-drying or freeze-drying.”

“Sediments were dry-sieved using U.S. Standard sieves to characterize the grain size distribution. Initially, in order to reduce sample heterogeneity, the >2 mm size fraction was sieved out and archived and is not used in the grain size distribution or chemical extractions. About 100 grams of dried sediment was weighed for separation into the following size fractions: 1.0-2.0 mm (very coarse sand), 0.5-1.0 mm (coarse sand), 0.25-0.5 mm (medium sand), 0.125-0.25 mm (fine sand), 0.0625-0.125 mm (very fine sand) and <0.0625 mm (silt-clay). The different sieves were stacked in sequence with fining mesh sizes towards the bottom and placed on the Ro-Tap machine to be shaken 15 minutes. After shaking, sediments from each of the size fractions were weighed to obtain the grain size distribution. A small portion of split sediments was ground to -80 mesh in a ball crusher to reduce the heterogeneity present in non-sieved material for some of the analyses. A grinding time of only 10 to 20 seconds was used to prevent the sample from heating up as well as to cut down on possible contamination by metal from the grinder itself.”

A.6.2.1 Selective Extraction

“A combination of partial extraction techniques developed by Tessier et al. [122] and Chao and Zhou [123] was performed on the sediments to determine relative proportions of exchangeable arsenic (water soluble and affected by adsorption-desorption processes), arsenic associated with carbonates, amorphous iron and manganese oxides, and organic matter. The procedure used is as follows: about one gram of sediment, ground to -80 mesh, is agitated in 8 ml of 1M NaOAc adjusted to pH 8.2 for 1 h to remove exchangeable arsenic. Next, the residue from the exchangeable

extraction is agitated in 8 ml of 1M NaOAc adjusted to pH 5 for 4 hours to remove arsenic associated with carbonates. The resulting residue is then digested in 20 ml of 0.25M NH₂OH-HCl in 0.25M HCl heated to 50 °C for 30 minutes to extract arsenic associated with amorphous iron and manganese oxides. Extraction of arsenic bound to organic matter is achieved by adding the residue from the iron-manganese oxide digestion to 3 ml of 0.02 M HNO₃ and 5 ml of 30% H₂O₂ adjusted to pH 2 with HNO₃. This mixture is heated to 85 °C for 2 h after which an additional 3 ml aliquot of 30% H₂O₂ is added with continued heating for an additional 3 h. The use of 0.25M NH₂OH-HCl (hydroxylamine hydrochloride) in 0.25M HCl, described by Chao and Zhou [123], was used instead of the 0.04M NH₂OH-HCl in 25% v/v HOAc suggested by Tessier et al. [122] because of its greater selectivity for amorphous Fe and Mn oxides and reduced matrix effects.”

“All extractions were conducted in plastic centrifuge tubes to avoid loss of sample and cross contamination. Between each successive extraction samples were centrifuged at 10,000 rpm for 30 minutes and the supernatant pipetted off for analysis. Afterwards, 8 ml of distilled water was added and the residue again centrifuged for 30 minutes. The second supernatant was removed and discarded before addition of the next extracting reagent.”

A.6.2.2 HNO₃ Digestions

“Nitric acid extractions were conducted on each of the size fractions and on whole sediment samples. About 1 gram of sediment was added to 10 ml of 8M HNO₃, (1:1 HNO₃ and distilled water) and microwave-heated under pressure in sealed Teflon containers. This mixture was heated 12 minutes at 50 psi and followed by 30 minutes at 100 psi, about 180 °C. After cooling, extracts were filtered and diluted for analysis on the GFAA.”

The HNO₃ procedure dissolves many of the secondary minerals and organic matter, but not residual minerals and glasses. It also provides an estimate of the “total” acid leachable arsenic in the sediments, and represents arsenic that could be remobilized with changes in environmental conditions such as pH or Eh. USEPA indicates that the analysis provides a measure of the total amount of environmentally available metals.

A.6.2.3 Speciation of Arsenic in Sediments

“Speciation of As³⁺, As⁵⁺, MMAA and DMAA in sediments was achieved by using an ion-exchange chromatography method modified after Grabinski [124]. The apparatus consisted of a 10 cm glass column, 1 cm diameter, filled with AG-1X8 anion resin in the chloride form connected

by a capillary to a 26 cm glass column, also 1 cm diameter, filled with AG50W-X8 cation resin in the hydrogen form. Resins were 50-100 mesh allowing gravity flow rates of about 3 ml/min. The top and bottom of the anion column and the bottom of the cation column were capped with a porous polymer bed support, and a Luer fitting for flow control was used at the base.”

“Before use, the ion exchange columns were first conditioned and regenerated as described by Grabinski [124]. Initially, resin was packed into the columns with distilled water, then washed twice with successive elutions of 1.5 M NH_4OH (70 ml), 1.0 M HCl (70 ml), 0.48 M HCl (70 ml) and 0.006 M (25 ml) trichloroacetic acid (TCA). After the first sample had been run, columns were regenerated by washing with the same successive elutions only once after each additional use.”

“Validation of the ion-exchange method was done using the sediment extracting reagent (0.1 M H_3PO_4) before running samples. This was carried out with prepared standard solutions of 250 ppb As^{3+} , As^{5+} , MMAA and DMAA in 0.1 M H_3PO_4 . Initially, each arsenic species was run separately to determine sample collection ranges and to validate separation. After sample collection ranges were determined, mixed standards containing known amounts of all 4 arsenic species were run to determine sample recoveries. Average recoveries for each of the species ranged as follows: As^{3+} (84%), MMAA (96%), As^{5+} (79%) and DMAA (79%). This extraction procedure provides semi-quantitative results for comparison between arsenic species and for comparison of the same species between different sample stations.”

“The effect of the H_3PO_4 extract on arsenic species was also investigated before sample analysis. Three sets of mixed standards in H_3PO_4 were run through the ion-exchange columns immediately after preparation, and an additional 3 sets run 1.5 h after preparation. No significant difference was observed between samples indicating no oxidation of As^{3+} during the time required for sediment extraction and centrifuging.

“Samples were run through the columns by using successive additions of 0.006 M TCA (55 ml), 0.2 M TCA (8 ml), 1.5 M NH_4OH (55 ml) and 0.2 M TCA (50 ml). The first 29 ml of sample collected from the column contained As^{3+} , 29 to 60 ml MMAA, 60 to 90 ml As^{5+} and 90 to 140 DMAA. A description of the elution process is as follows: during the first elution with 0.006 M TCA (pH~2.5) As^{3+} is present as a neutral species and travels through the column to be collected in the first 29 ml. MMAA is also a neutral species under these conditions and is eluted after the As^{3+} and collected in the 29 to 60 ml fraction. While As^{3+} and MMAA are being eluted As^{5+} and DMAA retain a charge and stick to the anion and

cation resins. As^{5+} is converted to its neutral form when the 0.2 M TCA reaches it in the anion resin and is collected in the 60 to 90 ml fraction while DMAA is strongly retained on the cation exchange resin. The DMAA is converted to its anionic form and moves from the cation resin to the bottom anion resin with the addition of 1.5 M NH_4OH . The final elution with 0.2 M TCA converts the DMAA to a positively charged species removing it from the anion resin to be collected in the 90 to 140 ml fraction.”

“The procedure used in H_3PO_4 extract sediment analysis is as follows: about 1 gram of sediment, ground to <80 mesh, was added to 10 ml of 0.1 M H_3PO_4 and shaken for 1 h in a plastic centrifuge tube. Samples were centrifuged for 30 minutes at 10,000 rpm, then 5 ml of sediment extract was pipetted on to the top of the ion-exchange column. The column was eluted until the sample was level with the resin bed, after which the first elution with 55 ml of 0.006 M TCA was begun. The first 5 ml of eluant, collected while leveling the sample with the resin, was discarded and the As^{3+} fraction was collected from 5 to 29 ml. The other As species were collected in the ranges described previously. Analyses were conducted by GFAAS with calibration of the instrument in the same matrix as the sample (H_3PO_4).”

A.7. SEDIMENT MINERALOGY

In addition to the partial extractions, Welch also conducted petrographic analysis of sediments to classify the rock and or mineral type present [106]. This included thin section analysis and modal analysis or rock or mineral type comprising the sediments at all sampling stations. Text in block quotations is from Welch.

A.7.1. Carbonate Analysis

“Carbonate was present in very small amounts and was measured by pressure difference, due to acid evolved CO_2 , and gas analysis using a quadrupole mass spectrometer. A glass vacuum reaction vessel was used that had a glass partition at the bottom creating two open, but separated chambers. The reaction vessel fit into a glass neck with a Teflon valve allowing the vessel to be sealed. This apparatus was fitted to a system of vacuum lines in contact with a capacitance manometer for pressure measurements. The system of vacuum lines is also set up to send a gas sample directly to a Balzers model QMG 125 quadrupole mass spectrometer.”

“Initially, sediment ground -80 mesh was oven dried at 105 °C for about 10 minutes to remove excess moisture. Afterwards, about 1.5 g of sediment was placed in one chamber of the reaction vessel and 4 ml of

concentrated H_3PO_4 was pipetted into the other. The apparatus was sealed with vacuum grease and attached to the vacuum lines. Low and hi-vacuum pumps were used to create a vacuum in the reaction vessel and were allowed to pump down overnight to remove adsorbed water and gas from the sample. The following day a downward extension on the vacuum line, filled with glass beads, was immersed in a cold trap of dry-ice in ethanol for removal of water. When the pressure in the vacuum line reached about 0.0000 mbar the initial pressure was recorded and the reaction vessel sealed off and tipped, allowing the acid to react with the sediment. The reaction was allowed to proceed for two hours, during which time the vacuum lines were pumped down to about 0.0000 mbar. Next, the vacuum pumps were sealed off and the reaction vessel opened allowing the evolved gas to fill a known volume of vacuum line connected to a capacitance manometer and cold trap. After two minutes the reaction vessel was sealed off to prevent possible leakage of air into the system. About 30 to 45 minutes were required for the pressure to equilibrate, due to removal of water from the vacuum lines by the cold trap. The final pressure and temperature was then recorded and the sample sent to the quadrupole mass spectrometer for gas analysis.”

“Before analysis, background intensities of H_2O , N_2 , O_2 , Ar and CO_2 gasses were measured when the pressure in the mass spectrometer was less than 2×10^{-7} mbar. Next, a valve was opened allowing the sample to enter the mass spectrometer. A leak valve was used to maintain a pressure in the spectrometer of 2×10^{-6} mbar. After a few moments, the intensities of H_2O , N_2 , O_2 , Ar and CO_2 gasses from the sample were recorded. Mole percentages of each of the gasses were calculated and corrected from the sample intensities.”

“Determination of the time required for reaction was made by recording pressure increases with time after reacting a sample with acid. After two hours, in a sample containing the largest amount of carbonate, 97% of the total gas had been evolved. The largest possible sample size, about 1.5 to 2 g was used to obtain the maximum precision possible. One sample, done in triplicate, was used to provide a detection limit of 0.05% carbonate which was calculated as two times the relative standard deviation. A second sample, containing less carbonate, was also done in duplicate with reproducibility better than 0.05%. Although, the amount of evolved CO_2 could be measured very precisely, the exact proportions of CO_2 resulting from dissolution of CaCO_3 , MnCO_3 , MgCO_3 can not be determined. As a result, values are reported as % carbonate not as % CaCO_3 .”

A.7.2. Electron Microprobe Analysis

“Polished one-inch round sections were examined by a Comica SX-100 electron microprobe. An accelerating voltage of 15 kV and a probe current of 20 nA was used. Iron oxides were visible as discrete grains and as oxidized mafic grains that still retained relict textures. No manganese minerals were detected with the microprobe. The distribution of arsenic within iron oxides was examined by conducting line scans on two different grains. Scans began in the center and proceeded in a line towards the outer edge of the grain. Output data from the line scans consisted of the number of counts of Fe and As at points along the traverse. The microprobe was also used to make point-count measurements of arsenic contents in iron-oxides relative to background glasses. Point count measurements do not provide a concentration of arsenic, only the number of counts of arsenic in one phase relative to another allowing comparison between the two.”

A.7.3. Reflectance Spectrophotometry

“A method of visible light reflectance spectrophotometry, outlined by Barranco et al., [125], was used to identify the types of iron oxides present in sediments. About 5 drops of water were added to 0.1 to 0.15 g of ground sediment, which was then mixed to make a thin slurry on a petrographic slide and dried. Samples were run on a Perkin-Elmer Lambda 6 spectrophotometer relative to a barium sulfate standard for the wavelength range 250 to 850 nm. Output data consisted of percent total reflectance vs. wavelength. Data was processed and enhanced by taking the first derivative of % reflectance and plotting it against wavelength.”

A.7.4. Surface Area Measurements

“Surface area measurements were conducted on a Monosorb direct-reading surface area analyzer (Quantachrome) using 30 mole % N₂ with 70 mole % H₂ carrier gas. Before analysis, whole sediments were heated overnight in a muffle furnace at 430 °C for removal of organic matter. The Monosorb was calibrated following factory recommended procedures. About 1 to 1.5 g of sample was placed in a u-shaped glass sample tube with holder, leaving space above the sample so that gas flow was not impeded. The sample tube was then placed in an “out-gassing” station and heated with a heat gun for about 2 minutes to drive off excess moisture. After cooling, the sample tube and holder is moved to a “sample” receptacle and immersed in a liquid nitrogen bath, during which time the Monosorb records an adsorption signal. When the adsorption

signal is completed the sample tube is removed from the bath and the desorption signal begins. When the desorption signal is completed the Monosorb displays the surface area in square meters. This number is divided by the sample weight to determine m^2/gm of sediment. Though no standard reference material was available for determination of accuracy, triplicate measurements were made on 60-100 mesh Silicar silica gel produced by Mallinckrodt, which reported a surface area of $480 \text{ m}^2/\text{g}$. Triplicate measurements conducted on the silica gel were $598 \text{ m}^2/\text{g} \pm 7.8$. Triplicate measurements on Rio Salado samples, were 1.52 ± 0.09 ."

A.7.5. Determination of Total Organic Carbon (TOC)

"Percent TOC was determined by loss-on-ignition. About 10 g of un-sieved sediments were oven dried at 105°C for 3 to 4 h and weighed, then placed in a muffle furnace and heated at 430°C for 24 h. After cooling, sediments were re-weighed to determine the amount lost-on-ignition, representing TOC. Contribution to the sediment weight loss by structural water expelled from clays is insignificant due to the fact that clays were present in non-detectable amounts. Also, carbonates do not to affect the loss-on-ignition value at temperatures of 430°C [126]."

A.7.6. X-Ray Diffraction

"An attempt was made to separate clays for identification by X-Ray diffraction (XRD). Removal of organic matter was done by addition of 5 to 6 g of $>63 \mu\text{m}$ sediments to 10 ml of Clorox (NaOCl) adjusted to pH 9 with HCl. This mixture is heated 15 minutes in a boiling water bath, then centrifuged for 5 minutes and decanted. This procedure is repeated several times until the decanted liquid is clear and shows no brown coloration indicating oxidized organic matter. Afterwards, the $> 63 \mu\text{m}$ sample is placed in a beaker with distilled water and several drops of Calgon to keep the clays dispersed. This mixture is stirred, and after 10 minutes settling time 2 ml is pipetted on to a petrographic slide for XRD on a Rigaku DMAX/2 X-Ray diffractometer. Dissolution of the organic matter with 0.02 M HNO_3 and 30 % H_2O_2 following the procedure of Tessier et al. [122], described previously, was also tried. The same technique of clay dispersion and slide preparation was used on these samples as well."

A.7.7. X-Ray Fluorescence

“Values of total As, Fe and Mn were determined by X-ray fluorescence (XRF) on a Phillips PW 2400 instrument at the New Mexico Bureau of Mines and Mineral Resources lab. Ground non-sieved sediments were used to make pressed powder pellets that were analyzed using standard procedures.”

A.7.8. Barium Arsenate

Barium arsenate investigations were conducted by the author. Barium arsenate $Ba_3(AsO_4)_2$, and the monohydrate $Ba_3(AsO_4)_2 \cdot H_2O$, have a very low solubility in water. It has been postulated that barium or calcium arsenate may exert a strong control on available arsenic by its precipitation. Barium arsenate and the monohydrate have not been observed in nature. Following the determination that quantifiable barium is introduced to Rio Salado at the Powerline spring, an investigation was conducted to determine if barium was precipitating arsenate downstream of that point. Saturation index modeling with PHREEQC indicated that Barium and Calcium arsenates were oversaturated in the river water.

Air-dried sediment aliquots of ~500 g were sieved and the -200 mesh fraction discarded and the remainder placed in Nalgene 1L bottles and mechanically rolled for several hours to abrade the outer grain surfaces. The abraded samples were sieved again and the -200 mesh fraction retained. XRD was used on this fraction to evaluate the presence of barium arsenates. All sample tested did not indicate the presence of insoluble barium or calcium arsenates. In order to increase the sensitivity of the XRD method, portions of the -200 mesh retained fraction were placed in lithium polytungstate solution with a density >3.0 g/ml and centrifuged. In theory, barium arsenate with a density of 5.1 g/cc should be separated by this method. The monohydrate, with a density of 1.93 would not be concentrated by this method. The heavy liquid separation was successful in separating heavy minerals as was evidence by a strong hematite peak in the XRD scan (hematite's density is 5.24) and the large volume reduction of the sample. Barium arsenate was not detected in any of the heavy liquid separates. Although thermodynamically stable, barium arsenate was not found in Rio Salado.

A.7.9. Algae Digestions and Arsenic Speciation

“About 0.5 g of ground, dried algae was added to 10 ml of concentrated HNO_3 in a capped Teflon microwave vessel. Samples were microwave heated at 55% power under 40 psi for 10 minutes allowing 5 minutes to reach pressure, followed by 55% power at 85 psi for 10 minutes allowing 5 minutes to reach pressure and finished with heating at 55% power and 100 psi for 10 minutes allowing 5 minutes to reach pressure. After cooling, 30% H_2O_2 was added until the effervescence ceased, then an additional 2 ml 30% H_2O_2 was added and allowed to digest overnight.

Digestion overnight was done to give the solution time for the H₂O₂ to dissipate, otherwise the 30% H₂O₂ will oxidize the graphite tube in the GFAA. Samples were then filtered and diluted for analysis by GFAA.”

“Speciation of arsenic present in the algae was done using the same technique as described previously for stream sediments. Digestion by HNO₃ and 30% H₂O₂ (USEPA SW-846 Method 3050) gave results for total arsenic in algae, leaving no visible trace of algae afterwards. The digestion procedure for speciation is less destructive and provides qualitative data on relative amounts of each species present. The method does not completely digest the algae nor does it liberate all the arsenic present.”

A.7.10. Plant Digestions

Plant samples were removed from frozen storage and thawed at room temperature. The samples were classified roughly according to plant type (e.g. Grass 1, Grass 2) and segregated by station. From 2-15 g of wet-weight plants were cut up using medical grade stainless steel scissors into pre-weighed aluminum foil boats and dried at 95-105 °C for 24 hours. The samples were weighed again then digested according to USEPA Method SW-846 3050 (concentrated nitric acid and 30% hydrogen peroxide reflux). Samples were filtered using 0.45 µm Millipore cellulose acetate then diluted to a known volume (100 ml). Arsenic analysis, as total arsenic, was conducted using the GFAA and data reduced to mg/kg dry weight. A portion of the plant samples were retained for classification by a botanist (John D. Vitti) possessing familiarity with North American vegetation.

A.7.11. Rio Salado Plants

A.7.11.1 Arsenic Speciation of Algae

From Welch [106]:

“Algae contain between 18 and 68 ppm total arsenic on a dry weight basis which is predominantly As⁵⁺, but also contain measurable As³⁺, MMAA and DMAA. The two different morphological types of algae recognized at La Primavera also seemed to have differing capacities to uptake As. The algae types containing the highest concentrations of arsenic were those present as dense mats covering the rocks and stream bottom near the source where waters are the hottest. The filamentous algae that generally occurred in cooler waters contained lower total As.”

A.7.11.2 Arsenic in Plants

Rio Salado plants were collected and analyzed for arsenic to: 1) Look for trends in plant concentrations that could provide insight into arsenic pathways at Rio Salado; 2) Provide data to estimate what arsenic levels would be expected in organic stream detritus; and, 3) Identify plant types that have elevated arsenic levels and might be candidates for phytoremediation.

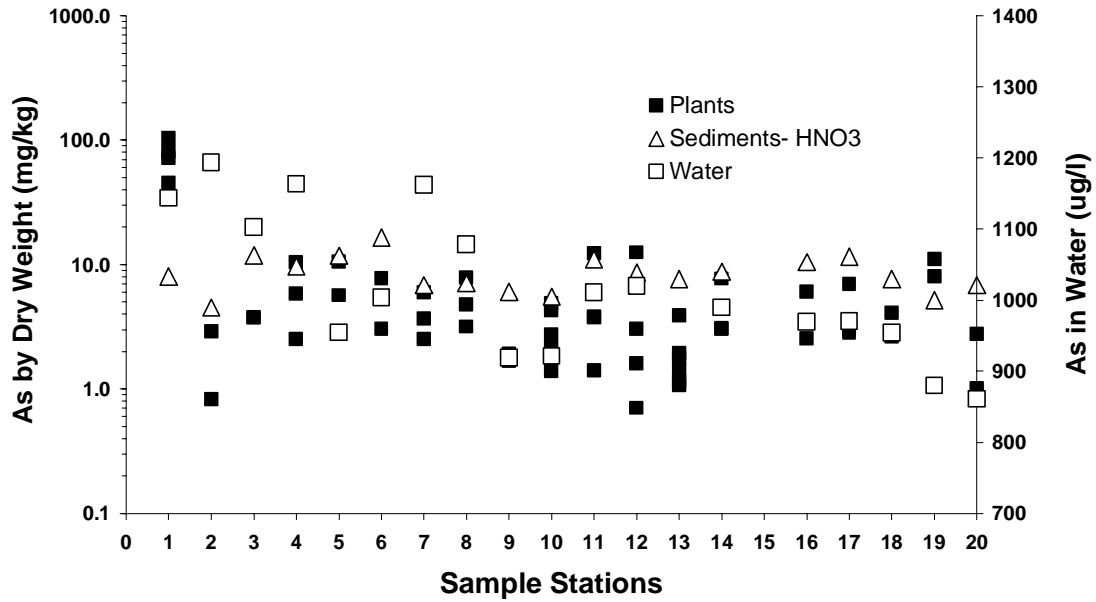


Figure A-5. Extraction of arsenic from plants, sediments, and water.

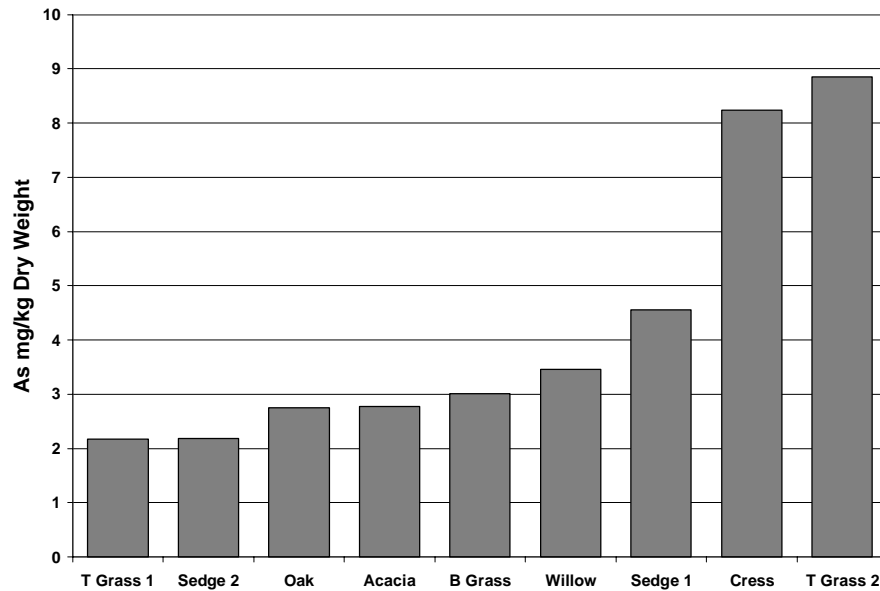


Figure A-6. Arsenic in plants by field name.

The arsenic in plants analysis reveals a few trends. Other than Station 1, with anomalously high values, no distinct trend in arsenic content was observed. Figure A-5 depicts arsenic concentrations in plants for all sample stations. There is good correlation between sediment values and arsenic in plants, a relationship not unexpected. A proportionality to water concentrations is much more tenuous, but there is a trend. The mean concentration of arsenic (censoring values from Station 1) in most of the plants lies below 3 (mg/kg) dry weight with SEDGE 1 slightly higher at 4.5 mg/kg and CRESS and TALL GRASS 2 substantially higher at 8.2 and 8.9 mg/kg, respectively. This is graphically depicted in Figure A-6. The minor organic fraction of the sediments should be locally derived and should not bias the sediment concentrations.

A.7.11.3 Plant Descriptions and Taxonomy

Plants were identified by John D. Vitti as well as the partial specimens allowed. Eight specimens are identified here. Seven are identified to the genus level; four of these seven include probable species level identification and two include possible species level identification. The remaining three of the ten specimens are identified to the family level only; two include probable genus level identification. Generally accepted common names are also listed [129, 130, 131]. The identification nomenclature follows current botanical convention:

Family level identification = Family.

Genus level identification = *Genus* Authority. [Family].

Species level identification = *Genus species* Authority. [Family].

Citations in the broader literature are given as found, or either without the Authority or without the Family listed (i.e., *Genus* [Family] or *Genus* Authority).

LOCAL OAK. A species of Oak, *Quercus* L. [Fagaceae]. Hardwood trees or shrubs of the temperate and tropical Northern Hemisphere. Worldwide: 450-500 species. Approximately 250 species occur in the Americas with Mexico as the center of distribution. Probably Netleaf Oak, *Quercus rugosa* Nee. [Fagaceae], the distinguishing characteristic being elaborately netted leaf venation.

TALL GRASS 1. A species of Fingergrass or Windmill Grass, *Chloris* Swartz. [Graminae]. Perennial or annual grasses of tropical and subtropical regions. Worldwide: 60-70 species. At least 10 species common in Mexico. Possibly *Chloris virgata* Sw. [Graminae], the distinguishing characteristic being racemes densely floriferous from tip to base.

BERMUDA GRASS. A species of *Hilaria* HBK. [Graminae]. Perennial grasses mostly with rhizomes or stolons. The genus consists of nine species, mainly distributed in southern North America. Possibly *Hilaria ciliata* (Scribn.) Nash. [Graminae], the distinguishing characteristic being bearded nodes.

TALL GRASS 2. A member of the Rush Family, Juncaceae. Perennial or annual grass-like herbs of temperate regions. Worldwide: 8 or 9 genera and 300-350 species. Two genera occur in the northern hemisphere: *Juncus* and *Luzula* accounting for approximately 300 species. Distinguished by culms filled with sponge-like pith. Probably a species of *Juncus* L. [Juncaceae].

CRESS. A species of False Loosestrife, *Ludwigia*, [Onagraceae]. Perennial herbs, mostly, of moist, warm regions. Worldwide: 70-80 species. Many common to Mexico.

Probably Water Purslane, *Ludwigia palustris* (L.) Elliott. [Onagraceae], the distinguishing characteristics being elliptic-ovate leaves and rooting at nodes.

ACACIA. A species of *Lysiloma* Benth. [Leguminosae]. Shrubs or trees of tropical and subtropical regions. The genus consists of 30-35 species of tropical America. Probably Watson Borderpod Acacia, *Lysiloma watsonii* J.N.Rose. [Fabaceae], the distinguishing characteristics being densely pubescent leaves and twigs and long, flat, cordlike-margined fruit.

WILLOW. A species of *Pluchea* Cass.[Compositae]. Malodorous, willowlike herbs or shrubs of warm or tropical regions. Worldwide: 40 species, mostly New World.

Probably *Pluchea salicifolia* (Mill.) Blake. [Compositae], the distinguishing characteristic being the dentate, conspicuously decurrent leaves terminating as foliaceous stem wings.

SEDGE 1. A member of the Sedge Family, Cyperaceae. Mostly perennial grass-like herbs widely dispersed around the globe. Worldwide: 75-80 genera and about 3200 species. Distinguished by solid, three-sided culms.

SEDGE 2. A member of the Rush Family, Juncaceae. Perennial or annual grass-like herbs with small regular persistent flowers. Worldwide: 8 or 9 genera and 300-350 species of temperate regions. Two genera occur in the northern hemisphere: *Juncus* and *Luzula* accounting for approximately 300 species. Distinguished by culms filled with sponge-like pith. Probably a species of *Juncus* L. [Juncaceae].

A.8. RIO SALADO TABULAR DATA

Table A-10. In-stream arsenic species concentration: Unfiltered samples ($\mu\text{g/L}$).

Station	As ³⁺	MMAA	As ⁵⁺	DMAA	Sum of Species	Total As	MMAA (%)	DMAA (%)	MMAA+DMAA (%)
1	0	0	1095	182	1290	1109	0%	14%	14%
2	64	0	1088	102	1267	1189	0%	8%	8%
3.3 (PM)	0	0	1171	113	1296	1042	0%	9%	9%
3.6 (AM)	0	41	973	228	1248	1073	3%	18%	22%
4	0	13	1178	91	1287	1142	1%	7%	8%
5	0	0	1076	62	1146	937	0%	5%	5%
6	0	0	1014	32	1052	985	0%	3%	3%
7	0	25	1048	171	1246	1119	2%	14%	16%
8	11	18	986	127	1141	1065	2%	11%	13%
9	0	24	827	28	883	909	3%	3%	6%
10	0	16	889	101	1005	897	2%	10%	12%
11	0	16	1038	107	1162	1002	1%	9%	11%
12	145	27	888	96	1156	983	2%	8%	11%
13	0	0	235	28	274	242	0%	10%	10%
14	26	16	968	96	1106	949	1%	9%	10%
16	13	13	1055	63	1144	909	1%	6%	7%
17	0	13	911	52	981	935	1%	5%	7%
18	0	20	956	36	1011	903	2%	4%	6%
19	0	0	867	16	892	848	0%	2%	2%
20	0	11	878	22	911	804	1%	2%	4%

Table A-11. In-stream arsenic species concentration: Filtered samples (µg/L).

Station	As ³⁺	MMAA	As ⁵⁺	DMAA	Sum of Species	Total As	MMAA (%)	DMAA (%)	MMAA+DMAA (%)
1	0	18	1130	146	1293	1065	1%	11%	13%
2	69	23	1085	94	1269	1121	2%	7%	9%
3.3 (PM)	0	11	1178	91	1284	1126	1%	7%	8%
3.6 (AM)	0	34	998	154	1193	1088	3%	13%	16%
4	0	18	1188	72	1281	1109	1%	6%	7%
5	0	0	1044	24	1077	970	0%	2%	2%
6	0	148	962	18	1130	964	13%	2%	15%
7	0	20	918	121	1060	1119	2%	11%	13%
8	16	50	896	94	1055	1046	5%	9%	14%
9	0	23	827	83	932	893	2%	9%	11%
10	0	16	750	74	840	888	2%	9%	11%
11	0	23	951	80	1058	722	2%	8%	10%
12	133	27	815	70	1044	983	3%	7%	9%
13	0	0	218	22	254	227	0%	9%	9%
14	28	23	756	66	872	911	3%	8%	10%
16	15	45	1006	36	1102	918	4%	3%	7%
17	0	0	957	51	1023	918	0%	5%	5%
18	0	18	956	33	1006	890	2%	3%	5%
19	0	0	1083	9	1098	821	0%	1%	1%
20	0	11	981	25	1017	756	1%	2%	4%

Table A-12. Unfiltered water samples, major elements.

Station	Ca ppm	Na ppm	Mg ppm	K ppm	SiO ₂ ppm	Ba ppb	Al ppb	Mn ppb	Fe ppb	Li ppm	Sr ppb	Mo ppb	Cu ppb	As ppb
1	3.2	296	0.19	13.6	531	ND	7	56.83	88.2	1.02	10.0	40.7	1.30	1109
2	3.8	312	0.20	13.7	533	ND	7	79.2	14.0	1.04	10.1	37.4	1.28	1189
3.3 (PM)	3.4	280	0.27	13.5	504	ND	9	77.6	28.2	1.02	9.1	39.8	1.38	1042
3.6 (AM)	3.6	280	0.28	13.3	518	ND	10	117.2	26.7	1.01	9.7	40.5	1.65	1073
4	3.4	306	0.26	13.5	522	ND	9	28.9	50.1	1.04	10.4	41.7	1.34	1142
5	3.7	276	0.28	13.6	496	ND	10	148.9	2.0	0.95	10.2	35.6	1.47	937
6	2.7	270	0.20	14	514	ND	7	10.4	0.6	0.97	6.9	42.9	0.12	985
7	3.8	300	0.30	13.6	513	ND	11	28.7	42.0	1.04	9.5	35.2	2.11	1119
8	3.7	298	0.29	14.1	505	ND	10	40.0	23.2	1.02	9.0	38.6	1.68	1065
9	4.2	275	0.33	13.7	452	ND	12	90.4	5.2	0.94	8.1	31.8	2.18	909
10	4.1	275	0.32	13.7	454	ND	9	43.2	4.0	0.91	8.4	37.2	2.53	897
11	3.7	287	0.32	13.9	482	ND	17	32.5	14.0	0.94	9.9	36.3	1.12	1002
12	3.8	280	0.60	13.8	488	6.4	24	63.5	32.0	0.91	9.9	37.2	1.29	983
13	2.5	64	1.38	3.7	254	ND	9	1.3	4.4	0.23	5.6	24.0	1.23	242
14	3.7	270	0.63	13.4	478	5.6	19	39.6	30.3	0.91	9.7	35.9	1.34	949
16	3.7	266	0.63	13.7	488	5.1	17	29.3	23.5	0.9	9.05	38.5	2.63	909
17	3.7	265	0.63	13.6	469	5.4	19	35.3	20.3	0.9	9.4	37.9	1.45	935
18	3.5	266	0.65	12.9	459	5.0	17	20.4	18.3	0.9	8.6	37.9	1.42	903
19	3.7	255	0.94	12.6	442	4.9	42	12.7	26.7	0.83	10.5	36.1	1.31	848
20	3.4	244	0.93	12.2	421	3.9	56	10.9	52.5	0.77	9.9	35.4	1.43	804
Powerline		280		22.6			103	74.9	0.8					
Agua Dulce		68		4.5			8	273.4	0.2					

Table A-13. Filtered water samples (0.45 µm), major elements.

Station	Ca ppm	Na ppm	Mg ppm	K ppm	SiO ₂ ppm	Ba ppb	Al ppb	Mn ppb	Fe ppb	Li ppm	Sr ppb	Mo ppb	Cu ppb	As ppb
1	3.8	292	0.19	12.7	486	ND	12	64.0	10.9	1.01	10.5	36.4	1.40	1065
2	3.8	306	0.19	13.2	511	ND	8	66.5	14.2	1.02	10.9	34.0	1.26	1121
3.3 (PM)	3.1	307	0.25	13	504	ND	11	90.2	26.4	1	9.2	35.5	1.36	1126
3.6 (AM)	3.5	297	0.28	13	494	ND	22	104.9	41.5	0.98	11.0	35.9	2.19	1088
4	3	295	0.25	13.3	513	ND	7	26.3	21.8	0.98	8.7	36.3	1.15	1109
5	3.7	290	0.3	13.5	476	ND	55	165.1	5.9	0.98	11.5	29.0	1.27	970
6	2.8	267	0.21	13.5	519	ND	7	61.1	3.9	0.93	9.7	39.8	0.55	964
7	3.8	294	0.3	13.5	507	ND	9	18.5	36.8	0.99	10.4	29.7	1.00	1119
8	3.8	285	0.32	13.6	500	ND	5	37.5	19.2	0.95	9.0	31.9	1.00	1046
9	4.2	268	0.34	13.6	446	ND	9	53.2	7.6	0.87	8.1	25.9	1.14	893
10	4.2	269	0.34	13.6	465	ND	13	38.2	2.1	0.86	8.5	24.9	1.12	888
11	3.8	289	0.32	14.2	488	ND	10	26.6	10.8	1	9.6	29.4	1.10	722
12	3.8	271	0.62	13.8	477	6.2	12	50.0	20.6	0.96	9.4	20.1	3.24	983
13	2.6	68	1.41	ND	251	ND	8	1.8	1.0	0.22	5.4	31.1	1.16	227
14	3.7	254	0.65	13.4	462	4.5	5	30.8	28.7	0.92	9.4	31.1	1.36	911
16	3.8	265	0.64	13.4	458	5.9	11	23.9	178.3	0.93	10.6	28.7	1.29	918
17	3.7	260	0.61	13.4	471	5.4	8	21.9	148.3	0.91	9.5	28.9	1.32	918
18	3.6	262	0.63	12.9	476	4.6	7	22.1	25.7	0.92	9.7	28.2	1.11	890
19	3.7	242	0.91	12.7	440	3.7	5	7.2	16.4	0.84	11.7	27.9	1.88	821
20	3.5	226	0.91	12.4	412	3.5	6	7.1	31.6	0.75	10.2	23.5	2.74	756

Table A-14. Anions and uncorrected alkalinity.

Station	Cl ppm	F ppm	Br ppm	B ppm	SO ₄ ppm	CO ₃ ppm	HCO ₃ ppm	NO ₃ ppm
1	93.1	14.8	0.81	7.3	26.8	ND	416	0.3
2	92.6	14.9	0.46	8.7	27.8	ND	392	ND
3.3 (PM)	92.6	15.7	0.37	7.1	28.5	ND	424	ND
3.6 (AM)	91.7	15.5	0.37	4.3	27.8	ND	408	ND
4	89.9	15.9	0.39	7.3	28.8	80	328	0.1
5	73.6	13.7	0.06	6.8	20.1	ND	328	0.1
6	79.2	15.0	0.50	9.4	20.3	88	300	0.1
7	92.0	16.0	0.42	8.9	28.5	56	320	ND
8	86.5	15.5	0.36	7.8	25.8	76	334	0.1
9	73.8	13.3	0.42	8.8	18.6	ND	368	0.2
10	75.4	14.0	0.25	9.3	19.1	104	270	0.1
11	82.5	15.1	0.33	5.7	22.9	160	236	ND
12	77.1	14.6	0.27	6.6	21.8	88	308	ND
13	16.9	6.1	ND	4.1	6.5	ND	88	ND
14	74.2	15.1	0.29	6.5	22.1	40	336	ND
16	75.9	14.7	ND	5.2	21.7	152	252	0.3
17	76.1	14.5	0.23	5.1	21.8	152	256	0.1
18	74.5	14.6	0.32	5.0	21.3	96	280	ND
19	70.9	13.8	0.27	4.7	20.3	144	220	ND
20	63.9	12.5	0.05	4.3	18.2	140	284	ND

Table A-15. Arsenic concentrations of time series samples.

Station	Date	As (ppb)	Station	Date	As (ppb)
RC-1	1/6/98	1284	RC-4	1/7/98	931
RC-1	1/6/98	1245	RC-4	1/7/98	976
RC-1	1/7/98	1120	RC-4	1/12/98	1019
RC-1	1/7/98	1164	RC-4	1/12/98	972
RC-1	1/13/98	1069	RC-4	1/13/98	931
RC-1	1/13/98	1211	RC-4	1/13/98	924
RC-3	1/6/98	1044	RC-7	1/12/98	654
RC-3	1/6/98	992	RC-7	1/12/98	718
RC-3	1/7/98	1044	RC-8	1/13/98	990
RC-3	1/7/98	1034	Powerline	1/7/98	906
RC-3	1/12/98	1006	Powerline	1/7/98	942
RC-3	1/12/98	997	Powerline	1/12/98	843
RC-3	1/13/98	1072	Powerline	1/12/98	938
RC-3	1/13/98	1037	Powerline	1/13/98	805
RC-3	1/13/98	981	Powerline	1/13/98	933
			Agua Dulce	1/11/98	186

Table A-16. Sediment Eh, organic carbon (TOC), and grain size distribution (Welch, 1999).

Location	Eh (mV)	TOC wt.%	<63 um	63-125 um	125-250 um	250 um - 0.5 mm	0.5-1.0 mm	1-2 mm
1	280	1.5	1.1	2.1	16.0	23.5	33.3	24.0
2	200	1.8	0.9	2.9	18.4	21.4	28.6	27.7
3 a.m.	80	2.0	0.3	1.8	18.0	18.8	29.4	35.6
3 p.m.	325	1.9						
4	310	1.7	0.4	3.2	16.9	23.5	31.2	24.8
5	200	2.5	2.0	9.2	25.4	26.1	20.8	16.5
6	267	3.0	2.4	6.1	17.2	27.4	30.5	16.4
7	220	2.6	1.7	6.9	22.2	27.1	29.6	12.6
8	230	1.6	0.2	1.9	15.8	25.6	27.4	29.1
9	212	1.9	1.9	1.9	6.2	16.6	37.0	36.4
10	250	1.8	1.6	2.4	6.1	16.9	35.8	37.3
11	210	3.0	1.7	5.2	18.0	30.4	28.0	15.0
12	225	1.8	2.1	5.9	16.4	18.9	29.9	26.9
13	200	3.1	1.8	4.8	14.2	26.0	33.2	20.0
14	70	2.3	2.8	6.4	18.1	29.3	30.2	13.2
16	280	3.1	14.8	14.4	53.1	15.0	1.8	0.9
17	290	3.7	1.3	5.2	27.3	40.8	19.0	6.4
18	280	1.3	0.1	1.9	13.1	23.0	34.5	27.3
19	350	1.3	0.8	3.1	11.3	17.3	33.5	34.1
20	340	1.2	0.0	0.2	1.7	11.8	47.0	39.3
Agua Dulce		1.5	0.3	1.1	8.2	25.5	32.6	32.2
Average		2.1	1.9	4.3	17.2	23.2	29.7	23.8
Standard Deviation		0.7	3.2	3.3	10.5	6.5	8.7	10.8

Table A-17. Arsenic bound in each size fraction as % of total arsenic and BET surface area (Welch, 1999).

Location	BET Surface Area (m ² /g)	<63 um	63-125 um	125-250 um	250 um -0.5 mm	0.5-1.0 mm	1-2 mm
1	0.7	3.9	3.0	10.4	12.9	52.0	17.8
2	0.8	1.3	3.6	16.9	20.5	31.9	25.8
3 a.m.		1.1	2.3	15.5	20.0	28.2	32.8
3 p.m.	1.2						
4	1.0	1.2	5.4	22.5	26.6	18.5	25.8
5	1.4	6.2	9.7	20.1	24.5	22.4	17.0
6	2.0	3.3	5.3	11.7	22.0	35.1	22.7
7	1.4	2.8	7.4	18.7	16.6	24.8	29.7
8	1.0	0.5	2.7	19.9	24.5	27.4	25.1
9	1.5	5.6	2.1	8.1	15.8	33.3	35.1
10	1.4	2.7	3.2	5.1	14.1	32.3	42.6
11	2.1	7.8	10.8	23.7	21.2	16.7	19.7
12	1.3	3.7	6.2	19.1	19.0	22.1	29.8
13	1.8	5.7	6.9	17.4	23.0	29.6	17.4
14	1.5	7.5	10.7	34.5	18.5	17.2	11.6
16	2.7	27.2	13.7	44.2	12.6	1.5	0.8
17	2.5	1.3	4.4	23.9	43.0	23.5	3.9
18	1.0	0.3	2.4	12.7	25.8	33.0	25.9
19	1.4	1.4	3.2	10.1	16.9	41.1	27.2
20	1.3	0.1	0.2	1.5	11.2	36.1	51.0
Agua Dulce	2.3	1.1	2.1	9.3	26.3	32.9	28.4
Average		3.0	4.8	15.8	21.2	29.4	25.8
Standard Deviation		2.5	3.1	7.8	7.0	8.7	10.6

Table A-18. Counts of arsenic measured for iron oxide and glasses by electron microprobe (Welch, 1999).

Sample ID	Mineral	Counts (As)	Sample ID	Mineral	Counts (As)
1	FeOx	2389	1	glass	1536
1	FeOx	2375	1	glass	1421
1	FeOx	2257	1	glass	1558
1	FeOx	3273	1	glass	1657
1	FeOx	2598	1	glass	1572
1	FeOx	2667	1	glass	1626
1	FeOx	2135	5	glass	1510
1	FeOx	2927	5	glass	1560
5	FeOx	4695	5	glass	1576
5	FeOx	6688	5	pyroxene	1966
5	FeOx	4398	8	glass	1582
5	FeOx	3226	8	glass	1628
5	FeOx	3059	9	glass	1518
8	FeOx	2407			
8	FeOx	2162			
8	FeOx	3231			
9	FeOx	3005			
Average FeOx		3140	Average glass		1593

Table A-19. Description of sediment >2 mm (Welch, 1999).

Location	Petrologic Description
1	75% pumice, 20% welded tuff fragments, 5% obsidian, <1% grains coated with FeOx's, minor plant fragments and some algae coatings on larger grains
2	58% welded tuff fragments, 30% pumice, 10% obsidian, 2% grains coated w/FeOx's, trace organic matter
3.6 (AM)	70% pumice, 20% welded tuff fragments, 8% obsidian, 2% grains coated w/FeOx's, <1% organic matter as twig and leaf fragments and algae coatings
3.3 (PM)	70% pumice, 20% welded tuff fragments, 8% obsidian, 2% grains coated w/FeOx's, <1% organic matter as twig and leaf fragments and algae coatings
4	50% welded tuff fragments, 33% pumice, 15% obsidian, 2% grains coated w/FeOx's, <1% organic matter as leaf and twig fragments
5	65% pumice, 20% welded tuff fragments, 12% obsidian, 3% grains coated w/FeOx's, <1% organic matter as leaf and twig fragments
6	80% pumice, 15% welded tuff fragments, 2% obsidian, 2% grains coated w/FeOx's, 1% organics-twigs, some algae coatings (sample has relatively less >2mm sed)
7	80% pumice, 13% welded tuff fragments, 6% obsidian, 1% grains coated w/FeOx's, <1% organic matter as leaf and twig fragments
8	80% welded tuff fragments, 10% pumice, 8% obsidian, 2% grains coated w/FeOx's, <1% organic matter as twig and leaf fragments
9	60% welded tuff fragments, 15% obsidian, 12% pumice, 2% grains coated w/FeOx's, <1% organic matter as leaf and twig fragments
10	60% welded tuff fragments, 25% pumice, 12% obsidian, 3% grains coated w/FeOx's, trace organic matter present
11	45% welded tuff fragments, 45% pumice, 10% obsidian, 2% grains coated w/FeOx's, <1% organic matter as leaf and twig frags and algae coatings on larger grains
12	15% obsidian, 50% welded tuff fragments, 32% pumice, 3% grains coated with FeOx's, <1% as leaf and twig fragments
13	70% obsidian, 20% pumice, 6% welded fragments, 2% grains coated w/ FeOx's, 2% organic matter as leaves and twigs
14	50% welded tuff fragments, 40% pumice, 8% obsidian, 2% grains coated w/FeOx's, <1% organic matter as leaf and twig fragments
16	69% pumice, 25% welded tuff fragments, 5% obsidian, 1% grains coated w/FeOx's, Trace organics (almost no sediment >2mm represented ~ 1-2% of total at that site)
17	80% pumice, 12% welded tuff fragments, 4% organic matter as leaf and twigs, 3% obsidian, 1% grains coated w/FeOx's
18	45% pumice, 33% welded tuff fragments, 20% obsidian, 2% grains coated w/FeOx's, <1% organic matter as leaf and twig fragments
19	75% welded tuff fragments, 17% pumice, 6% obsidian, 2% grains coated w/FeOx's, <1% organic matter as twig and leaf fragments
20	43% pumice fragments, 30% obsidian, 25% welded tuff fragments, 2% grains coated w/FeOx's, <1% organic matter as twig and leaf fragments and algae coatings
Agua Dulce	50% welded tuff fragments, 45% pumice, 4% grains coated w/FeOx's, 1% obsidian, trace organic matter

Table A-20. Fe, Mn, and As extracted by HNO₃ from whole sediment (Welch, 1999).

Location	Sample mass (g)	Fe (mg/kg)	Mn mg/kg	As (mg/kg)
1	1.280	1798	102	3.7
2	1.120	2342	33	4.4
3.6 (AM)	1.120	2236	45	4.1
3.3 (PM)	1.010	1699	225	5.9
4	1.050	1721	201	5.1
5	1.020	1276	147	12.8
6	1.150	3484	1045	15.3
7	1.090	2110	257	6.3
8	1.340	2910	179	5.3
9	1.020	2941	304	7.1
10	1.090	2752	183	5.2
11	1.160	3886	294	10.4
12	1.340	1644	149	5.0
13	1.060	1896	23	2.9
14	1.110	1838	184	6.8
16	1.100	2005	593	11.1
17	1.160	2236	679	7.3
18	1.100	1821	510	6.6
19	1.210	2397	107	7.0
20	1.240	1852	129	3.0
Agua Dulce	1.390	4095	101	2.9

Table A-21. Fe, Mn, Al, Si, and As extracted by HNO₃ from -80 mesh sediment (Welch, 1999).

Location	Sample mass (g)	Fe (mg/kg)	Mn (mg/kg)	Al (mg/kg)	Si (mg/kg)	As (mg/kg)
1	0.956	2908	103	2166	492	8.0
2	0.931	3602	18	2621	227	4.5
3.6 (AM)	0.899	3713	55	2916	379	11.8
3.3 (PM)	0.992	3428	316	2127	343	9.7
4	1.202	2830	258	2263	310	6.1
5	0.907	2595	232	3452	269	11.8
6	0.820	3848	770	3402	297	16.6
7	1.000	2713	319	3470	405	6.8
8	1.017	3601	356	2968	335	7.1
9	0.983	3478	276	4610	215	6.1
10	1.372	3984	228	4482	178	5.5
11	0.829	3788	554	4597	138	11.0
12	1.088	3383	347	3006	343	8.6
13	1.008	2611	0	6957	306	7.7
14	0.993	3078	230	2990	310	8.8
16	0.877	2981	634	4139	352	10.5
17	1.130	3024	800	4406	216	11.6
18	0.900	2923	526	2055	307	7.6
19	1.150	3642	120	3808	128	5.2
20	0.891	3415	189	3043	346	6.8
Agua Dulce	0.885	4569	56	8785	276	3.5

Table A-22. Fe, Mn, Al, Si, and As extracted by Chao reagent with ground -80 mesh sediment (Welch, 1999).

Sample ID	Sample mass (g)	Fe (mg/kg)	Mn (mg/kg)	Al (mg/kg)	Si (mg/kg)	As (mg/kg)
1	0.967	511	76	155	259	0.7
2	1.038	602	0	183	273	0.5
3.6 (AM)	1.123	560	24	223	252	1.3
3.3 (PM)	1.012	484	280	153	344	2.1
4	1.100	635	244	182	272	1.2
5	0.983	515	302	254	272	1.5
6	0.977	556	907	256	357	1.4
7	0.910	146	316	181	240	1.3
8	0.832	633	377	192	301	1.1
9	0.955	534	357	325	365	1.0
10	0.913	568	221	307	346	1.0
11	1.000	814	613	345	349	2.0
12	1.045	798	375	206	334	1.3
13	0.847	719	0	514	411	1.1
14	0.931	623	225	204	304	1.2
16	1.013	690	746	252	360	5.1
17	1.007	706	948	243	411	7.2
18	0.969	730	498	160	242	1.3
19	1.012	767	104	277	328	0.7
20	0.926	741	182	232	359	0.9
Agua Dulce	1.042	722	67	408	428	0.5

Table A-23. As species, Fe, and Mn extracted by 0.1M H₃PO₄ with ground -80 mesh sediment (Welch, 1999).

Location	Sample mass (g)	As ³⁺ (mg/kg)	As ⁵⁺ (mg/kg)	DMAA (mg/kg)	MMAA (mg/kg)	Fe (mg/kg)	Mn (mg/kg)
1	0.980	0.3	1.5	ND	ND	333	71
2	1.200	0.3	0.6	ND	ND	415	9
3.6 (AM)	1.170	0.7	2.6	ND	0.3	383	35
3.3 (PM)	0.970	0.6	2.4	ND	0.3	106	106
4	1.000	0.5	1.4	ND	ND	449	224
5	0.930	0.8	2.7	ND	0.4		
6	0.940	0.4	2.2	ND	ND	307	420
7	1.110	0.5	2.0	ND	0.2	70	115
8	1.060	0.5	1.6	ND	ND	345	246
9	1.090	0.4	1.7	ND	ND	324	263
9 b	0.950	0.5	2.0	ND	ND		
10	1.110	0.6	2.5	ND	ND	286	158
10 b	1.050	0.3	1.1	ND	ND		
11	0.990	0.8	4.1	ND	0.4	456	377
12	1.040	0.5	2.9	ND	ND	484	238
13	1.020	0.8	2.4	ND	0.3	434	16
14	1.000	0.7	2.3	ND	ND	327	183
16	0.990	0.8	4.8	ND	0.3	434	462
17	1.010	1.3	7.1	0.5	0.7	347	456
18	1.030	0.6	2.0	ND	0.3	421	345
19	0.990	0.4	1.4	ND	ND	524	87
20	1.120	0.4	1.4	ND	ND	447	138
Agua Dulce	1.060	0.4	1.7	ND	ND	534	54

Table A-24. Results of Tessier partial extractions (Welch, 1999).

As in Sediment Components (mg/kg)				
Location	Exchangeable	Carbonate	Fe/Mn Oxide	Organic
3.3 (PM) (a)	0.47	0.54	1.54	0.81
3.3 (PM) (b)	0.54	0.47	1.55	1.02
11	0.69	0.99	2.17	1.49
17	0.88	1.17	4.05	2.67
7	0.49	0.6	0.8	1.01
13	0.32	0.57	0.4	2.14
19 (a)	0.27	0.24	0.3	0.74
19 (b)	0.31	0.26	0.2	0.67
Mn in Sediment Components (mg/kg)				
Location	Exchangeable	Carbonate	Fe/Mn Oxide	Organic
3.3 (PM) (a)	0	32.9	265	0
3.3 (PM) (b)	0	22.1	255.1	0
11	0	36.5	566.6	42.20
17	0	123.6	701	78.20
7	0	33.6	298.7	14.4
13	7.9	7.9	0	0
19 (a)	0	30.8	79.6	12.50
19 (b)	0	36.8	56.6	13.40
Fe in Sediment Components (mg/kg)				
Location	Exchangeable	Carbonate	Fe/Mn Oxide	Organic
3.3 (PM) (a)	0	0	525.5	406.7
3.3 (PM) (b)	0	0	493.2	472.6
7	0	0	204.6	286.1
11	0	0	690.6	396
13	0	0	530.1	0
17	0	0	506	347.8
19 (a)	0	9	566.6	437.6
19 (b)	0	14	463.2	355.4

Table A-25. XRF determinations of elemental concentrations in whole sediment, mg/kg unless noted (Welch, 1999).

Sample	Sr	Rb	Th	Pb	Ga	Zn	Cu	Ni	Fe	Mn	Cr	Ba	V	As	U	Y	Zr	Nb	Mo	Fe ₂ O ₃ (%)	MnO (%)	TiO ₂ (%)
1	14	134	16	14	22	89	28	40	16017	387	340	56	4	6	6	47	540	50	4	2.29	0.05	0.16
1 b	14	134	16	14	22	88	5	7	15178	387	60	57	4	6	5	48	539	49	3	2.17	0.05	0.16
1 c	14	134	16	15	21	97	12	14	15458	387	131	53	3	6	6	47	540	50	4	2.21	0.05	0.16
1 d	14	131	15	14	22	88	5	6	15248	387	62	58	ND	6	5	47	537	49	4	2.18	0.05	0.16
2	28	137	17	14	23	91	5	7	16787	387	58	98	11	6	5	46	515	50	3	2.4	0.05	0.29
3.6 (AM)	23	140	16	15	23	91	5	7	15807	387	75	83	9	9	6	48	526	51	3	2.26	0.05	0.19
3.3 (PM)	25	140	17	16	23	98	5	6	18186	697	65	90	10	10	6	49	532	52	4	2.6	0.09	0.25
4	26	140	17	15	23	89	5	6	14968	542	63	94	ND	7	7	47	512	49	3	2.14	0.07	0.17
5	6	166	20	22	24	113	7	6	14199	465	60	24	ND	13	8	63	442	63	4	2.03	0.06	0.11
6	21	159	18	20	23	110	5	6	16227	1239	47	58	5	20	7	56	442	58	5	2.32	0.16	0.14
7	16	144	17	17	23	93	5	4	14339	697	10	69	ND	10	6	50	499	52	3	2.05	0.09	0.15
8	26	136	16	15	22	96	5	5	15458	774	63	93	5	8	6	44	499	49	4	2.21	0.1	0.18
9	27	147	18	20	24	101	15	6	15528	620	49	88	7	9	6	51	499	56	4	2.22	0.08	0.19
10	41	143	17	17	23	100	6	7	16577	542	67	149	10	8	6	51	491	54	4	2.37	0.07	0.21
11	15	145	17	18	23	104	10	6	15528	852	55	70	4	13	7	53	491	54	4	2.22	0.11	0.15
12	24	139	15	15	23	95	6	6	15598	697	69	112	5	10	6	47	502	51	3	2.23	0.09	0.18
13	13	151	18	20	24	104	5	7	15038	310	88	52	ND	9	7	54	507	60	3	2.15	0.04	0.15
14	18	139	17	16	22	97	7	6	15458	542	52	73	7	10	6	47	416	51	3	2.21	0.07	0.17
16 a	18	139	17	17	22	96	9	12	14409	929	102	84	ND	13	5	48	477	51	3	2.06	0.12	0.15
16 b	18	137	17	16	23	95	7	9	14129	929	72	82	6	13	5	49	478	51	3	2.02	0.12	0.14
17	11	145	18	17	23	102	6	8	14828	1239	76	78	4	16	6	52	479	53	3	2.12	0.16	0.13
18	27	134	16	15	22	93	8	5	14548	774	55	117	4	9	5	45	499	47	3	2.08	0.1	0.17
19	27	168	19	17	24	102	6	7	16017	387	70	98	8	9	7	59	559	63	3	2.29	0.05	0.18
20	23	156	17	16	23	99	6	6	15388	465	58	95	5	7	7	53	557	57	4	2.2	0.06	0.17
Agua Dulce	31	231	22	24	29	140	10	8	16787	310	55	80	7	6	8	77	688	95	2	2.4	0.04	0.17

Table A-26. Mineral surface sorbing sites determined by HNO₃ digestion on -80 mesh sediment.

Station	Fe mg/kg	Ferrihydrite Strong Sites (molal)	Ferrihydrite Weak Sites (molal)	Goethite Sites (molal)	Gibbsite Sites (molal)
1	2908	9.5E-04	3.8E-02	2.8E-03	2.2E-03
2	3602	1.2E-03	4.7E-02	3.5E-03	2.6E-03
3 a.m.	3713	1.2E-03	4.9E-02	3.6E-03	2.9E-03
3 p.m.	3428	1.1E-03	4.5E-02	3.4E-03	2.1E-03
4	2830	9.3E-04	3.7E-02	2.8E-03	2.3E-03
5	2595	8.5E-04	3.4E-02	2.5E-03	3.5E-03
6	3848	1.3E-03	5.0E-02	3.8E-03	3.4E-03
7	2713	8.9E-04	3.6E-02	2.7E-03	3.5E-03
8	3601	1.2E-03	4.7E-02	3.5E-03	3.0E-03
9	3478	1.1E-03	4.6E-02	3.4E-03	4.6E-03
10	3984	1.3E-03	5.2E-02	3.9E-03	4.5E-03
11	3788	1.2E-03	5.0E-02	3.7E-03	4.6E-03
12	3383	1.1E-03	4.4E-02	3.3E-03	3.0E-03
13	2611	8.5E-04	3.4E-02	2.6E-03	7.0E-03
14	3078	1.0E-03	4.0E-02	3.0E-03	3.0E-03
16	2981	9.8E-04	3.9E-02	2.9E-03	4.2E-03
17	3024	9.9E-04	4.0E-02	3.0E-03	4.4E-03
18	2923	9.6E-04	3.8E-02	2.9E-03	2.1E-03
19	3642	1.2E-03	4.8E-02	3.6E-03	3.8E-03
20	3415	1.1E-03	4.5E-02	3.3E-03	3.1E-03

Table A-27. Mineral surface sorbing sites determined by HNO₃ digestion on whole sediment.

Station	Fe mg/kg	Ferrihydrite Strong Sites (molal)	Ferrihydrite Weak Sites (molal)	Goethite Sites (molal)	Gibbsite Sites (molal)
1	1798	5.9E-04	2.4E-02	1.8E-03	2.2E-03
2	2342	7.7E-04	3.1E-02	2.3E-03	2.6E-03
3 a.m.	2236	7.3E-04	2.9E-02	2.2E-03	2.9E-03
3 p.m.	1699	5.6E-04	2.2E-02	1.7E-03	2.1E-03
4	1721	5.6E-04	2.3E-02	1.7E-03	2.3E-03
5	1276	4.2E-04	1.7E-02	1.2E-03	3.5E-03
6	3484	1.1E-03	4.6E-02	3.4E-03	3.4E-03
7	2110	6.9E-04	2.8E-02	2.1E-03	3.5E-03
8	2910	9.5E-04	3.8E-02	2.8E-03	3.0E-03
9	2941	9.6E-04	3.8E-02	2.9E-03	4.6E-03
10	2752	9.0E-04	3.6E-02	2.7E-03	4.5E-03
11	3886	1.3E-03	5.1E-02	3.8E-03	4.6E-03
12	1644	5.4E-04	2.2E-02	1.6E-03	3.0E-03
13	1896	6.2E-04	2.5E-02	1.9E-03	7.0E-03
14	1838	6.0E-04	2.4E-02	1.8E-03	3.0E-03
16	2005	6.6E-04	2.6E-02	2.0E-03	4.2E-03
17	2236	7.3E-04	2.9E-02	2.2E-03	4.4E-03
18	1821	6.0E-04	2.4E-02	1.8E-03	2.1E-03
19	2397	7.8E-04	3.1E-02	2.3E-03	3.8E-03
20	1852	6.1E-04	2.4E-02	1.8E-03	3.1E-03

Table A-28. Mineral surface sorbing sites determined by H₃PO₄ digestion on -80 mesh sediment

Station	Fe mg/kg	Ferrihydrite Strong Sites (molal)	Ferrihydrite Weak Sites (molal)	Goethite Sites (molal)	Gibbsite Sites (molal)
1	333.2	1.1E-04	4.4E-03	3.3E-04	1.6E-04
2	415.1	1.4E-04	5.4E-03	4.1E-04	1.8E-04
3 a.m.	383.3	1.3E-04	5.0E-03	3.7E-04	2.2E-04
3 p.m.	105.8	3.5E-05	1.4E-03	1.0E-04	1.5E-04
4	449.2	1.5E-04	5.9E-03	4.4E-04	1.8E-04
5	324.0	1.1E-04	4.2E-03	3.2E-04	2.6E-04
6	307.3	1.0E-04	4.0E-03	3.0E-04	2.6E-04
7	69.9	2.3E-05	9.2E-04	6.8E-05	1.8E-04
8	345.1	1.1E-04	4.5E-03	3.4E-04	1.9E-04
9	323.8	1.1E-04	4.2E-03	3.2E-04	3.3E-04
10	285.7	9.3E-05	3.7E-03	2.8E-04	3.1E-04
11	455.6	1.5E-04	6.0E-03	4.5E-04	3.5E-04
12	484.1	1.6E-04	6.3E-03	4.7E-04	2.1E-04
13	433.7	1.4E-04	5.7E-03	4.2E-04	5.2E-04
14	326.5	1.1E-04	4.3E-03	3.2E-04	2.1E-04
16	434.1	1.4E-04	5.7E-03	4.2E-04	2.5E-04
17	346.5	1.1E-04	4.5E-03	3.4E-04	2.4E-04
18	420.6	1.4E-04	5.5E-03	4.1E-04	1.6E-04
19	523.8	1.7E-04	6.9E-03	5.1E-04	2.8E-04
20	446.5	1.5E-04	5.8E-03	4.4E-04	2.3E-04

Table A-29. Mineral surface sorbing sites determined by Chao reagent digestion on -80 mesh sediment.

Station	Fe mg/kg	Ferrihydrite Strong Sites (molal)	Ferrihydrite Weak Sites (molal)	Goethite Sites (molal)	Gibbsite Sites (molal)
1	511	1.7E-04	6.7E-03	5.0E-04	1.6E-04
2	602	2.0E-04	7.9E-03	5.9E-04	1.8E-04
3 a.m.	560	1.8E-04	7.3E-03	5.5E-04	2.2E-04
3 p.m.	484	1.6E-04	6.3E-03	4.7E-04	1.5E-04
4	635	2.1E-04	8.3E-03	6.2E-04	1.8E-04
5	515	1.7E-04	6.7E-03	5.0E-04	2.6E-04
6	556	1.8E-04	7.3E-03	5.4E-04	2.6E-04
7	146	4.8E-05	1.9E-03	1.4E-04	1.8E-04
8	633	2.1E-04	8.3E-03	6.2E-04	1.9E-04
9	534	1.7E-04	7.0E-03	5.2E-04	3.3E-04
10	568	1.9E-04	7.4E-03	5.6E-04	3.1E-04
11	814	2.7E-04	1.1E-02	8.0E-04	3.5E-04
12	798	2.6E-04	1.0E-02	7.8E-04	2.1E-04
13	719	2.4E-04	9.4E-03	7.0E-04	5.2E-04
14	623	2.0E-04	8.2E-03	6.1E-04	2.1E-04
16	690	2.3E-04	9.0E-03	6.7E-04	2.5E-04
17	706	2.3E-04	9.2E-03	6.9E-04	2.4E-04
18	730	2.4E-04	9.6E-03	7.1E-04	1.6E-04
19	767	2.5E-04	1.0E-02	7.5E-04	2.8E-04
20	741	2.4E-04	9.7E-03	7.2E-04	2.3E-04

A.9. DATA QUALITY

A.9.1. Reagents and Standards

Trace metal grade reagents were used when available. Fisher Trace Metal HCl and NH₄OH were diluted as necessary. These reagents were used for column preparation and regeneration that does not require very precise molarity, and they were not standardized. HCl and NH₄OH used for ion exchange chromatography eluant were standardized to pH values within ± 0.05 units of optimal. The maximum error from this simplification is less than 10% for HCl and less than 1% for NH₄OH. TCA for elution was made from Sigma ACS reagent solid and could be formulated by dilution to precise molar concentrations. The measured pH of the 0.006 M trichloroacetic acid (TCA) was 2.25 ± 0.05 and the 0.2 M TCA was 1.05 ± 0.05 at 23.2 °C. The pH was checked when stock solutions were made.

With the exception of MMAA, all arsenic standards were obtained from Sigma. MMAA could not be located through the normal chemical suppliers. MMAA was obtained from Dr. Dean Carter of the University of Arizona. As³⁺ standards were prepared from American Chemical Society (ACS) certified reagent grade arsenic trioxide. As³⁺ standards were prepared the day of use as a 1.000 g/L arsenic stock solution by dissolution in 100 ml of hot 1.0 M trace metal grade HCl and dilution to 1 liter with Type I (ASTM) water. Complete oxidation of As³⁺ standards to As⁵⁺ in two weeks was observed during this effort. Partial oxidation has been observed in less than 12 hours. Attempts were not made to preserve the As³⁺ standards. As⁵⁺ and DMAA standards were prepared from ACS reagent sodium arsenate and Sigma Ultra cacodylic acid as 1.000 g/L arsenic stock solutions by dissolution in 1 liter of Type I water. Since only ~50 mg of MMAA was made available to this effort, a 52 ppm as arsenic stock solution was prepared by dissolving 0.0201 g of MMAA in 100 ml of Type I water.

A.9.2. Quality Assurance

Design of this project incorporated a data quality objective (DQO) development process early in its inception. It was recognized that this data might be used for risk assessment, risk management, or comment on rulemaking. Balanced with this was the necessity to limit analytical and field costs. Data quality objectives had to be set to meet these competing priorities.

A DQO process was used to define the sampling and analysis program described here. The DQO process was created by the USEPA in the late 1980's for use in the Superfund program as part of a general, and ongoing, revision of their quality assurance and quality control practice, regulation, and guidance. The DQO process borrows heavily from elements of Terzhagi's observational method and other well accepted experimental design principles. USEPA's objective was to create a publicly-acceptable quality framework for environmental data collection that would meet the needs of environmental compliance and risk assessment at lowest cost. The intended purpose of the DQO process is to ensure that:

1. The questions to be answered through data collection and analysis are well defined;
2. The data collected is of known quality;
3. An acceptable level of uncertainty for answers to the questions is specified; and
4. The cost, amount, and quality of data necessary to answer questions are critically evaluated.

The DQO process enabled establishment of the following findings and objectives.

1. Combining arsenic analysis with surface water flow measurement allows evaluation of the sources and sinks of arsenic, kinetics of arsenic transformations, and the role of other chemicals in arsenic behavior.
2. High levels of arsenic may make it easier to inspect the system for processes that are known to occur, but have elusive quantification.
3. Speciation of arsenic was required because the species distribution was unknown.
4. A broad range of analysis is required to allow detailed evaluation of water-mineral chemistry and mechanistic modeling of system geochemistry.
5. Sample aliquots were preserved appropriately and were large enough to allow additional analyses to be conducted if data gaps are identified.
6. Analytical techniques should be comparable to a US laboratory protocol or peer reviewed publications.
7. Physical and chemical parameters such as temperature, pH, Eh, streamflow needed to be measured.
8. Sediment mineralogy, physical properties, and surface chemistry required investigation.
9. The density of measurements was selected to arsenic speciation and partitioning at different scales.
10. The uncertainty in the data and interpretation was hoped to be comparable to that of a preliminary risk assessment or initial remedial investigation.
11. Plan review was accomplished before project implementation.

The data set was very broad in terms of the analysis conducted and was found to be of good accuracy and precision. At this point it was determined that exploratory modeling using a thermodynamically based, mechanistic SC approach was possible with the existing data set. Correction of a few data gaps and inclusion of the Rio Salado sediment data [106] was required for modeling. The predictions are made using thermodynamic properties and assume equilibrium conditions.

All data collection met project-specific precision, accuracy, representativeness, completeness, and comparability criteria (PARCC parameters) or it was determined that an out-of-control event had taken place and the data used with caution if used at all. Chemical analyses should meet the precision and accuracy standards of SW-846 in order for the data to be acceptable. Generally, the reconnaissance data met these requirements. However, due to the novel and exploratory use of the data, full SW-846 QA (matrix spikes, matrix spike duplicates, and internal laboratory QA programs) was not invoked. Some methods, such as ion exchange chromatography and sediment partial extraction do not have SW-846 equivalents. All non-SW-846 analytical methods used have been peer reviewed, published in peer reviewed journals, or developed as part of this effort.

Sample types were determined based on the environmentally significant repositories of arsenic at the field site, namely water, geomeia, and plants. The sample locations for the reconnaissance survey were selected based on several factors. The first

was to limit the number of sample locations to 20 for the reconnaissance survey so that all locations could be sampled within time and budget constraints. Next was to ensure that all major arsenic sources (thermal springs) be sampled directly. Samples are also desired at each of the existing flow structures and above and below the coalescence between first and second order streams to separate arsenic contributions and effects. An approximate sample spacing of 500 meters within the watershed was selected to enable the study to observe arsenic transformation kinetics on the scale that it had been noted in Hot Creek, California [48]. Additional sample locations were filled in at approximately this spacing. Finally, two sample locations were selected at a distance of 2 and 6 km downstream of RC-8 to examine far-field geochemistry.

All sample containers were new HDPE (Nalgene or equivalent) bottles or pails. All containers were cleaned with Alconox detergent and warm water, triple rinsed with tap water, triple rinsed with Type I water, and allowed to air dry with openings down. Following drying, caps were replaced and sample containers stored in zip-closure plastic bags for transportation to the field. Any other field sampling equipment was field cleaned immediately following use with 1.0 M Fisher Trace Metal grade HCl, and triple rinsed with Type I water. All field sampling equipment was cleaned nightly with an Alconox wash, triple rinse with Type I water, and air drying. No sampling equipment was exposed to the high-arsenic tap water available at the field site.

All water samples were containerized and preserved according to USEPA SW-846 accepted methods. Samples remained in the sample team custody throughout the sampling event and were transported to the laboratory in the custody of the sampling team. Water and sediment samples were stored at $4 \pm 2^\circ\text{C}$ until analysis. SW-846 mandated holding times were met. All sample locations are identified alphanumerically. Sample numbers were recorded in the project logbook. These numbers will be used to track the samples until final disposal.

Data was obtained from the analytical laboratory in electronic format to minimize transcription errors. A copy of the raw data was archived along with copies of logbooks and other data that would be difficult to reproduce. Spreadsheets were used for data manipulation and unit conversions. A number of types of exploratory statistical methods were used to examine the data for trends and outliers, such as box and whisker plots or analysis of distributions using histograms and probability plots.

All data to be collected was used for the evaluation of arsenic environmental chemistry. The initial parameter lists were broad in order to orient the study to a reduced set of analyses for following work. Surface water flow data was needed to evaluate mass balance and determine reaction kinetics and partitioning. Sediment data is needed to evaluate solid-water partitioning coefficients. All of the data obtained, in either raw or reduced form was used to develop the conceptual model and calibrate and validate the numerical model(s). In order to model an environmental system, the mathematical formulation of the model must be capable of accurately representing the physical system that is being modeled. This was accomplished by comparing the model output to an analytical solution for a simple system. This was accomplished for the public domain codes. Models were verified for successful computer installation by running example data sets and by comparison with the supplied test data set outputs. Code modifications were documented. There were no problems in code compiling. After any code modification, a test data set was used to demonstrate that the computer code produces a

correct solution to the mathematical model, and that the mathematical model is a valid solution to the physical problem. Once this was accomplished and documented, the code was considered to be verified. Following verification steps input parameters were systematically varied to produce a valid model of the physical system under consideration. Once the calibration target was met or exceeded (Rio Salado model), the model is ready for use for predictions (Florida Model).

Other quality assurance activities included logging of all field and lab data in bound logbooks, noting out of control events and their resolution, written preplanning of all activities, and following standard field and laboratory hygiene and safety practices. All equipment was used and maintained according to manufacturer's instructions. Malfunctioning equipment was removed from service until repairs were made. Backup equipment was available for most needs.

A.9.3. Quality Control

The GFAA and FAA use autocalibration procedures based on standard dilution. FAA methods for the analytes of interest are routinely run at the NMBMMR laboratory and no modification of the standard methods was necessary to achieve accurate reproducible results. This was not true for ion-exchange chromatography samples that were strongly attenuated by matrix and arsenic species effects. Special procedures were implemented in order to meet PARCC parameters for these samples.

In the case of the GFAA arsenic analysis in acidified total metals samples, little or no matrix effect was noted. The calibration curve for these samples was developed using 20 and 50 ppb standard solutions of As^{5+} in Type I water acidified to $\text{pH} < 2$ with ultra pure HNO_3 . All analytical methods used a five point calibration curve. A blank and a 20 ppb standard were analyzed at the rate of 1 in 20. Calibration reslope was performed every 20 samples and recalibration every 40. It was noted that there was some negative bias with the mean value of 20 ppb standard (36 measurements) being 17.9 ppb. The GFAA is able to achieve detection at 1.0-1.5 ppb without matrix effects. For this effort a practical quantification limit (PQL) was set to 2.0 ppb, a value greater than the mean of the blank (36 measurements) plus two standard deviations, that gives a reproducible absorbance peak (RMS error $< 10\%$ for 3 analyses).

The samples from the arsenic speciation exhibited strong matrix effects. In order to correct for this effect, standards were made by spiking eluant from a blank ion exchange separation. The blank eluant did not have detectable arsenic before the spike. This was also a control check for the regeneration process since the columns had been used with arsenic standards before the blank eluant run. The 0-55 ml fraction was used to prepare the standard for As^{3+} and MMAA analysis, the 55-85 ml fraction for As^{5+} analysis, and the 95-140 ml fraction for DMAA analysis. These standards were all spiked from the As^{5+} stock solution to 20 and 50 ppb strength. A NITS traceable standard was tested, providing a result of 56.6 ppb with a true value of $56.02 \pm 0.73 \mu\text{g/L}$ arsenic as As^{5+} . Duplicates were run to spot-check unexpected values, however, there was no systematic use of duplicates. A double peak in the absorbance was also noted for the speciation matrices. The ramp and drying times for the GFAA were adjusted until this was not problematic. Arsenic analysis by GFAA is generally subject to recovery, accuracy, and precision problems. This is evidenced by the USEPA SW-846 acceptable

limits for Method 7061 (GFAA) of 60-140% for accuracy (% recovery), precision of 0-40% (reproducibility) at a method detection limit of 1.4 ppb and reporting limit of 2.0 ppb. These problems were also noted in this effort.

Quantification limit studies were not performed for aqueous analytes other than arsenic since they are run routinely at the NMBMMR laboratory and/or the current level of investigation does not require greater accuracy and precision than was available to this study. There is an exception, phosphate as PO_4 . Phosphate is known to affect arsenic SC. The NMBMMR IC, as normally configured, has a PQL for phosphate of 100 ppb. The corresponding detection limit is ~60 ppb. It is possible that <60 ppb of phosphate could noticeably affect arsenic speciation when the arsenic level is closer to the phosphate level. This is in an arsenic and phosphate concentration range that may be common. Using the standard IC setup, phosphate was not detected in Rio Salado waters. It would improve the present and future work to lower the PQL for phosphate at the NMBMMR laboratory.

A.9.4. Rio Salado Data Quality Assessment

Samples are generally representative of the site conditions because deviations were not made from acceptable sampling practice for the media of interest. With the exception of arsenic speciation, chemical data is 'complete' because >90% of all data collected meets PARCC requirements within project standards. The chemical data is comparable to other data collected using SW-846 protocols. The DMAA data obtained is suspect and the achievable phosphate PQL should be lowered for low-arsenic work.

Speciation of Arsenic in Water

Investigation of the speciation of arsenic in the environment requires the ability to preserve the arsenic species before analysis, or to separate the species before transformation takes place. Given the uncertainties in the preservation of arsenic species, field separation was selected. Separation is initiated within minutes of sample collection. Uncertainties associated with sample preservation are eliminated. In order to accomplish this, an existing ion chromatography separation method for As^{3+} , As^{5+} , MMAA, and DMAA was modified for field use [124].

A.9.4.1 Speciation Method Modification

The published method uses 9 cm of anion exchange resin (100-200 mesh, AG-1X8, Bio-Rad) and 26 cm of cation exchange resin (100-200 mesh, AG50W-X8, Bio-Rad) in a single 1×35 cm nitrogen pressurized glass column to separate these four arsenic species. Since nitrogen pressurization was not practical for field use, gravity flow and 50-100 mesh resin was used to allow separation in a reasonable time. Using gravity, the flow rate was maintainable at about 3 ml/min. Separations were completed roughly one hour after sample introduction.

A second modification was the use of two glass columns in series connected by a capillary tube, a 1×10 cm column for the anion resin at the bottom, and a 1×30 cm upper column for the cation exchange resin, rather than a single column containing both resins in layers. There were several reasons for this modification. Occasionally Grabinski's columns required repacking to remove air bubbles that caused non-ideal flow conditions [124]. The anion and cation exchange resin must not be mixed during this process.

Laboratory testing indicated that this would be difficult on a stream bank. By keeping the cation resin separate, it is possible to remove air bubbles by agitating the resin with a pipette. The anion resin is back flushed with a wash bottle to remove air bubbles. Another reason is that capillary connections between columns can provide for peak sharpening by allowing the main mass to catch up with the diffuse peak. All columns were stock borosilicate glass "Econo-Columns" from Bio-Rad. Prior to packing, all columns and connectors were cleaned with Alconox detergent and warm water, triple rinsed with tap water, triple rinsed with 1.0 M Fisher Trace Metal grade HCl, triple rinsed with Type I water, and allowed to air dry with openings down or covered with Kim-Wipe laboratory tissue. The anion column was filled with a 10 cm bed of AG-1X8 resin in the chloride form and capped top and bottom with a porous polymer bed support and Luer fitting. The cation column was filled with 26 cm of AG50W-X8 resin in the hydrogen form using a porous polymer bed support and Luer fitting at the base. The capillary used is a Luer connector. All columns were slurry filled with resin using Type I water and preconditioned before used.

Column conditioning, elution, and regeneration generally followed the method outlined by Grabinski. Following packing, the columns were conditioned by rinsing with 70 ml of Type I water, then two ordered series of 70 ml aliquots each of 1.5 M NH₄OH, 1 M HCl, and 0.48 M HCl. Arsenic species were not used in preconditioning. Grabinski states that "several" of the same series were used for preconditioning in his work, preceded by introduction of 50 µg each of As³⁺, As⁵⁺, MMAA and DMAA. Grabinski and this effort both used a single series to regenerate the columns between elutions. This effort preconditioned the columns with 25 ml of 0.006 M trichloroacetic acid (TCA) following the 1.50 M NH₄OH, 1.00 M HCl, and 0.48 M HCl series (before sample introduction) as suggested by Maiorino and Aposhian [114]. Grabinski did not mention preconditioning with TCA. Columns were also stored overnight, saturated with 0.006 M TCA in the laboratory and field.

A.9.4.2 Speciation Method Performance

Arsenic speciation methods were researched to find a procedure suitable for field use. No organic/inorganic arsenic method was found that was directly transferable to the field. The Grabinski method was selected for modification and testing in the laboratory. The most important factor to evaluate was if gravity flow variable head ion exchange chromatography could be used to resolve the arsenic species of interest. Recovery of arsenic standards was tested and limited optimization of the procedure conducted. There remains considerable room for refinement of the procedure. Time and budget did not allow detailed experimentation with the separation method for this project. Following determination that the gravity flow method would separate the four arsenic species of interest, in the concentration range expected at Rio Salado, the method was taken to the field.

Grabinski indicates good arsenic recovery rates (96-107%) at total arsenic concentrations below 500 ppb. The modifications to the method resulted in lower recoveries than published by Grabinski. The results obtained from the lab and field separations still provide useful data. Grabinski had noted that separation efficiency tailed off at total arsenic concentrations of greater than 500 ppb (1 µg in 2 ml). Sample recoveries tabulated in Table A-30 indicate this problem clearly. I did not try to increase

recovery rate prior to field implementation of the modified method. There is also peak overlap for MMAA and As^{3+} at 1.0 ppm concentration that is not apparent in Grabinski's data. Ion exchange chromatographic methods were used to separate the arsenic species into separate aliquots for analysis by graphite furnace atomic absorption quantification.

Table A-30. Ion exchange chromatography - GFAA recovery rates.

Method	As^{3+}	MMAA	As^{5+}	DMAA
Grabinski	104%	100%	97%	99%
Modified 250 ppb	90%	85%	116%	77%
Modified 1000 ppb	92%	75%	63%	43%

The ion chromatography method depends on the property of arsenic species to change charge depending on pH. Referring to the Table A-31 of weak acid disassociation constants (pK_a) below it is clearly seen that pH has a strong influence on the ionic charge of arsenic species. As^{3+} , as HAsO_2 , As^{5+} as H_3AsO_4 , and MMAA are either neutral or negatively charged oxyanions at pH values from 1-12. DMAA can act as an anion, neutrally charged, or a cation dependent on pH.

Table A-31. Acid disassociation constants for arsenic compounds.

Species	Below pK_1	pK_1	$\text{pK}_1 \leftrightarrow \text{pK}_2$	pK_2	Above pK_2	pK_3
As^{3+}	neutral	9.18	anion			
As^{5+}	neutral	2.22	anion	6.98	anion	11.60
MMAA	neutral	3.41	anion	8.18		
DMAA	cation	2.60	neutral	6.27	anion	

It is this principle that allows separation of these four arsenic species by ion exchange chromatography. Below a pH of 9.18, As^{3+} is a neutral species, above that pH it is an anion. For As^{5+} below pH 2.22, As^{5+} is neutral, above that pH it is negatively charged. Below a pH of 3.41, MMAA is a neutral species, above that pH it is an anion. DMAA below a pH of 2.60 is in the cation form, between 2.6 and 6.27 it is neutral and above pH 6.27 it is an anion. By selective use of eluant, it is possible to take advantage of these differences and separate the four species.

The elution process is as follows. The sample is gently introduced to the top of the cation exchange column using a 2 ml class A pipette (± 0.006 ml). The stopcock on the base of the column is opened and 2 ml of the 0.006 M TCA is wasted. As in the Grabinski method, the sample is then eluted using 55 ml of 0.006 M TCA, 8 ml of 0.2 M TCA, 55 ml of 1.5 M NH_4OH , and 50 ml of 0.2 M TCA that are gently decanted into a gravity fed reservoir. Since gravity flow is used, flow rates are variable as the head on the column changes.

The arsenic species separations work in the following manner. In 0.006 M trichloroacetic acid, $\text{pH} < 2.5$, the As^{3+} and MMAA exist in solution as uncharged species, the As^{5+} exists primarily as an anionic species, and DMAA is dominantly a cation. Most of the DMAA is retained at this pH on the cation exchange column. Elution of the neutral As^{3+} is not retarded by cation and anion exchange resins and elutes the first 25 ml. The second fraction of the eluted solution (25 to 55 ml) contains the MMAA. Although the MMAA is also predominantly uncharged, it elutes behind the As^{3+} . The literature did not contain any detailed, plausible explanations of this behavior. It is probable that the MMAA is weakly retained due to non-polar interactions or other processes that are not well understood at this time. The retardation of the MMAA is

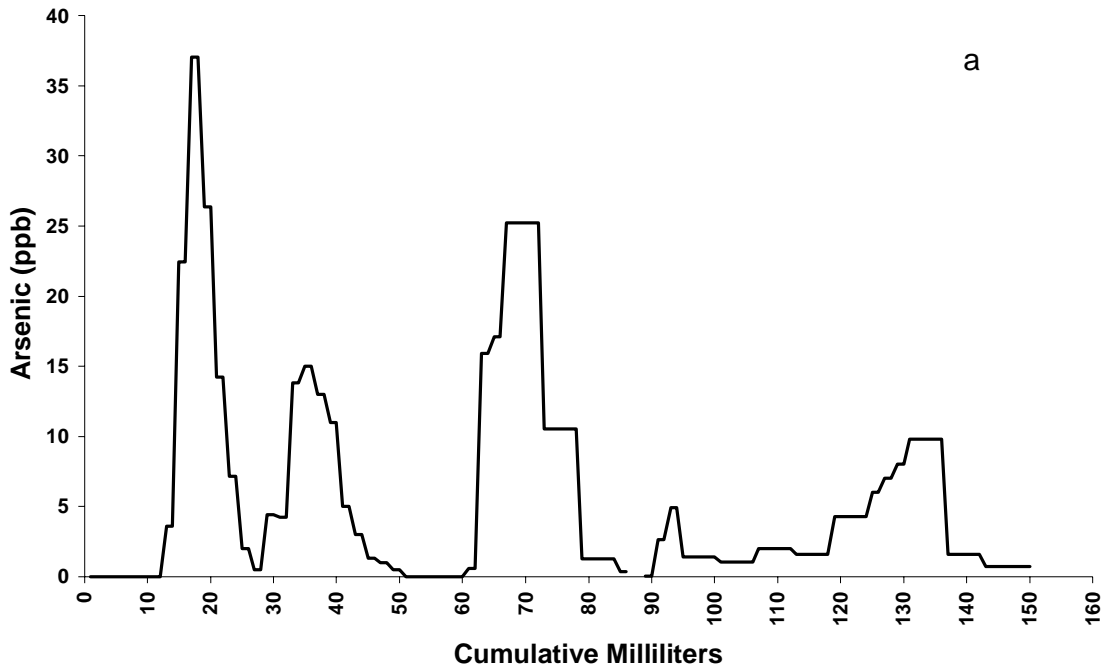
consistent. The resin column now contains the As^{5+} species strongly bound on the anion exchange resin and the DMAA species strongly bound on the cation exchange resin. The addition of 8 ml of 0.2 M TCA lowers the pH to less than 1.0. The DMAA is retained strongly on the cation exchange resin. As the more concentrated TCA enters the anion resin, As^{5+} is converted into its neutral form and is collected in the 55 to 85 ml fraction. The only arsenic species left in the chromatographic column is the DMAA on the cation resin. Addition of the solution of 1.5 M NH_4OH (pH~12) converts the DMAA into its anionic form, strips it from the cation exchange and carries it into the anion exchange resin at the bottom of the column where it is strongly retained. Finally, the addition of 0.2 M TCA strips the DMAA species by converting it to its neutral and cationic forms to be collected in the 85 to 140 ml fraction.

Referring to the validation run arsenic elution points, Figure A-7a, it can be seen that there is definite separation between the arsenic species. Figure A-7b depicts the elution curve of 1000 ppb standards. The graph on the left depicts the separate arsenic species eluting when a mixed standard with 250 ppb of As^{3+} , As^{5+} , MMAA and DMAA is used. Based on these and other validation runs, the 0-25 ml aliquot was collected as As^{3+} , the 25-55 ml aliquot as MMAA, the 55-85 ml aliquot as As^{5+} , and DMAA in the 85-140 ml fraction. The overlap in the As^{3+} and MMAA peaks is of some concern at higher concentrations. As evidenced in Figure A-7a the As^{3+} -MMAA peak separation is good at a concentration of 250 ppb.

There are some problems with the separation of DMAA using the method as employed in January 1998. The method used here quantified significant amounts of DMAA (20-200 ppb). Two other researchers (Eric Crecelius, Battelle Marine Sciences Laboratories and Walter Goessler, University of Austria-Graz), did not find DMAA in sub-samples of the Rio Salado water samples. Crecelius and Goessler did not find DMAA in either the filtered HNO_3 preserved samples or unfiltered unpreserved samples that were sent to them in July, 1998. Ion exchange laboratory validation had shown successful separation of DMAA from other arsenic species.

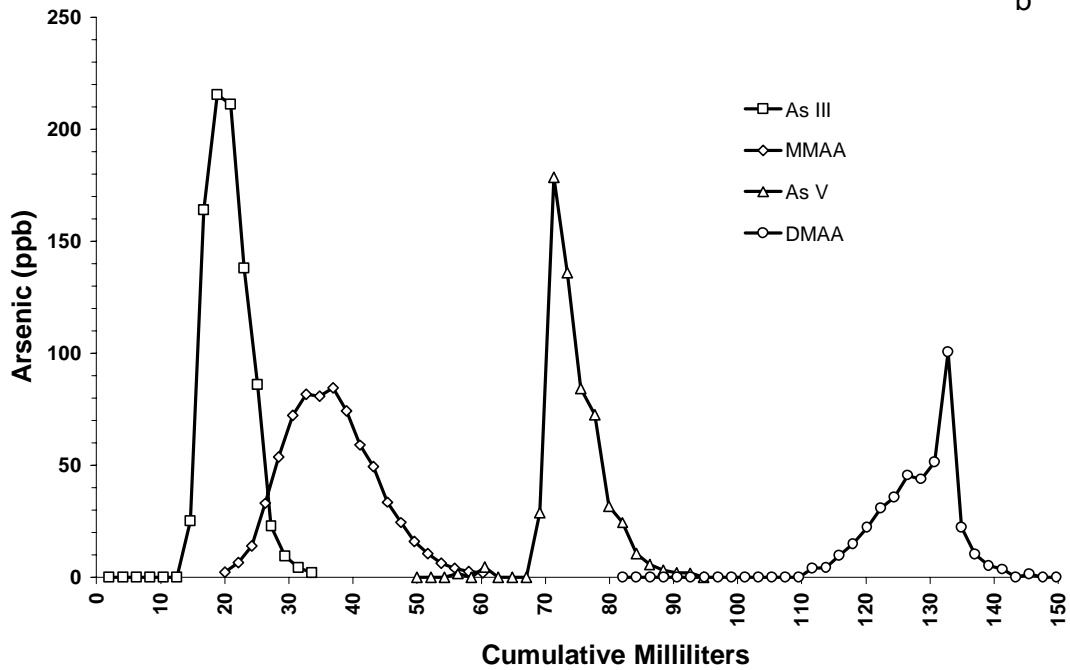
During the laboratory testing before the January 1998 sampling event, analysis of the eluant in the 110-160 ml range was not done when only As^{5+} standards were used. Testing after the January sampling did examine this area of the As^{5+} elution. The problem lies in that the peaks at 115 and 135 ml points create a false positive for DMAA. A confounding factor for this being an explanation of DMAA false positives is that the mass of As present in the 'late' As^{5+} eluant is far less than the mass of As found in the field collected DMAA eluant fractions. This is shown in Figure A-4. The triangles are the amounts of late arsenic that show up in the eluant at >110 ml after As^{5+} standards have been run through the column. The dark diamonds and squares are DMAA values for the field samples. Only a few samples fall below the 1000 ppb As^{5+} 'late peak' mass line. This would appear to indicate that the DMAA seen is not a result of the As^{5+} bleeding through to the DMAA eluant. If the 'DMAA' seen in the field samples is indeed As^{5+} , a constant ratio would be expected, since the 'late' eluted As^{5+} (filled triangles Figure A-4) concentrations are quite linear with respect to the concentration of the As^{5+} introduced to the column.

Mixed Standards 250 ppb



a

Individual Standards 1000 ppb



b

Figure A-7. Examples of early validation runs for ion exchange separation of arsenic species.

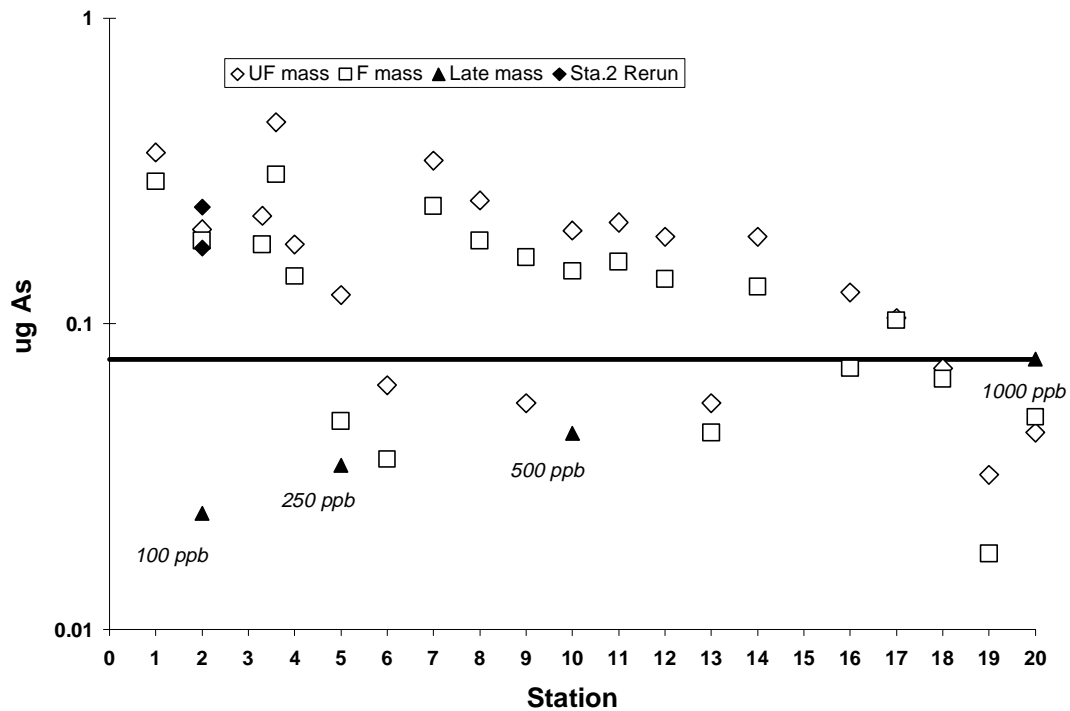


Figure A-8. Comparison of the late mass peaks produced by As^{5+} and the mass of 'DMAA' detected at Rio Salado.

I found that the ratio of DMAA to As^{5+} or Total As is not constant, implying that they are not proportional and are not correlated. As^{5+} and Total As ratios are relatively constant, implying a relationship. When taken all together, the column evidence indicates the presence of DMAA in substantial concentrations, not related to As^{5+} concentration, but only if other evidence to the contrary is ignored. A 2 ml aliquot of the unpreserved Station 2 sample (anion) from January 1998 was run through the column twice in October 1998. The eluted 'DMAA' mass is plotted as light diamonds in the figure. These 'DMAA' values are almost identical to the values determined from field elution. It is difficult to explain the amount of 'late' arsenic showing up in Station 2 based on the bleed through of As^{5+} observed during the DI water tests (triangles). Subsequent testing using the Grabinski method as published, and as modified here, failed to replicate the published finding that 8 ml of 0.2 M TCA is sufficient to elute all As^{5+} from the column. These methods result in a late peak for As^{5+} in the DMAA elution range. It was found that 40 ml of 0.2 M TCA was required to cleanly elute the As^{5+} peak and eliminate the late peak.

In summary, DMAA is a common constituent in surface waters. The detected 'DMAA' is suspect given the number of confounding factors. The observation of MMAA in absence of As^{3+} (no possibility of peak overlap) and Welch's observation of MMAA and DMAA in sediments and algae is definitive evidence that there is organic As in the Rio Salado system. DMAA is more likely to be present in natural waters than

MMAA [43, 44, 60, 81, 82]. There should be DMAA in Rio Salado waters but quantification was prevented due to problems with the speciation method.

APPENDIX B FLORIDA INVESTIGATION

A review of data on arsenic-contaminated sites was conducted with the assistance of Southern Company Services. The objective of the review was to identify sites that are suitable for investigation of the transferability of the model used at Rio Salado. The mechanistic SC model used for Rio Salado was successful. However, it was unknown if it could be used at other sites by collecting only the data necessary to constrain the model. This is in contrast to Rio Salado where the conceptual model was developed through detailed examination of the site. Two sites were identified that had characteristics that made them suitable for evaluation of the transferability of the model. Analysis of the sediments and water allow a determination of the accuracy of the SC approach in predicting the sorbed arsenic concentration on the sediments. Tyndall Air Force Base (AFB) and Fort Walton, Florida have shallow groundwater plumes that contain elevated levels of arsenic. Ditches are groundwater discharge points at Tyndall AFB and Fort Walton. Where the arsenic plume crosses a ditch contaminated surface water is found. Contaminated ditches represent ideal sampling points to collect sediment-water pairs for the purpose of this effort because:

1. It is relatively easy to collect high quality samples using only hand equipment;
2. The depth of penetrations can be minimized; and,
3. Water samples can be collected without use of wells or penetrometers.

B.1. SAMPLING AND ANALYSIS

At Tyndall AFB all paved roads have adjacent drainage swales. Ditch Reach 4 crosses groundwater known to be arsenic-contaminated. Arsenic has been detected in surface water in the swale. This swale was sampled at three locations. The original intent was to be near both endpoints and the midpoint of the ditch. Field relocation of two sample locations was necessary to meet sampling objectives. At each sample location, a sediment-water pair was collected.

The Fort Walton plume is proximal to a ditch on the east and south sides. The open ditch was sampled near the headwall east of Jet Stadium and in the open section southwest of Robinwood Drive SW. It was planned to take a sample west of Bass Avenue, but this location was not suitable for sample collection in support of model testing. Sample locations in the open reaches were set based on field conditions and the discretion of the sampling team. The sample locations for Tyndall AFB and Fort Walton Beach are described in Table B-1.

Other than field measurements, separations, and the X-ray fluorescence (XRF) analysis conducted at the University of New Mexico, all analytical procedures were conducted at New Mexico Institute of Mining and Technology (NMIMT) and New Mexico Bureau of Mines and Mineral Resources (NMBMMR) facilities. The principal

instruments used for water and sediment extract analyses are an IL Video Model 12 flame atomic absorption spectrophotometer (FAA), Varian 600 Zeeman graphite furnace atomic absorption spectrophotometer (GFAA), and Dionex 4000 ion chromatograph (IC). The determinations and analyses that were performed for this effort are listed in Table B-2. Tabular analytical data for all analyses described here are found in a following section of this appendix.

Table B-1. Florida sampling station locations.

Station	Description	Use
FW-1	Fort Walton Beach downstream sample. Robinwood Drive SW location. Open drainage channel with natural bottom. Sample location at the end of point bar ~5 m from headwall on downstream side of Robinwood Drive. Flow rate ~0.1 m ³ /s. Sediments are medium to fine sands with orange staining.	Sediment-water pair
FW-2	Fort Walton Beach upstream sample. Jet Stadium sample location. Sample location from middle of submerged section ~10 m north of Hollywood Blvd. Sediments are medium to fine sands with orange staining.	Sediment-water pair
T-1	Tyndall AFB 'upstream' sample. 10 m NW of Reach 4 upstream headwall. Sample collected using wide diameter shallow piezometer.	Sediment-water pair
T-2	Tyndall AFB 'center' sample. 15 m NW of Reach 4 upstream headwall. Sample collected using wide diameter shallow piezometer.	Sediment-water pair
T-3	Tyndall AFB 'downstream' sample. 20 m NW of Reach 4 upstream headwall. Sample collected using wide diameter shallow piezometer.	Sediment-water pair

Table B-2. Florida data collection.

Parameter	PQL ¹	Method	Comments
Field Measurements			
pH	± 0.02 units	Field Probes	Calibrated daily and checked frequently through the day.
Conductivity	±10 µS/cm	Field Probes	
Temperature	± 1 °C	Field Probes	Calibrated daily against temperature corrected KCl standard.
Eh	± 10 mV	Field Probes	
Alkalinity	5 mg/L as CaCO ₃	Titration	Measured with calibrated probes and mercury thermometer. Platinum electrode values corrected for Ag/AgCl reference electrode (add 200 mV to meter reading). Field titrated alkalinity at pH 8.3 and 4.5 endpoints. Performed in the field daily.
Metals			
Aluminum	0.5 mg/L	FAA	
Antimony	0.5 µg/L	GFAA	
Arsenic	0.001 mg/L	GFAA	
Barium	0.003 mg/L	GFAA	
Boron	0.5 mg/L	GFAA	Boron not detected
Cadmium	0.01 µg/L	GFAA	
Calcium	0.1 mg/L	FAA	
Chromium	0.4 µg/L	GFAA	
Cobalt	0.3 µg/L	GFAA	
Copper	0.8 µg/L	GFAA	
Iron	0.2 µg/L	GFAA	
Lithium	0.05 mg/L	GFAA	Lithium not detected
Lead	0.4 µg/L	GFAA	
Magnesium	0.05 mg/L	FAA	

Parameter	PQL ¹	Method	Comments
Manganese	0.4 µg/L	GFAA	
Molybdenum	1.5 µg/L	GFAA	
Nickel	0.2 µg/L	GFAA	
Potassium	0.1 mg/L	FAA	
Selenium	0.9 µg/L	GFAA	Selenium not detected.
Silica	15 µg/L	GFAA	
Silver	0.02 µg/L	GFAA	
Sodium	0.2 mg/L	FAA	
Strontium	0.1 µg/L	GFAA	
Vanadium	2.4 µg/L	GFAA	
Zinc	0.2 µg/L	GFAA	
Anions			
Total Bromine	1 mg/L	IC	Bromine not detected
Chloride	1 mg/L	IC	
Fluoride	0.2 mg/L	IC	
Nitrate	0.1 mg/L	IC	
Phosphate	0.025 mg/L	Colorometric	
Sulfate	0.1 mg/L	IC	
Sediments		Comments	
Sediment preparation was highly variable and dependent on the analytical method used.	Sequential Extraction (Tessier Method) for Fe, Mn, and Al concentrations. Strong acid (USEPA SW-846 Method 3051) digestion for Fe, Mn, and Al concentrations. Hydroxylamine hydrochloride extraction for Fe, Mn, and Al concentrations (Chao reagent). Trace elements by XRF. Total organic carbon by loss on ignition.		

¹Practical Quantification Limit Note: mg/L = parts per million (ppm) and µg/L = parts per billion (ppb)

B.1.1. Tyndall AFB

A reconnaissance of Tyndall AFB was not conducted before sampling. Photographs and drawings of the site were examined for planning. It was apparent that the ditches contain a shallow layer of organic muck. This was not the material desirable to sample for the purpose of validation. In order to collect a representative sediment-water pair the muck layer was removed and a temporary 6" PVC casing with screened perforations installed through the layer to the cleaner sands below. Casing installation was started the morning of January 7, 2000 after obtaining the necessary permit from the Base Engineer's office. Casings were advanced using a bucket hand-auger to remove sediments through the casing while driving with hammer taps from the top. This was continued until the casing was advanced into the sediments 0.3-0.5 meters. The operation was repeated until the casing was installed in the originally planned configuration of one casing near each headwall of Reach 4 with one casing located approximately in the center. I created a caisson that would allow upward groundwater flow from the bottom and discharge through the screened perforations driven by the natural hydraulic gradient. The caisson sequestered 1-2 liters of water from the muck. The intent was to be able to collect a water sample of a liter or more in as representative a manner as practical. The water should have very recently been in equilibrium with the sediments. Following collection of the water sample, a disturbed sample of the sediment formerly in equilibrium with the water was collected.

Inspection several hours after installation revealed that the center and downstream casings were not installed in locations with groundwater up flow. The field decision was made to relocate those casings closer to the upstream headwall where up flow conditions were observed. Relocation was accomplished on the morning of January 8, 2000. The casings were moved to straddle location T-2 that had indicated good hydraulic connection. T-2 was purged several times while T-1 and T-3 were installed. Following installation of T-1 and T-3, these casings were purged of 10-20 liters of water by frequent removal of a liter or two of water over the course of a few hours. Sampling was initiated with T-2 with all sampling finished the same day. Water samples were collected by evacuating the caisson, collecting field parameters and collecting samples after the caisson has refilled, filtering one 500 ml sample (metals), and two 500 ml unfiltered samples (metals and anions). The filtered and unfiltered aliquots were subsampled and the arsenic in the subsamples speciated in the field using ion exchange chromatography. Separation was conducted using the modified Grabinski method described in Appendix A and the modified Ficklin [95] method described by Miller et al. [132]. Disturbed sediment samples were collected from the sediments at the base of the in-place casing using a hand auger immediately following collection of water samples. All sample containers and preservation (other than arsenic speciation) were according to USEPA SW-846 protocol.

B.1.2. Fort Walton Beach

A reconnaissance of the Fort Walton drainage was not conducted before sampling. Photographs and drawings of the site were examined to plan the sampling. Fort Walton site sediment-water pairs were collected from a drainage ditch that bounds the plume on the southern and eastern sides a distance of ~300 m from the application area of the herbicide. The drainage is typical of an urbanized small stream, with steeply incised banks and a narrow riparian boundary between the channel and built up areas. Much of the stream channel in the plume area is routed through buried drains. The sampled sections were open channels. The stream bottom was composed of loose sediments with submerged point bars and other fluvial structures. The channel was surprisingly free of refuse given the location and setting. Water depth varied from 0-50 cm with most of the water ~20 cm deep. Sediment water pairs were collected from the upstream faces of submerged point bars in the drainage at two locations, FW-1 and FW-2. Water and sediment samples were collected on January 9, 2000 in the manner described in Appendix A for Rio Salado sediment-water pairs. Sample preservation and analysis was identical to that used at Tyndall AFB. Sampling was completed January 9, 2000.

FW-1 was located farthest downstream of the substation. The sample was taken on the downstream side of the culvert that crosses under Robinwood Drive SW. The drainage is about 10 meters wide at this point. Approximately half the width of the drainage was flowing water at the time of sampling. A large point bar, located just downstream of the headwall was sampled on its submerged upstream face. FW-2 was located adjacent to Jet Stadium (a city recreational area) ~300 m due east of the substation. The drainage is about 5 meters wide at this location. The channel is

deeply incised with the stream water level approximately three meters below ground surface. A small point bar with a broad upstream face was selected for sampling.

B.1.3. Field Parameters

Field parameters of pH, conductivity, temperature, and oxidation-reduction potential (ORP) were measured using calibrated probes. The alkalinity values and other field data are presented in Table B-3. Field measurements, with exception of alkalinity, were made within several minutes of sample collection. All meters were calibrated and stored according to the manufacturer's instructions and cleaned between uses with a Type I water rinse. Occasional physical cleaning of probe sensors was accomplished with Kim-Wipes® tissue or cotton swabs. All calibrations, equipment malfunctions, or failures to spot check were recorded in the project logbooks.

A Cole-Parmer TDSTestr 40 with a temperature compensated range of 0-1999 and 0-199 $\mu\text{S}/\text{cm}$ and accuracy of $\pm 2\%$ of full scale was used to monitor conductivity. A conductivity calibration standard of 1333 and 133 $\mu\text{S}/\text{cm}$ was used to check instrument response several times a day. The instrument was calibrated to the same standards daily before use. An OMEGA model PHH-82 meter was used to measure pH and ORP. The glass-bulb gel-filled combination electrode pH meter has a range of 0-14 pH units, resolution of 0.01 pH units, and accuracy of ± 0.02 pH units over an automatically temperature compensated range of 0-70°C. Fresh National Institute of Testing and Standards (NITS) traceable pre-mixed buffer solutions of 4.01, 7.00, and 10.01 pH units at 25°C, accurate to ± 0.02 pH units (OMEGA), were used for daily calibrations. The true buffer values were calculated using the manufacturer supplied temperature dependent pH corrections appropriate for each buffer.

Table B-3. Florida field parameters.

Station	Date	Time (CST)	Temp(°C)	Conductivity ($\mu\text{S}/\text{cm}$)	pH	ORP (mV)	CO_3^{2-} (ppm)	HCO_3^- (ppm)
T-1	1/8/00	1401	15.6	97	5.07	103	0	10.1
T-2	1/8/00	1050	15.5	111	4.85	128	0	13.0
T-3	1/8/00	1613	15.6	60	5.00	105	0	19.1
FW-1	1/9/00	938	17.3	284	6.95	354	0	118.3
FW-2	1/9/00	1224	20.5	264	6.74	327	0	127.2

The ORP meter is a platinum electrode type with range of ± 1000 mV, resolution of 1 mV, and accuracy of ± 15 mV. The ORP meter is factory calibrated at time of manufacture and is not intended for user adjustment. The meter is referenced to the Ag/AgCl electrode in the pH sensor with the meter reading the differential voltage between the Pt and Ag/AgCl electrodes. This reading is corrected to Eh by addition of the standard potential for the Ag/AgCl electrode (200 mV) to the meter reading. Temperature was measured with a mercury thermometer with resolution of 0.1°C and accuracy of ± 0.2 °C.

Alkalinity was determined by titrating a 50 ml sample with standardized 0.020 N H_2SO_4 to phenolphthalein (colorless, pH~8.3) and bromcresol green-methyl red (light pink, pH~4.5) endpoints. Titrations were conducted at the end of each field day. Carbonate (CO_3^{2-}) concentrations can be estimated as two times the phenolphthalein alkalinity. The bicarbonate (HCO_3^-) concentration estimate is the bromcresol green-

methyl red alkalinity, minus two times the phenolphthalein alkalinity. The Tyndall alkalinity values are low enough that a substantial portion of the alkalinity is probably non-carbonate.

B.2. SPECIATION OF ARSENIC IN WATER

Investigation of the speciation of arsenic in the environment requires the ability to preserve the arsenic species prior to analysis, or to separate the species before transformation takes place. Given the uncertainties in the preservation of arsenic species, field separation was selected. Separation is initiated within minutes of sample collection. Uncertainties associated with sample preservation are eliminated. In order to accomplish this, two existing ion chromatography separation methods were modified for field use [87, 124]. The first method was the four species method previously used at Rio Salado for As^{3+} , As^{5+} , MMAA, and DMAA. The second method is designed primarily for the separation of As^{3+} and As^{5+} and has been shown to yield false positives for As^{3+} when MMAA and/or DMAA are present.

As presented in Appendix A, the four species arsenic separation method exhibited some problems with DMAA, providing false positives. This was rectified before employing the method in Florida. In addition, a two species method modified from that published by Fickin [95, 132] was used in parallel with the four species method.

B.3. SEDIMENT EXTRACTIONS

Sediment extractions on the Florida samples repeated the selective extractions and microwave assisted HNO_3 digestion used on the Rio Salado samples by Welch [106]. Manganese was not evaluated in the Florida extractions. Manganese oxides were not included in the Rio Salado model as sorbing phases and therefore it was not necessary to analyze the Florida extracts for comparison purposes. An additional extraction method often used by soil scientists for evaluation of iron hydroxides and oxides, citrate-bicarbonate-dithionate, was also employed.

B.3.1. Selective Extraction

A combination of partial extraction techniques developed by Tessier et al. [122] and Chao and Zhou [123] was performed on the sediments to determine relative proportions of exchangeable arsenic (water soluble and affected by adsorption-desorption processes), arsenic associated with carbonates, amorphous iron and manganese oxides, and organic matter. The procedure used is as follows: about one gram of sediment, coned and quartered from air dried field samples, is agitated in 8 ml of 1M NaOAc adjusted to pH 8.2 for 1 h to remove exchangeable arsenic. Next, the residue from the exchangeable extraction is agitated in 8 ml of 1M NaOAc adjusted to pH 5 for 4 hours to remove arsenic associated with carbonates. The resulting residue is then digested in 20 ml of 0.25M $\text{NH}_2\text{OH-HCl}$ in 0.25M HCl heated to 50 °C for 30 minutes to extract arsenic associated with amorphous iron and manganese oxides. Extraction of arsenic bound to organic matter and crystalline oxides is achieved by adding the residue from the iron-manganese oxide digestion to 3 ml of 0.02 M HNO_3 and 5 ml of 30% H_2O_2 adjusted to

pH 2 with HNO₃. This mixture is heated to 85 °C for 2 h after which an additional 3 ml aliquot of 30% H₂O₂ is added with continued heating for an additional 3 h. The use of 0.25M NH₂OH-HCl (hydroxylamine hydrochloride) in 0.25M HCl, described by Chao and Zhou [123], was used instead of the 0.04M NH₂OH-HCl in 25% v/v HOAc suggested by Tessier et al. [122] because of its greater selectivity for amorphous Fe and Mn oxides and reduced matrix effects.

All extractions were conducted in plastic centrifuge tubes to avoid loss of sample and cross contamination. Between each successive extraction, samples were centrifuged at 10,000 rpm for 30 minutes and the supernatant pipetted off for analysis. Afterwards, 8-12 ml of Type I water was added and the residue again centrifuged for 30 minutes. The second supernatant was removed and discarded before addition of the next extracting reagent.

B.3.2. HNO₃ Digestions

Nitric acid extractions were conducted on whole sediment samples. About 1 gram of sediment was added to 10 ml of 8M HNO₃, (1:1 HNO₃ and distilled water) and microwave-heated under pressure in sealed Teflon containers. This is equivalent to USEPA SW-846 Method 3051. This mixture was heated 12 minutes at 50 psi and followed by 30 minutes at 100 psi, about 180 °C. After cooling, extracts were filtered (0.45 µm) and diluted for analysis.

The HNO₃ procedure dissolves many of the secondary minerals and organic matter, but not residual minerals and glasses. It also provides an estimate of the “total” acid leachable arsenic in the sediments, and represents arsenic that could be remobilized with changes in environmental conditions such as pH or Eh. USEPA indicates that the analysis provides a measure of the total amount of environmentally available metals.

B.3.3. Citrate-Bicarbonate-Dithionate Extractions

The citrate-bicarbonate-dithionate (CBD) extraction method was used only on the Florida samples. The CBD method [85] is designed to remove amorphous coatings and crystals of iron oxide from soil. With time and testing, it is now considered appropriate for this use and determination of extractable aluminum, silica and manganese. The CBD extraction is not very effective on highly crystalline oxides of aluminum, silica and manganese. The extraction is conducted on approximately 1.0 g of air dried sediment. Sediments are then combined with 40 ml of 0.3 M sodium citrate and 5 ml of 1 M NaHCO₃ solution in a 100 ml centrifuge tube. The contents are mixed by shaking and the tube placed in a 75 to 80°C water bath. The sediments are stirred with a glass rod until they reach 75 to 80°C. At that point, about 1 g of Na₂S₂O₄ (dithionate) powder is added, the solution stirred thoroughly for 1 minute and intermittently for 5 additional minutes. Then an additional 1 g portion of Na₂S₂O₄ is added and the digestion continued for 10 more minutes, stirring occasionally. The use of various flocculating agents to the extract to assist in separating the supernatant from the residue is often suggested for the CBD method. Rather than using that method the sample was centrifuged at 10,000 rpm for 15 minutes and the supernatant decanted for analysis.

B.3.4. Speciation of Arsenic in Sediments

The phosphoric acid (H₃PO₄) extraction and speciation method used on the Rio Salado samples was repeated using Florida samples. The results were very poor. Very little arsenic was recovered from these extractions. Spikes were not recovered. After several attempts, exhibiting similar results, the effort to speciate the arsenic on the Florida sediments by phosphate extraction were abandoned. Welch had difficulty with the method on the Rio Salado samples, but satisfactory results were obtained. A laboratory artifact is suspected rather than an issue with the method's utility. The source of the difficulty with the Florida sediments was not investigated.

B.4. SEDIMENT PETROLOGY AND MINERALOGY

The Florida sediments are a relatively simple system from a mineralogical perspective. At both sites the dominant (>99%) mineral present is quartz. Sediments are dominantly sand sized. Non-quartz grains are composed of shell fragments, urban debris, residual minerals, organic fragments, and unidentifiable material. These non-sand components comprise 1% or less of the total sediment volume. The following classification is used: 1.0-2.0 mm (very coarse sand), 0.5-1.0 mm (coarse sand), 0.25-0.5 mm (medium sand), 0.125-0.25 mm (fine sand), 0.0625-0.125 mm (very fine sand) and <0.0625 mm (silt-clay).

At Fort Walton Beach the sediments are very coarse to very fine quartz sand with occasional grains to 3 mm, very poorly sorted, with subangular to subrounded grains. FW-2 has a distinct orange staining on the grain surface absent at FW-1. Tyndall AFB Reach 4 sediments are fine to medium quartz sand very poorly sorted, with subangular to subrounded grains. The sediments have a gray cast that may be related to the overlying muck layer.

B.4.1. Determination of Total Organic Carbon (TOC)

Percent TOC was determined by loss-on-ignition. About 10 g of un-sieved sediments were oven dried at 105 °C for 3 to 4 h and weighed, then placed in a muffle furnace and heated at 430 °C for 24 h. After cooling, sediments were re-weighed to determine the amount lost-on-ignition, representing TOC. Contribution to the sediment weight loss by structural water expelled from clays is insignificant due to the fact that clays were present in non-detectable amounts. Also, carbonates do not to affect the loss-on-ignition value at temperatures of 430 °C [126].

B.4.2. X-Ray Fluorescence

Values of total metals were determined by X-ray fluorescence (XRF) on the instrument at the University of New Mexico geology laboratory. Ground whole sediments were used to make pressed powder pellets that were analyzed using standard procedures. This instrument does not have the required sensitivity for arsenic. Total arsenic was determined by reflux digestion with perchloric-nitric-hydrofluoric acids.

B.5. FLORIDA TABULAR DATA

Table B-4. Concentration of As, Fe, Al, Si by sediment extraction method.

HNO₃	As (mg/kg)	Fe (mg/kg)	Al (mg/kg)	Si (mg/kg)
FW-1	2.718	642.9	1338.6	ND ¹
FW-2	3.712	1240.1	3716.3	ND ¹
T-1	0.431	18.9	212.1	ND ¹
T-2	0.637	13.1	106.3	ND ¹
T-3	3.410	14.8	142.1	ND ¹
T-1 Dup	0.689	23.8	241.2	ND ¹
CBD	As (mg/kg)	Fe (mg/kg)	Al (mg/kg)	Si (mg/kg)
FW-1	0.569	32.4	342.1	570.7
FW-2	0.421	96.3	570.5	623.8
T-1	0.936	2.4	680.3	777.9
T-2	0.438	5.2	235.2	521.2
T-3	0.492	2.9	260.4	600.6
T-1 Dup	0.747	1.5	546.9	703.1
Exchangeable NaOAc pH 8.3	As (mg/kg)	Fe (mg/kg)	Al (mg/kg)	Si (mg/kg)
FW-1	0.364	0.8	13.2	73.1
FW-2	0.306	0.8	15.1	91.9
T-1	0.188	0.7	17.8	91.9
T-2	0.238	0.4	7.5	75.0
T-3	0.191	0.3	12.2	68.6
T-1 Dup	0.209	0.5	12.5	88.0
Carbonate NaOAc pH 8.3	As (mg/kg)	Fe (mg/kg)	Al (mg/kg)	Si (mg/kg)
FW-1	0.768	21.7	39.0	52.2
FW-2	1.012	28.7	29.4	24.0
T-1	2.430	7.1	772.3	762.9
T-2	1.777	6.5	109.5	617.1
T-3	5.484	8.6	119.4	649.0
T-1 Dup	1.368	7.6	502.8	966.2
Amorphous Oxides Chao Reagent	As (mg/kg)	Fe (mg/kg)	Al (mg/kg)	Si (mg/kg)
FW-1	0.339	18.1	63.2	8.1
FW-2	0.244	28.2	104.7	52.2
T-1	0.126	1.2	129.1	0.0
T-2	0.001	2.4	19.0	0.0
T-3	0.001	2.9	16.3	0.0
T-1 Dup	0.139	2.1	93.1	0.0
Organic and Crystalline Oxides	As (mg/kg)	Fe (mg/kg)	Al (mg/kg)	Si (mg/kg)
FW-1	0.125	131.3	373.9	155.1
FW-2	0.197	180.8	632.2	209.4
T-1	0.103	9.2	79.5	115.3
T-2	0.156	3.3	9.2	2.8
T-3	2.216	2.6	15.4	3.1
T-1 Dup	0.160	24.5	91.6	107.2
Total by XRF or Digestion (mg/kg)	As (mg/kg)	Fe (mg/kg)	Al (mg/kg)	Si (mg/kg)
FW-1	14.7	552	4160	457202
FW-2	44.4	795	5796	447807
T-1	14.2	379	3880	458091
T-2	13.6	365	2758	459025
T-3	32.0	252	2945	457623
T-1Dup	10.8	355	3132	457156

Table B-5. Florida anions in water.

Station	Cl ppm	SO ₄ ppm	F ppm	NO ₃ ppm	PO ₄ ppm
T-1	19.9	43.8	0.28	0.95	100
T-2	16.9	13.5	0.26	0.81	50
T-3	8.6	13.4	0	0.44	100
FW-1	14.8	5.1	0	0.92	225
FW-2	12.4	4.5	0	1.39	350

Table B-6. Arsenic concentration in water (ppb).

Station	Total Unfiltered	Total Filtered	As III by Two Species Method	As V by Two Species Method	As III by Four Species Method	As V by Four Species Method	MMAA by Four Species Method	DMAA by Four Species Method
FW-1	10.7	9.5	4.6	5.2	6.3	7.5	0.0	0.0
FW-2	10.2	9.7	4.0	4.6	5.0	7.5	0.0	0.0
T-1	210.7	189.9	123.2	19.4	137.5	24.4	4.5	8.1
T-2	524.2	474.7	214.0	160.0	207.5	150.0	43.5	33.0
T-3	107.2	71.1	42.0	6.2	34.4	15.0	4.5	8.7

Table B-7. Arsenic species as percentage of total filtered arsenic concentration in water and method recovery as compared to the total (ppb).

Station	As III by Two Species Method	As V by Two Species Method	Two Species Method % Recovery	As III by Four Species Method	As V by Four Species Method	MMAA by Four Species Method	DMAA by Four Species Method	Four Species Method % Recovery
FW-1	48%	55%	103%	66%	66%	0%	0%	131%
FW-2	41%	47%	89%	52%	52%	0%	0%	103%
T-1	65%	10%	75%	72%	72%	2%	4%	151%
T-2	45%	34%	79%	44%	44%	9%	7%	104%
T-3	59%	9%	68%	48%	48%	6%	12%	115%
Average FW	45%	51%	96%	59%	59%	0%	0%	117%
Average Tyndall	50%	31%	81%	50%	50%	5%	6%	112%

Table B-8. Unfiltered water sample analytical results.

Station	Ag (ppb)	Al	Ba (ppb)	Ca	Cd (ppb)	Co (ppb)	Cr (ppb)	Cu (ppb)	Fe (ppb)	K	Mg	Mn (ppb)	Mo (ppb)	Na	Ni (ppb)	Pb (ppb)	Sb (ppb)	Si (ppb)	Sr (ppb)	V (ppb)	Zn (ppb)
FW-1	0.06	1.27	82	34.6	0.02	0.6	0.8	11.5	68.0	9.3	1.98	6.7	3.9	21	2	ND	7.9	799	311	2.8	39
FW-2	0.04	1.43	125	34	0.04	0.1	0.7	6.6	27.0	10	1.50	5.2	2.6	18	1.9	ND	3.6	2272	420	ND	30
T-1	0.13	3.66	ND	7.5	0.23	0.4	0.5	8.9	11.1	1.8	3.03	2.1	ND	6	1.5	1.1	0.9	1605	11	5.7	13
T-2	0.22	1.98	ND	8.5	0.19	0.8	1.2	12.6	26.0	1	1.74	2.0	ND	10	3	3.7	2.2	3299	20	ND	26
T-3	0.24	2.32	ND	7.8	0.03	0.2	1	5.3	36.0	2.1	1.26	3.4	ND	4	4	2.5	2.7	2197	72	ND	20

Table B-9. Filtered water sample analytical results.

Station	Ag (ppb)	Al	Ba (ppb)	Ca	Cd (ppb)	Co (ppb)	Cr (ppb)	Cu (ppb)	Fe (ppb)	K	Mg	Mn (ppb)	Mo (ppb)	Na	Ni (ppb)	Pb (ppb)	Sb (ppb)	Si (ppb)	Sr (ppb)	V (ppb)	Zn (ppb)
FW-1	ND	1.95	68	34	0.02	0	0.7	1.9	23.0	8	1.99	12.0	2.7	21	0.7	ND	6.9	801	304	ND	124
FW-2	ND	1.98	110	34	0.02	0	0.9	3.3	23.0	8.1	1.52	9.6	1.6	18	1.2	ND	6.8	1849	372	2.5	93
T-1	ND	2.44	ND	7.3	0.04	0.2	0.5	3.7	2.1	0.5	2.40	2.3	ND	6	0.5	0.7	3	646	17	ND	12
T-2	ND	2.55	ND	7.9	ND	0.2	0.9	7.4	21.0	1.2	1.71	15.7	ND	13	0.4	2.7	ND	1542	17	ND	30
T-3	ND	2.57	ND	4.1	ND	0.3	ND	4.5	1.0	2.1	0.81	2.0	ND	6	0	1.1	ND	1001	44	ND	20

Table B-10. Arsenic by partial extraction methods as compared to arsenic by total digestion.

Station	HNO ₃	CBD	Exchangeable	Carbonate	Amorphous Oxides	Organic and Crystalline Oxides	Tessier Total	Digestion
FW-1	18%	4%	2%	5%	26%	1%	34%	100%
FW-2	8%	1%	1%	2%	1%	0%	4%	100%
T-1	3%	7%	1%	17%	1%	1%	20%	100%
T-2	5%	3%	2%	40%	0%	1%	43%	100%
T-3	11%	2%	1%	6%	0%	7%	13%	100%
T-1 Dup	6%	7%	2%	13%	1%	1%	17%	100%

Table B-11. Mineral surface sorbing sites determined by HNO₃ digestion.

Station	Fe (mg/kg)	Ferrihydrite Strong Sites (molal)	Ferrihydrite Weak Sites (molal)	Goethite Sites (molal)	Al (mg/kg)	Gibbsite Sites (molal)
FW-1		643	2.6E-04	1.0E-02	7.8E-04	3.0E-03
FW-2		1240	4.6E-04	1.8E-02	1.4E-03	7.7E-03
T-1		19	7.2E-06	2.9E-04	2.1E-05	4.5E-04
T-2		13	4.8E-06	1.9E-04	1.4E-05	2.2E-04
T-3		15	5.3E-06	2.1E-04	1.6E-05	2.8E-04
T-1Dup		24	8.9E-06	3.5E-04	2.6E-05	5.0E-04

Table B-12. Mineral surface sorbing sites determined by citrate-bicarbonate-dithionate (CBD) digestion.

Station	Fe (mg/kg)	Ferrihydrite Strong Sites (molal)	Ferrihydrite Weak Sites (molal)	Goethite Sites (molal)	Al (mg/kg)	Gibbsite Sites (molal)
FW-1	32	1.3E-05	5.2E-04	3.9E-05	342	7.7E-04
FW-2	96	3.6E-05	1.4E-03	1.1E-04	571	1.2E-03
T-1	2	9.2E-07	3.7E-05	2.8E-06	680	1.4E-03
T-2	5	1.9E-06	7.7E-05	5.7E-06	235	4.8E-04
T-3	3	1.0E-06	4.1E-05	3.1E-06	260	5.2E-04
T-1D	1.5	5.6E-07	2.3E-05	1.7E-06	547	1.1E-03

Table B-13. Mineral surface sorbing sites determined as the sum of all Tessier sequential extraction steps

Station	Fe (mg/kg)	Ferrihydrite Strong Sites (molal)	Ferrihydrite Weak Sites (molal)	Goethite Sites (molal)	Al (mg/kg)	Gibbsite Sites (molal)
FW-1	172	7.0E-05	2.8E-03	2.1E-04	489	1.1E-03
FW-2	238	8.9E-05	3.6E-03	2.6E-04	781	1.6E-03
T-1	18	6.9E-06	2.8E-04	2.1E-05	999	2.1E-03
T-2	13	4.6E-06	1.8E-04	1.4E-05	145	3.0E-04
T-3	14	5.2E-06	2.1E-04	1.5E-05	163	3.3E-04
T-1D	35	1.3E-05	5.2E-04	3.8E-05	700	1.5E-03

Table B-14. Mineral surface sorbing sites determined by the Chao reagent step of the Tessier sequential extraction.

Station	Fe (mg/kg)	Ferrihydrite Strong Sites (molal)	Ferrihydrite Weak Sites (molal)	Goethite Sites (molal)	Al (mg/kg)	Gibbsite Sites (molal)
FW-1	18	7.3E-06	2.9E-04	2.2E-05	63.2	1.4E-04
FW-2	28	1.1E-05	4.2E-04	3.1E-05	104.7	2.2E-04
T-1	1	4.6E-07	1.8E-05	1.4E-06	129.1	2.7E-04
T-2	2	8.7E-07	3.5E-05	2.6E-06	19.0	3.9E-05
T-3	3	1.1E-06	4.2E-05	3.2E-06	16.3	3.3E-05
T-1D	2	7.8E-07	3.1E-05	2.3E-06	93.1	1.9E-04

Table B-15. Porosity, density, and organic carbon content (TOC).

Station	Bulk Density (g/cc)	Porosity	Calculated Particle Density (g/cc)	Solids to Water Ratio (kg/kg)	% TOC ¹	% TOC ²
FW-1	1.60	0.354	2.480	4.53	0.41%	0.48%
FW-2	1.58	0.380	2.550	4.16	0.54%	0.74%
T-1	1.50	0.355	2.331	4.23	0.61%	0.64%
T-2	1.53	0.376	2.452	4.08	0.25%	0.16%
T-3	1.54	0.383	2.489	4.01	0.25%	0.28%
T-1D	1.50	0.360	2.338	4.15	0.54%	0.53%

¹ Analysis by Loss on Ignition conducted at New Mexico Institute of Mining and Technology.

² Analysis by Loss on Ignition conducted at University of New Mexico.

B.6. DATA QUALITY

B.6.1. Reagents and Standards

Trace metal grade reagents were used whenever available. Fisher Trace Metal HCl and NH₄OH were diluted as necessary. These reagents are used for column preparation and regeneration that does not require very precise molarity and they were not standardized. The maximum pH error from this simplification is less than 10% for HCl and less than 1% for NH₄OH. HCl and NH₄OH used for ion exchange chromatography eluant were standardized to pH values within ± 0.05 units of optimal. TCA for elution was made from Sigma ACS reagent solid and could be formulated by dilution to precise molar concentrations. The measured pH of the 0.006 M TCA was 2.25 ± 0.05 and the 0.2 M TCA was 1.05 ± 0.05 at 23.2 °C. The pH was checked when stock solutions were made and periodically thereafter.

With the exception of MMAA, all arsenic standards were obtained from Sigma. MMAA could not be located through the normal chemical suppliers. MMAA was obtained from Dr. Dean Carter of the University of Arizona. As³⁺ standards were prepared from American Chemical Society (ACS) certified reagent grade arsenic trioxide. As³⁺ standards were prepared the day of use as a 1.000 g/L arsenic stock solution by dissolution in 100 ml of hot 1.0 M trace metal grade HCl and dilution to 1 liter with Type I (ASTM) water. Complete oxidation of As³⁺ standards to As⁵⁺ in two weeks was observed during this effort. Partial oxidation has been observed in less than 12 hours. Attempts were not made to preserve the As³⁺ standards. As⁵⁺ and DMAA standards were prepared from ACS reagent sodium arsenate and Sigma Ultra cacodylic acid as 1.000 g/L arsenic stock solutions by dissolution in 1 liter of Type I water. Since only ~50 mg of MMAA was made available to this effort a 52 ppm as arsenic stock solution was prepared by dissolving 0.0201 g of MMAA in 100 ml of Type I water.

B.6.2. Quality Assurance

Design of this project incorporated a data quality objectives development process early in its inception. It was felt that this data might eventually be used for risk assessment, risk management, or comment on rulemaking. Balanced with this was the necessity to limit analytical and field costs. Data quality objectives had to be set to meet these competing priorities.

A Data Quality Objectives (DQO) process was used to define the sampling and analysis program described here. The DQO process was created by the USEPA in the late 1980's for use in the Superfund program as part of a general, and ongoing, revision of their quality assurance and quality control practice, regulation, and guidance. The DQO process borrows heavily from elements of Terzhagi's observational method and other well accepted experimental design principles. USEPA's objective was to create a publicly acceptable quality framework for environmental data collection that would meet the needs of environmental compliance and risk assessment at lowest cost. The intended purpose of the DQO process is to ensure that:

1. The questions to be answered through data collection and analysis are well defined;
2. The data collected is of known quality;
3. An acceptable level of uncertainty for answers to the questions is specified; and,
4. The cost, amount, and quality of data necessary to answer questions are critically evaluated.

The DQO process enabled us to establish the following findings and objectives. The primary objective was to obtain samples from a location other than Rio Salado to test the transferability of the modeling process to other locations. This being the case, sampling and analysis should be as comparable to that conducted at Rio Salado as is reasonably possible. Only the data necessary to support model testing should be collected. Plan review was accomplished before project implementation by Mary McLearn of EPRI.

All data collection met project-specific precision, accuracy, representativeness, completeness, and comparability criteria (PARCC parameters) or it was determined that an out-of-control event had taken place and the data used with caution if used at all. Chemical analyses should meet the precision and accuracy standards of SW-846 in order for the data to be acceptable. Generally, the reconnaissance data met these requirements. However, due to the novel and exploratory use of the data, full SW-846 QA (matrix spikes, matrix spike duplicates, and internal laboratory QA programs) was not invoked. Some methods, such as ion exchange chromatography and sediment partial extraction do not have SW-846 equivalents. All non-SW-846 analytical methods used have been peer reviewed, published in peer reviewed journals, or developed as part of this effort.

The sample locations for the Florida effort were selected based on several factors. The first was to identify sites where the limit and extent of arsenic contamination was known. Sampling of sediment-water pairs needed to be accomplished without the use of drilling equipment or expansive effort. The number of sites to be investigated was limited to two and the samples to be collected were limited to a total of six.

All sample containers were new high-density polyethylene (Nalgene or equivalent) bottles. All containers were cleaned with Alconox detergent and warm water, triple rinsed with tap water, triple rinsed with Type I water, and allowed to air dry with openings down. Following drying, caps were replaced and sample containers stored in zip-closure plastic bags for transportation to the field. Any other field sampling equipment was field cleaned immediately following use with 1.0 M Fisher Trace Metal grade HCl, and triple rinsed with Type I water. All field sampling equipment was cleaned nightly with an Alconox wash, triple rinse with Type I water, and air drying.

All water samples were containerized and preserved according to USEPA SW-846 accepted methods with exception of arsenic speciation samples. Samples remained in sample team custody throughout the sampling events and during transportation to the laboratory. Water and sediment samples were stored at $4^{\circ}\text{C} \pm 2^{\circ}\text{C}$ (iced in the field, refrigerated in the laboratory) until analysis. SW-846 mandated holding times were met. All sample locations are identified alphanumerically. Sample numbers were recorded in the project logbook. These numbers will be used to track the samples until final disposal.

Whenever possible, data was obtained from the analytical laboratory in electronic format to minimize transcription errors. A copy of the raw data was archived along with copies of logbooks and other data that would be difficult to reproduce. Spreadsheets were used for data manipulation and unit conversions. The parameter lists are broad in

order to emulate the sampling and analysis conducted at Rio Salado. Sediment data is needed to evaluate solid-water partitioning coefficients. All of the data obtained, in either raw or reduced form was used to calibrate and validate the numerical model.

Other quality assurance activities included logging of all field and lab data in bound logbooks, noting out of control events and their resolution, written preplanning of all activities, and following standard field and laboratory hygiene and safety practices. All equipment was used and maintained according to manufacturer instructions. Malfunctioning equipment was removed from service until repairs were made. Backup equipment was available for most needs.

B.6.3. Quality Control

The GFAA and FAA use autocalibration procedures based on standard dilution. FAA methods for the analytes of interest are routinely run at the NMBMMR laboratory and no modification of the standard methods was necessary to achieve accurate reproducible results. This was not true for ion-exchange chromatography samples that were strongly attenuated by matrix and arsenic species effects. Special procedures were implemented in order to meet PARCC parameters for these samples. The arsenic methods outlined in Appendix A were used for the Florida samples. Arsenic quantification has improved at the NMBMMR laboratory since the analysis of the Rio Salado samples. Routine quantification on natural waters is below 1 ppb with reproducibility within 10-15%. Using multiple injection techniques on the GFAA detection can be lowered to 0.2 ppb in many matrices.

Detailed quantification limit studies were not performed for aqueous analytes other than arsenic. This does not preclude the standard procedure of assigning practical quantification limits (PQL's) based on two standard deviations of the blank signal achieved during analysis. This is for routine analysis without significant matrix effects and is reflected by the PQL's in Table B-1.

B.6.4. Florida Data Quality Assessment

Samples are generally representative of the site conditions because deviations were not made from acceptable sampling practice for the media of interest. The chemical data is comparable to other data collected using SW-846 protocols. There is an exception, phosphate as PO₄. The NMBMMR IC, as normally configured, has a PQL for phosphate of 100 ppb. The corresponding detection limit is ~60 ppb. Phosphate is known to affect arsenic SC. It is possible that <60 ppb of phosphate could noticeably affect arsenic SC when the arsenic level is close to the phosphate level. Using the standard IC configuration phosphate was not detected in Rio Salado waters (Appendix A). Therefore, a molybdate blue colorimetric method sensitive to 10 ppb and quantifiable in 25 ppb increments to 500 ppb was used to evaluate phosphate in the Florida samples.

The two species arsenic speciation method used at the Florida sites suffered from some low recoveries. It was later identified that the elution point of As⁵⁺ using this method is very sensitive to the resin preparation technique. The low recoveries are

probably due to elution of As^{5+} past 100 ml of eluant. Since total arsenic is used for the modeling effort the conclusions reached from the modeling effort are not impacted.

APPENDIX C
CD-ROM OF DATA AND MODEL OUTPUT

The CD-ROM is found in a pocket inside the back cover of the bound dissertation.